INVESTIGATING THE INTERACTIONS OF POLYCATIONS WITH NUCLEIC ACID AND THE MECHANISMS OF DELIVERY

A THESIS

SUBMITTED TO THE FACULTY OF

UNIVERSITY OF MINNESOTA

BY

DUSTIN SPROUSE

IN PARTIAL FULFILLMENT OF THE REQUIREMENTS

FOR THE DEGREE OF

DOCTOR OF PHILOSOPHY

THERESA M. REINEKE

May 2015

Acknowledgements

The author would like to acknowledge the contributions from other authors from his prior published papers, the guidance of Theresa Reineke, the members of the committee, and the funding that made this work possible.

The author would also like to thank Yogesh Dhande, Nilesh Ingle, Karen Grinnen, and Haley Philips for assistance with biological assays, and Anton Sizov, Swapnil Tale, Scott Forbey, Yaoying Wu, Jeff Ting, Tushar Navale, Adi Ish Am Radian, Chris Macosko, and Bharat Wagh for helpful scientific discussions. Thank you to Letitia Yao, who helped with temperature and kinetic NMR experiments, Nancy Thao for help with regulatory, Jim Marti in the nanomaterials characterization facility, and Courtney Meeker for proof reading and editing.

This project was partially funded by the National Institutes of Health (NIH) program (1 DP2 OD00666901) and partially funded by the National Science Foundation through the University of Minnesota MRSEC under Award Number DMR-1420013. Part of this work was carried out in the College of Science and Engineering Characterization Facility, University of Minnesota, which has received capital equipment funding from the NSF through the UMN MRSEC program under Award Numbers DMR-0819885 and DMR-1420013, and part of this work was carried out in the College of Science and Engineering Minnesota Nano Center, University of Minnesota, which receives partial support from NSF through the NNIN program.

Dedication

This thesis is dedicated to Charles and Mercedes van der Spuy, two of the smartest, bravest, most humble, and influential people in my life. And to Gavin and Daphne Staats, the most loving, supportive, and accepting parents anyone could have asked for.

Abstract

Polymers - large macromolecules composed from many smaller subunits - have ever-growing uses and potentials in our lives. More specifically, cationically charged polymers have been widely explored as non-viral vectors to deliver nucleic acid to cells in an effort to regulate gene and protein expression. The polymeric vehicle must not only bind and complex with DNA to protect and deliver it to the targeted site, but also efficiently dissociate from the DNA and be non-toxic to the cell or host organism. Herein lies the wide array of polymers that must be rationally designed and synthesized in order for the delivery vehicle to perform its specific function.

At the turn of the century, two monumental achievements paved way for gene therapy. First, the Human Genome Project was completed. This milestone continues to unravel important information about the genetic basis of human health, disease, hereditary, and genetic dispositions. Second, RNA interference was discovered, an innate cellular pathway to control gene expression within cells. These discoveries afforded scientists the information necessary to move forward with controlling gene and protein expression profiles. More recently, CRISPR-cas technology was discovered, which allows scientists to permanently edit the genetic code by either regulating genes or adding, disrupting, deleting, or altering the specific base-pairs within the DNA sequence.

Herein, we investigate several classes of polymers and macromolecules for the complexation and delivery of nucleic acid, including: amino acids, dendrimers, micelles, and linear homo- and block polymers. Initially, it was shown that polymer type, length, charge, dispersity, and composition greatly affect the efficacy of these therapeutic delivery vehicles. With this in consideration we set out to explore some of the fundamental properties of polymeric vectors. Diblocks, triblocks, and statistical copolymers were designed and synthesized with varying amounts of primary and tertiary

amines. These were complexed with pDNA to from polyplexes and probed for their toxicity, stability, gene expression profiles, and mechanisms of membrane permeability. Amphiphilic polymers were also synthesized, which in aqueous environments spontaneously self assembled into core-shell structured micelles. These were probed for their ability to change size in different buffers and form different sized aggregates with DNA.

Table of Contents

List of Tables

List of Figures

Chapter 1.

POLYMERIC DELIVERY VEHICLES FOR EXOGENOUS NUCLEIC ACID DELIVERY

Synopsis:

Herein is described the structure-property relationships between polymers and their ability to interact with nucleic acids such as oligonucleotides, small interfering RNAs, and plasmid DNAs for delivery into cells in culture and in mammals. Polymer structure, composition, length, and dispersity have a strong influence on the ability for it to bind, condense, and complex nucleic acids, and to allow the composite material to function as a delivery agent. Numerous structural features are illustrated, and their effects on nucleic acid delivery into cultured cells is described. The features necessary for systemic delivery of nucleic acids in mammals are outlined, and examples of polymer delivery systems and their functions are illustrated. Finally, a few examples of polymer-based delivery of nucleic acids in humans are presented.

A version of chapter 1 is to to be published in the module: Materials Science and Materials Engeneering. Sprouse, D.; Reineke, T. M.; Davis, M. E. *Elsevier* **2015**.

1.01 Introduction

At the turn of the century, the Human Genome Project was completed and this milestone continues to unravel important information about the genetic basis of human health, disease, hereditary, and genetic dispositions. At the same time, RNA interference (RNAi), an innate cellular pathway to control gene expression, was also discovered. These breakthroughs have opened up completely new fields of medicine and research in controlling gene expression to understand biological processes, combat disease, and improve human health. The broad field of polymer science is playing an exciting role in inspiring and advancing new discoveries in the area of nucleic acid delivery for research tool and drug development. Many different polynucleotide types are currently being examined for these purposes; for example, high molecular weight plasmid DNA (pDNA), oligodeoxynucleotides (ODNs) of various lengths, small interfering RNA (siRNA), micro-RNA (miRNA), mRNA, and piwi-interacting RNA (piRNA). These biological macromolecules do not readily enter cells without a delivery vehicle and are easily and quickly degraded by ubiquitous nucleases present in the extra and intracellular environment. Nucleic acids, being large, negatively charged, and hydrophilic, do not diffuse through the cell membrane. The negative charge on the phosphodiester backbone of DNA is "repelled" by the negatively-charged cell surface (due to glycoproteins, glycosaminoglycans, and proteoglycans). Thus, in general, naked nucleic acids need a delivery vehicle for transport into the cell. The delivery vehicle is responsible for many essential functions (Figure 1): (1) it must compact various sizes of nucleic acids into nanoparticle complexes (termed polyplexes) that are similar in size and shape to viruses, (2) protect nucleic acids from premature release and enzymatic degradation, (3) promote specific cell surface binding and internalization (endocytosis), and finally (4) release the cargo at the proper intracellular location without toxic side effects. It is worth noting the

challenges encountered in the design of these materials; although the polymeric vector must bind nucleic acids with high stability to protect its payload during extra- and intracellular transport, the material must also release the nucleic acid once at the proper cellular location to perform its functional effect. Another important consideration is that the features needed to promote high delivery of polynucleotides into cell culture in vitro do not necessarily lead to the best systems for in vivo delivery. Thus, three important additional functions must be added to the list above. For systemic administration the polymer vehicle must (5) promote polyplex dispersion and stability from aggregation in physiological salt and serum concentrations, (6) minimize recognition and clearance by the immune and reticuloendothelial systems, and (7) localize to the target tissues/organ and be internalized into the cells of interest for successful in vivo efficacy.

In this chapter, we focus on the impressive role that polymers are playing in the in vitro and in vivo delivery of nucleic acids. We outline the basic features needed in a biomaterial to be utilized for this application. Several classes of polymers, including linear, hyperbranched, dendrimers, block copolymers, micelles, and stars polymers have been developed and extensively studied for this application and are summarized for this purpose. How these materials interact with nucleic acids and the important characterization assays used to study polymer-nucleic acid binding, nanoparticle formation, and cellular delivery are also discussed. Next, we outline in vitro delivery studies, their successes and developments with these complexed systems and the structure-activity relationships and features needed to progress into in vivo studies. Finally, our chapter is concluded by outlining the few ongoing human clinical trials.

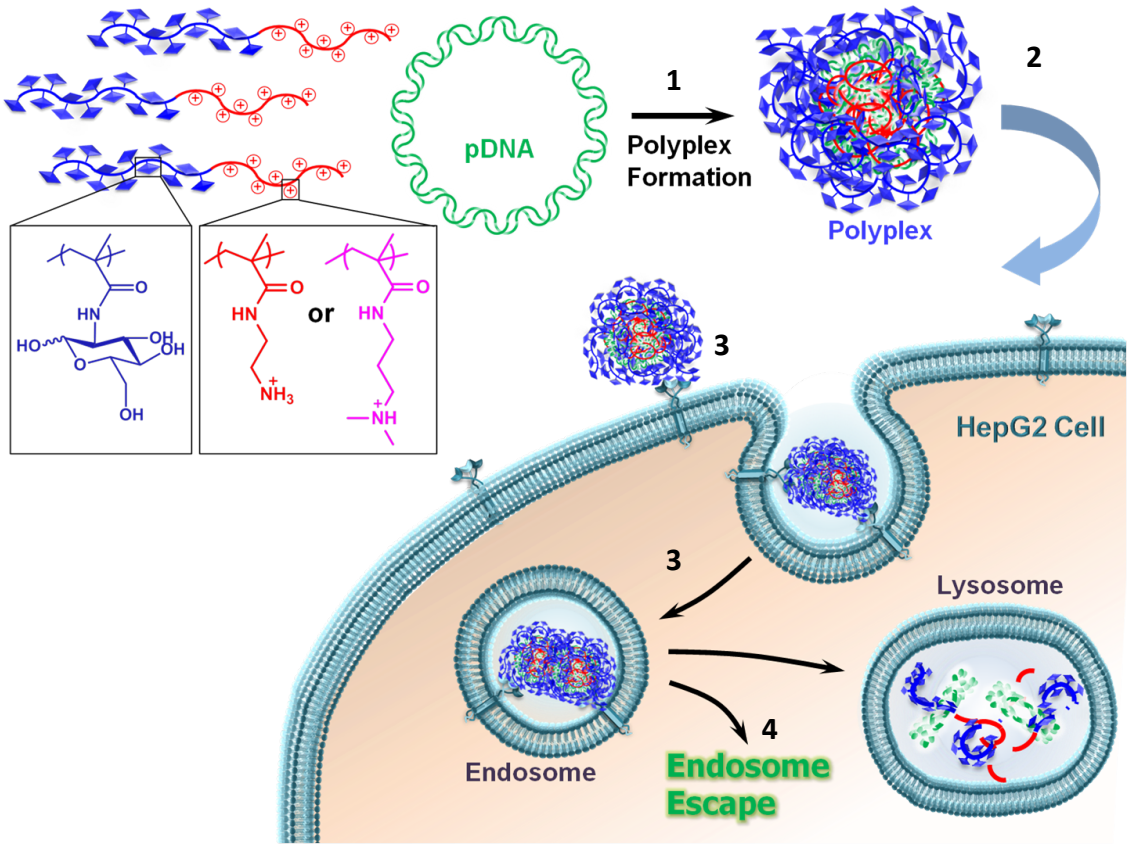

Figure 1: Schematic of polyplex formation and transfection. 1) Polycation binds electrostatically to plasmid DNA (pDNA) to form a polyplex nanoparticle, 2) the polyplexes are added to cells in transfection media, and 3) the polyplexes associate with the cellular membrane or receptors and are internalized, usually via endocytosis into an endosome. 4) Endosomes carry the polyplexes into the cell where 4) the polyplexes must escape the endosomes to avoid degradation in lysosomes. The delivery vector must then release its nucleic acid cargo either in the cytoplasm or nucleus (depending in the desired destination) for effective delivery. Figure adapted from [1].

1.02 Polymer Vehicles for Nucleic Acid Delivery

1.02.1 Basics of Polyplex Formulation and Delivery

Polymeric and dendritic macromolecules are typically created to contain a variety of functionalities and features to promote the cellular delivery of nucleic acids. First and foremost, the polymer must be hydrophilic component, water soluble, and promote interactions with polynucleotides. Macromolecules typically used for nucleic acid delivery mainly have a cationic nature (polycations) and their interactions with polynucleotides are driven mainly by electrostatic interactions with the negatively charged phosphate backbone. This process typically causes charge neutralization of the phosphodiester groups and compaction into colloidal complexes termed "polyplexes" or "micelleplexes". In the design of polycation vehicles, various types of charge centers are typically incorporated into the polymer structure to promote binding to DNA and RNA. For the most part, polycation vehicles are designed containing various types of amines (primary,[2-4] secondary,[5,6] tertiary,[7] quaternary,[8] imines,[9] and imidizoles[10]) that either have a cationic "hard charge" or "soft charge" that can be protonated within the physiological pH range. Hydrogen bonding has also been found to play a role in nucleic acid binding and compaction, Reineke et al., have suggested that H-bonding between polycations and nucleic acids can help stabilize polyplex formation by reinforcing the interactions within.[11-13] Kabanov et al. have been examining the use of polyoxomers termed pluoronics (A–B–A amphiphilic block copolymers of poly(ethylene oxide) and poly(propylene oxide), for nucleic acid delivery.[14] These structures appear to promote some interaction with nucleic acids, cellular uptake, and trafficking without electrostatic interactions. In fact, the nature of the interaction between polyoxomers and nucleic acids and how these polymers promote cellular delivery and alter intracellular trafficking is

under study, but new evidence suggests that this might be due to competitive binding and hydrophilic/hydrophobic interactions.

When polyplexes are formed, the formulation conditions of combining the polymer, dendrimer, or micelle with the polynucleotide can vary greatly depending on the type and structure of the material, nucleic acid, cell, and/or if in vitro or in vivo conditions are being examined. Thus, the field of nucleic acid delivery typically utilizes some conventions in describing the formation of polyplexes and ratios of macromolecules utilized. Polyplexes are usually formed in aqueous conditions by pipetting a solution of the studied polymer or dendrimer into a solution of the polynucleotide of study and allowing the solution to "incubate" or sit for a certain length of time to allow electrostatic binding, complexation, and formation of the nanoparticles. As previously mentioned, most typically, the vehicle is a polycation and the positive charges reside on the nitrogen (N) containing groups along the backbone and the negative charges on the polynucleotide reside on the phosphodiester (P) groups. Thus, when considering the formation of polyplexes, a molar ratio of the nitrogens to phosphates (typically termed N/P ratio) is used to denote the formulation of the nanoparticle complexes. Typically, this is calculated by determining the molar ratio of the nitrogens (able to be protonated) in the polymer repeat unit divided by the ratio of each nucleotide base. If a "hard charge" is present on the polymer, for example a quaternary ammonium group or imine, the charge ratio of total positive charges on the polymer to total negative charges from the nucleic acid present within the colloidal complex mixture are reported. It should be noted that if a "charge ratio" is used for the calculation with groups such as primary, secondary, or tertiary amine, the charged state of the amines can change dramatically in the physiological pH range from about 4.5 – 7, and this notation is likely not accurate for these variable-charged polymer. This is not true for polycations whose

charge centers remain positively-charged throughout this pH range (that is, pKa > ~8.5) such as quaternary ammonium, amidine, or guanidinium groups.

Most typically for in vitro nucleic acid delivery (also called "transfection"), a positive N/P or molar ratio is used; this corresponds to not only charge neutralization of the polynucleotide backbone but an over charging of the polyplexes with a positive charge. Polyplexes are typically formulated to have a size within the 20-500 nm range in water, and exhibit characteristic colloidal behavior. The overall positive charge on the complexes facilitates colloidal stability of the polyplexes from aggregation in water due to electrostatic repulsion. The concentrations, solvents, additives, and other factors can dramatically influence the size and morphology. Once a solution containing colloidal complexes stabilized by their cationic charge is subjected to media containing a high concentration of salts, nucleotides, amino acids, carbohydrates, serum and other nutrients, the morphology, size and colloidal stability can change. For nucleic acid delivery to cultured cells, the size, morphology, and aggregation characteristics of polyplexes are not typically optimized as many studies have found that a variety of nanoparticle sizes and shapes can be internalized by cultured cells.[15] In fact, some studies have shown that polyplex aggregation and precipitation can actually improve delivery in cultured cells.[16] However, for in vivo delivery, polyplex size and shape must be optimized for each clinical goal and aggregation must be avoided.[17] Careful characterization of polyplexes and their behavior in culture media and blood is needed and many tools are being used to study their behavior, which is discussed extensively in section 1.03 of this review. Colloidal stability of polyplexes represents one of the major challenges for pharmaceutical development and this issue is discussed in this review in sections 1.05 and 1.06. As briefly mentioned above, electrostatics are not necessary to fully drive the complexation,[11,12] particularly if the polymer vehicle does not contain cationic groups, such as the case of the polyoxomers.[14] Also, it should be noted that some synthetic forms

of nucleic acids are also being developed that do not have a polyanionic backbone, such as peptide nucleic acids and morpholinos, and these structures tend to be more stable from nucleases and a review of this area is beyond the scope of this article.[18,19]

1.02.2 Examples of Cationic Polymeric Vehicles

The field of polymer-based nucleic acid delivery continues to grow at a very rapid pace and many novel and interesting structures continue to be published. In general, the polymer vehicle should be benign within biological systems; if the material is highly toxic, this can cause unwanted side effects. If the polymer is toxic, high cell death, apoptosis (programmed cell death), and cell necrosis are inevitable and significantly limit the applicability of the material as a research tool and for clinical use. In addition to effective delivery, a major difficulty in this field has been overcoming the toxicity issue of synthetic materials. Unfortunately, some delivery vehicles that promote high cellular internalization tend to cause cellular damage and death.[20,21] Many of the systems published have not thoroughly studied and compared polymers (both toxicity and delivery efficacy), based on their chemical structure, in order to predict the biological profiles and behavior of them. This is challenging because research is being focused on modifying existing structures with groups such as polyethyleneglycol (PEG), carbohydrates, peptides, and other biocompaticle molecules to lower the toxicity and some examples of these studies are discussed in detail in section 1.04 of this chapter.

Indeed, polymer structure plays a very large role in the delivery efficiency, efficacy of polynucleotide biological activity, and toxicity. For example, when considering a polymer vehicle, different counterions,[22,23] linear versus branched,[24,25] block versus statistical,[26,27] and/or short versus long[28-31] analogs of the same chemical

structure can yield very different results. While many unique and creative systems continue to be published, a full review of all the systems that have been synthesized and studies for this purpose is beyond the scope of this review. Here, we introduce a few major classes of materials that are making an impact in the field of polymer/dendrimer/micellular-based nucleic acid delivery (Figure 2): a) polyethylenimine (PEI), b) amino acids, c) dendrimers, d) chitosan, e) β-cyclodextrin polymers, f) polyglycoamidoamines (PGAAs), g) poly(β-aminoesters), and h) *N,N*-dimethylaminoethyl methacrylate (DMAEMA).

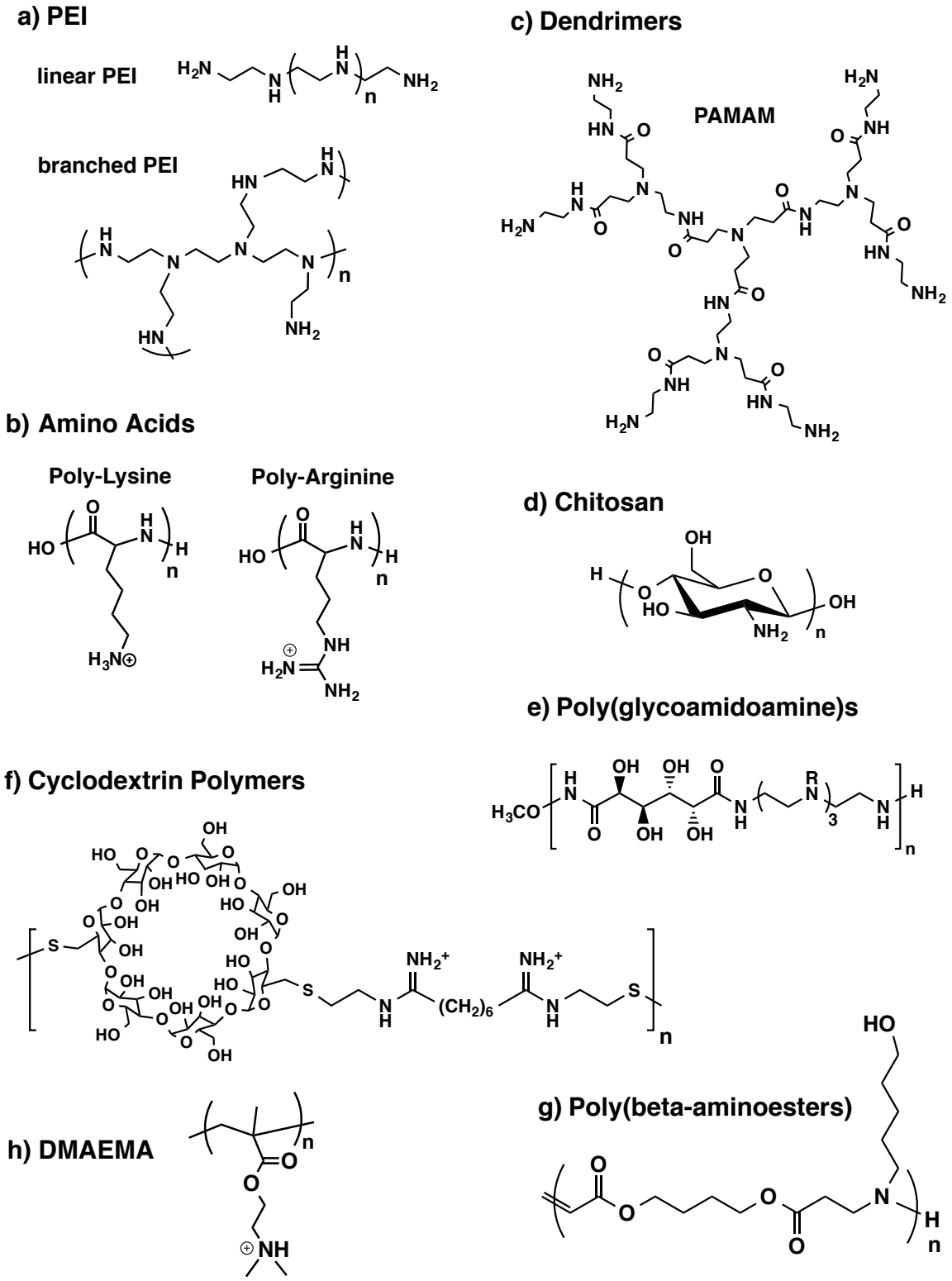

Figure 2: Structures of the polymeric nucleic acid delivery vehicles reviewed herein.

When polyplex formulations are prepared with these cationic materials, the "overall" molar ratio, charge ratio, or N/P ratios are reported and almost always biological testing of polyplex formulations are done at a variety of ratios. However, it should be noted that the overall ratio of formulation may not be representative of the "actual" ratio of the nanoparticle complexes within that formulation.[32] Once a charge ratio threshold is crossed (this is likely structure-dependent), additional positive charge (polymers) no longer contribute to the charge ratio of the complexes themselves, thus, excess polycation molecules remain free in solution and the uncomplexed molecules could contribute to an increase in transfection efficiency and toxicity profiles. For example, Fahrmeir et al. have developed an electrophoresis method to purify excess linear PEI (both PEGylated and unmodified) from the polyplex solutions.[33] After removal of the excess polymer, the final PEI polyplexes (unmodified and PEGylated) had a final N/P ratio of about 2.4-2.6, and about 60% of the total amount of PEI used to formulate polyplexes at an N/P ratio of 6 was found to be in excess. Removal of the excess polymer resulted in a marked decrease in toxicity, particularly in vivo.[33] However, there is also evidence that excess polymer can facilitate in significantly more efficient cellular uptake of polyplexes in vitro, and that excess PEI chains contribute to the subsequent intracellular trafficking.[34] Thus, the importance to test a wide range of N/P ratios is needed to understand how the amount may differ from in vitro and in vivo assays.

1.03 Polyplex Characterization

1.03.1 Physicochemical Characterization Methods of Polyplexes

The physicochemical characterization of nucleic acid complexes with polymers and dendrimers is very important to understanding the binding affinity, complex stability, size, shape, and colloidal behavior in physiological conditions. In studying polyplex formation, there are many analytical methods that are typically used to study polyplex/dendriplex/micelleplex formation and have been reviewed very nicely by Shcharbin et al.[35] The standard "essential set" of tools consists of the following three categories: a) analysis of charge/molar ratio (gel electrophoresis/dye-exclusion assay/zeta potential), b) analysis of hydrodynamic diameter of complexes in solution (DLS), and c) analysis of size and shape of the complexes in dried/frozen state (TEM/SEM/AFM).

To conceptualize the amount of polymer needed to neutralize the nucleic acid's charge, a conventional agarose gel electrophoresis shift assay is typically used. When electrophoresed, uncomplexed nucleic acid migrates quickly through the gel toward the anode, but when complexed, the nucleic acids migrate much slower or remain in the well and are unable to migrate (because they reside in a larger complex that is charge neutral and cannot travel through the agarose gel). Consequently, gel electrophoresis allows a comparison of formulations prepared at various charge or N/P ratios and enables calculation of the minimum ratio required to neutralize and complex ~100% of the nucleic acid (Figure 3a).[36,37] An extension of the gel electrophoresis assay involves prior incubation of a formulation in a medium to simulate the conditions encountered during delivery (often containing a nuclease or nuclease-containing serum). After the incubation event, the nucleic acid is subsequently released by addition of a displacing agent, such as heparin sulfate or sodium dodecyl sulfate (SDS). The intensity of the intact "liberated"

nucleic acid, when compared to that from a control sample in which the same formulation not exposed to nucleases, sheds light on the ability of the polyplex formulation to protect the nucleic acid from degradation.[32,38]

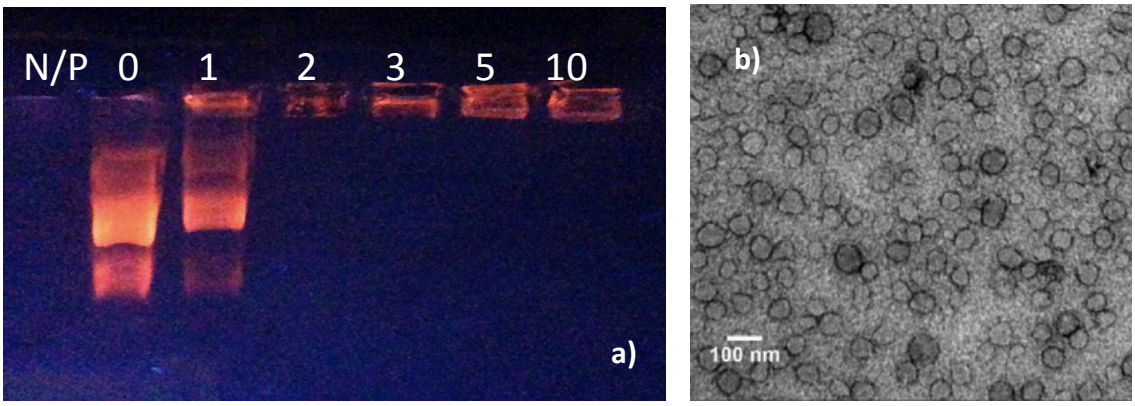

Figure 3 Examples of polyplex characterization via gel electrophoresis and transmission electron microscopy. a) Gel electrophoresis shift assay of a polymer bound to pDNA at the N/P ratios indicated. N/P = 0 indicated pDNA only, which migrates with the electrophoretic field. At N/P = 2 the polymer binds pDNA and prevents migration with the electrophoretic field. Figure generated by the author. b) Transmission electron micrograph (TEM) of polyplexes. Figure adapted from [39].

Assays using intercalating dyes (i.e. ethidium bromide, PicoGreen®, and RiboGreen®) can also be used to indirectly measure the polymer-polynucleotide binding affinity. Intercalating dyes exhibit an increase in fluorescence intensity upon interaction with double-stranded nucleic acid, but their fluorescence is rapidly quenched when the dye is displaced. The formulation of polyplexes can alter the intercalation degree in an observable manner and is related in part to the polymer-nucleic acid binding affinity.[40] However, it should be noted that this assay is not a direct measure of binding affinity as other factors such as electrostatics, changes in DNA/RNA secondary structure, H-

bonding etc. can alter the degree of intercalation.[11,12] Also, this technique is not sensitive to detect subtle changes in the binding affinity and other more quantitative methods such as isothermal titration calorimetry which offers more accurate binding constants.[11,12]

Zeta potential is frequently used to measure the charge of polyplexes at the shear plane. The zeta potential is the electric potential that exists at the electrical double layer of ions and counterions that surrounds a particle. There are several ways to measure zeta potential, which include electrokinetic, electrophoresis (electrophoretic light scattering), electroacoustics (acoustic impedance and sound attenuation), and electrostatic (streaming potential). Whichever measurement technique is used, it is imperative that the environment of the nanoparticles is known. The pH, ionic strength, and concentration of the solution can have a large effect on the zeta potential and these parameters should be mentioned along with the zeta potential measurement. In general, an approximate threshold value of 20 mV (positive or negative) separates minimally-charged (-20 to +20 mV) from highly-charged (<-20 or >+20 mV) complexes. The implications of colloidal complex surface charge play a large role in their aggregation behavior in physiological salt and serum conditions. Surface modification of polyplexes with neutral components, such as poly(ethylene glycol) (PEG), not only act to shield the surface charge and reduce zeta potential but increase steric stabilization, which has been shown to provide an increase in plasma circulation time in vivo.[41,42] That being said, PEGylation has also been shown to decrease overall transfection efficiency, and for this reason, stimuli-responsive systems are being developed to cleave off the PEG groups after cellular uptake.[41]

Dynamic light scattering is a technique used in conjunction with zeta potential measurements to analyze polyplex size (average hydrodynamic diameter) distribution. Because the formation of polyplexes can result in a polydisperse mixture of nanoparticle sizes and shapes (including uncomplexed components), multiple peaks can result. Thus, typical reported data include average hydrodynamic diameter and polydispersity. Most

software associated with DLS instrumentation permits assessment of a multimodal size distribution,[43] but such data are often unreported or underreported. The default assumption of a single, Gaussian distribution may not be appropriate for the majority of polymer-nucleic acid complex formulations that are analyzed by DLS. Most models and instrumentation software assume the particles to be a uniform sphere, which again, is not necessarily accurate since polyplexes are often observed in rod and toroid-like morphologies.[5,40] Also, polyplex formulations are sometimes passed through a filter (e.g., a 0.2 μm or 0.45 μm syringe filter) prior to DLS assessment. However, this practice can reduce/eliminate unwanted signal from large particles, but such filtration necessarily leads to DLS data that are not representative of the entire as-formulated complex mixture. Unless an identical filtration procedure is to be followed for all in vitro and in vivo efficacy and safety assessments of the formulation, use of filtration solely for DLS measurement is not warranted. In this field, there is a need for an assessment of the various instruments and data processing approaches, including the assumptions and uncertainties involved in each, as well as the establishment of a "standard protocol" that can be followed to ease comparison of data among different researchers, materials, and instruments. As such assessment and protocols have been developed for TiO_2 nanoparticles.[44] Multi-angle laser light scattering has also been used to understand and calculate the number of macromolecules in a nanoparticle (number of polymers and number of nucleic acids) within a polyplex.[31,45] For example, Bartlett and Davis have calculated that their average polyplex structure is made up of about 9750 β-cyclodextrin polymer chains and 2110 siRNA (21 base pairs) molecules (degree of polymerization of 5).[31]

For the direct visualization of the size and shape of the colloidal complexes in the frozen, vitrified, or dried state, transmission electron microscopy (TEM), scanning electron microscopy (SEM), and atomic force microscopy (AFM) are used. To achieve

proper visual image contrast with TEM and SEM, the nanoparticles must be coated or negatively stained and uranyl acetate tends to be very common. TEM is also a tool to look at polyplexes within cells in high resolution and assess their cellular internalization and intracellular trafficking (see Figure 3b). Mishra et al. have performed studies with TEM to monitor the intracellular trafficking of unmodified polyplexes formed with pDNA and branched PEI (25 kDa) and linear β-cyclodextrin polymers and compared these date with their PEGylated variants.[16] They have found that unmodified polyplexes enter cells as large aggregates, are localized to the perinuclear region, which leads to high gene expression; however, these aggregates are not relevant for in vivo use. PEGylated variants remain as discrete 100 nm entities even during internalization. While PEGylation sometimes leads to a decrease transgene expression, these conditions are favorable for in vivo use. Cryo-TEM is arguably more accurate for particle visualization than TEM; it does not require sample drying as the samples are vitrified in solution for examination.[43] However, lower availability of this instrument type and difficulties in sample preparation deem this technique less popular over all for polyplex study. To this end, due to the wide availability and abilities for in situ polyplex study, AFM is becoming a more popular technique for polyplex morphology characterization. Unlike the previously mentioned techniques, AFM facilitates three dimensional characterization of polyplex size and shape.[32]

Many other characterization techniques have also been employed to enhance the knowledge in the formation and make up of polyplexes. For example the use of polyanions such as heparin can also be used as competitors to dissociate the polyplexes (concentration of competitor needed to dissociate polyplex is related to polyplex stability) and polyplex dissociation is monitored via agarose gel electrophoresis.[30,38,46] Along with the other methods (i.e., intercalating dye assays), these measures of "binding strength" are indirect and do not show subtle differences in the binding affinity nor offer accurate

binding constants. To this end, isothermal titration calorimetry (ITC), a more analytical measure of binding affinity, became popular as a technique to assess polyplex formation. Use of ITC as a tool to characterize polymer/nucleic acid binding allows for the thermodynamic parameters to be directly obtained and subtle binding differences (between similar chemical structures) to be delineated.[11,12,47] For example, Prevette et al. have found that by altering the stereochemistry of the hydroxyl units along the backbone of poly(glycoamidoamine)s can lead to orders of magnitude difference in the polymer-pDNA binding constants and that both electrostatics and hydrogen bonding contribute to the overall mode of binding.[11] These subtle differences and effects are not observed with indirect methods of studying binding, but can be through more quantitative methods.

1.03.2 Transfection and Toxicity Characterization of Polyplexes In Vitro

For the preliminary in vitro biological screening of polyplex delivery efficiency and toxicity, several standard assays are used for performance comparison, 1) analysis of cellular uptake via flow cytometry and/or fluorescent microscopy, 2) analysis of cellular transfection efficiency by monitoring the expression of a reporter gene such as luciferase, β-galactosidase, or green fluorescent protein (GFP) (or for siRNA gene knockdown), and 3) toxicity analysis by several methods such as total protein, dye exclusion, MTT, and enzyme leakage assays.[48] Depending on the disease of interest, these standard assays are done in a large variety of cell lines, most typically, human embryonic kidney cells (HEK293), SV40 transformed monkey kidney fibroblasts (COS-7), human breast cancer (MCF-7), human primary glioblastoma cells (U87), and human cervical carcinoma cells (HeLa) are used for preliminary studies.

Polyplex uptake is typically assessed by transfecting cells with polyplexes formed with nucleic acids labeled with a fluorescent tag (such as Cy5, rhodamine, fluorescein, and the alexa fluor classes of dyes).[5,48,49] In some cases, the polymer or dendrimer can also be labeled with a fluorophore and cellular internalization is monitored of both the polymer and the nucleic acid. The assessment is then typically made by one or more of the following techniques: measurement of the cell lysate fluorescence, fluorescence microscopy (wide field or confocal miscroscopy) of the cells after polyplex exposure, and measurement of the cell population fluorescence (both the number of positive cells and intensity) by flow cytometry. When using these techniques for analysis of polyplex cellular uptake, care must be taken to avoid potential key issues. For example, it is important to properly remove polyplexes that are associated to the cell membrane (but not internalized) by washing or treating the cultured cells with heparin or commercially available treatments such as CellScrub™ (Genlantis) prior to analysis. It should be mentioned that the effect of adding fluorophores to the polymer or pDNA on polyplex uptake and intracellular trafficking is not currently known. For this reason, radio-labeling the systems can be performed; however, this technique requires special facilities. Finally, as with all in vitro assessments of polyplexes in adherent cultured cells, one should be cognizant that this system may not be a good estimate of in vivo performance, particularly for polyplexes administered systemically and/or for polyplexes targeting circulating (non-adherent) cells (discussed in sections 1.05 and 1.06).

Transfection efficiency is monitored to determine the delivery efficiency of the polymeric vehicle. The nature of the assessment of transfection efficiency depends on the type of nucleic acid being delivered. For the delivery of pDNA, the assessment is made by measurement of transgene expression of a reporter gene. As mentioned, reporter genes, such as luciferase, β-galactosidase, or GFP, are observed and efficiency is based on the number of cells positive and fluorescence/color intensity (Figure 4).[36,50] The data

are standardized to results from the positive (pDNA delivered by a commercial transfection reagent) and negative controls (untransfected cells and cells transfected with pDNA only and polyplexes formed with non-coding pDNA). For the delivery of oligonucleotides or small interfering RNA (siRNA), performance is measured by the amount of protein knocked down from the basil expression profile, i.e. the reduction of the target gene expression level[51,52] (usually measured as mean fluorescence intensity). However, the assessment of efficacy (target gene knockdown) can be and is often made at the mRNA level in addition to (or instead of) the protein level. Quantitative reverse-transcription PCR (qRT-PCR) is frequently used to quantify target gene transcript levels relative to an endogenous "housekeeping" control, such as GAPDH or β-actin.[53,54] This approach, nonetheless, only allows determination of relative levels of target gene transcript among various samples. If a pDNA encoding the target gene is available, it can be used to establish a standard curve that permits determination of absolute target gene transcript levels. It is important to take into account the cell viability when observing siRNA knockdown as this may lead to false-positive results. To avoid this, negative controls should contain scrambled RNA sequences and polymer only samples, while positive controls are usually commercially available reagents such as Lipofectamine®, HiPerFect, or DharmaFECT.

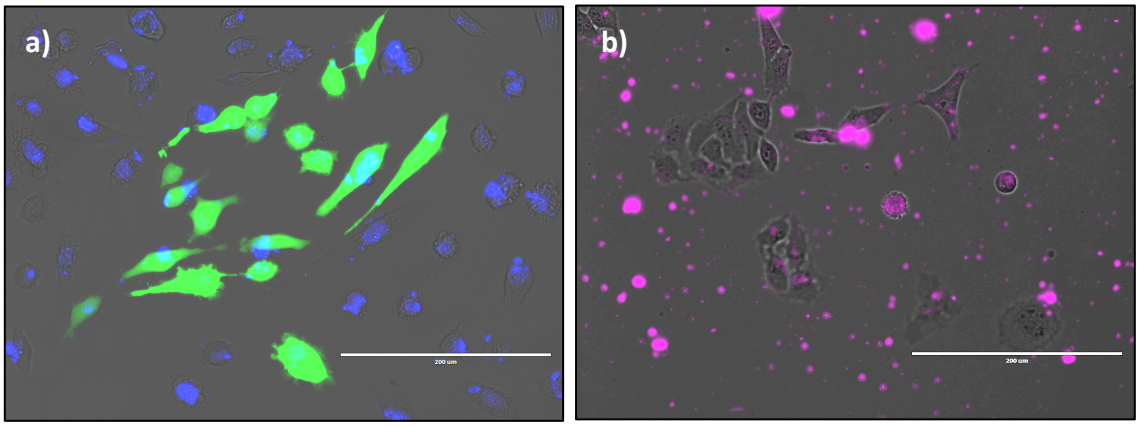

Figure 4: a) HeLa cells imaged with Cy-5 labeled polyplexes (purple overlay) four hours post transfection. b) 48 hours post transfection HeLa cells transfected with polyplexes formed with pDNA encoding for green fluorescent protein (GFP). Nuclei are stained blue with dapi. Figures generated by the author.

For the assessment of cytotoxicity of a polymer-nucleic acid formulation in vitro, there are several commonly used techniques: total protein assay, dye exclusion, MTT assay, and membrane leakage of enzymes such as lactate dehydrogenase (LDH) or adenylate kinase (AK) assays. Assessment of total protein content is made with the assumption that, for an experiment involving adherent cultured cells, any protein within the remaining cells will be released into the culture medium upon lysis of the cell membrane. The total protein concentration in the cell lysate solution is measured spectrophotometrically, such as via BioRad's DC Protein Assay.[8] This conventional assay is also used to normalize transgene expression data by total protein content, particularly when reporting luciferase gene expression. While this normalization can be useful, it can also be misleading as highly toxic formulations may yield extremely high apparent transfection efficiency (as a result of division by a small total protein value). An alternative test of cytotoxicity involves detachment of adherent cultured cells (or

collection of suspended cultured cells by centrifugation) and resuspension in a buffer containing a dye,[55] such as trypan blue or propidium iodide. The intact cell membrane of healthy cells prevents the dyes from entering the cell, while the compromised cell membrane of apoptotic cells allows dye entry. Consequently, when such a cell suspension is visualized using a hemacytometer (for trypan blue) or flow cytometer (for fluorescent propidium iodide), counts of viable vs. non-viable cells can be rapidly and accurately made. Another assessment of cytotoxicity involves the addition of MTT ((3-(4,5-dimethylthiazol-2-yl)-2,5-diphenyltetrazolium bromide), a yellow compound which is reduced to formazan, a purple compound, in living cells. The MTT assay is typically performed using a multiwell plate format, and a solubilization solution (often DMSO or SDS in dilute HCl) is used to dissolve the otherwise-insoluble formazan. The intensity of the resulting purple solution is measured spectrophotometrically.[56] Like the MTT assay, the LDH assay takes advantage of the difference in cell membrane integrity between viable and non-viable cells. For the LDH assay, the analyte, lactate dehydrogenase (LDH), is normally sequestered inside viable cells but is released in the cell culture medium, where it can be measured, by non-viable cells.[57,58] A similar assay monitoring AK has also been used as a variant by Reineke et al.; the advantage of monitoring AK is that this protein is smaller and allows the detection of smaller imperfections in the cellular membrane as a potential cause of cytotoxicity.[59] Most toxicity assays tend to be destructive to the cells; however, a recent product by Dojindo quantifies viable cell number, proliferation, and cytotoxicity. Similar to the MTT assay, the Cell Counting Kit-8 (CCK-8) assay allows colorimetric assays with a highly water-soluble tetrazolium salt. The yellow salt (WST-8) is reduced by dehydrogenase activities in cells to an orannge formazan dye, which is soluble in the tissue culture media. The amount of formazan dye reduced is proportional to the number of living cells.[60,61]

Another alternative for determining cytotoxicity in adherent cultured cells involves the use of real time-cell electronic sensing (RT-CES) equipment. Cells are plated into special multi-well plates through which a current is passed at defined time intervals. The impedance of that current is correlated to the density of adherent cells in the well through calculation of a "cell index" that is measured over the duration of the experiment. The greatest advantage of the RT-CES assay is that cell assessment can occur continually over the entire course of the experiment. For example, the cells need not be removed from the flask or tissue culture plate to be assessed. This advantage is countered by the heightened cost of the RT-CES plates and related equipment vs. that required for the aforementioned methods.[52,62]

1.04 Polymer Composition and the Structure Relationship to DNA Binding and Delivery from In Vitro and In Vivo Studies

As described in the previous sections, many characterization tools are utilized to examine the formation of polymer-polynucleotide complexes, their colloidal behavior and morphology, and their transfection and toxicity profiles in a wide array of cell types. Numerous fundamental studies of these characteristics, on an increasingly large amount of diverse and creative structures, continue to be published and unfortunately cannot be reviewed in full here. In the following section, we discuss a number of materials that have been thoroughly studied in vitro and discuss their structure-activity relationships. As shown previously in Figure 2, we have selected eight general classes of synthetic polynucleotide delivery vehicles to review in this section and discuss the general impact of their structure on the biological properties in vitro: a) polyethylenimine (PEI), b) amino acids, c) dendrimers, d) chitosan, e) β-cyclodextrin polymers, f) poly(glycoamidoamine)s (PGAAs), g) poly(β-amino ester)s, and h) Poly(N,N-dimethaminoethyl methacrylate) (DMAEMA).

1.04.1 Polyethylenimine (PEI)

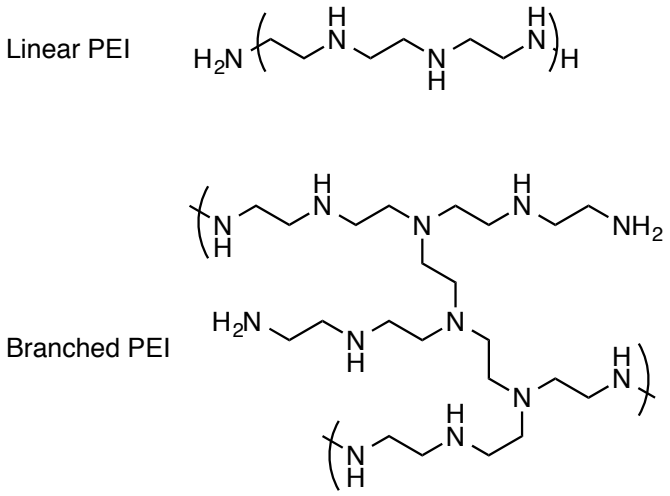

Figure 5. General Structures of linear and branched Polyethylenimine.

Polyethyleneimine (PEI) is one of the most widely studied polymeric delivery vehicles for polynucleotides. PEI is commercially available, and as shown in Figure 5 and Figure 2a, it is commonly sold as a linear polymer (L-PEI or Jet-PEI^{TM}), branched (B-PEI), and as different molecular weights of these motifs. The structure of this vehicle consists of its repeating ethyleneamine groups and high charge density, as ever third atom along the backbone is an amine group that can potentially house a positive charge. Due to the generally high delivery efficiency, several morphologies (branched versus linear and different molecular weights) of the unmodified structure along with numerous modifications of the PEI backbone have been made and heavily examined in vitro. In particular, it is accepted that PEI does present some toxicity to cultured cells, but this has been shown to be highly dependent on cell type and molecular weight. However, structural modification by various means (i.e., PEGylation, acetylation, carbohydrate substitution) has been successful at decreasing toxicity associated with this material and some examples are discussed below.

One of the first examples of using PEI as a transfection vehicle was published in 1995 by Behr and coworkers.[63] This study presented the high efficiency of B-PEI (800 kDa was used for most of the studies) for transfection in a number of common cell lines (3T3, COS7, HepG2, K562, HeLa, MRC-5) and primary cells (rat brain endothelium and chick embryonic neurons). They also showed that the efficiency of this polymer was comparable or higher to a common lipopolyamine (Transfectam^{TM}) and orders of magnitude higher than poly-L-lysine. In addition, this study revealed that B-PEI was able to transfer oligonucleotides into the nucleus of postmitotic neurons, a cell type normally very difficult to transfect. In a related study, Godbey and coworkers have shown that molecular weight (600, 1200, 1800, 10,000, and 70,000 Da) of B-PEI significantly affects the efficiency of this delivery vehicle in human endothelial cells.[28] At low molecular weights (600-1800 Da), B-PEI does not promote transfection nor expression of a GFP reporter gene (pEGFP-N1). However, the higher molecular weights promoted transfection, where the 70 kDa B-PEI sample yielded gene expression in around 15-30% of the cells and the 10 kDa sample yielded expression in an average of 10% of cells. It should be noted here that Godbey and coworkers reported the gel filtration chromatography results of the B-PEI samples used in this study and the high molecular weight versions were both quite polydisperse (Đ) (70 kDa B-PEI: M_w = 216,000 Da, M_n = 17,000 Da, Đ = 12.93; 10kDa B-PEI: M_w = 7,600 Da, M_n = 5,600 Da, Đ = 1.36).[28] These uncertainties in molecular weights and high dispersity indices likely play a role in the observed toxicity, efficiency, and reproducibility of the data, and should be carefully analyzed when using commercially available polymers for delivery studies.

In the above studies, it was reported that B-PEI at the reported molecular weights did not cause significant toxic effects in the cell types studied, however, Kissel and coworkers have performed extensive studies on PEI and have shown that depending on the structural characteristics, this vehicle can have low or high toxic effects in vitro. For

example, they have found that as the molecular weight increases, in vitro toxicity increases.[64] By examining derivatives of B-PEI (1,616 kDa and 11.89 kDa) and found that the higher molecular weight analog showed significant toxic effects to the cells, and noticed that this polymer caused plasma membrane permeability (as seen by LDH leakage and microscopy assays).[64] In addition, when comparing the transfection efficiency in serum of these two molecular weight B-PEI versions, the 11.89 kDa version was not affected by serum. Collectively, these results show that molecular weight of B-PEI can affect the toxicity, transfection efficiency, and serum stability of B-PEI polyplexes. Generally, toxic effects are observed with B-PEI, particular at high molecule weights[65] but a lower molecular weight window appears to exist where transfection, lower toxicity, and serum stability can be observe with B-PEI between 5-25 kDa.[66] However, it should be noted that when very low molecular weights are studied (generally below 10 kDa), higher N/P ratios (20-70) are needed to observe decent gene expression.[64] The effects of N/P ratio, chain length, crosslinking, disulfide linkage, excess cationic polymer, and linear vs. branched PEI have profound outcomes on toxicity and transfection efficiency; these structure-relationships and outcomes have been studied in detail by Wu and co-workers.[34,67-72]

As PEI generally promotes very high nucleic acid delivery and is readily available, many different derivatives have been studied to improve the toxicity profile of this material. For example, a very common modifying agent to decrease toxicity and increase colloidal stability are derivatives of polyoxomers such as PEG. Kissel et al. and Kabanov et al. have published many studies to examine how polyethyleneoxide derivatives affect the complexation and delivery of nucleic acids. Kabanov et al. found that PEGylated PEI was still able to form polyplexes with ODN and pDNA and PEG generally increases the solubility of the complexes.[73] The same group later reported the complex stability in salt and serum and a transfection comparison of B-PEI (both 2 and

25 kDa versions) modified with either polyethylene oxide or Pluronic 123 (P123).[74] Modification of PEI with PEO generally causes a significant decrease in transfection efficiency,[74] likely due to decreasing polyplex interactions with the cell surface. P123-modified PEI, however, still retained high transfection efficiency as the pluronics appear to have the ability to interact with cellular membranes and the authors have attributed this to the surfactant-like qualities of these molecules. In a similar study, Kissel et al. all looked at a series of PEGylated 25kDa B-PEI derivatives (Figure 6).[75] In that study, it was found that the PEG grafting density and morphology significantly affects the toxicity profile of these systems. As shown by the data in Figure 6, the surface of the B-PEI should be mostly shielded by PEG to decrease toxicity (as determined by LDH leakage assay). The derivatives all appeared to have similar luciferase reporter gene expression values but one derivative [PEI(25k)-g-PEG(550)35] appeared to yield the highest expression efficiency. Also, when the surface of b-PEI is covered with PEG, it should be noted that a much higher N/P ratio (20 and 30) is needed to promote transfection.[75] In a later study, the same group has also looked at these PEGylation morphologies on siRNA delivery.[76] A slightly different trend was noted; it was found that as the surface grafting density was lowered (and individual PEG length increased), siRNA-mediated gene knockdown increased (the more PEG surface coverage on b-PEI, the lower siRNA efficacy). This effect was attributed to both the stability of the siRNA cargo from RNase degradation and the possible effect of longer PEG molecules facilitating cytoplasmic release of the siRNA. It is interesting to note that the nucleic acid type also plays a large role in the delivery efficiency. Double stranded DNA and siRNA have many similarities and differences that must be accounted for when delivering these therapeutics;[77] in particular, the site of delivery (different regions of the cell) is crucial for sustained protein expression or knockdown.

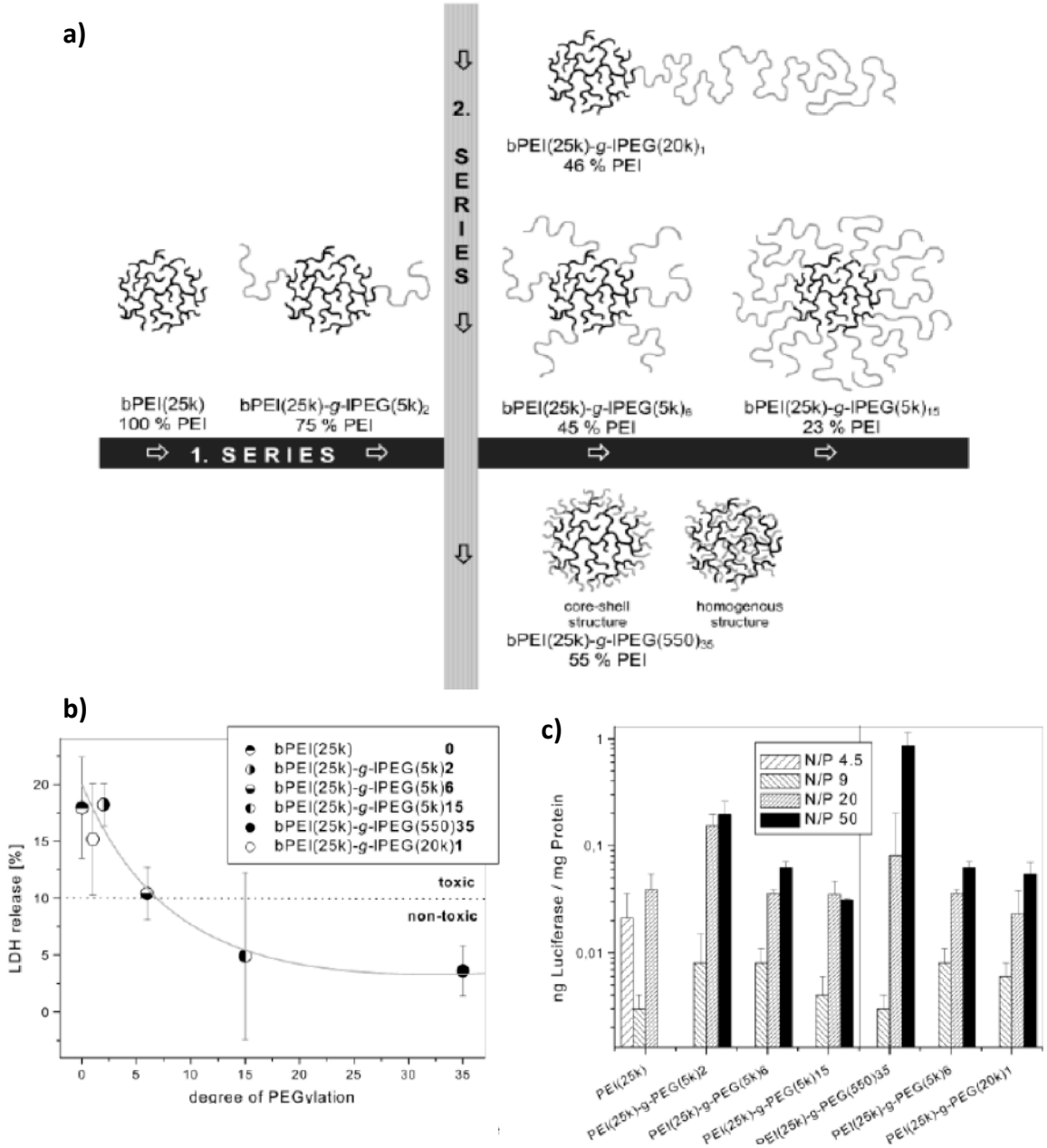

Figure 6: a) Branched PEI (bPEI 25 kDa, black) grafted in various ways with PEG (grey). b) Correlation of the degree of PEG grafting (average number of PEG blocks per one PEI molecule) with cytotoxicity of the polyplexes as determined via LDH release at N/P = 20. c) Transfection efficiency of the various polyplexes at different N/P ratios in NIH 3T3 cells. Figure adapted from [75].

Recently, Kim and coworkers have created related but opposite structures by functionalizing a novel multi-arm (6 arms) PEG star core macromolecule with linear PEI (25kDa) arms.[78] The L-PEI molecules are exposed on the surface of the PEO core structure and two motifs were created, where all six PEO arms were functionalized with L-PEI (MAPEG-$LPEI_6$) and where only about 3 PEO arms linked to L-PEI (MAPEG-$LPEI_3$). When comparing these novel motifs to L-PEI (25 kDa), the macromolecules formed more uniform polyplexes with lower zeta potential, and the transfection efficiency of the MAPEG-$LPEI_6$ derivative was similar in efficiency to L-PEI and higher in efficiency when compared to the MAPEG-$LPEI_3$. In particular, the transfection efficiency in serum was higher for the MAPEG-$LPEI_6$ derivative overall.

Many other PEI motifs continue to be created and examined for their structure-property relationships in vitro. For example, the PEI backbone has been modified with acetyl groups, galactose, and β-cyclodextrin. Pack et al. performed an interesting study by simply acetylating the backbone of B-PEI to understand the effect of lowering the buffering capacity and charge density of this polymer.[79] Three modified B-PEI versions were created by differing the degree of PEI acetylation from 15, 27, and 43 (PEI-Ac_{15}, PEI-Ac_{27}, PEI-Ac_{43}) respectively. All versions were found to bind pDNA and the subsequent polyplexes were slightly larger in size than that formed with unmodified PEI. Interestingly, by decreasing the buffering capacity with acetylation of the amines, transfection actually increased with the degree of acetylation (and unmodified PEI yielded the lowest transgene expression). The authors attributed this effect to a few possibilities: 1) the acetylated versions could have increased the polyplexes ability to dissociate from the pDNA, exposing it to transcription, 2) increasing the lipophilicity of the polymer could result in higher membrane permeation, and/or 3) possibly changing the mechanisms of intracellular trafficking. Davis and coworkers also created versions of L-PEI and B-PEI that were grafted with β-cyclodextrin and studied these systems in vitro

and in vivo.[80] With the branched PEI variant, it was found that as the degree of β-cyclodextrin grafting increased (5, 6, 7, 8, 10, 12, 16% of amines grafted with β-CD), both the in vitro transfection efficiency and toxicity decreased. Grafting percent of 5-8 resulted in only an order of magnitude decrease in luciferase activity, however, 10 percent grafting resulted in two orders of magnitude decrease and 12, and 16 percent resulted in almost no luciferase expression. It was also found that the IC_{50} parameters were proportional to the degree of grafting, at low grafting of 5 and 8% the IC_{50} values were 2 and 5-fold higher, and with even higher levels of grafting (12-16%) the IC_{50} values increased over 20-fold. For the β-cyclodextrin modified variants, 8% grafting of B-PEI and 12% grafting of L-PEI were found to be the best for plasmid delivery. The investigators also went onto further test polyplexes formed with these variants for salt stability and in vivo delivery. The β-cyclodextrin was then used as a noncovalent handle to include PEG conjugates to improve salt and serum stability and in turn blood circulation time. Kissel et al. examined substituting B-PEI with galactose groups as a means to improve targeted polyplex delivery to liver hepatocytes.[58] Galactose substitution of PEI yielded polymers with degrees of substitution ranging from 3.5, 9.7, and 31% of all PEI amino groups. Increasing the degree of substitution compromised DNA complexation, led to an increased complex size, and decreased the zeta potential. While increasing the degree of galactose substitution on PEI reduced the cytotoxicity. In HepG2 hepatocytes, the variant that gave the best gene expression had a galactose substitution degree of 3.5% and at N/P of 5 the expression was nearly the same as unsubstituted PEI. This is likely due to the fact that the higher substituted variants do not stably complex pDNA. In NIH 3T3 fibroblasts, a similar effect was seen, as the degree of substitution increased, luciferase expression decreased. However, the fact that high gene expression was noticed in ASGPR-negative cells suggests that this system is not yet

optimized for hepatocyte targeting. Many other studies continue to be performed with various forms of PEI to optimize this system for in vitro and in vivo delivery.

1.04.2 Amino Acids

In this section we will focus on two of the 21 proteinogenic α-amino acids found in eukaryotes, lysine and arginine, and the polymers thereof – poly-*L*-lysine (PLL) and polyarginine (PArg). Both these polymers have been studied in vitro and in vivo with promising results.

Poly-L-lysine (PLL) is a polypeptide vehicle that is also commonly utilized for the delivery of nucleic acids (Figure 2b). The advantages of utilizing polypeptide vehicles for delivery, particularly for clinical applications, lies in the fact that these polymers can be prepared via solid phase and automated synthetic procedures and thus samples of specific molecular weights (numbers of lysine units) and low dispersity can be readily prepared. One of the first reports of utilizing a PLL vehicle was published in 1987 by Wu and Wu where they developed the system as a soluble alternative to the calcium phosphate precipitation method commonly used to transfer pDNA into cultured cells.[81,82] In this study, they used a commercial source of PLL (69 kDa, Sigma) and coupled it directly to a galactose-terminated asialoglycoprotein, asialoorosomucoid (ASOR), to create the first targeted pDNA delivery vehicle to liver hepatocytes. In vitro transfection studies were completed by examining chloramphenicol acetyltransferase enzyme activity in both Hep G2 and SK-Hep1 cells. The presence of enzyme activity in Hep G2 cells and the lack of enzyme activity in SK-Hep1 cells revealed the ability of the ASOR-conjugated PLL system to specifically delivery pDNA to hepatocytes. A year later, the same group published an in vivo study with this same vehicle system that showed

specific polyplex uptake and gene expression in the liver with a lack of uptake in other organs.[82]

PEGylated versions of PLL have also been studied. Wolfert et al. have found that a block copolymer of PLL (9.6 kDa, Sigma) and PEG (10 kDa) was able to complex with pDNA, although this block copolymer yielded unusually shaped and disperse polyplexes as observed in AFM images (toroid and worm-like structures).[83] This effect has been further studied in detail by the same group[84] and also the group of Kataoka and coworkers[85] where the conjugation of PEG to PLL increased both polyplex solubility, decreased the size, and increased the stability from dissociation. Furthermore, Wolfert et al. examined the transfection of PLL and a PEGylated variant (PLL 9.6 kDa; and an A-B type block co-polymer of PEG-PLL, 10,000-10,000 Da) and the PEGylated systems surprisingly yielded about 125-fold higher gene expression in HEK293 cells when compared to unmodified PLL and this affect was not fully understood.[83]

In the above studies various molecular weights of PLL were used and thus comparing the data from different studies is difficult due to the known dependence of the biological properties on the polymer molecular weights. Thus, Kano et al. have studied molecular weights of PLL of 28 and 40 kDa and PEG molecular weights of 2, 5, and 10 kDa were examined in vivo for efficacy of siRNA delivery in metastatic lung tumors.[86] Interestingly, only the polyplex variants created with 40 kDa PLL grafted with 5 or 10 kDa PEG remained in the tumor tissue for 100 hours and this affect is likely related to the larger molecular weight. The system with 10 kDa PEG remained in circulation for longer periods of time and these structures also successfully protected siRNA from degradation in serum conditions.

Davis et al. have performed significant studies on PLL in vitro and in vivo. One study revealed that the length of PLL can affect polyplex size, delivery, and the duration of transgene expression both in vitro and in vivo.[87] PLL of 9.7 and 53.7 kDa were

conjugated to peptides that target the serpin enzyme complex receptor (for neuron, hepatocyte, and macrophage cells). Polyplexes formed with the longer PLL vehicles were generally smaller (around 25 nm for 53.7 kDa PLL and 39 nm for 9.7 kDa PLL) and the longer vehicles protected pDNA from nuclease degradation for a longer time duration. Transfections completed in HuH7 cells with these vehicle types also revealed that transgene expression was higher and of longer duration with the higher molecular weight PLL variants. The authors reported that luciferase expression was observed in this cell type for up to 40 days with the longer PLL chains.

The differences between PLL and polyarginine (PArg) in condensing and complexing with DNA was studied back in the early 70's,[88] but the use of PArg to transfect cells with nucleic acid in vitro was only exploited in the 90's.[89] Polyarginine, like PLL, is protonated in physiological conditions; this is a result of the basic guanidinium functional group on the peptide side chain (Figure 2b). While various lengths of PArg (5,000 -15,000 Da) have been studied, it appears that longer residues are not associated with increased transfection, in fact longer polymers and higher N/P ratios resulted in polyplexes being associated on the surface of the membrane; however, when shorter oligoarginines were used the transfection efficiency increases, meaning that polymer charge is not the driving force for polyplex membrane translocation.[90]

While PArg is quite capable of condensing and carrying nucleic acids (and derivatives which will be mention later) its use as a cationic delivery vehicle is limited. However, its application as a cell penetrating peptide (CPP) to permeabilize the membrane of cells and transfect large payloads makes this oligomer important to the field of cellular delivery. It was accidently discovered in 1988 that a protein named Tat (transactivator of HIV transcription) had an ability to translocate the cellular membrane.[91,92] More specifically the Tat peptide, being very basic and hydrophilic, contains six arginines and two lysines, and when conjugated to other exogenous proteins,

including β-galactosidase, their internalization into cells significantly increased.[93] In vivo delivery of this 120 kDa Tat-β-galactosidase chimaera was also investigated and β-galactosidase activity was detected in a number of different organs including the brain.[94]

Various analogs of polyarginine and oligoarginine have been synthesized and investigated. For example, Futaki compared polyarginine (5,000 -15,000 Da) to octoarginine and reported them to have the same transfection efficiency in COS-7 cells at an N/P ratio of 1.6. However, when octoarginine was N-terminal stearylated, it was found to give 100 times the amount of luciferase activity, comparable to that of their positive control – Lipofectamine.[90,95,96] Interestingly, when comparing the *L* and *D* enantiomers of the same oligoarginine lengths, the *D* configuration had higher cellular uptake after just 15 mins at room temperature, but when the *D* enantiomer was compared to polyguanidine peptoids, cellular uptake was comparable on most samples after just 4 minutes of transfection, but when the $(CH_2)_3$ linker in *D*-oligoarginines was doubled to $(CH_2)_6$ cellular uptake increased two fold.[97]

Remarkably, the cellular uptake of arginine containing polymers or arginine CPPs has little to do with its cationic behavior and has been reported to simultaneously use at least three endocytic pathways, but is not dependent on any endocytic or pinocytic events, and can occur without disruption of the cellular membrane.[98-100] The cytotoxicity of polyarginine is low even up to 50 μM (15% cell death), at which transduction is high (>95%); however, Stenzel et al. has recently made zwitterionic guanidine-based polymers with a methacrylate polymer backbone, and investigated the toxicity of zwitterionic vs. cationic arginine moieties and concluded that the cationic charge and positive zeta potential is the main cause of toxicity, and that is not the cationic charge interaction with the membrane, but the guanidinium groups alone that are responsible for high cellular uptake.[101] Adding to this, when arginine was methylated at the guanidinium group there

was an 80% decrease in transfection, and when dimethylated there was a 95% decrease.[102]

When directly comparing the same molecular weights (10 kDa) of PEI, PLL, and PArg coated silica nanoparticles for siRNA delivery and GFP knockdown in human brain, breast, and prostate cancer cell lines, cell viability and fluorescence quantification assays revealed that PArg-coated vectors are the most effective in promoting gene knockdown and are the least toxic. TEM images of transfected cells showed that PArg-coated nanoparticles entered cells through cell transcytosis, while PLL and PEI coated nanoparticles entered cells through endocytosis.[103]

Zhang has investigated a biodegradable amphiphilic triblock polymer comprised of PEG (2000 Da), PLA (3000 Da), and PArg (2300 Da) for the delivery of siRNA in vivo. Not only did previous in vitro cytotoxicity and hemolysis assays demonstrate that the triblock micelles had greater cell viability and haemocompatibility than that of PEI and oligoarginine, but they exhibited a 65% inhibition of EGFR expression in MCF-7 cells - comparable to that of Lipofectamine. When the siRNA micelleplexes were administered intravenously, tumor growth in nude mice was significantly inhibited. Owing to these micelleplexes stability and low cytotoxicity there was no positive activation of the innate immune system or body weight loss over the experimental period of 18 days.[104]

1.04.3 Dendrimers

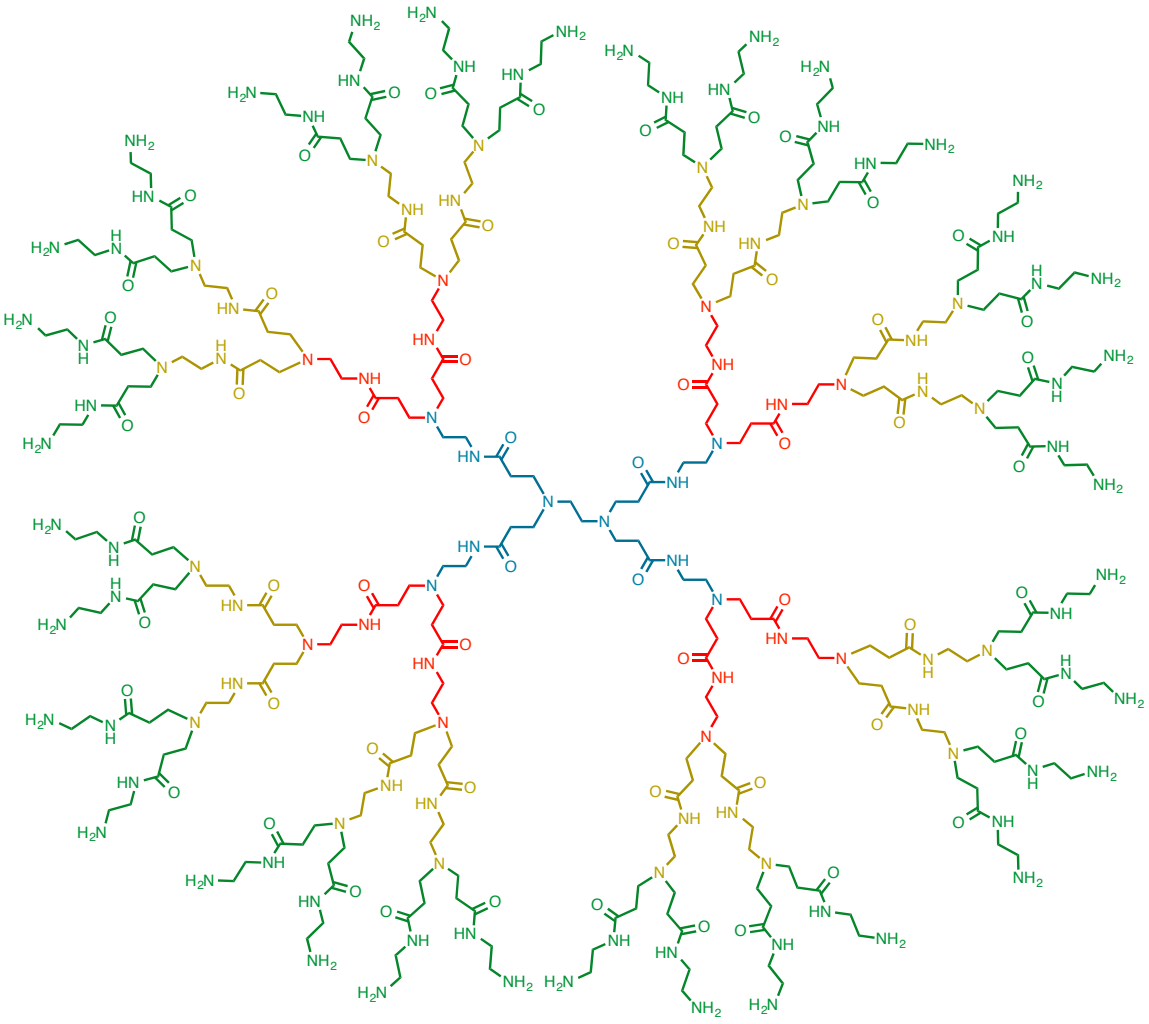

Figure 7. A third generation PAMAM dendrimer. The core (G0) is in blue, G1 is in red, G2 is in yellow, and G3 is in green.

Dendrimers have uniformly branched and symmetric architectures that have numerous end groups. For nucleic acid delivery purposes, dendrimers are a unique platform as they offer a multi-functional scaffold for potential chemical modifications with groups to improve colloidal stability or tissue specificity. As shown in Figure 2c and Figure 7, one of the most common dendrimer structures used for nucleic acid delivery is polyamidoamine (PAMAM) or Starburst dendrimer. Several core geometries (i.e. NH_3 or ethylenediamine) and multiple generations have been studied for nucleic acid delivery. The first examples of utilizing this structure for polynucleotide delivery was reported in 1993 by Haensler and Szoka, where they examined pDNA transfection efficiency in CV-1 cells with PAMAM dendrimers with an ammonia core from generations G2-G10.[105] They observed that luciferase reporter gene expression peaked at an N/P ratio of 6 and 10 with G6 dendrimer (10^{10} RLU/mg protein) and they reported the toxicity of this species to be lower than PLL in CV-1 and SD68 cells. In 1996, Tomalia and Baker also published a related study describing the transfection of a variety of PAMAM dendrimer structures.[106] They examined generations G3-G10 of two different types of dendrimers (based on NH_3 and ethylenediamine cores) and while all of these materials complexed pDNA, only G5-G10 were active for transfection. In a Rat2 cell line, as the generation increased, the transfection efficiency increased (paralleling with the increase in surface charge) with a plateau in gene expression occurring at G8. These dendrimers yielded a very large increase in transfection efficiency over that of DEAE-dextran, however, it was also reported that adding DEAE-dextran to the transfection media further increased the transfection efficiency of the PAMAM dendrimers. After these studies, Tang and Szoka published a follow up study that revealed that "fracturing" the dendrimer via heat treatment to produce a degraded and polydisperse macromolecule actually results in a greater than 50-fold increase in transfection efficiency.[107] In a related study, Szoka and Verkman compared the in vitro buffering capacity of second generation PAMAM

(coupled to pDNA) to polyplexes formed with PEI and PLL.[108] This study revealed data supporting the proton sponge hypothesis where both the polymers that contain titratable amines (PAMAM and PEI) in the physiological pH range increased Cl^- accumulation in endocytic vesicles and an increase in size of these vesicles was noted at 30-75 min post transfection. This was subsequently followed by an increase in transgene expression, but this was not noted with the PLL polyplexes. This study provided some evidence that incorporating titratable amines into the vehicle structure leads to cellular internalization through mechanisms leading to vesicle acidification and swelling. However, how the pDNA gets from the cytoplasm to the nucleus is still not clear.

Table 1. The calculated thearecical properties of amine surface functional PAMAM dendrimers by generation number. Information supplied by Dendritech Inc.

Generation	Molecular Weight (Da)	Measured Diameter (Å)	Surface Groups
0	517	15	4
1	1,430	22	8
2	3,256	29	16
3	6,909	36	32
4	14,215	45	64
5	28,826	54	128
6	58,048	67	256
7	116,493	81	512
8	233,383	97	1024
9	467,162	114	2048
10	934,720	135	4096

The impact of PAMAM dendrimer generation on cell growth and viability was examined by Prestidge et al. in HeLa and HEK293T cells.[7] As the concentration of the dendrimer (generations G2, G4, and G6) was increased (concentrations from 100 -1000

nM), cell growth diminished. Similarly, as the generation of the dendrimer increased the viability decreased. In both cell types, cell growth remained normal up to a concentration of 500 nM but at higher concentrations, cell growth was negatively impacted. While the complete mechanisms of toxicity are not yet clear, the cytotoxicity has been hypothesized to be, in part, attributed to the strong interaction these molecules have with the cell surface that can cause permeablization. While the proton sponge hypothesis states that materials able to buffer endosomes could lead to enhanced delivery (polyplexes avoid degradation in lysosomes and are released into the cytoplasm), it has also been hypothesized that lysosomal rupture could lead to cell signaling events that trigger apoptosis. Thomas et al. found that PAMAM dendrimers are internalized into cells in a manner that involve the lysosomal pathway,[109] while PAMAM/pDNA dendriplexes are predominantly taken up by caveolae-mediated endocytosis, and PAMAM dendriplexes coated with chondroitin sulfate are internalized via macropinocytosis.[110] However, additional studies suggest that cell internalization of this class of vehicles may be size dependent. Thomas et al. also has shown that as the buffering effect and lysosomal pH increases, cell death and apoptosis increased, and this was found to be directly proportional to the number of surface primary amines on the dendrimer. The mechanism appears to be through a mitochondria-mediated apoptosis event. Interestingly, by acetylating the surface of the dendrimer, toxic effects in the concentrations studies were abolished.[109]

A recent in vitro and in vivo study done by Imamura et al. found dendriplexes with PAMAM (G5) and pDNA to have high luciferase gene expression in the spleen of male ddY mice. Although these dendiplexes were toxic to B16-B10 cells (60% viability), when the cationic dendriplexes were additionally complexed to chondroitin sulfate (a sulfated glycosaminoglycan), resulting in a negatively (zeta potential) charged dendriplex complex, the toxicity diminished completely. And more interestingly, the negatively

charged complexes had equal or better gene expression profiles. The chondroitin sulfate dendriplexes also had less agglutination with erythrocytes, higher gene expression in the liver and spleen, and were not inhibited by amiloride (macropinocytosis inhibitor).[110] Overall, it appears that encapsulating the PAMAM dendriplexes with this cytoprotective chondroitin sulfate leads to stable, nontoxic, and efficient delivery vehicles that have potential for use in humans.

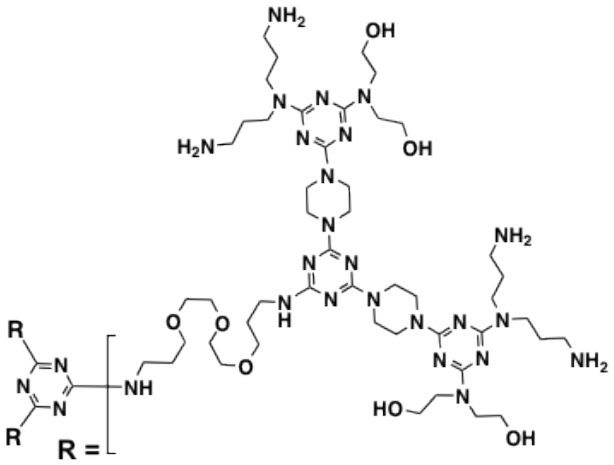

Figure 8: Structure of dendrimer F2-1 created by Simanek et al. [111].

While PAMAM dendrimer has been widely studied, other dendrimer forms are also being designed and developed for nucleic acid delivery. For example, Simanek and Kissel have pioneered the development of dendrimers based on melamine for the delivery of drugs and nucleic acids.[111] Simanek et al. have developed a number of triazine dendrimers that differ in generation (G1, G2, or G3), number of terminal amine groups (6, 12, or 24), and flexibility of the core (by adding an ethylene oxide functionality linking the triazine core to the branched arms). The group measured the cytoxicity of the differing structures and found it to range between 20-500 μg mL^{-1}) and the cytoxicity was

found to increase with the generation and the core structure also affected toxicity. The presence of a flexible PEG core did help to decrease toxicity of the higher generations. Transfection efficiency was examined on the family of 5 structures and compared to PEI and PAMAM. While the analogs without PEG yielded modest transfection efficiency, one particular analog with the PEG core (F2-1; Figure 8) yielded transfection efficiency higher than PEI and Superfect in L929 and MeWo cells.

1.04.4 Chitosan

Chitosan is a natural polysaccharide that has been widely explored for the delivery of nucleic acids. The compound is derived via the deacetylation of chitin yielding repeated glucosamine and N-acetyl glucosamine units bonded via β(1→4) glycosidic bonds (see Figure 2d).[4,112,113] Chitosan is widely studied because this biopolymer is commercially available, low in cost, biodegradable and contains functional groups (primary and secondary hydroxyls and primary amines) that can be readily modified via simple chemistry. The amino groups in chitosan also have a pK_a value of about 6.5, therefore offering a polycationic nature, which promotes association and polyplex formation with nucleic acids.[114,115] It has been found that the hydrolysis of chitin, however, is often heterogeneous in nature and can result in localized blocks of N-acetyl-2-amino-2-deoxyglucose units along the backbone of this biopolymer.[116] The influence of this heterogeneity on polyplex formation and nucleic acid delivery is not well studied, as it is difficult to characterize and reproduce. Commercially-available chitosan is typically reported to be around 80% deacetylated, however, methods to produce 100% deacetylated product have been published.[117] Dispersity in molecular weights is also widely found and can also significantly affect the bioactivity of this vehicle. The influence of these structural properties on the bioactivity has been extensively reviewed, and chitosan with an average molecular weight of 10 kDa containing a deacetylation degree ≤ 80% is typically suggested for nucleic acid delivery applications.[113]

The use of chitosan as a nucleic acid delivery vehicle was first reported by Mumper and coworkers in 1995.[118] Further studies on chitosan were published by the same group in 1998 examining the role of chitosan molecular weight (variants of 7, 32, 102, and 540 kDa) on polyplex formation and pDNA delivery efficiency in COS-1 cells.[4]

That study revealed that a decrease in molecular weight from 540 to 7 kDa caused a similar decrease in polyplex size, from about 500 nm to 100 nm. In the absence of serum, the chitosan variants having molecular weights of 230 and 102 kDa yielded the highest transgene expression; however, in serum-containing media, the 540 kDa chitosan vehicle yielded the highest gene expression. It is speculated that either large molecular weight variants help in protecting the nucleic acids from nuclease degradation and/or the larger polyplex size could facilitate precipitation onto adherent cells and promote internalization. Studies by Ishii et al. have found that large chitosan polyplex aggregates can absorb onto the cell surface and promote endocytosis.[119]

The deacetylation degree of chitosan has been found to play a critical role in the observed transfection efficiency, where typically values ranging from 65-80% are desired. To examine this parameter, Kiang et al.[120] have synthesized chitosan variants with different degrees of acetylation. Transfection studies in vitro with HEK293, HeLa and SW756 cells revealed that transgene expression is dependent on both the molecular weight and degree of acetylation. The chitosan variants having the largest fraction of primary amines (highest deacetylation degree) offered the highest transgene expression in vitro (more stable polyplexes in serum). However, in vivo, the results were not complementary. The differently acetylated versions were administered to mice via intramuscular injection and the high-deacetylation degree chitosan was found to be the least efficient. As previously mentioned, this study supports many others that have found significant differences in polyplex behavior between in vitro and in vivo experiments.[120] Huang et al.[29] revealed very similar results in vitro that showed highly deacetylated chitosans offer higher transfection in A549 cells because they protected pDNA from degradation. Correlation between zeta potential, cellular uptake, and transfection efficiency was shown and suggested that the high electrostatic interactions between the polyplex and the cell membrane mediate increased cellular uptake with highly

deacetylated chitosans.[29] Similar effects were observed when examining siRNA delivery to H1299 human lung carcinoma cells; polyplex stability and efficacy was generally higher for larger molecular weights and highly deacetylated chitosans.[121]

Most studies to date have proposed that cationic polymers need to have a high buffering capacity in the endosomal pH range (4~7) in order to mediate escape from the endosome by the proton sponge effect. In a study by Richard et al. the ionization behavior of chitosan and chitosan/DNA polyplexes was examined and compared to that of PEI and PLL on a molar basis, and it was discovered that chitosan has a higher buffering capacity than PEI, but the formation of chitosan/DNA polyplexes reduces chitosan's buffering capacity by 2 fold due to the negative electrostatic environment of nucleic acids. Their data suggest that chitosan may mediate endosomal escape partially through the proton sponge mechanism, but depends on the presence and amount of excess chitosan polymer.[122]

While chitosan has yielded promising biocompatibility, many different chemical modifications have been examined to improve the transfection efficiency. A common modification has been to graft PEI-like structures onto the backbone of chitosan in an attempt to increase the number of amines and thus the buffering capacity while maintaining low cytotoxicity. Kim et al. first examined this by physically formulating PEI (not chemically grafting) with chitosan and forming polyplexes with pDNA.[123] This formulation technique increased pDNA transfection efficiency (as compared to chitosan only) in HeLa, A549 and 293T cells. Wong and coworkers[124] chemically grafted low molecular weight PEI (M_n = 206 Da) to water-soluble chitosan (M_n = 3.4 kDa) via cationic polymerization of aziridine from the amine groups of chitosan. Chitosan-g-PEI/pDNA formed polyplexes (at a low N/P ratio of 2.5) reached a transfection efficiency similar to that of polyplexes formed with 25 kDa PEI (in serum-free media) at a high N/P ratio of 40 - in HeLa, HepG2, and primary hepatocytes. Howerver, the cell viability

studies, reported for chitosan-g-PEI and PEI polymers (not in polyplex form), showed that chitosan-g-PEI had a 7-fold higher LD_{50} than PEI.

More recently, chitosan (200 kDa, degree of acetylation ~90%) was functionalized with folic acid and 4-imidazolecarboxaldehyde and complexed with GFP encoding pDNA. These pH sensitive polymers had little to no toxicity in HeLa, HepG2, and CHO cells; however, the polyplexes were only slightly toxic (70% viability at 50 μg/mL with HepG2 and 90% viability at 50 μg/mL with CHO cells). The GFP expression of these chitosan-imidazol-folic acid polyplexes was higher than that of PEI, Lipofectamine, unmodified chitosan, and chitosan-imidazol polyplexes. Furthermore, they had higher ex vivo gene loading and release profiles in more acidic environments (pH 5 vs. 7), suggesting that these vehicles could deliver genetic cargo selectively to cancer cells, and can specifically target the folate receptor on tumor cells, facilitating cell uptake via the folate receptor -mediated pathway.[125]

1.04.5 Poly(glycoamidoamine)s

As previously discussed, PEI and chitosan have been very commonly studied materials for the delivery of nucleic acids in vitro and in vivo. While PEI has many examples of high delivery efficiency, depending on the structural characteristics, the cytotoxicity of this material has been a limiting factor in some instances. Chitosan, a highly biocompatible naturally-derived biomaterial, has also shown promise; however, in its unmodified state, this structure is typically disperse and has displayed moderate delivery efficiency, and these characteristics have prompted researchers to explore modification of the backbone with ethyleneamines and other structures to improve efficacy. In conjunction with these strategies, Reineke et al. have explored copolymerizing various carbohydrate structures with ethyleneamine monomers to create a series of polymers termed poly(glycoamidoamine)s (or PGAAs; Figure 2e). In 2004, the first example of this strategy was published where esterified glucose was polymerized with diethylenetriamine, triethylenetetramine, tetraethylenepentamine, and pentaethylenehexamine to derived polymers containing 1-4 secondary amines in the polymer repeat unit.[126] These new glycopolymers were found to bind and compact pDNA into polyplexes and successfully transfect BHK-21. The analog created by polymerizing esterified glucose with pentaethylenehexamine (termed D4) yielded high transgene expression comparable to PEI but with much lower cytotoxicity.

These initial promising results prompted the creation and study of a larger family of 16 analogous polymers with three other carbohydrate diastereomers in a series of papers published by Reineke et al. (Figure 9).[36,126,127] This family of structures were synthesized by copolymerizing dimethyl-*meso*-galactarate (G), D-mannaro-1,4:6,3-dilactone (M), or dimethyl-L-tartrate (T) in addition to esterified D-glucarate (D). These glyco-monomers were polymerized with the series of oligoethyleneamine comonomers

[diethylenetriamine (1), triethylenetetramine (2), tetraethylenepentamine (3), or pentaethylenehexamine (4)] via step-growth polymerization to generate a series of polymers (D1 – D4, G1 – G4, M1 – M4, T1 – T4) with degrees of polymerization (*n*) around 11–14 (Figure 9). From this follow up work, it was discovered that while all of the polymers were able to form polyplexes with pDNA, the carbohydrate type and ethyleneamine number were found to play a key role in the delivery efficiency (G4 generally was the most effective in a variety of cell types). The delivery efficiency was generally very similar to PEI but much higher than chitosan; however, the PGAAs revealed similar cell viability profiles to chitosan in a variety of mammalian cell types: BHK-21, HeLa, HepG2, and H9c2(2-1).[36,38,126] Studies in a cardiomyoblast (H9c2(2-1)) cell line showed high levels of transgene expression; this result was attributed to the high levels of polyplex cellular internalization in both serum-free and serum-containing media (nearly 100% of cells were positive for FITC-pDNA). Using a similar polymer synthesis strategy, the effect of increasing the number of secondary amines in the polymer backbone from four to five and six, as well as the effect of polymer branching on delivery efficacy and toxicity was also investigated.[24] In general, the linear and branched PGAAs yielded slightly larger polyplexes when compared to their analogs containing 4 secondary amines. However, polyplexes formed with the branched galactose and tartrate polymers and generally all of the linear polymer PGAA analogs containing five and six ethyleneamines did not significantly swell or aggregate in serum-containing media, suggesting the higher secondary amine number within these PGAAs could help to prevent serum-mediated aggregation. Increasing the amine number, however, did not generally enhance transfection efficiency but the increase in amines did increase cytotoxicity.

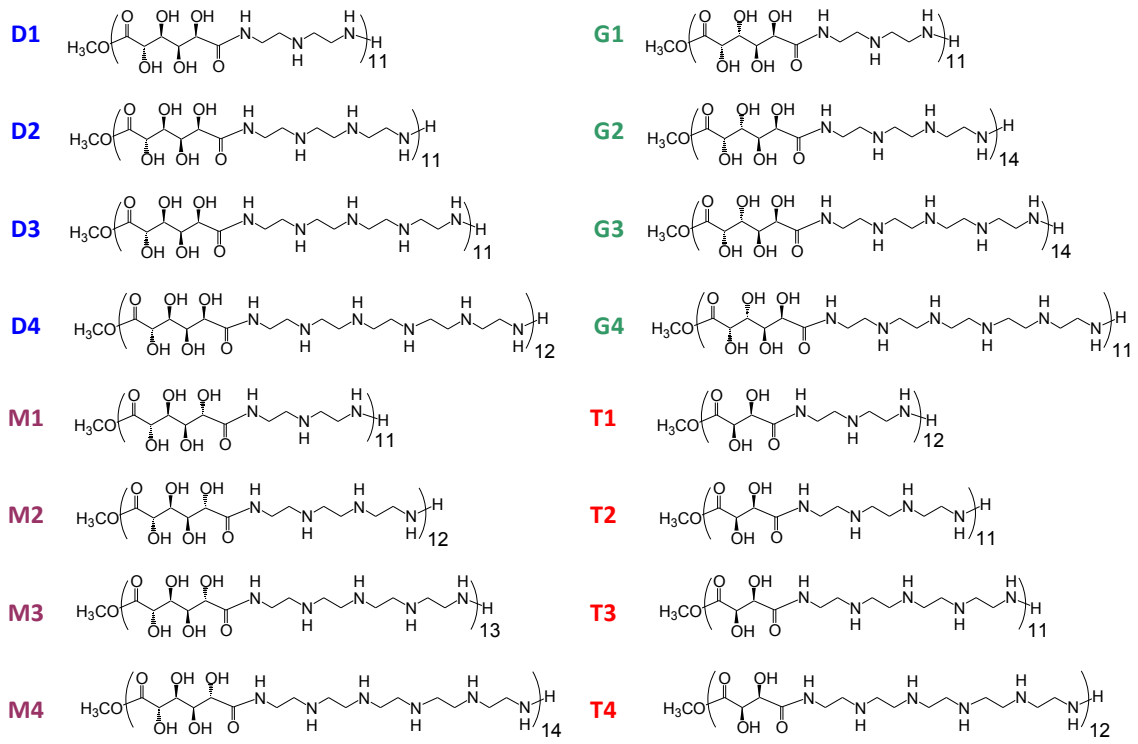

Figure 9: Schematic structures of the sixteen PGAAs. Figure adapted from [127].

The promising initial transfection and toxicity studies on these PGAA structures prompted Reineke et al. to examine the biophysical interactions of the polymer with pDNA. Several analytical techniques such as dynamic light scattering, isothermal titration calorimetry, circular dichroism, and infrared spectroscopy have been used to probe the polymer structural attributes that lead to pDNA encapsulation and effective cellular delivery. It has been discovered that PGAA-pDNA binding occurs through a combination of electrostatic and hydrogen bonding forces.[11] While electrostatics provides a means to bring the polycation (PGAA) and polyanion (pDNA) together and initially associate, the closer-range hydrogen bonding force likely affords greater polyplex stability. It has been hypothesized that the buffering capacity of the polymer vehicle can have a significant endosomal release of polyplexes and in turn, transgene expression. Further studies on these polymers were carried out to measure the percentage of amines that can be protonated during endosome acidification via titration experiments. This study examined and compared the buffering capacity of the D-glucaroamidoamine (D1-D4), L-tartaroamidoamine (T1-T4), and spermine-monomer analogs of these polymer (DS and TS incorporate butylene groups between neighboring secondary amines, thereby increasing the amine spacing) to the observed cellular internalization, gene expression, and cytotoxicity properties.[128] With this study, an interesting trend emerged: as the amine number increased in the polymer repeat unit, the delivery efficacy and gene expression increased, yet, the buffering capacity decreased. The polymers created with the spermine monomers, DS and TS, yielded higher gene expression than the D2 and T2 analogs, but had substantially lower buffering capacity. The results obtained in this publication go against the proton sponge hypothesis of endosomal escape and gene delivery, and since has been further investigated.[129-132] The spermine-containing polymers also exhibited much higher toxicity, suggesting the charge spacing and charge density plays a significant role in biocompatibility. This study revealed that ethylene spacers between the

amine groups lead to more biocompatible delivery and also showed that higher polymer buffering capacity does not necessarily correlate with higher gene expression. To further explore the mechanism of cytotoxicity and nuclear membrane permeabilization, polymer T4 and G4 (Figure 9) were studied in whole cells and in isolated nuclei with flow cytometry and confocal microscopy.[20] The results revealed that when pDNA was complexed with PGAA polymers, association with the nuclei was inhibited in isolated nuclei compared to whole cells, this suggests that intracellular components play a vital role in pDNA nuclear import. Amongst other things published in this work, it was discovered that the ability to directly permeabilize the nuclear envelope, which may contribute to cellular toxicity, increases gene expression efficiency, and that free polymers are able to cross the nuclear membrane without their pDNA cargo, indicating different modes of internalization for free polymers and polyplexes. Thereafter, polymer T4 was compared to PEI and studied for its mechanism of cytotoxicity,[13] it was shown that polycations with the highest amount of protein expression and toxicity are capable of inducing nuclear membrane permeability. But also, polymer length, charge, the presence or absence of hydroxyl groups, and polyplex size effect protein expression and toxicity.

A unique characteristic that emerged with these PGAA polyamides is that they rapidly degrade under physiological conditions. Interestingly, replacement of the carbohydrate with an alkyl chain or replacement of the oligoethyleneamine units with ethylene oxide units lead to polymers that do not hydrolyze after 120 h of incubation in phosphate buffered saline.[133] It has been hypothesized that synergy between the presence of both hydroxyl groups and ethyleneamine groups along the polymer chain facilitate hydrolysis. In correlation with these degradation results, the polymers that do not degrade suffer from lower transgene expression, suggesting that polymer degradation facilitates pDNA release and availability for transcription. This feature of these polymers has been

exploited to develop layer-by-layer polyelectrolyte films via dip coating of pDNA and PGAAs on quartz slides for the controlled release of nucleic acids.[134]

In addition to monosaccharides, disaccharides have also been incorporated into these PGAA structures by the Reineke group (Figure 10). Trehalose, a disaccharide composed of two glucose units linked via an α-(1→1) glycosidic bond has been incorporated into a PGAA motif. This carbohydrate has been shown to have cryo- and lyo-protective properties, and prevents aggregation and fusion of proteins with lipids; this property has been attributed to the molecular geometry and large hydration sphere surrounding the trehalose molecule.[135,136] For these reasons, trehalose was incorporated into a polycation backbone to build a unique delivery vehicle that may help to prevent aggregation of polyplexes in physiological salt and serum conditions. Previous work has shown that polyplexes can aggregate rapidly and are cleared from the blood in vivo.[137,138] Successful results previously described by Liu et al.[36,38] and Reineke and Davis[139] prompted Srinivasachari et al. to synthesize a series of trehalose (Tr)-containing PGAA polymers, with similar ethyleneamine numbers (1-4) to the previous PGAA structures, but with an increased carbohydrate size and polymer length, in order to understand these structural attributes in stable polyplex formation and transfection efficiencies.[5] The series of trehalose-based polymers (Tr1-Tr3) were synthesized via the "click reaction" of acetylated-diazido trehalose and a series of dialkyne-oligoethyleneamines (1-3) (Figure 10). The polymers bind pDNA stably at N/P = 2 according to gel electrophoresis experiments. TEM studies revealed that the polyplexes have either spherical or rod-like morphologies with diameters around 50-125 nm. In general, these polyplexes do aggregate but as the ethylene amine linker increases in the polymer vehicle, polyplex aggregation degreases.

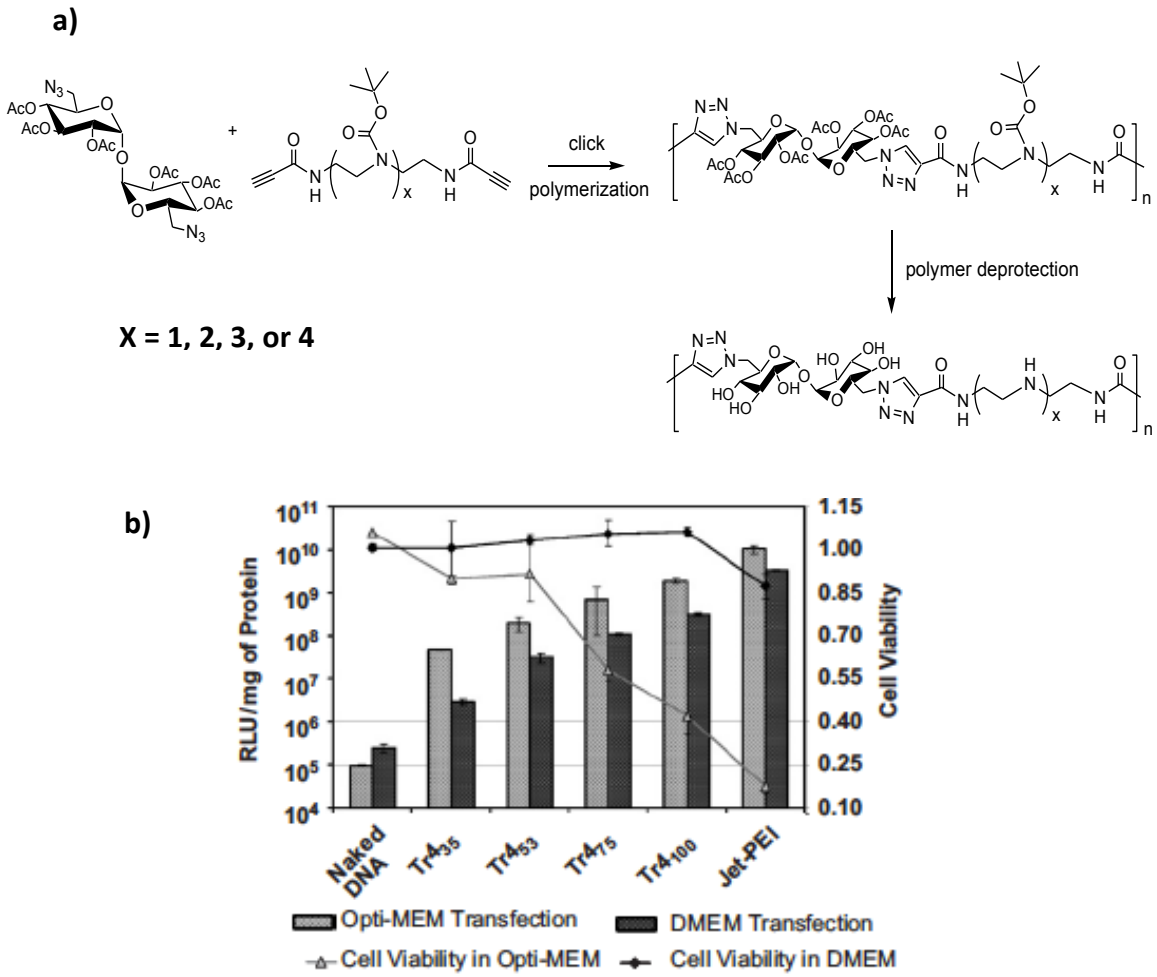

Figure 10: a) Click glycopolymer synthesis and characterization data where x = 1 (Tr1), 2 (Tr2), 3 (Tr3), or 4 (Tr4). The degree of polymerization has been systematically varied from 35-100. b) Transfection data as determined by luciferase reporter gene assays in Hela cells with polyplexes formed from Tr4 at N/P = 7 (PEI N/P = 5). As the degree of polymerization increases, the transfection efficiency increases, both in the presence and absence of serum (DMEM and Opti-MEM, respectively). In the absence of serum, the toxicity also dramatically increases with the polymer length. Figure adapted from [5,30].

In a follow up paper, trehalose polymers with four ethyleneamine units were synthesized (Tr4). The degree of polymerization of these analogs was varied to assess the influence of polymer length on biological properties.[30] Molecular weight played a moderate role, polyplexes formed with Tr4 polymer with a degree of polymerization over 35 appeared to have lower aggregation in serum-containing culture media. Transfection studies with HeLa cells in serum-containing media revealed that Tr3 and Tr4 were the most effective vehicles for pDNA transfection, which could be attributed to the decreased tendency of the polyplexes to aggregate under these conditions.[5,30] When compared to the positive control, PEI, polyplexes formed with Tr3 yielded higher cellular uptake but slightly lower gene expression, whereas Tr4 polyplexes yielded slightly lower expression in Hela cells, but higher expression in H9C2(2-1) cells in serum-free and slightly lower in serum-containing media. The trehalose-based polymers exhibit comparably low toxicity (greater than 80% cell viability) in serum-containing media at N/P = 7, whereas PEI displays a much higher toxicity profile in the cell lines. These results show that incorporation of trehalose imparts favorable biological properties. Further studies performed on these systems to examine the binding to pDNA revealed that polyplex stability improved as a function of increasing the number of amines and degrees of polymerization in both Opti-MEM and DMEM. The polymers with greater amine stoichiometry have been shown to promote favorable DNA binding and stable polyplex formation due to a combination of electrostatic and hydrogen bonding interactions with the pDNA. The combination of these forces help to promote interactions of the polymer backbone via both electrostatics with the phosphodiester backbone and hydrogen bonding with the nucleobases.[12] In contrast to Tr4, Tr1 did not show evidence of direct interaction with the nucleobases; the interaction appears to be more electrostatic in nature with lower amine stoichiometry. The higher amount of secondary amines in the longer Tr4 polymers

likely promotes binding cooperativity, which likely plays a role in increasing pDNA binding and polyplex stability.

While the Tr4 polymers with lower degrees of polymerization (i.e. 35 and 53) did not reveal cytotoxic effects in transfection experiments conducted in both the absence and presence of serum, as the degree of polymerization was further increased (75 and 100), some toxic effects were found in the absence of serum, but were still much lower than PEI. However, in the presence of media containing serum, all lengths of the trehalose polymers revealed high delivery efficiency without cytotoxicity. In HeLa cells, as the degree of polymerization increased, so did transfection efficiency; however, in H9c2 cells the transfection remained constant despite an increase in polymer length (in both the presence and absence of serum).[30] These results suggest that these favorable properties in the serum are important for developing these materials towards various in vivo applications.

To compare the effect of charge center type on the biological properties of these oligoethyleneamine charge centers (PGAAs), a family of poly(glycoamidoguanidine)s (PGAG)s were synthesized and studied.[130] The PGAG polymers complexed pDNA at lower N/P ratios than their PGAA analogs (T1 and G1) and formed polyplexes around 100 nm in size. Interestingly, the substitution of the guanidinium group into the backbone of the polymer resulted in oligomers that were not cytotoxic (at all N/P ratios tested), and had high cellular uptake and good transgene expression in HeLa cells as compared to the amine-containing analogs (G1 and T1).

More recently, the Reineke group has studied 4D spatiotemporal cellular imaging with their Tr4 polymers and other commercially available reagents. The data suggests that the structural characteristics of polyplexes play an important role in determining the intracellular polyplex size, trafficking kinetics, and delivery mechanisms. First, the smaller polyplexes formed the majority of the intracellular polyplex population for all

polymer vehicle types when compared to larger polyplexes. Second, the smaller sized polyplexes trafficked faster and reached the perinuclear zones quicker than larger polyplexes of the same polymer class. The trehalose-containing polyplexes trafficked the fastest and appeared to maintain this state up to 24 hours, subsequently, the trehalose polymer Tr4 showed the highest gene expression. This suggests that trafficking speed to the nucleus is important against enzymatic degradation and nucleases in the cytoplasm. Third, polyplexes were internalized by a caveolae/Rab-5-dependent pathway, and avoided late endosomes (Rab 7), with the exception of jetPEI polyplexes. Fourth, the nature of the chemical backbone in the polymer plays a vital role in uptake, trafficking, and kinetics.[140]

1.04.6 Cyclodextrin Polymers

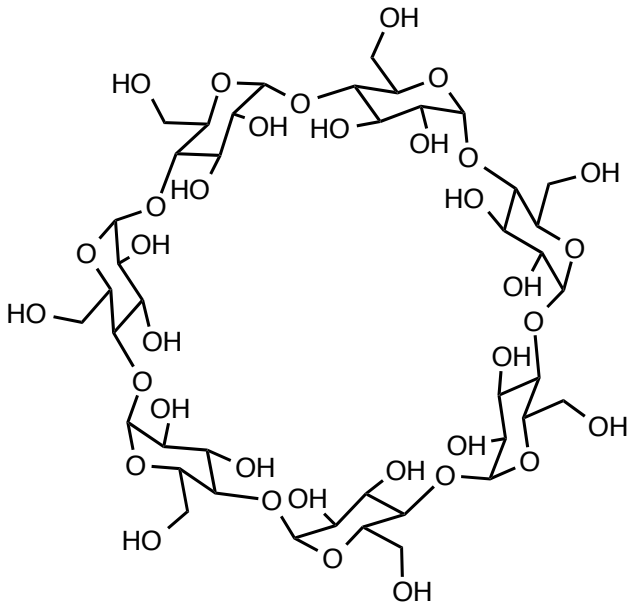

Figure 11. The structure of *β*-cyclodextrin.

Cyclodextrins (CDs) are cup-shaped molecules comprised of cyclic oligomers of glucose. The differing structures composed of 6, 7 or 8 glucose units are subsequently named α-, β- or γ-cyclodextrin, respectively. The three-dimensional structure of a CD is such that the cavity is relatively hydrophobic when compared to the exterior, and thus the cavity can be used to imbibe hydrophobic compounds to create host-guest complexes. The ability of CDs to form inclusion complexes has been exploited in CD drug formulations throughout the world and, for this reason, a significant knowledge base on CD behavior in humans is available. With Sporanox, the i.v. (intravenous) dose contains 8 grams of CD, which is evidence that CDs have relatively low toxicity. Additionally, these structures are neither immunogenic nor metabolized by human enzymes. β-CDs complexed with hydrophobic meso-tetraphenylporphyrin have shown that the β-CD complexes avoid endosomes by using a direct transmembrane pathway – making these

drug and gene carriers favorable among scientists.[141] These properties in combination with their ability to form inclusion complexes led Davis and coworkers to use CDs in the design of their novel delivery vehicles, which advanced to the clinic. Most of the discussion below is based on an article previously published by Davis et al.[10]

As illustrated in Figure 2f, one of the first linear β-cyclodextrin (β-CD) polymer nucleic acid delivery vehicle created by the Davis Group was synthesized by the condensation of a 6A,6D-dideoxy-6A,-6D-di(2-aminoethanethio)-β-cyclodextrin with dimethylsuberimidate (DMS).[9] The resulting polycation contains repeating β-CDs and amidine groups that are completely protonated at physiological pH (the pKa of the amidine group is approximately 12). These polycations are short [molecular weight (M_w) below 10 kDa] and have low dispersities.[9,142] Short polycations (approximately 10 charges per chain) have several advantages. First, as previously discussed, toxicity is generally known to decline with decreasing molecular weight for polycation delivery vehicles.[64] Second, recognition by complement proteins and the detrimental events occurring as a consequence of this step also decreases with decreasing polycation length.[143] Third, at these low molecular weights, the individual polycation chains are small enough to be renally cleared (short polycations can be displaced by nuclear proteins to release the active nucleic acid).

The CD polymers self-assemble with nucleic acids to form dense, spherical, and positively charged polyplexes (as observed from cryoTEM, stereoscopic field emission SEM, and zeta potential studies).[142] As previously mentioned, the mass of these polyplexes have been obtained by using multi-angle, laser light scattering (MALLS) techniques.[45] The polyplexes can be formed with polydispersities below 0.02 (0.02 is the generally accepted upper limit for the definition of monodisperse particles), so that the measured values from MALLS accurately represent the average of the sample. For example, polyplexes with diameters of approximately 70 nm contain 1–2 plasmids (if the

plasmid is around 5–6 kbp) and approximately 1500 polymer strands. These β-CD polymer-based polyplexes have been shown to deliver nucleic acids into cells and yield gene expression values that are similar to other non-viral transfection systems such as Superfect, Lipofectamine, and PEI.[9,142] Davis et al. revealed in these studies that charge ratios well above 2 are necessary for decent gene expression with the β-CD polymers, and that these polycations do not reveal significant toxicity in vitro (even at very high charge ratios).

In follow up studies, Davis et al. prepared over 30 different analogous CD polymers to explore how polycation structure affects gene delivery and cellular toxicity and some selected examples are highlighted below. Initially, the spacing (4-10 methylene units denoted as CDP4-CDP10) between the amidine charge centers along the CD polymer backbone was varied (Figure 2f).[142] The molecular weight and dispersity of these materials are similar with average degrees of polymerization of about 4–5 and very low dispersity values. These β-CDPs self-assemble with pDNA to give polyplexes of similar size and surface charge. However, the properties of these delivery vehicles differ in their stability profile during the exposure to DNA-cleaving enzymes or heparin sulfate (a large polyanion used for displacing the CD polymer from pDNA).[142] For example, CDP6-based polyplexes showed complete stability in the presence of DNA-cleaving enzymes (indicating complete encapsulation of the pDNA) while CDP5- and CDP7-based polyplexes did not. Interestingly when comparing the biological properties of all of these analogous materials, CDP6 yielded the highest gene expression, while CDP8 was the least toxic.[142]

To further pursue the relationships between charge distribution along the polycation backbone and cellular toxicity, another series of polycations that had similar degrees of polymerization and dispersities were prepared. These polycations had variations in: (i) the linkers between the amidine sequences that contained either

methylenes (hydrophobic), a trehalose sugar (hydrophilic), or a β-CD group (very hydrophilic), (ii) in the distances between the charge centers by differing the linker length/sugar sizes (trehalose vs. β-CD), and (iii) the distances between the amidine centers (AP6, which contains 6 methylenes, vs. AP7, which contains 4 methylenes).[139] It should be noted here that polycation AP5 is identical to β-CDP6 (just a difference in nomenclature for different publications). All of these polycation analogs self-assembled with pDNA to form polyplexes of similar size and had zeta potentials greater than 30 mV in de-ionized water. The gene delivery efficiencies were dependent on the polycation used, but in general the delivery efficiency did not exceed the original synthesized polycation delivery platform, β-CDP6 (AP5).[139] When the toxicity of the polymer analogs (AP1–AP7) was compared, the carbohydrate size played a significant role. In general, increasing the carbohydrate size decreases toxicity, and as shown in Figure 12, when AP1, AP3 and AP5 were compared, clearly, the more hydrophilic the polycation, the lower the cellular toxicity. From this study, it was also discovered that the charge center distance from the sugar effects toxicity; the longer the distance, the greater the toxicity.[8] Charge centers other than amidines have been investigated with the CD polymers. Polymers QP1-QP4 were prepared to be analogous to the amidine polymers but to contain quaternary ammonium groups instead. In general, the quaternary ammonium-charged polymers exhibited lower gene delivery efficiencies, but had similar toxicities to their amidine analogs.[8]

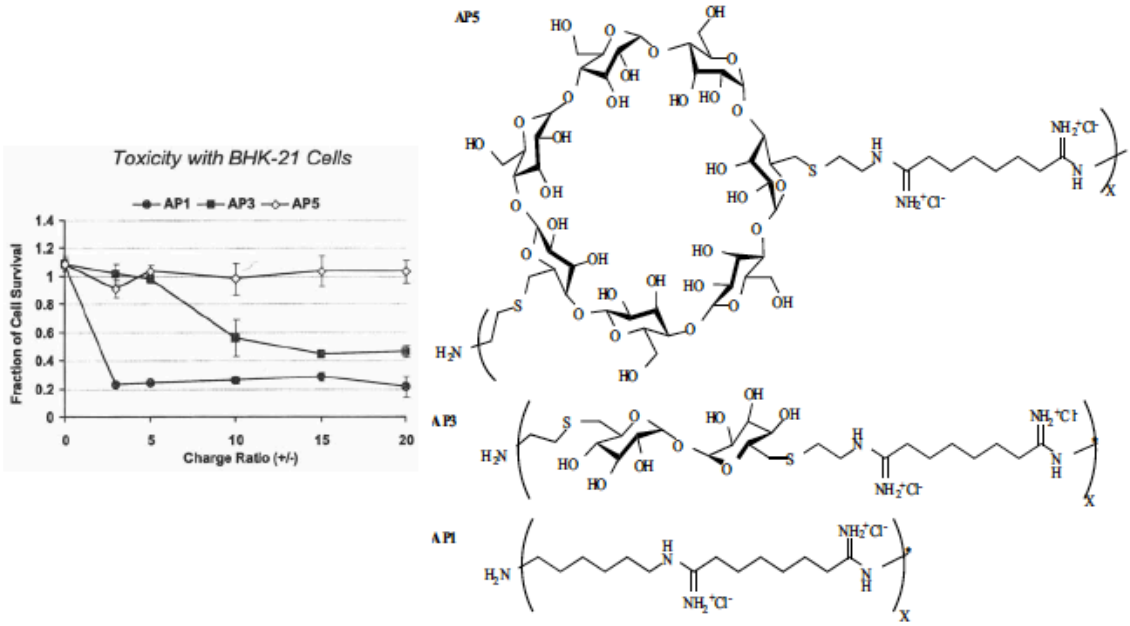

Figure 12: Three examples of the analogous polymer structures (AP5=CDP). As the hydrophobicity of the polymer increases, toxicity significantly increases concomitantly. Figure adapted from [10].

To examine whether the cyclodextrin type and functionalization site on the cyclodextrin cups play a role in the observed structure-bioactivity relationships, β- and γ-cyclodextrin derivatives were prepared by Davis et al.[37] In that study, 3A,3B-dideoxy-3A,3B-diamino-β- and γ-CDs were prepared (as opposed to the 6A,6D-dideoxy-6A,6Ddiamino-β-CDs) and the spacer length and type between the cyclodextrin and amidine charge centers was varied from ethylenediamine, butamethylenediamine, hexamethylenediamine, and diaminetriethylenedioxide. The β- and γ-cyclodextrin monomers (with the different linkers) were all polymerized with dimethylsuberimidate to create a series of eight analog structures. From this study, the cyclodextrin type did not appear to play a role in the delivery efficiency, but incorporating the larger γ-cyclodextrin appeared to slightly lower the toxicity.[37] Also, it was found that the transfection efficiency and toxicity were affected by the spacer length and type that separates the CD from the charge center. In general, the longer the spacer, the higher the observed toxicity.[37] Interestingly, this result was similar in nature to the trend observed with the AP1–AP7 series.[139] From these structure-property studies, it was concluded that the best overall performance for in vitro gene delivery (highest delivery efficiency/gene expression with low toxicity) was achieved with CDP6 (also denoted AP5). This polycation will be referred to and denoted as β-CDP in all discussions in sections 1.05 and 1.06.

In tandem with the above structure property studies, the ability of the cyclodextrin within these delivery vehicles to form inclusion complexes was exploited by Davis et al. to functionalize β-CDP in a noncovalent manner with PEG and targeting moieties. Adamantane (AD) derivatives are known to form inclusion complexes with β-CD and have association constants on the order of 10^4–10^5 M^{-1}.[144] Also, inclusion complexes between adamantane that have been end-capped with poly(ethylene glycol) (PEG)[145] and poly(glucosamine methacrylamide)[146] have been compared and contrasted. The Davis

group utilized these concepts to develop a new method for the surface modification of their polyplex formulations with PEG and other targeting groups (Figure 13). In their structures, a targeting ligand was coupled on the distal end of the PEG opposite from the adamantane which may also contain a short anionic segment to help tune the polyplex surface charge in order to avoid nonspecific charge interactions with the cell surface.[147] The adamantane (AD) formed inclusion complexes with exposed β-CDs on the polyplexes thus modifying the particle surfaces. The surface modifications occured from the self-assembly of the AD-PEG-targeting materials with β-CD-containing polyplexes.[147] Interestingly, the Davis group also found that the polyplexes need not be formed first and that the AD forms inclusion complexes with β-CD polymers first and then binds and compacts nucleic acids into polyplexes. Solutions of β-CD-containing polycations and AD-containing modifiers have been prepared and they spontaneously self-assemble when mixed with nucleic acids to form stabilized particles with diameters of approximately 70 nm with excellent uniformity and allows for formulation at high concentrations. The surface modifications of the β-CD-based polyplexes endow the particles with properties appropriate for systemic application (Figure 13). The further development and use of these concepts to form in vivo-relevant delivery vehicles are discussed in sections 1.05 and 1.06.

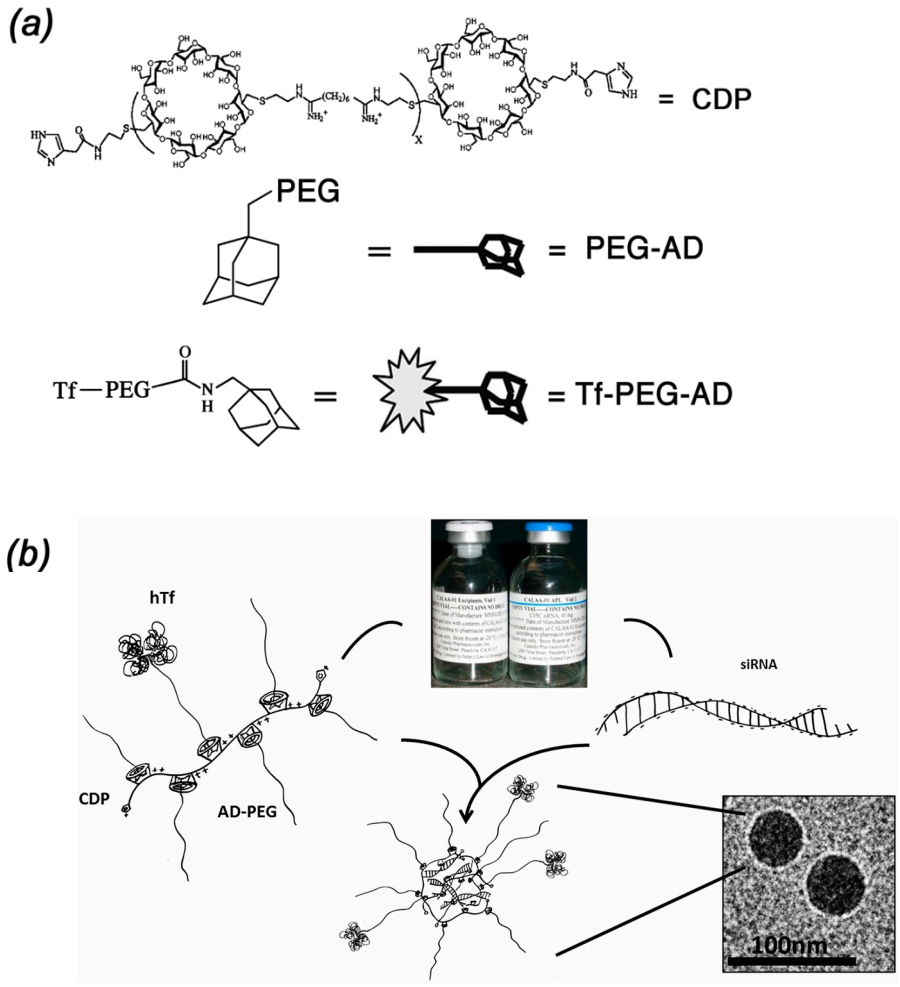

Figure 13: Components and formulation of targeted nanoparticle-containing siRNA. (a) The delivery components are: (i) a water soluble, linear cyclodextrin-containing polymer (CDP), an adamantane (AD)-PEG conjugate (PEG M_w of 5,000), and (iii) the targeting component that is an adamantane conjugate of PEG (PEG M_w of 5,000) that has human transferrin (Tf) conjugated at the end opposite to the adamantane. (b) The formulation contains two vials, one with siRNA and the other with the delivery components. When the two vials are mixed together, the targeted nanoparticles form via self-assembly of the four components. Figure from [148,149].

The interesting properties of the PGAAs previously discussed and β-cyclodextrin polymers developed by Davis et al. further inspired Reineke et al. to design a series of novel macromolecule vehicles using β-CD as the core framework. The 6-positions of the glucose units were functionalized with pendant arms containing a terminal primary amine and oligoethyleneamines of varying length (between 0-4; Figure 14).[59] The core was coupled to the arm units via a 1,2,3-trizole linkage utilizing 1,3-dipolar cycloaddition (the click reaction). These "click clusters" were designed to offer a synthetic approach that yields a reproducible and monodisperse vehicle platform, which could yield benefits for clinical development. Also, the versatility in functional groups and noncovalent interactions with the β-cyclodextrin core offer a means to further functionalize these materials. The click clusters were generally found to bind and compact pDNA into polyplexes at N/P ratios greater than 2, yielding nanoparticles between 80-130 nm. The analogs that had arms containing 2, 3, and 4 secondary oligoethyleneamine units protected pDNA from nuclease degradation when incubated in serum at 37 °C for up to 48 h. The delivery of Cy5-labeled pDNA into HeLa and H9c2(2-1) cells was successfully observed, and the internalization was comparable to commercial reagents such as JetPEI™ and SuperFect; however, with dramatically lower toxicity. It was found that transgene expression generally increased with increasing secondary amine content and N/P ratio in both cell lines. The analogs with 3 and 4 secondary amines had gene expression values similar to the commercial controls and lower N/P ratios (such as 5) yielded higher gene expression. The analogs with lower numbers of ethyleneamines offered minimal gene expression at low N/P ratios. Further studies of these β-CD polymers included forming inclusion complexes with adamantane and either end-capping them with PEG or poly(glucosamine methacrylamide) in order to understand stability, uptake, and reporter gene expression.[146]

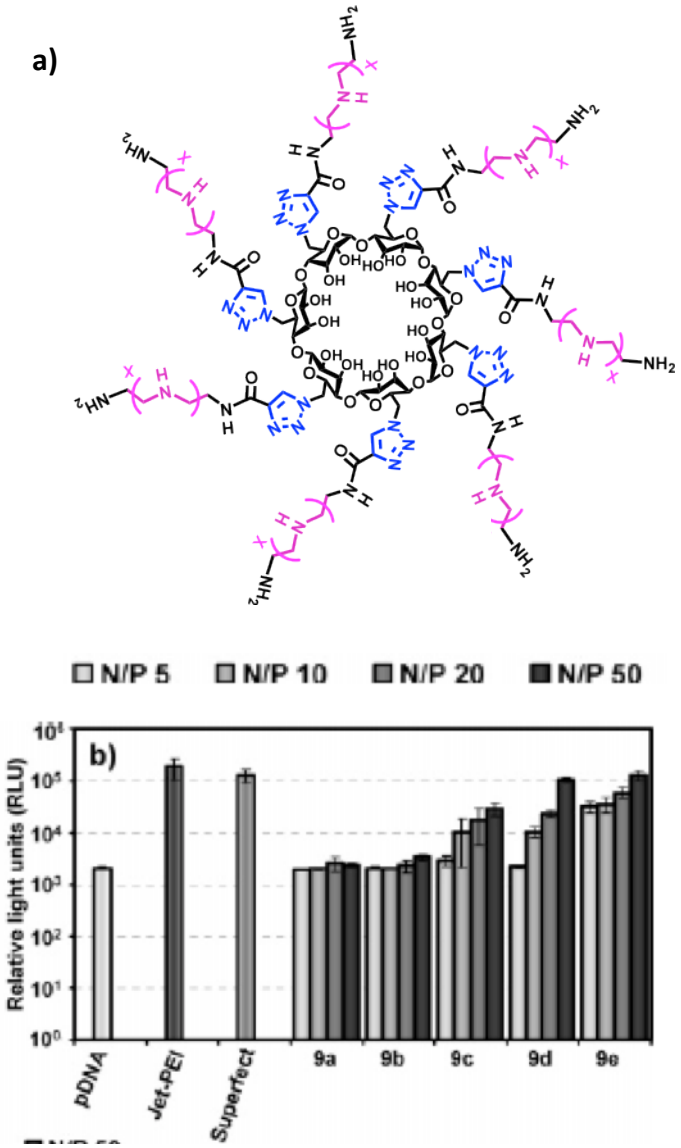

Figure 14: a) Structures of the click cluster delivery vehicles; five monodisperse structures were developed that vary in the length of the oligoethyleneamine arms where x = 0 (9a), 1 (9b), 2 (9c), 3 (9d), and 4 (9e). Transfection increases as the arm length increases, without having a dramatic effect on cytotoxicity. Figure adapted from [59].

While the click cluster vehicles offer a promising monodisperse scaffold, linear polymer analogs were created by Reineke et. al. to further understand the structure-property relationships of this nucleic acid delivery vehicle class.[150] The β-CD scaffold was difunctionalized with azide groups and polymerized with the dialkyne-functionalized oligoethylenamines to derive the target linear β-CD polymers containing between 1-4 ethyleneamines within the repeat unit (Cd1-Cd4; all containing weight averaged degrees of polymerization between 44 and 49). Because of the interesting results with the previously published systems,[5,30,36,128] analogs of Cd4 with weight-averaged degrees of polymerization of 27, 47, 93, and 200 were also created to study the effect of β-CD polymer length. These β-CD polymers showed similar pDNA binding, polyplex size, and zeta potential profiles as observed with the click clusters and the trehalose polymers. Some similar trends were noticed with these structures as seen in previous studies performed by the same group on the trehalose polymers; polyplexes formed with Cd2, Cd3, and Cd4 were internalized significantly better than Cd1 polyplexes, while altering the Cd4 polymer length (degree of polymerization) did not appear to significantly affect internalization nor gene expression. Also, polyplexes formed with polymer Cd3 revealed slightly higher expression levels than polyplexes formed with Cd4.

Recently, polymers CD4, Tr4, and G4 were compared for their ability to deliver pDNA and siRNA in vitro to U-87 (glioblastoma) cells. While delivery efficacy differs significantly as a function of carbohydrate type, nucleic acid type, dose, polymer length, and amount of excess polymer, the results indicate that the trehalose polymers (Tr4) were more effective for pDNA delivery, yet the β-cyclodextrin polymers (CD4) offered higher siRNA delivery and gene knockdown. Interestingly, the smaller carbohydrate analogs of both T4 and G4 were completely ineffective for siRNA delivery yet had high pDNA delivery and gene expression, and free uncomplexed polymer in solution appeared to play a key role in promoting siRNA uptake and gene knockdown.[151]

1.04.7 Poly(β-amino ester)s

Poly(β-amino ester)s are hydrolytically-active compounds that have been routinely examined by the research group of Langer et al. These materials are formed via step-growth polymerization by the Michael addition of a variety of diacrylate comonomers with a number of amine-containing monomers (Figure 2g and Figure 15). This synthetic approach has facilitated a large library of degradable polymers to be generated in a short amount of time for screening toward nucleic acid delivery activity. In an early publication, Lynn et al. created a very large library of 140 structurally unique polymers by reacting 7 diacrylates with 20 different amine monomers.[152] The resulting structures varied greatly in molecular weight profiles (from 2000 to 50,000 Da) and, of these structures, only 70 were water-soluble and 56 of the 140 compounds bound pDNA according to gel electrophoresis shift assays. These 56 compounds were further screened for their activity to delivery pDNA containing the luciferase reporter gene. Furthermore, of these 56 structures that bound pDNA, only seven structures mediated gene expression, and only two structures (B14 and G5) yielded gene expression similar to Lipofectamine 2000.[152] In a follow-up study, this approach was applied to thousands of compounds.[153]

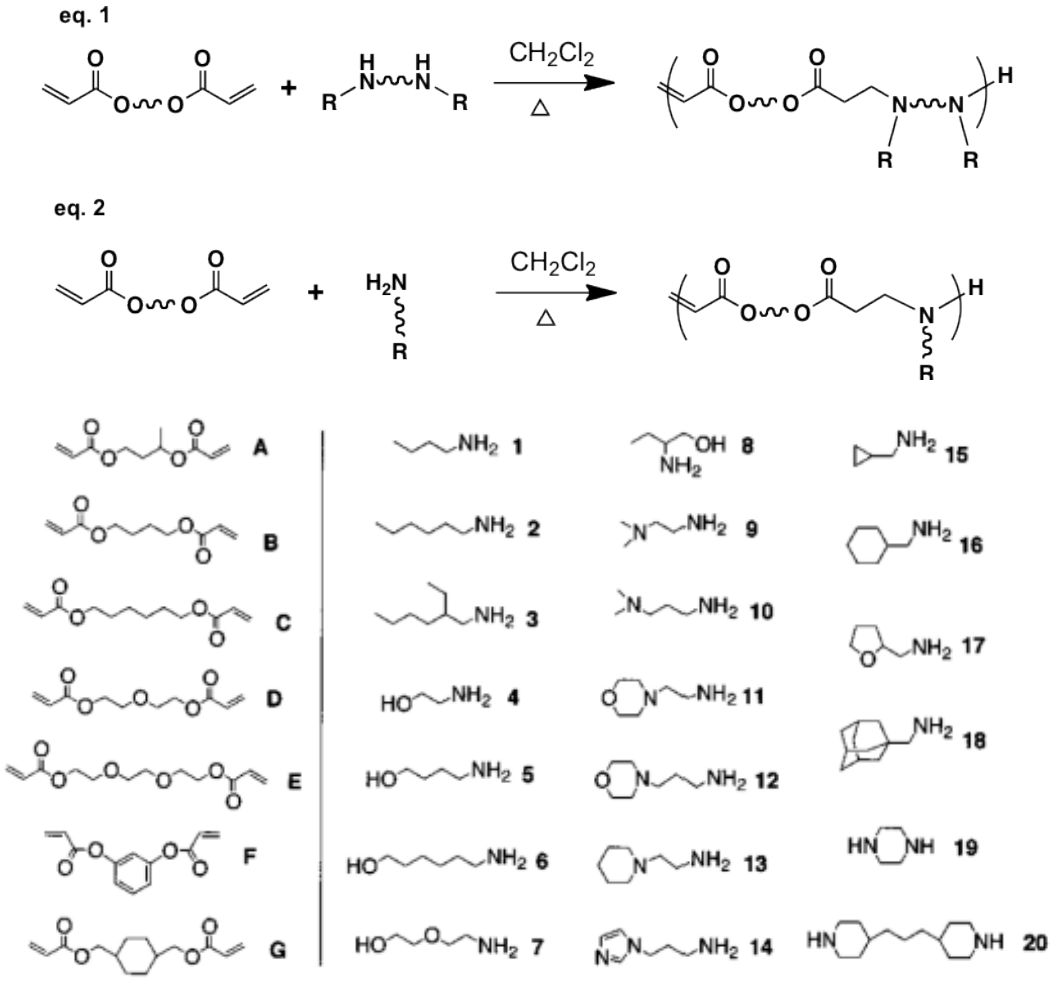

Figure 15: a) Synthesis of the poly(β-amino ester)s created by Langer et al. Two approaches to the synthesis have been taken by reacting a diacrylate monomer with a diamine (eq. 1) or a diacrylate with a monoamine monomer (eq.2). b) Examples of some of the monomers explored by Langer et. al. to create their poly(β-amino ester) library. Figures adapted from [152,153]

Next, the same group further examined two of their most effective compounds in depth that contained pendent hydroxyl groups termed Poly-1 and Poly-2.[154] These two structures were created by copolymerizing 1,4-butanediol diacrylate (Poly-1) or 1,6-hexanediol diacrylate (Poly-2) with 1-aminobutanol. In that study, 12 different lengths of each structure were created that ranged in molecular weight from 3350 to 18,000 Da and the effect of polymer to DNA ratio was also examined as a variable. In addition, the role of the polymer end groups were examined as another variable in this study and these parameters were found to have a dramatic effect on the delivery efficiency in COS-7 cells.[154] Interestingly, the polymer variants with acrylate-terminated were completely lacking in delivery and expression efficiency. However, the polymers with the amine-terminated ends yielded very high gene expression efficiency. Also, in general, high molecular weights (between about 13-15 kDa) and higher polymer/DNA ratios (about 110-150) of the amine-terminated variants yielded higher gene expression and Poly-1 offered higher efficacy than Poly-2. With respect to toxicity, Poly-1 also yielded a lower toxicity profile in cultured cells.[154] The Langer group has taken these structure-property relationships further to examine some of their poly(β-amino ester)s in human umbilical vein endothelial cells (HUVEC) in the presence of serum as models for cardiovascular disease treatment.[155] The compounds with the pendent hydroxyl groups created by copolymerizing 1,4-butanediol diacrylate with 1-aminopentanol (termed C32: Figure 2g) yielded good transfection efficiency with HUVEC and COS-7 cells. A similar approach has also been taken for the delivery of suicide genes for prostate and ovarian cancer treatments.[156,157] It is fascinating that, in all of these studies, the poly(β-amino ester) derivative that yields the highest efficacy consistently is the C32 derivative.

The Langer group has since utilized these materials for functional delivery of siRNA in HeLa cells.[158] For the delivery of siRNA, an interesting approach was taken; first, gold nanoparticles were coated with PEG derivatives containing terminal thiol

groups.[158] Next, siRNAs were linked directly to the surface of the gold nanoparticles via disulfide bonds and then the poly(β-amino ester) compound C32 (Figure 2g),[159] modified with one of various end structures, was added to electrostatically coat the surface of the siRNA-functionalized nanoparticles. Remarkably, when the poly(β-amino ester)s were used directly as a siRNA transfection reagent (without the gold nanoparticles), the poly(β-amino ester) compounds did not show knockdown to luciferase gene expression. However, when the poly(β-amino ester)s were combined with the siRNA-coated gold nanoparticles, effective luciferase knockdown was observed. The poly(β-amino ester) C32 derivative that offered the most effective gene knockdown was the C32 derivative modified with tertiary amine endgroups.[158]

1.04.8 Poly(N,N-dimethaminoethyl methacrylate) (DMAEMA)

Here, the discussion of poly(N,N-dimethylaminoethyl mathacrylate) (DMAEMA) (Figure 2h) will be divided into three sections: linear homopolymers, block polymers, and macromolecular structures such as stars and micelles. While DMAEMA has been in use for decades, its first reported use as a transfection agent was in 1996 by Hennink et al..[160] Since, there have been many studies on its binding and dissociation with DNA, and herein a few of the positive in vitro and in vivo results will be mentioned. DMAEMA polymer is easily synthesized, both low and high molecular weights with low dispersities can be formulated, and is desirable as a delivery vehicle for multiple reasons. First, it is a weak polyelectrolyte with a pK_a around 7.5 (depending on polymer length), making DMAEMA pH sensitive and partially protonated at physiological pH. Due to its high buffering capacity it was originally thought to facilitate endosomal escape through the proton sponge mechanism,[161,162] but that mechanism has since been disproved.[163] Second, it has a reported LCST of 38 ºC at pH 9, 45 ºC at pH 7, and 69 ºC at pH 4 making it temperature sensitive.[164] Third it is less toxic and more biodegradable than PEI with an IC_{50} = ~ 40 μg/ml.[165] Fourth, this polymer contains only tertiary amines but reaches 90% of the transfection efficiency of branched PEI (25kDa) and Lipofectamine.[165] The mechanism of binding between DMAEMA and DNA has been studied in detail by the Hennink group both physically and computationally.[166] It is interesting to note that there are three types of interactions occurring, 1) an ionic interaction (strong) between the positively charged amino groups and the negatively charged phosphate groups in DNA, 2) hydrogen bonding (medium) between the NH of adenine and the carbonyl in the ester group of the polymers, and 3) intrapolymeric interaction (weak) between the positively charged amino group and the carbonyl group within a polymer chain. Therefore, as the degree of protonation in the polymer increases the “binding” between the two

macrostructures increases and the polymer comes into a more fixed position in the major groove of DNA.[166]

Several aspects of DMAEMA have been investigated, such as the role of molecular weight, polyplex size, pH, ionic strength, temperature, viscosity, N/P ratio, and the presence of stabilizers. Interestingly, DMAEMA with high molecular weight (>150 kDa) forms smaller polyplexes (≈190 nm) and is more efficient in transfecting cells, but as a result is more cytotoxic, whereas low M_w polymers form large polyplexes (≈1 μm).[167] It appears that transfection efficacy and cytotoxicity are related to polymer molecular weight. An optimum (good efficiency and mild toxicity) molecular weight seems to be 200 kDa for pDNA[167] and 20 kDa for siRNA[168]. While transfection is good, the stability and toxicity are moderate (13 kDa at N/P=3 has a 80% viability; and at N/P=6 has a 60% viability (COS-7 cells)),[161] several strategies have been implemented to reduce the toxicity without affecting transfection, such as designing block polymers, PEGylation, end group modification, crosslinking, etc.

While the effect of PEGylation does result in more colloidally stable polyplexes in physiological conditions, the transfection efficiency decreases.[162,168-170] Adding blocks of ethylene glycol methacrylate and methyl methacrylate had the same results.[171]

One idea to reduce toxicity while maintaining strong binding to DNA is to decrease the DMAEMA molecular weight and incorporate primary amines [2-aminoethyl methacrylate (AEMA)]. AEMA is more hydrophilic, can bind more tightly to DNA, and has a higher pK_a.[26,161] Previously, Reineke et al. had shown that diblocks of AEMA and 2-deoxy-2-methacrylamido glucopyranose (MAG) formed very stable polyplexes (≈100 nm) even in biological media, were nontoxic, and had high uptake into cells (80%),[39] but due to the strong association between pDNA and AEMA there was little expression even though polyplex uptake was high (80%). Building on this in vitro study, Sprouse and Reineke adjusted the length of AEMA, MAG, and DMAPMA (*N,N*-

dimethylaminopropyl methacrylamide), it was noticed that homopolymers of DMAPMA and AEMA had excellent cell uptake (≈ 90%), but were not colloidally stable and DMAPMA was toxic (≈ 50% cell viability).[1] All diblocks synthesized that incorporated a hydrophilic MAG block resulted in stable polyplexes. While the block length of MAG had little effect on the transfection or toxicity, the lengths of cationic block did affect both properties. Interestingly, cell type played a major role in efficiency, the glycopolymers had higher cellular uptake and transfection efficiency in HepG2 cells over HeLa cells, signifying that the MAG sugar block could aid in hepatocyte transfection. This lead Sprouse and Reineke to investigate a series of polymers in which the cationic block length remained constant while the ratio of primary (AEMA) to tertiary (DMAEMA) amines varied.[26] The results suggest that there is a careful balance between toxicity and transfection, incorporating more DMAEMA leads to higher gene expression but at the cost of higher toxicity, while a 1:1 ratio of AEMA-*block*-DMAEMA leads to optimal polymers that still offer high transfection efficiency. Moreover, the authors investigated the difference between block polymers and random copolymers. Statistical copolymers have previously been shown to be less toxic and sometimes to have enhanced gene expression,[172,173] and Sprouse confirmed this as statistical copolymers always had greater cell survival than their block polymer counterparts. More interesting was the mechanism of toxicity, it was shown that DMAEMA is able to permeabilize the cell membrane, and uncomplexed DMAEMA polymers enter cells just as efficiently as polyplexes do, yet cause more toxicity. This was attributed to the cellular and nuclear membrane being destabilized as cell apoptosis is triggered, yet, GFP and luciferase expression are high.[26] The Reineke group has also investigated secondary and quaternary amines in Hep G2 cells.[174] Interestingly, the secondary amines [N-methylaminoethyl methacrylate (MAEMA)] showed the best results when transfected in biological serum, with lowest cytotoxicity, highest uptake, and higher GFP expression than PEI. These

results have prompted an investigation of diblocks of MAG and MAEMA in vivo with mice, which is currently ongoing.

Over the past few years, star shaped and comb shaped structures containing DMAEMA have been investigated for their ability to bind, deliver, and transfect cells more effectively than linear DMAEMA polymers. One star shaped example by Neoh et al. uses β-cyclodextrin at the core with DMAEMA side arms extending outward.[175,176] The star shaped structures exhibited lower cytotoxicity and higher gene transfection over high molecular weight DMAEMA homopolymers. When the length of the DMAEMA was fixed, the fewer the arms, the lower the toxicity. Conversely, when the molecular weight was held constant, the shorter the DMAEMA arms, the less toxicity was observed. Again, there was a balance between number of arms and transfection efficiency; stars with 21 arms possess the lowest transfection efficiency, while stars with 4-7 arms had the highest.[175]

Of course the synthesis of di- or multi-block polymers that incorporate DMAEMA with a hydrophobic segment can give rise too much more complex and sometimes ordered macrostructures. Micelles have received a lot of attention lately for their ability to be nucleic acid delivery vehicles as they can be preassembled into stable structures, studied or altered, and then complexed with not only genetic cargo, but also hydrophobic small molecules, such as therapeutics, imaging agents, and sensors (Figure 16).[164,177-180] There have been several studies investigating these duel purpose delivery vehicles and comparing them to polyplexes in vitro and in vivo. Won et al. compared PEG-BA-DMAEMA (BA = butyl acrylate) with diblocks of PEG-DMAEMA and homopolymers of DMAEMA and tested them with pDNA in vitro with HeLa cells. These initial results suggest that micelleplexes are not advantageous with pDNA delivery.[181] While the micelleplexes had similar toxicity and aggregation profiles in serum containing media, they tended to interact with erythrocytes more, and they had lower gene

transfection efficiency. However, when the same polymers were tested in vitro with siRNA, the micelles had better efficacy and in vivo biodistribution properties.[182] It was reported that micelleplexes had an enhanced siRNA delivery performance without increasing toxicity. This increase in delivery was attributed to the alternative way that micelles are internalized as opposed to polyplexes. In the same conditions, micelleplexes had better in vitro gene silencing and in vivo tumor accumulation over polyplexes of DMAEMA and PEG-DMAEMA.[182] Other scientists have had success with similar micellular systems.[183-189] It appears that the length of DNA plays a very important roll with the complexation of micelles.

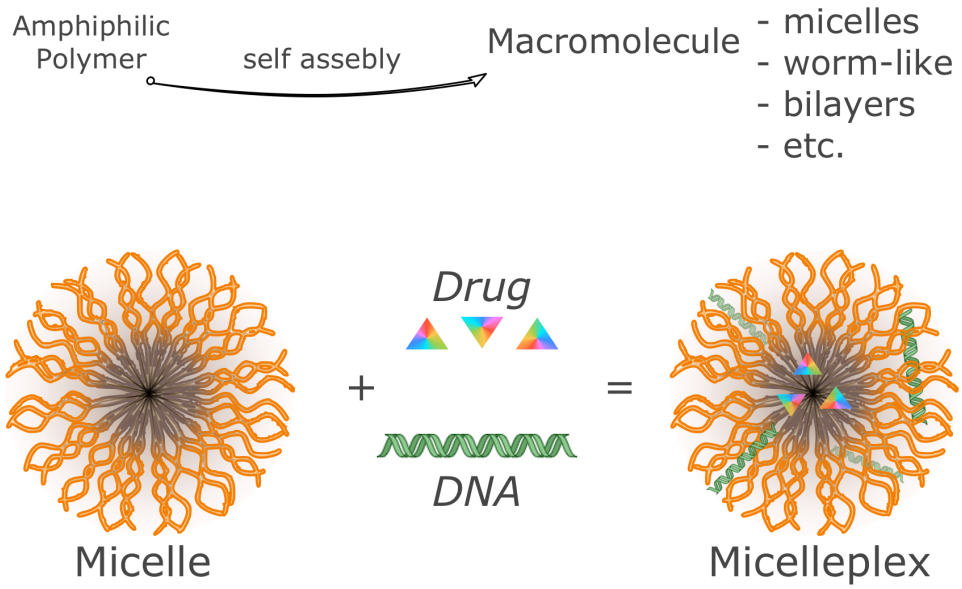

Figure 16: The self assembly of macromolecular structures from hydrophilic-hydrophobic (amphiphilic) polymers, and the complexation of these macromolecular structures with nucleic acid and/or encapsulation of hydrophobic drugs to form stable duel purpose delivery vehicles. Figure generated by the author.

1.05 Introduction to In Vivo Nucleic Acid Delivery with Polymers

Three major classes of barriers that need to be overcome in the development of systemically administered, polymeric, in vivo nucleic acid delivery systems are: barriers to formulation and manufacturing, extracellular barriers, and intracellular barriers. The intracellular barriers have been described above. They must also be overcome in vivo. One of the issues in creating an effective, systemic delivery vehicle is to impart properties to allow in vivo use without destroying essential features for intracellular delivery. Additionally, delivery systems that are optimized for in vitro delivery are not necessarily the best delivery systems for in vivo applications. For example, polyplexes will normally aggregate in the presence of serum. These aggregates then can precipitate onto cell in culture and give high transfections. Polyplexes of this type when injected via mouse tail vein quickly aggregate and are collected in the first capillary bed that they encounter – that is, the lung. For systemic administration, the polymer delivery system should form particles that do not aggregate. In most cases, these particles are sub-200 nm. For simplicity, the polymer-nucleic acid composites described below (will include components other than the polymer and the nucleic acid) will be called nanoparticles (even though some would argue that nanoparticles should be 100 nm diameters or smaller – that upper limit is arbitrary). Well constructed nanoparticles will not aggregate in serum and when used in vitro, will not contact cells as efficiently as with polyplexes that aggregate and sediment onto the cells (see time scale for diffusion of nanoparticles vs. sedimentation[44]). Thus, well-constructed nanoparticles for systemic administration in general will not be as effective for in vitro transfection. The key point is that the intracellular trafficking and nucleic acid release characteristics do need to be maintained for use in vivo, but because of the nature of the other properties that are necessary for successful circulation and targeting, the nanoparticles may not be optimal for in vitro

transfection reagents. In addition to the intracellular barriers, extracellular barriers to use such as polymer toxicity, in vivo stability, and immunogenicity are major issues, and are discussed below (these sections are modified (to include nucleic acids other than plasmids) and updated from Hwang and Davis[190]). After describing the barriers that need to be overcome for in vivo delivery, a polymeric delivery system will be described to provide a specific example of how one polymer system was developed from the laboratory to the clinic.[17,191]

1.05.1 Formulation Barriers

1.05.1.1 Nanoparticle concentration

Cationic polymer-mediated delivery of nucleic acid-based drugs at a therapeutic dose requires high concentrations of nanoparticles. If not stabilized correctly, aggregation of these colloidal systems can occur with neutral particles, in concentrated solutions, or in the presence of salt. Formulation of polyplexes at near-neutral zeta potentials results in rapid aggregation of the polyplexes due to van der Waals interactions. For charge-mediated uptake utilized with some in vitro studies, this problem is bypassed by formulating polyplexes with positive zeta potentials. However, positively-charged polyplexes aggregate more readily as their concentration increases and they quickly precipitate out of solution above their critical flocculation concentration. For example, polylysine-based polyplexes precipitate at 20 μg DNA per mL water,[192] thereby severely limiting the injectable dosage of these particles. The concentration of nanoparticle formulations can increase with the hydrophilicity of the cationic polymers. Conjugation of hydrophilic polymers or proteins to the cationic polymers also increases polymer solubility. PEGylated (polyethylene glycol-conjugated) polylysine-based nanoparticles show no aggregation even at neutral zeta potentials.[85,193] The solubility of PEG-PLL

particles depends on the degree of PEGylation[194] and molecular weight of PEG,[195] with formulated concentrations as high as 2 mg DNA per mL water.[194] Ogris et al. were able to concentrate PEGylated PEI to 400 μg mL^{-1} in water without precipitation.[196] Dextran-modified PLL also increases the solubility of complexes of 40 μg of DNA per mL,[197] as does conjugation of water-soluble proteins such as transferrin (increases the concentration of polylysine-based nanoparticles to 300 μg DNA per mL water[192]). Thus, injection of cationic polymer-based nucleic acid therapies at a pertinent dose generally requires concentrations of nanoparticles above their critical flocculation concentration. Efforts to raise nanoparticles concentration limits by increasing their hydrophilicities and by providing steric stabilization have resulted in formulations that can be used for systemic administrations in humans at therapeutic concentrations.[191]

1.05.1.2 Nanoparticle storage

In addition to formulation stability, nanoparticles need to have significant shelf-storage stability in order to be practical as a bedside medicine. Nanoparticles that contain plasmids are stable in solution in the presence of a protectant such as 10% sucrose and if stored at 4 °C. Even under these precautions, the supercoiled plasmid form disappears with time.[198] Lyophilization of nanoparticles presents a viable alternative for storage. Issues of importance for nanoparticle preservation by lyophilization are summarized in a review by Anchordoquy and Koe.[199] A lyoprotectant is crucial for maintaining nanoparticle size and ultimately transfection potential. Various types of sugars (sucrose, trehalose, lactosucrose, β-cyclodextrin, etc.)[200] have been successfully used as lyoprotectants and are hypothesized to prevent aggregation by hydrogen bonding with polymer/plasmid complexes or by forming a protective glassy matrix.[201] Freeze-drying in the presence of these sugars can result in nanoparticles with no decrease in activity even

after storage for at least 10 months.[198] Nanoparticles with protein-based ligands such as transferrin can also be successfully preserved by lyophilization.[202] Thus, it appears that lyophilization of nanoparticles in the presence of a lyoprotectant is a generally useful method for storage since it does not seem to depend strongly on polymer structure. While storage data for nanoparticles containing nucleic acids other than plasmids are not available, it is likely that the use of lyoprotectants will also be utilized in these types of formulations.

1.05.2 Extracellular barriers

Extracellular barriers in systemic delivery involve hurdles to nucleic delivery encountered from the point of injection to the surface of the cellular target. For cationic polymer-based systems, these barriers typically include the toxicity of the nanoparticles, interactions with serum proteins, extracellular matrices and non-specific cell surfaces, clearance by the innate immune system, aggregation due to physiological salt conditions and evasion of the adaptive immune response. Ideally, the nanoparticle should: (i) remain nontoxic, small and discrete, (ii) bypass the immune system and (iii) interact only with the cells of interest. Efforts to prepare polymer systems that endow nanoparticles with these characteristics are discussed below.

1.05.2.1 Toxicity

A major drawback of nanoparticles formulated using cationic polymers that has limited their progress towards use in clinical trials is toxicity. Although the molecular basis of toxicity is unclear, the internalization profile and polycationic nature of the polymers appears to be the main origin of toxicity. Thus, recent efforts to develop

polymers with reduced toxicity have focused on low molecular weight polymers, biodegradable polymers, and polymers with reduced cationic charge density.

Polyethylenimine,[203,204] polylysine,[204] and some dendrimers[21] suffer from toxicity in mammals. The LD_{50} of high molecular weight forms of PEI and polylysine polymers (25 kDa) in mice range from 5-30 mg/kg when complexed to DNA.[205,206] Low molecular weight preparations of PEI[64] and PLL[84] are significantly less toxic to cultured cells. Cyclodextrin-based polymers (M_w ~6000) demonstrate low toxicity, with an LD_{40} of 200 mg/kg in mice.[142] In addition, low molecular weight chitosan also shows significant increase in tolerability in vitro over long-chain chitosan.[207] Biodegradable polymers such as poly(β-amino esters) also have reduced toxicity, possibly by reduction to smaller units after internalization.[208] Polymer detoxification has also been achieved by reducing cationic charges. Glycolylation of amine groups in PEI, PAM, and PLL reduces the number of free amines and introduces hydrophilic residues. Glycolylation of 70% amine groups in PEI resulted in a polymer with low cytotoxicity even at N/P ratio of 30.[63,209] PEGylation of polylysine by reacting with the primary amine groups also reduces the polymer amine content and yields polymers with significantly lower toxicities.[2,194] Polymers with high charge density, e.g., PEI and polylysine, tend to have higher toxicities. Hwang et al. showed that the distance separating the charge centers on cyclodextrin-containing polymers effects the toxicity with shorter distances yielding higher toxicity materials.[142] Finally, in vivo formulations can sometimes contain polymer that is bound to the nucleic acid and also free uncomplexed polymer. These two fractions may have different toxicities.[26] Fahrmeir et al. showed that with PEI complexed to plasmids in formulations that also contained non-complexed PEI, mice receiving those formulations exhibited severe toxicity.[33] Formulations purified to remove the free PEI were well tolerated when administered to mice.[33] Thus, for this case, the free PEI appears to be the major source of toxicity in the formulation; however, in other cases the

uncomplexed PEI polymers seems to aid in gene transfection and intracellular trafficking.[34] A further histological analysis of major organs indicates that the presence of uncomplexed polymer elicits toxicity only to the organ that is associated with the clearance of the complexes from the circulation system.[185]

1.05.2.2 Salt and serum stabilization

Systemic delivery of nanoparticles has been limited due to particle aggregation upon injection. Cationic nanoparticles, while stable in water, aggregate in ionic solutions due to a decrease in the protective electrostatic double layer. The physiological salt concentration (~150 mM) is more than sufficient for inducing rapid aggregation of the nanoparticles.[210] Injection of PEI-based nanoparticles into mice results in 50% lethality, and the likely cause is by blockage of lung vasculature with aggregated nanoparticles.[196] In addition to salt-induced aggregation, serum proteins readily adsorb onto positively charged particles, initiating rapid blood clearance by macrophage uptake (a first step in the removal of polyplexes by the innate immune system). Polylysine-based particles are eliminated quickly with a half-life less than 5 minutes. Clearance from blood has been shown to correlate with the amount of plasma associated with the particles.[211] One approach to minimizing salt-induced aggregation and non-specific protein or cell surface adsorption is steric stabilization with hydrophilic polymers. Steric stabilization can be achieved by grafting a "brush" layer of hydrophilic polymers to the surface of nanoparticles, thereby decreasing particle-particle and particle-protein interactions. Hydrophilic polymers used for polyplex modification include PEG, MAG,[1,39] HPMA (N-(2-hydroxypropyl)methacrylamide),[3,195] oligosaccharides[6,195] and soluble proteins.[212] By far the method that is used most for steric stablization of nanoparticles is PEGylation, which is described in more detail in the nextsection.

1.05.2.2.1 Stabilization by PEGylation

Attempts to provide salt and serum stabilization of nanoparticles by PEGylation have yielded mixed results. The issues of concern when discussing PEGylation include the length of PEG, PEG grafting density, and method of PEGylation. Conjugation of PEG to cationic polymers often reduces the charge density of the polymers by reacting away cationic amine groups while adding hydrophilic, bulky polymer fragments. Thus, PEGylation can reduce the nucleic acid binding efficiency of cationic polymers and alter the thermodynamics of plasmid DNA condensation. PEGylation of PEI (M_w 2000, "PEI2K", DP ~ 45) resulted in nanoparticle structures of complexed plasmid DNA with thick threads and donuts, whereas PEG-PEI25K condensed plasmid DNA to small dense granules without extended threads.[74] The PEG-PEI2K-based nanoparticles were not capable of plasmid DNA transfection. PEGylation of PLL4K (polylysine with M_w 4000, DP = 19) altered the nanoparticle structure from toroids to rods. In addition, these structures were not stable against salt-induced aggregation, unlike PEG-PLL10K that offered salt stabilization.[210] PEGylation of thermine derivatives (~4 charges per chain) also prevents plasmid DNA condensation.[213] Vinogradov et al.[73] and Kwok et al.[194] report successful plasmid DNA condensation after PEGylation of short polycations (PEG-PEI2K & PEG-Polyspermine and Alk-CWK18, respectively); however, in the latter case condensation was determined by light scattering (assumes spherical particles) for measurements and therefore would be unable to accurately reveal changes in nanoparticle structure. The PEI2K-PEG complexes are stable at physiological salt conditions while the PEG-CWK18 complexes give high concentrations in water.

Steric stabilization occurs by protection of particle surfaces with hydrophilic polymers. The thickness of the protective layer, i.e., the M_w of PEG, therefore influences

the degree of particle protection. Analysis of plasma protein adsorption to PEG-coated nanoparticles of sizes 160-270 nm as a function of PEG thickness revealed decreased protein adsorption with increased M_w. PEG2K was able to reduce protein adsorption by 43% while PEG5K reduces protein adsorption by 73%. Further increases in PEG length offer only marginal increases in protein protection, indicating PEG5K to be a critical length for steric stabilization of nanoparticles in this size range.[214] Indeed, PEGylation of PEI-based nanoparticles with PEG3400 only slows salt-induced aggregation while PEG6K completely prevents aggregation in physiological salt conditions. PEG6K was also more effective than PEG3400 in preventing complement activation and serum binding.[212]

The degree of stabilization is also influenced by the density of the PEG layer. PEGylated-nanoparticle studies determined the threshold PEGylation density (by weight %) for maximum reduction of protein adsorption to nanoparticles to be 5%, with total adsorbed protein content decreasing as PEG density increased. The average distance between PEG strands at this density was calculated to be 1.4 nm.[214] It should be noted that while PEG significantly decreases protein adsorption, adsorption cannot be completely eliminated due to the inability to completely coat particle surfaces. Nevertheless, protection from complement activation by PEGylation of PEI/DNA complexes depends on the amount of PEG associated with the particle surface.[215] PEG coating of nanoparticles, in addition to providing salt and serum protection, can also reduce non-specific cellular uptake as a function of PEGylation density. PEG5K-PEI25K particles have reduced transfection potential that is dependent on PEG grafting density: 10% modification of PEI amine groups renders the polyplexes completely inactive.[74] PEG550-PLL25K nanoparticles transfect optimally with 10% PEG grafting. Further increases in PEGylation reduce transfection, most likely by inhibiting uptake. Increasing the density of high M_w PEG also affects the plasmid DNA binding affinity of the cationic

polymer, both by sterically interfering with plasmid DNA binding interactions and by reducing the number of cationic charges available for binding. High PEG:PLL ratios in PEG5K-PLL10K polymers result in decreased DNA binding and polyplexes with worm-like structures.[193] Therefore the following dichotomy exists: higher grafting densities and longer PEGs are necessary to maximize salt and serum stabilization; however, these conditions lead to particle destabilization and low transfection efficiencies. An approach to circumvent this problem is to PEGylate or coat the cationic polyplexes after nanoparticle formation in order to minimize disruption of DNA binding.[216]

Two examples of post-polyplex PEGylation formation are by Ogris et al.[196] and Finsinger et al..[215] Ogris modified transferrin-PEI (Tf-PEI) or PEI-based polyplexes by reacting activated PEG5K to primary amino groups in the PEI molecules.[196] This PEGylation method therefore modifies only surface-available amine groups and prevents nanoparticle instability due to hydrophobic polymers trapped in the nanoparticle core. One-third of the primary amine moieties in PEI were modified by the reaction with the PEG5K without any change in nanoparticle size. In addition, the PEGylated nanoparticles were stable in ionic solutions up to 70 mM. PEGylation prevented plasma-mediated aggregation and significantly increased blood circulation (33% of the PEGylated nanoparticles remained in blood 30 minutes after injection in mice versus 6% of unmodified particles). In addition, tumor-site expression was increased after systemic injection of PEGylated DNA/Tf-PEI nanoparticles over unmodified polyplexes.[196] Finsinger et al. also PEGylated preformed PEI and PLL polyplexes by the addition of anionic peptide-PEG conjugates. The anionic peptide self-assembled to the polyplex surface by electrostatic interactions. The coated particles also retained their size and demonstrated steric stabilization against physiological salt conditions and proteins such as BSA.[215]

Many of the features discussed above for PEG stabilized nanoparticles containing pDNA also exist with nanoparticles carrying other types of nucleic acids. Reviews on polymeric carriers of antisense oligonucleotides and siRNA[185,217,218] and polycation-based nanoparticle delivery of siRNA[219] are available. The PEG density and PEG M_w are important parameters with short nucleic acid delivery[31,191,220] as outlined above with the delivery of plasmids. For example, Bartlett and Davis reported that PEG of M_w 5000 was necessary to provide steric stabilization with 70 nm nanoparticles carrying siRNA. Using this size PEG, the nanoparticles had a PEG surface density of 43 pmol/cm^2. [31]

1.05.2.3 Evading the immune system

One of the most difficult extracellular barriers that the nanoparticles must overcome is the detection by the immune system. The immune system is very complex and has numerous pathways to clear nanoparticles. Overviews of the area of nanoparticle immunological properties are available.[221-223] Here, several mechanisms that are particularly important with polycation-based delivery of nucleic acids are discussed.

1.05.2.3.1 Toll-like receptors

Toll-like receptors (TLRs) are part of the innate immune system. Several of the TLRs are know to recognize nucleic acids. TLR-9 recognizes unmethylated CpG (cytosine guanosine dinucleotide) while TLR-3, TLR-7 and TLR-8 recognize RNA (double-stranded RNA with TLR-3 and single-stranded with TLR-7 and TLR-8). eg. TLR-3 interacts with and causes an immune response to Poly I:C, a common synthetic analog of dsRNA used in research. While there are several groups working on creating immunostimulatory oligonucleotides for cancer therapies,[224] designs to avoid TLR recognition are the more normal situation with polymer-nucleic acid nanoparticles.

siRNAs can stimulate immune responses via TLRs when certain delivery systems are utilized. Each system appears to have its own inherent ability to stimulate or evade the immune system. For example, numerous lipid-based systems do stimulate the immune system with siRNAs,[225] while some polymer-based systems do not.[191] If a particular delivery system does provide for immune stimulation with siRNAs, it is now known how to mitigate this stimulation by chemically modifying the siRNA.[225] Each new delivery system must be tested for its immunostimulatory potential. Interesting results are appearing. For example, PEI has been shown to be recognized by TLR-5.[226] This is a surprising result, demonstrating that non-natural polymers must be tested in vitro and in vivo in order to ascertain whether they will be immunostimulatory.

1.05.2.3.2 Complement activation

Complement provides a multifaceted defense system against infection.[227] It is known that negatively-charged liposomes activate complement via the classical pathway that involves antibodies while positively-charged liposomes activate complement through the alternative pathway that can be independent of antibody interactions.[228] Additionally, naked phosphorothioate oligonucleotides can activate complement by the alternative pathway.[229] Thus, polymer-based nanoparticles carrying nucleic acids have the potential to activate complement. Plank et al. reported that complement activation could limit the circulation half-life of polyplexes in vivo.[143] Also, complement-mediated hemolysis was obtained at elevated polymer concentrations with high molecular weight polymers.[31,143] The potential for complement activation by cationic polymers was found to strongly depend on polymer chain length; cationic oligomers were found to be weak activators of the complement system.[31,143] Polymer complexation with pDNA[211] or siRNA[31] also greatly reduces the potential for complement activation. Dash et al. studied the

mechanisms for polyplex clearance from the blood and found minimal contributions from complement at the concentrations tested.[211] Additionally, Heidel et al. reported no complement activation in non-human primates with a polymer-based nanoparticle carrying siRNA.[149] Thus, while polycations can activate complement, it does appear that properly formulated nanoparticles can be prepared that do not. This property must be tested prior to use in humans, and is it important to do so in non-human primates as they give the closest analog to behavior in humans.

1.05.2.3.3 Antibody production: specific antibodies to PEG

Nanoparticles containing polymers, nucleic acids and targeting ligands have numerous components that have the potential as individual species to elicit antibody production. For example, with the human transferrin-containing targeting ligands, injection into non-humans may stimulate antibodies to this human protein. Even in humans, this targeting ligand may also create antibodies as the protein is modified to allow for the conjugation to the nanoparticle. Heidel et al. reported a small titer antibody production to the human transferrin on nanoparticles administered i.v. to monkeys.[149] The antibodies were shown to bind the human transferrin (as opposed to other components of the nanoparticle) and they were not affecting the pharmacokinetics of the nanoparticles in multi-dosing studies.[149] More recently, antibody production has been observed for structures on nanoparticles that alone would not elicit antibody production. A major new discovery is that the presence of PEG on nanoparticles can elicit antibody production.[230-237] Individual PEG molecules do not cause antibody formation. However, PEGylated liposomes upon repeated injection in animals and humans produce IgM antibodies, that then rapidly eliminate the nanoparticles and can cause acute hypersensitivity upon dosing.[230,232-237] The antibody production has been observed with PEGylated liposomes

carrying siRNA.[236] Additionally, it is unlikely that only liposomes will produce this response as PEGylated poly(lactide) nanoparticles also show rapid clearance upon repeat injections in mice.[231] However, Heidel et al. did not observe IgM production or alterations in clearance upon repeat injections in monkeys.[149] The antibody production to PEGylated nanoparticles is relatively new and complete understanding of its origin is unknown at this time. Obviously, each new nanoparticle system needs to be investigated as altered clearance and the onset of hypersensitivity reactions upon repeat administration would not be acceptable for use in humans.

1.05.3 Example of in vivo application

Numerous polymer-nucleic acid composites have been investigated in animal studies. The most widely used polymeric systems are the polymers or variations of the polymers mentioned in section 1.04 (see Figure 2). There are also systems derived from natural polymers such as chitosan and collagen.[238,239] Below, a single system is outlined to show how some of the issues illustrated above are translated from the level of transfections in cells to the treatment of humans in the clinic (the following discussion is adapted from a presentation by Davis[191]).

The delivery system illustrated here is a three-component system (β-CD polymer, AD-PEG and AD-PEG-Tf: see Figure 13a) that was developed into a two-vial formulation where the delivery components are contained in one vial and the siRNA in a second vial (see Figure 13b). When the contents of the two vials are combined, they self-assemble into ca. 70 nm nanoparticles (see Figure 13b). These targeted nanoparticles are administered by i.v. to patients where they circulate (too large to escape via the kidney) and localize in tumors (see Figure 18). The human transferrin protein targeting ligand (Tf) on the nanoparticle is able to bind to TfR on cancer cells, and the nanoparticles can

be internalized via receptor mediated endocytosis (see Figure 17d). The β-CD polymer contains organic groups that are protonated around pH 6. This "chemical sensing" mechanism then triggers a number of processes that provide endocytic vesicle escape and nanoparticle release of the nucleic acid into the cytoplasm. Of importance is that each of the delivery components is sufficiently small so that when the nanoparticle disassembles into individual components, those components can be cleared from the body via the kidney. This delivery system was the first targeted, polymeric delivery system carrying a nucleic acid to reach human clinical trials.[191]

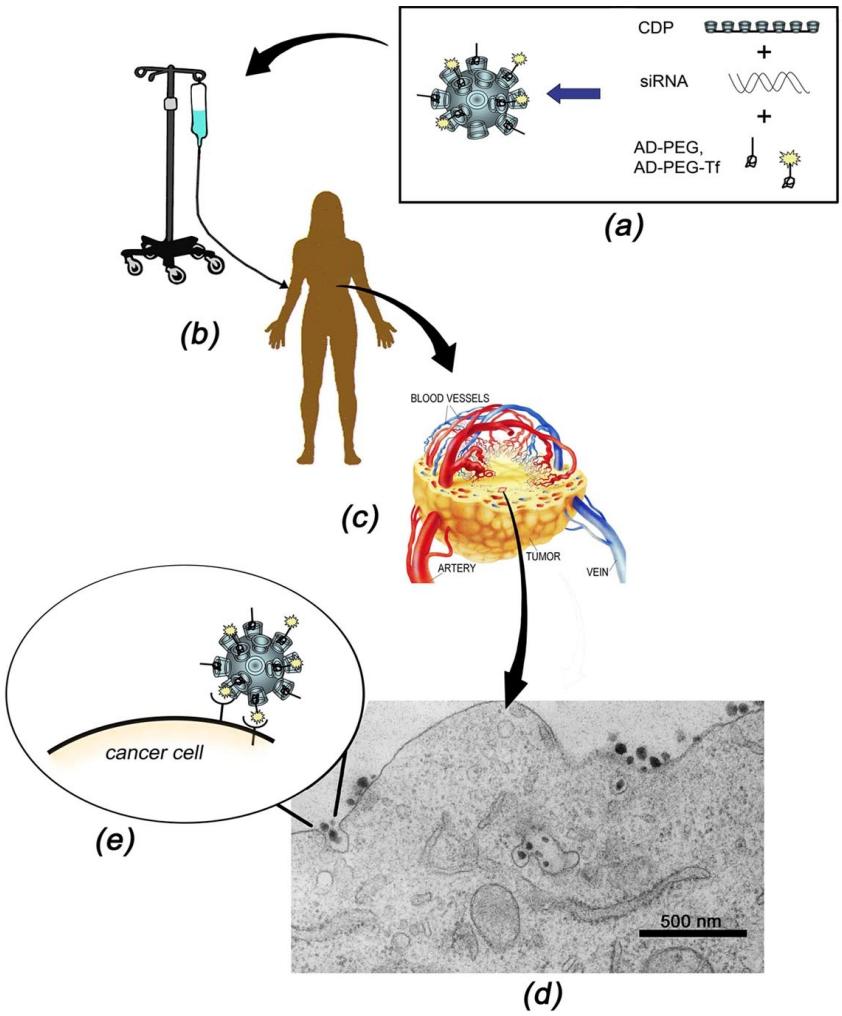

Figure 17: Schematic of how the targeted nanoparticles function. (a) Nanoparticles are assembled from the four components (see Figure 13). (b) Aqueous solutions of nanoparticles are infused into patients. (c) The nanoparticles circulate in the blood of the patient and escape via the "leaking" blood vessels in tumors. (d) Nanoparticles penetrate though the tumor and enter into cells by receptor-mediated endocytosis (transmission electron micrograph of 50 nm nanoparticles entering a cancer cell). Note that the nanoparticles enter and are initially located in vesicles within the cell and must escape and disassemble to delivery their payload. (e) Targeted nanoparticles can have numerous interactions (e.g.,Tf with its receptor) on the surface of the cancer cell that then stimulate the entrance into the cell. Figure from [191].

Initial animal experiments using the β-CD polymer, AD-PEG and AD-PEG-Tf delivery components utilized two different types of nucleic acids; namely, DNAzymes[240] and pDNA.[241] Results from those two investigations were consistent with one another and provided the basis for siRNA delivery in vivo. Intravenous injections of nanoparticles containing Cy-3-labelled DNAzymes were monitored by whole animal fluorescence imaging of tumor bearing mice.[240] Nanoparticles that did not contain AD-PEG or AD-PEG-Tf collected in the lungs presumably due to aggregation. However, when nanoparticles contained AD-PEG, there was no fluorescence observed in the lungs. These results suggested that the PEGylated particles did not aggregate in circulation. Tumor site fluorescence was obtained with nanoparticles containing AD-PEG and those with AD-PEG + AD-PEG-Tf. However, intracellular delivery within the tumor was only observed with the formulation that contained the AD-PEG-Tf. Intravenous injections of nanoparticles containing pDNA coding for the p53 gene were studied in nude mice bearing PC3 tumors (TfR positive and p53 null).[241] The nanoparticles were formulated with either AD-PEG or AD-PEG + AD-PEG-Tf. By using PCR methods, the biodistribution of the plasmid was determined. It was observed that the amount of the plasmid in the tumor was ca. 10% of the injected dose in the best cases and that there were no differences in the amounts of plasmid localized in the tumors when using nanoparticles that did or did not contain the AD-PEG-Tf. However, using RT-PCR, the amount of mRNA from the delivered p53 gene was measured. No mRNA was observed from the formulation absent of Tf, while the Tf containing formulation did give p53 mRNA.

The results of these two studies showed that the amount of nanoparticles localized in the tumors were independent of the presence of the targeting ligand (Tf). However, in both cases, the data are consistent with the Tf ligand providing greater tumor cell uptake (directly observed in the case of the DNAzyme and implied by the presence of the

mRNA for the case with the pDNA). Additionally, it is clear that the nanoparticles need to be PEGylated to provide for circulation without significant lung accumulation.

The initial demonstration of β-CD polymer-based delivery system formulated with siRNA (not chemically modified) utilized a disseminated murine model of Ewing's sarcoma.[242] siRNA against the breakpoint of the EWS-FLI1 fusion gene (siEFBP2) was shown to inhibit the gene product in vitro and that this inhibition provided an anti-proliferative effect. The rearrangement of the EWS and the FLI1 genes results in the EWS-FLI1 fusion gene that creates a transcription factor that regulates growth. Thus, elimination of this transcription factor by siRNA inhibition of the EWs-FLI1 mRNA can provide anti-proliferative effects. TC71 cells (TfR positive, EWS-FLI1 positive, human Ewing's sarcoma cells) constitutively expressing luciferase were injected into mice and their proliferation monitored by in vivo bioluminescent imaging. The treatment groups investigated were: (1) injection solution (D5W), (2) naked siRNA, (3) full formulation (illustrated in Figure 13) with a control siRNA (siCON), (4) full formulation with the anti-EWS-FLI1 siRNA (siEFBP2) and (5) formulation without the AD-PEG-Tf of the anti-EWS-FLI1 siRNA (siEFBP2). Only formulation (4) revealed any anti-tumor effects (Figure 18). Further studies indicated that the mRNA of the EWS-FLI1 gene was inhibited (Figure 19A) while other genes were not (Figure 19B) and no innate immune responses were obtained from any of these formulations. Thus, this work provided evidence to show that the correct sequence and the targeting agent were both necessary for biological efficacy. Further investigations with the β-CD polymer-based delivery system have been reported. Bartlett et al. showed via in vivo multimodal imaging (PET and bioluminescent) the kinetics of the biodistribution and gene inhibition function of the targeted and non-targeted versions of the nanoparticles.[32] Interestingly, the biodistribution amounts and kinetics were the same for the targeted and untargeted nanoparticles. Like with the delivery of the pDNA (p53 gene), the amount of siRNA

reaching the tumor was the same for the Tf targeted and non-targeted siRNA-containing nanoparticles. However, the luciferase gene inhibition was significantly greater for the Tf targeted nanoparticles. Thus, the primary effect of the Tf targeting ligand is to enhance tumor cell uptake not to change the amount localized in the tumor tissue. This conclusion has been obtained with a lipid-based delivery system as well.[243] Choi et al. created a series of PEGylated gold nanoparticles of constant size (80 ± 5 nm diameter) and constant zeta potential (-10 ± 0.5 mV) with variable targeting ligand (variations from 0-144 human protein transferrin molecules – Tf).[244] The biodistribution in tumor bearing mice were independent of the number of targeting ligands. However, the higher amounts of the targeting ligands greatly enhanced the number of nanoparticles localized into the cancer cells of the tumor from a systemic injection. Thus, there is a growing body of evidence supporting the concept that the targeting ligand on the nanoparticle does not influence tumor uptake but rather intratumoral distribution to the intracellular compartments of the cancer cells in the tumor tissue. That is not to say that a non-targeted nanoparticle does not enter tumor cells but rather that the targeted version of the nanoparticle should always outperform the non-targeted version.[244] Bartlett and Davis have shown this using a potent siRNA against ribonucleotide reductase subunit 2 (RRM2) in a murine tumor model.[245] The likely reason for the lack of anti-tumor efficacy with the non-targeted EWS-FLI1 siRNA was that the siRNA used in that study was not that potent (100 nM transfection in vitro gave 50% reduction in mRNA vs. ca. 1 nM transfection in vitro gave 50% reduction with RRM2). Given the results from these studies, the β-CD polymer-based delivery system was translated into clinical use.

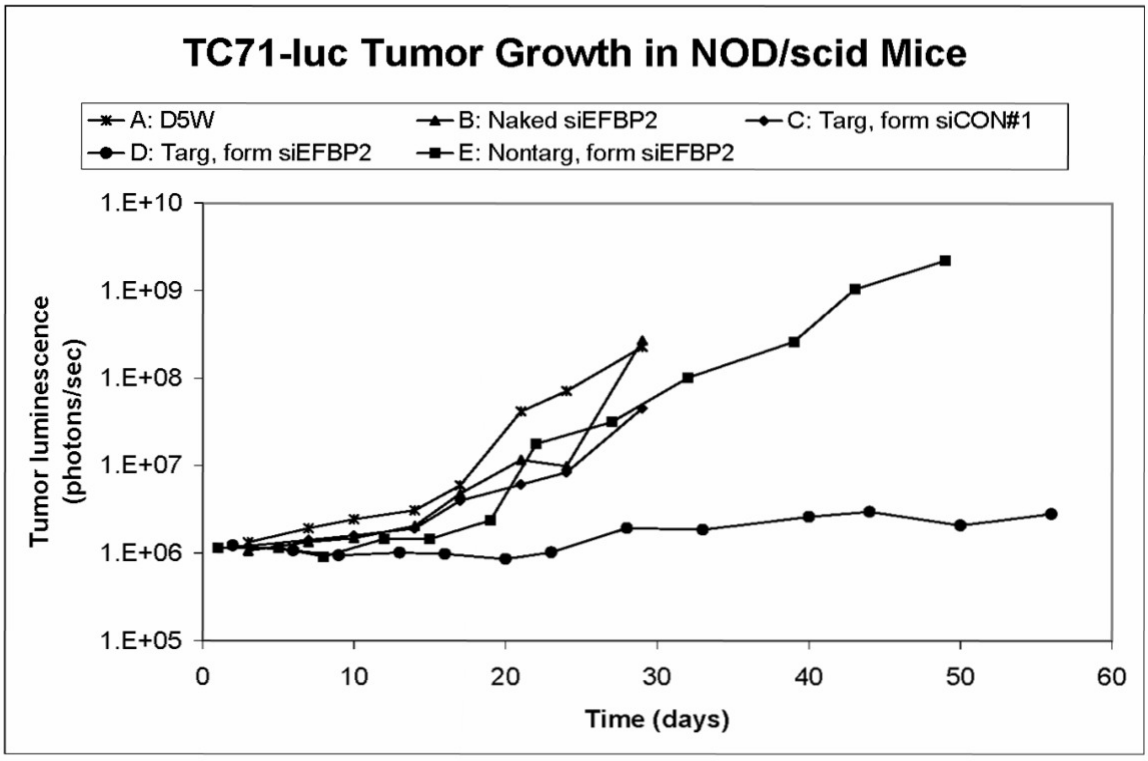

Figure 18: Effect of long-term delivery of siRNA formulations on growth of metastasized EFT in mice. Growth curves for engrafted tumors. The median integrated tumor bioluminescent signal (photons/sec) for each treatment group [n=8-10] is plotted versus time after cell injection. [Treatment groups: A, 5% (w/v) glucose only (D5W); B, naked siEFBP2; C, targeted, formulated siCON1; D, targeted, formulated siEFBP2; E, non-targeted, formulated siEFBP2.]. Figure adapted from [242].

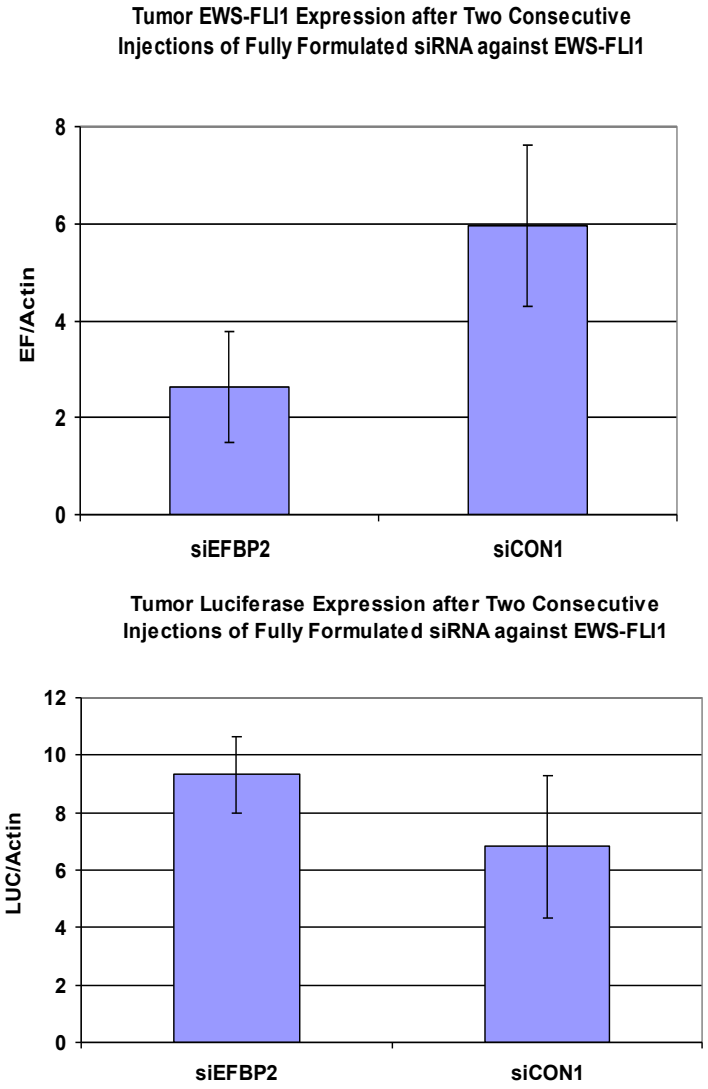

Figure 19: Effect of siEFBP2 formulations on mRNA. a.)EWS-FLI1 RNA level in tumors after two consecutive injections of fully formulated siRNA. b.) Luciferase (LUC) level in tumors after two consecutive injections of fully formulated siRNA. Formulated siEFBP2 or siCON1 were administered by LPTV injection on two consecutive days (Days 19 and 20) after injection of TC71-LUC cells. Tumors were harvested on the third day. RNA was extracted and mRNA levels were determined by qRT-PCR. Figure adapted from [242].

CALAA-01 is an experimental therapeutic that employed the β-CD polymer-based delivery system to formulate siRNA against ribonucleotide reductase subunit 2 (RRM2).[148] CALAA-01 employed Tf as the targeting agent and the siRNA was not chemically modified. The clinical material is a two vial formulation as illustrated in Figure 10A, potent siRNA against RRM2 was developed that exhibits significant antiproliferative activity in a broad spectrum of cancer types of human, mouse, rat and monkey.[52] The RRM2 sequence showed complete target site homology in mouse, rat and monkey and this greatly assisted in translating this siRNA into the clinic. A pilot safety study in non-human primates has been published.[149] This study was the first to show that multi-dosing of siRNA could be safely accomplished in a non-human primate. No complement activation and liver toxicities were observed at any dose level. When administered at 3 and 9 mg siRNA/kg, the nanoparticles were well tolerated. However, at 27 mg siRNA/kg, elevated levels of blood urea nitrogen and creatinine were observed indicating mild kidney toxicity (which was reversible). Additionally, at this dose level, IL-6 levels were increased (the cytokine IL-6 and other cytokines are indications of immune and other inflammatory responses). Multiple administrations spanning a timeframe of 17-18 days allowed for assessment of antibodies. Low titer, non-clearing (no changes in pharmacokinetics) antibodies to the human Tf on the nanoparticles were obtained. The antibodies were not against the PEGylated nanoparticles. This is important as clearing antibody generation in humans has been observed with PEGylated liposomes. In total, the multiple, systemic doses of the targeted nanoparticles containing the non-chemically modified siRNA were safely administered to non-human primates. Anti-tumor efficacy has been observed with mouse doses of 2.5-5.0 mg siRNA/kg in mice. Using body surface area normalizations, these dose levels translate to 0.6-1.2 mg siRNA/kg monkey. Thus, the predicted therapeutic window is quite large based on these data.

CALAA-01 is the first targeted delivery of siRNA in humans and was used to treat the first patient in a Phase I clinical trial in May 2008.[148,246] The Phase I trial design was a typical safety study, treating 24 patients with different solid tumors where standard-of-care therapies were not successful. CALAA-01 was administered via a 30 minute i.v. infusion on days 1, 3, 8, 10 of a 21 day cycle. The treatment of patients with CALAA-01 ushered in a new era of targeted experimental therapeutics. Other formulated siRNA therapeutics have followed, and these will be mentioned in the next section.

1.06 Polymer-Nucleic Acid Therapeutics in Human Clinical Trials

Over the past few years more and more polymeric/nucleic acid drugs have been tested in clinical trials, particularly with RNAi. Table 2 lists some of the trials that have been studied in this area. A few of these and others will be described below.

Table 2. Polymer-nucleic acid clinical trials.

Company	Drug	Target	Disease	Phase	Status	Identifier
Calando Pharmaceuticals	CALAA-01	RRM2	Solid Tumors	I	Terminated	NCT00689065
Silenseed	*siG12D LODER	KRASG12D	Pancreatic cancer	I II	Completed Recruiting	NCT01188785 NCT01676259
Arrowhead Research	**ARC-520	Conserved regions of HBV	HBV	I II II	Complete Recruiting Active	NCT01872065 NCT02065336 NCT02349126
BioCancell Ltd.	DTA-H19		Superficial Bladder Cancer, Ovarian Cancer, Pancreatic Neoplasms,	II II II	Complete Complete Active	NCT00826150 NCT00711997 NCT00595088
Sevion (Senesco)	SNS01-T	$eIF5A^{K50R}$ pDNA & eIF5A siRNA	B-cell cancer types - myeloma	I/II	Active	NCT01435720
Alnylam Pharmaceuticals	ALN-TTRsc ENDEAVOR	TTR - FAC	Transthyretin-mediated amyloidosis	I II II III	Recruiting Recruiting Active Recruiting	NCT01814839 NCT02292186 NCT01981837 NCT02319005

* Polymer scaffold loaded with siRNA directly administered to the tumor site.
** Polymer and siRNAs are a physical mixture and do not interact with each other. Polymer and siRNAs independently traffic to the various organs when administered to patients.

The first human clinical trial using a polycation-nucleic acid involved low molecular weight polylysine that was used to protect Poly I:C (polyinosine-polycytidylic acid: synthetic analog of double stranded RNA) from fast degradation by serum nucleases.[247] Poly I:C is used to stimulate an interferon response and thus an immune response that can lead to antitumor effects. Over the years there have been many (>40) Poly I:C/LC (Hiltonol) clinical trials; however, this drug has still not received FDA approval. Patients received systemic doses of this therapeutic by i.v. infusion. Toxicity responses observed in this study were hypotension, skin rashes, acute renal failure, and

polyarthralgia-myalgia. While significant serum interferon levels were detected, antitumor effects were not significant in adults; however, this drug still shows potential as an alternative to chemotherapy in children. Several Phase II trials currently being investigated include treating: brain tumors, central nervous system tumors, melanoma, myeloma, breast cancer, ovarian cancer, and adenomatous polyps.

Polylysine has shown potential in many studies and has been used in the clinic for several years. Two significant systems that utilized polylysine are (1) polylysine containing transferrin as a targeting ligand. This adenovirus enhanced transferrinfection (AVET) drug was used to deliver adenovirus into melanoma cells of patients.[248] The adenovirus, once internalized, delivers nucleic acid to the nucleus of the cells. Fifteen patients received skin injections of their own melanoma cells that were collected and then transfected ex vivo to produce the cytokine IL-2. This immunotherapy was well tolerated but was not investigated beyond the Phase I stage. (2) Low molecular weight polylysine (30 lysine units) terminated with PEG (10 kDa) was used to carry a gene encoding cystic fibrosis transmembrane regulator in a plasmid. The nanoparticles were administered to 12 patients via single intranasal dosing.[249] No serious adverse events were observed in this trial and evidence for gene transfer detected. Additionally, there was some functional data suggesting correction of chloride channel function. Unfortunately there have been no reports beyond the Phase I trial.

Polymers other than polylysine have been used in the clinic. PEI has been used to deliver plasmids for bladder cancer.[250,251] The H19 gene has been detected with high expression levels in human bladder cancers. A DNA plasmid that carries the gene for diphtheria toxin-A was combined with PEI for delivery to bladder cancer in humans. The initial treatment of two patients with confirmed high H19 expression using a direct injection into the bladder was first reported.[251] The treatments were well tolerated and evidence for ablation of the tumors provided. Of importance, no trace of the plasmid

could be detected in the bloodstream. Thus, the treatment did localize to the bladder without systemic exposure. Subsequently, the results from the Phase I/IIa clinical trial were published.[250] A total of 47 patients were treated and the overall results showed that the plasmid DNA delivered prevented new tumor growth in two-thirds of the patients and in 33% of the patients there was complete tumor ablation and in 64% there were no new tumors at 3 months. Prolonged time to recurrence was observed in responding patients, median time to recurrence was 11 months in all cases, and adverse events were mild.[252] This therapeutic, is currently in a Phase IIb clinical trial (active but not recruiting) as of early 2015.

As was mentioned above, the first polymer/siRNA targeted therapeutic nanoparticle that was used to treat a patient was in May of 2008. The nanoparticle contained human transferrin as the targeting ligand, a cyclodextrin-containing polymer, and siRNA.[191,246] The targeted nanoparticles were administered i.v. twice weekly. Results from this Phase I trial showed that the nanoparticle treatments were well tolerated, the nanoparticles localized intracellularly within melanoma tumor cells of patients in a dose-dependent manner (0.47-0.79 mg siRNA/kg), the targeted mRNA and protein were reduced by the treatment, and the correct mRNA fragment from the RNA interference mechanism of mRNA reduction was detected.[148,246] This clinical trial was terminated in 2013,[148] but was the first targeted polymeric based nucleic acid delivery vehicle. CALAA-01 shows the potential of these types of vectors, and may pave the way for future studies.

In 2008 Alnylam Pharmaculicals completed a Phase II trial of ALN-RSV01. This 88 patient study looked at delivering a chemically modified siRNA through inhalation to target respiratory syncytial virus. Since, Alnylam Pharmaceuticals has had several clinical trials involving polymer-DNA conjugates, some ongoing in Phase III trials. Their current Revusiran drug is an N-acetyl galactose based polymer chemically linked to

siRNA (see Figure 20). These GalNAc-siRNA conjugate platforms are administered subcutaneously and mainly target the liver (through the ASGP receptor). Data from the 26 patients in the pilot Phase II clinical trial with revusiran showed this drug to be well tolerated, rapid, dose dependent, and had good knockdown of mutant and wild-type transthyretin (TTR) protein (up to 98%), however, there were no significant changes observed in exploratory clinical measurements over the short experimental period. Revusiran was initially administered daily for 5 days and then weekly for 5 weeks at doses of 5.0-7.5 mg/kg. These positive data moved revusiran onto a Phase II trial in late 2013, and a Phase III trial in 2014. Revusiran is also currently on the FDA fast track approval list, and could be the first FDA approved polymer/RNA therapeutic. The current human clinical trials will show if this polymer platform can indeed demonstrate human translation and if so could enable a wide index of subcutaneous delivery of RNAi therapeuticsAlnylam also has a PEGylated lipid-based nanoparticle delivering siRNA, called Patisiran, in Phase II and III clinical trials (ongoing). This nanoparticle is comprised of hydrophobic lipid (Figure 20), a 2000 Da PEG polymer, cholesterol, and distearoylphosphatidylcholine, and has showed positive Phase I data.[253] The 49 patients in the study were split into two groups, whom were treated with different concentrations of two different lipid nanoparticles. Interestingly, the lipid formulations had similar physicochemical properties but different ionizable head groups, which appeared to play a key role determining potency.[254] The nanoparticles were all 100 nm in size and delivered intravenously, one time, but the second generation nanoparticle had more than twice the amount of gene knockdown for four times as long; showing the importance of pK_a (6.44) and head group ionization (see Figure 20). With a dose of 0.15 to 0.3 mg/kg of ALN-TTR02 (see Figure 20) the transthyretin knockdown ranged from 82% to 87%, and sustained reductions of 57 - 67% at 28 days. While there were no major side effects, 8% of subjects reported mild to moderate infusion-related reactions.[253] Phase II and III

clinical trials of Patisiran are ongoing, according to the companies website there are positive multi-dose results (see Figure 20) with sustained knockdown (>50%) for 28 weeks (injections administered every 4 weeks x 7).

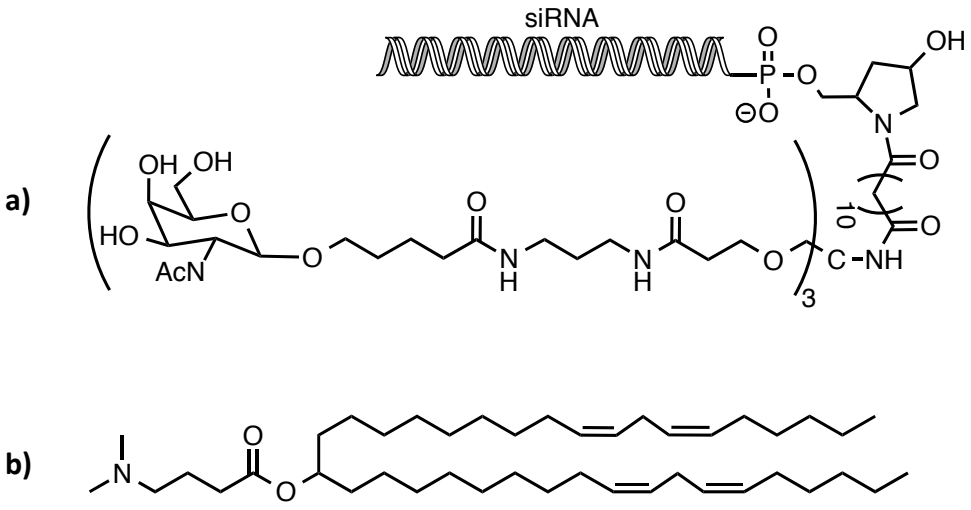

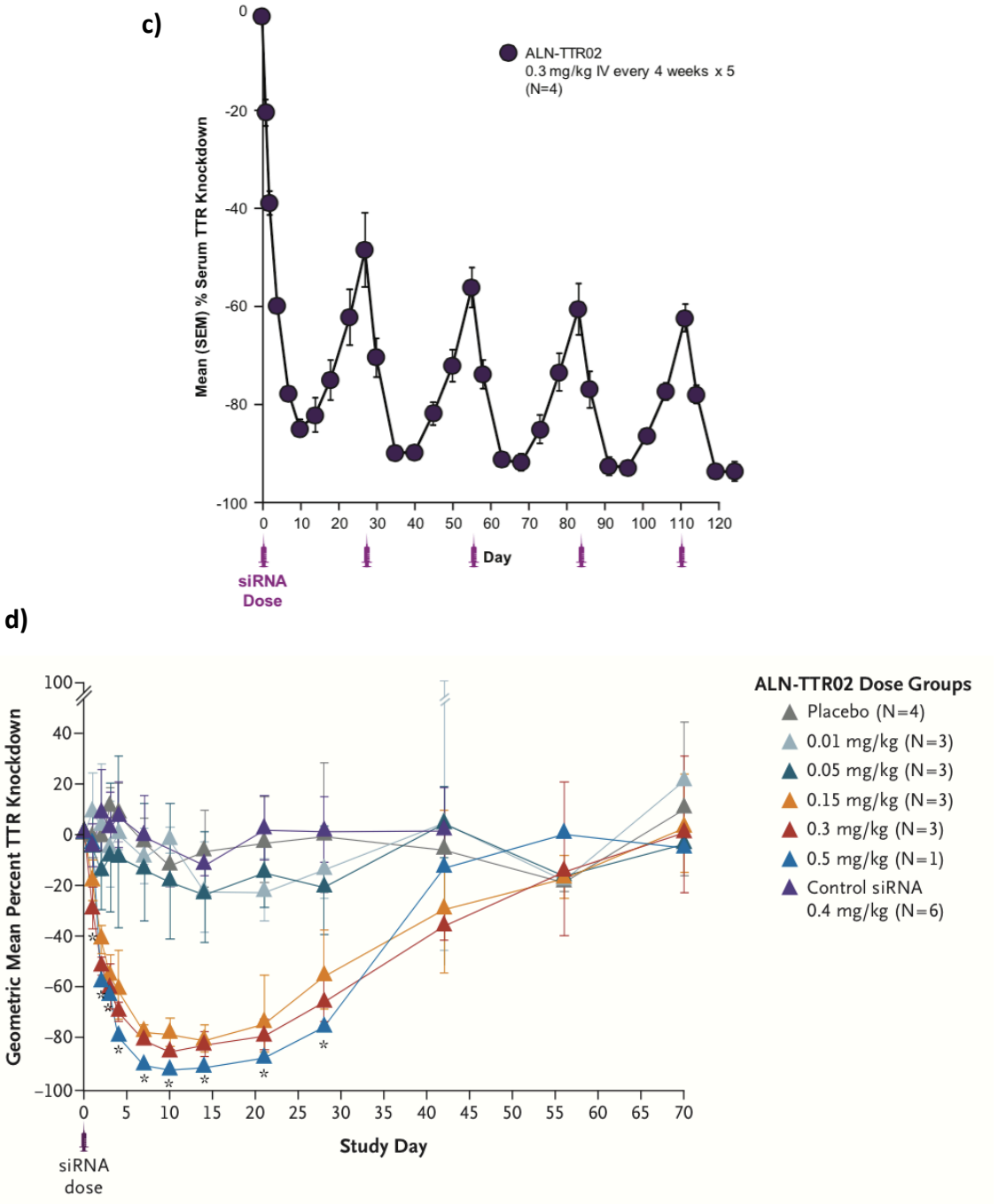

Figure 20: a) Revusiran (ALN-TTRsc) - a trivalent GalNAc carbohydrate ligand conjugated to siRNA to mediate targeted delivery to hepatocytes to treat amyloidosis. Revusiran is being used in Phase II and III clinical trials. b) The main component used in

the lipid formulation of Partisiran (ALN-TTR02), a lipid nanoparticle formulation used to encapsulate TTR-targeted-siRNA. Partisiran is in Phase II and III clinical trials. c) The dose dependent knockdown of Partisiran from a Phase I study. d) The multi-dose knockdown profile of Partisiran over four months with a 0.3 mg/kg dose administered five times via i.v. Figure adapted from [253].

Silenseed has completed a Phase I/IIa (2011-2013) trial with their LODER (LOcal Drug EluteR) polymer and is moving into a Phase II trial. The siG12D LODER drug comprises of a siRNA wrapped in a biodegradable polymer matrix that is injected into the pancreatic tumor during an endoscopic ultrasound biopsy procedure, and targets KRAS mRNA. The polymer conjugate is designed to slowly release the siG12D locally in the tumor and knockdown the mutated KRAS gene for a period of four months.[255,256] Fifteen patients were given LODER in a dose escalation design (0.025 mg, 0.75 mg, and 3.0 mg) as well as chemotherapy treatments simultaneously. The doses were all well tolerated, and no toxicity was observed. In fact, in all patients the tumor showed no progression for 12 weeks following treatment, 10 patients showed tumor regression, and median survival was increased by a few months.[257] This drug demonstrates the potential for locally administered polymer/nucleic acid conjugates, and is also being investigated in preclinical trials for prostate and brain cancer by Silenseed.

Sevion (previously Senesco) is currently in a Phase Ib/IIa clinical trial with their SNS01-T drug in patients with B-cell cancers. SNS01-T utilizes polyethylenimine (PEI) to self assemble the two (active) nucleic acid components.[258] These modulate apoptosis by delivering a siRNA and a pDNA that modulate Factor 5A (the eIF5A gene), which is the only known protein to be post-translationally modified with a hypusine residue.[259,260] The nanoparticles are delivered via intravenous infusion twice-weekly for 6 weeks followed by a 4 week observation period, then repeated at the next higher dose level;

starting at 0.0125 mg/kg (total nucleic acid dose), and increasing to 0.05 mg/kg, 0.2 mg/kg and 0.375 mg/kg (1:2 siRNA:pDNA wt/wt ratio). Sevion's siRNA and pDNA regulate the Facter 5A gene, which has the ability to control apoptosis and cell survival by controlling the expression of pro-apoptotic and anti-apoptotic proteins.[261] While the siRNA knocks down the eIF5A (pro-survival protein) the pDNA codes for a stable mutated eIF5A^{K50R} pro-apoptotic protein (single amino acid substitution), thus triggering cell death in B-cell specific cancers.[259] SNS01-T is a first-in-class modulator of eukaryotic translation initiation Factor 5A and is a promising target with broad potential application in multiple disease areas.[262]

Currently Arrowhead Research has two active Phase II trials involving their Dynamic PolyConjugates (DPC) delivery system involving siRNA–polymer therapeutics.[263] These conjugates (< 20 nm) take advantage of several interesting chemistries within cells (Figure 21). The siRNA is chemically conjugated via a hydrolysable S-S linkage to a cationic poly(butyl amino vinyl ether), which in turn is reversibly linked to GalNAc and PEG polymers, each component plays a specific role in the delivery process. First, the PEG acts as a shielding agent, prolonging circulation and enhances solubility, while the GalNAc targets the ASGP receptors on hepatocytes, and promotes uptake. Once the DPC is within the acidic environment of the endosome the GalNAc and PEG ligands are cleaved, resulting in a cationically charged poly(butyl amino vinyl ether). This membrane active polymer facilitates membrane disruption and endosomal escape. Thirdly, once the poly(butyl amino vinyl ether)-S-S-siRNA conjugate escapes the endosome, the disulfide bond is reduced in the cytosol, delivering the siRNA cargo.[264] This DPC system was administered in vivo through intravenous injection and effectively silenced two targeted genes (apolipoprotein B (ApoB) and peroxisome proliferator-activated receptor alpha (PPARA)) in the liver. Knockdown of ApoB was dose-dependent and resulted in lowered serum cholesterol levels.[265-267] In a Phase I

clinical trial, 36 healthy patients received ARC-520, doses ranged from 0.01 mg/kg to 2.0 mg/kg, all doses were well tolerated with no adverse side effects. Arrowhead is currently in Phase II trials and is focusing on patients with chronic hepatitis B virus, which is said to infect ~350 million people worldwide.

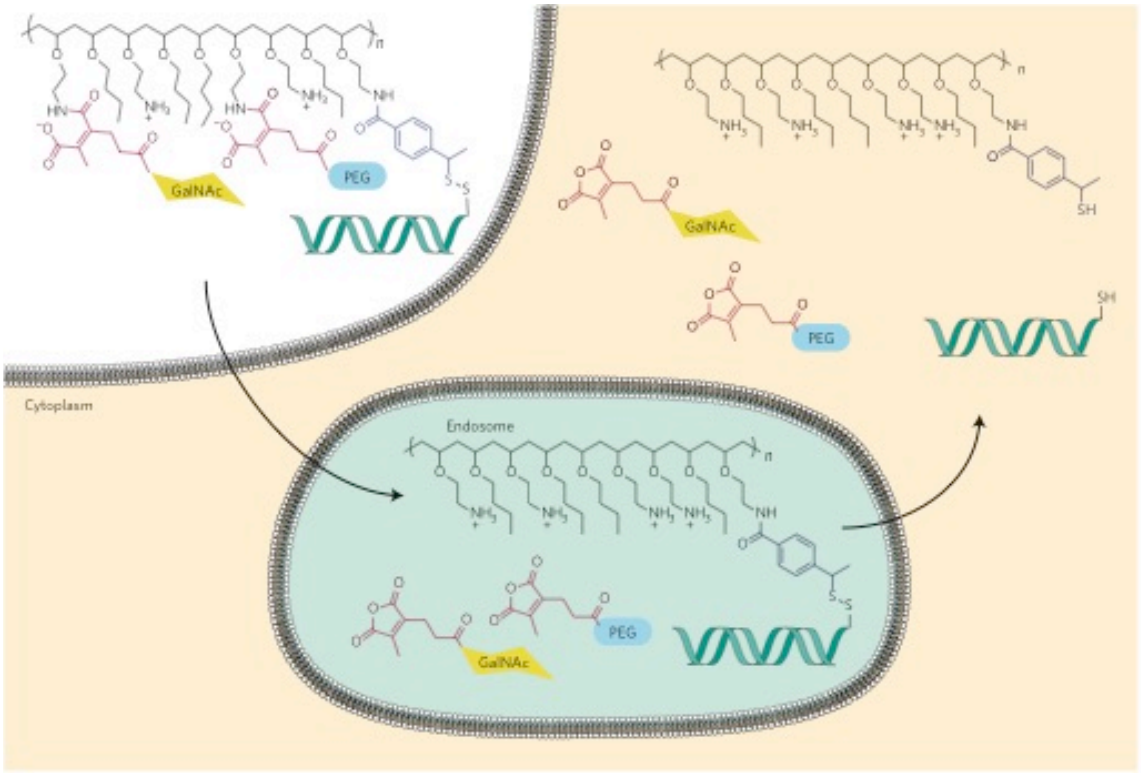

Figure 21: DPC materials are designed to respond to the acidic environment of the endosome and the reducing environment of the cytoplasm. In circulation, the polymer targets hepatocytes with the GalNAc targeting ligand. The membrane-disrupting poly(butyl amino vinyl ether) (black) is shielded by PEG. After cell uptake (endocytosis), the PEG chains are shed as the pH of the endosome lowers, exposing the polymer and causing endosomal release. In the cytoplasm, the disulphide bond linking the siRNA to the polymer is reduced, freeing siRNA to trigger RNAi. Figure from [263].

As we have mentioned, there are several ways being investigated to deliver nucleic acids to various target sites. This still remains the most challenging obstacle scientists in this field face: systemically-administered nucleic acids must survive in circulation long enough to reach their target tissue, circumvent clearance, enter the cells of target, travers the cellular matrix, dissociate from the "delivery packaging," and finally become incorporated into the nucleus or RNA-induced silencing complex (RISC), all while avoiding immunological side effects. A wide range of delivery techniques are being investigated, inhalation and injection were aforementioned, but other methods have been investigated as well. Oral delivery of siRNA therapeutics has been accomplished by engineering a β1,3-D-glucan-encapsulated siRNA particle (GeRPs).[268] The in vivo study had positive results, but unfortunately there have been no human trials involving this technique yet. There have been several articles published dealing with micro-needle arrays for the delivery of plasmid DNA[269] and siRNA[270] some even in Phase II clinical trials.[271] For example, TransDerm Inc. is currently investigating dissolvable micro-needles as well as a GeneCreme formulation, a topological delivery vehicle. Electroporation and jet injection have gained acceptance as delivery alternatives because they allow gene transfer into different tissues with naked DNA.[272-274] The gene gun uses pressurized air to force small volumes (3-10 μL) of naked DNA into targeted tissues, this technique is efficient for targeting small sites but has poor systemic and prolonged effects.[275] Several gene therapy trials have investigated non-viral gene integration (incorporation of new genetic material into the genome), such as the sleeping beauty transponson,[276,277] piggyBac,[278,279] and CRISPR-Cas9.[280-283] The discovery of these transponsons and gene editing systems are important to potentially cure genetic diseases by replacing or incorporating corrected sequences into the host genome.[284,285] In summary, there are many alternative routes for polymeric gene delivery, which makes up only a small portion of current gene therapy vectors (see Figure 22), the future success of

nucleic acid therapy lies heavily with the development of new and better targeted delivery vehicles and progress in human clinical trials.[286]

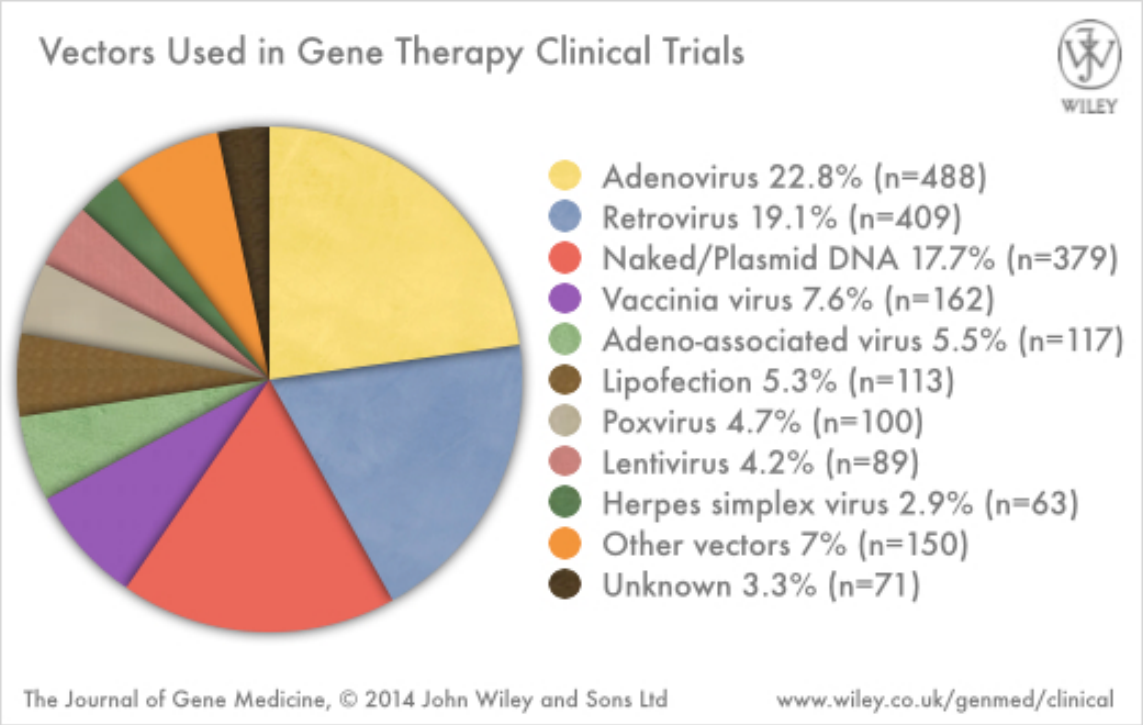

Figure 22 a) The total number of clinical trails up until 2014 divided into each trial Phase. b) The different vectors used in the total number of gene therapy trials to date. Figure adapted from [287].

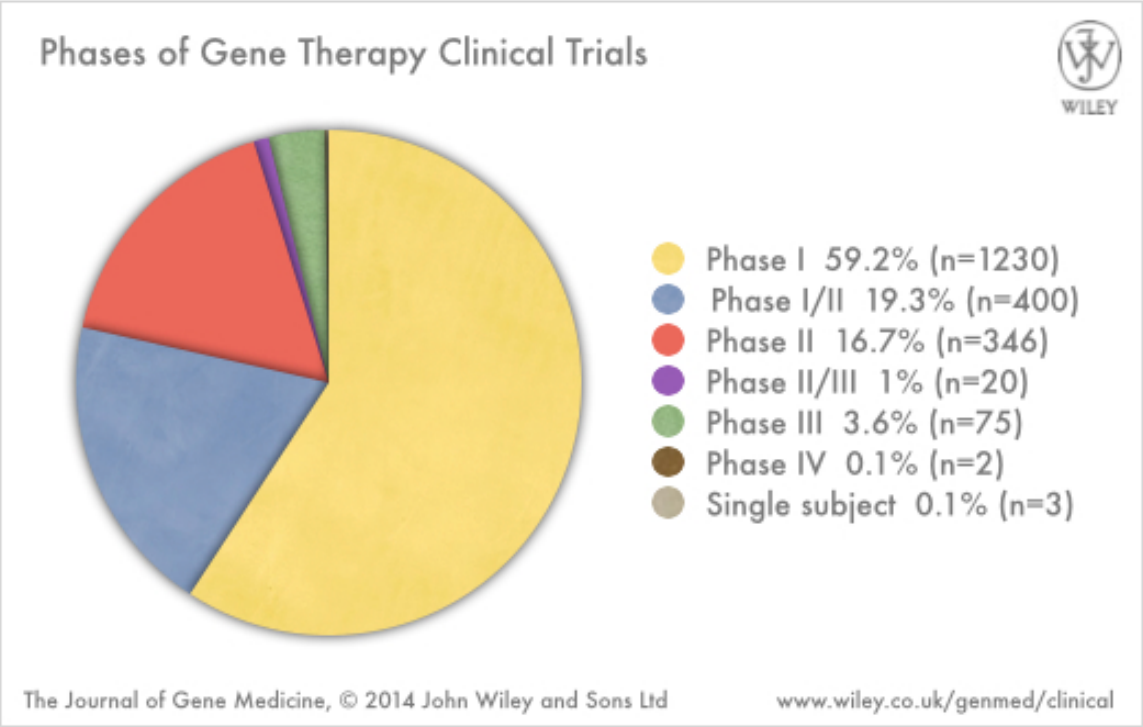

Figure 22 b) The different vectors used in the total number of gene therapy trials to date. Figure adapted from [287].

To date, there have been over 2000 gene therapy clinical trials worldwide, a few involving polymer-nucleic acid therapeutics that have had success in the clinic. At this time (beginning of 2015), only a handful are active while more are in the preclinical trial phases (most trials to date have been terminated or completed). As more clinical data are accumulated, the designs of the polymer components of the therapeutics are likely to improve. The key is that more human experience with polymer-containing therapeutics is needed. While animal experiments are useful, they are no substitute for human clinical trials. Our belief is that we are just at the beginning of the era of polymer-containing therapeutics. Clearly, there are many more polymer-drug conjugates that are being investigated in the clinic (primarily for cancer[287]), and our hope would be that polymer-nucleic acid therapeutics will follow this trend in the near future.

Chapter 2.

INVESTIGATING THE EFFECTS OF BLOCK VERSUS STATISTICAL GLYCOPOLYCATIONS CONTAINING PRIMARY AND TERTIARY AMINES FOR PLASMID DNA DELIVERY

Synopsis.

Herein is described the synthesis and characterization of nine novel polymers, and their efficacy of being DNA delivery vehicles. In an effort to find the right balance among nucleic acid uptake, toxicity, membrane permeability, and gene expression, the polymers, all similar in length, varied in composition between primary and tertiary amines, and their special arrangement (block vs. random). While tertiary amines are more toxic to cells they do have higher internalization and gene expression profiles; however these polyplexes were also not serum stable and aggregated over time. Microscopy and flow cytometry were used to visualize and quantify the amount of protein expression for each polymer respectively.

This chapter is adapted with permission from the refrence below. (Copyright 2014) Sprouse, D.; Reineke, T. M. *Biomacromolecules* **2014**, *15*, 2616–2628.

2.1 Abstract

Polymer composition and morphology can affect the way polymers interact with biomolecules, cell membranes, and intracellular components. Herein, diblock, triblock, and statistical polymers that varied in charge center type (primary and/or tertiary amines) were synthesized to elucidate the role of polymer composition on plasmid DNA complexation, delivery, and cellular toxicity of the resultant polyplexes. The polymers were synthesized via RAFT polymerization and were comprised of a carbohydrate moiety, 2-deoxy-2-methacrylamido glucopyranose (MAG), a primary amine group, *N*-(2-amino)ethyl methacrylamide (AEMA), and/or a tertiary amine moiety, *N,N*-(2-dimethylamino)ethyl methacrylamide (DMAEMA). The lengths of both the carbohydrate and cationic blocks were kept constant while the primary amine to tertiary amine ratio was varied within the polymers (see Figure 23). The polymers were characterized via NMR and size exclusion chromatography (SEC), and the polyplex formulations with pDNA were characterized in various media using dynamic light scattering (DLS). Polyplexes formed with the block copolymers were found to be more colloidally stable than statistical copolymers with similar composition, which rapidly aggregated to micron sized particles. Also, polymers composed of a higher primary amine content were more colloidally stable than polymers consisting of the tertiary amine charge centers. Plasmid DNA internalization, transgene expression, and toxicity were examined with each polymer. As the amount of tertiary amine in the triblock copolymers increased, both gene expression and toxicity were found to increase. Moreover, it was found that increasing the content of tertiary amines imparted higher membrane disruption/destabilization. While both block and statistical copolymers had high transfection efficiencies, some of the statistical systems exhibited both higher transfection and toxicity than the analogous block polymers, potentially due to the lack of a hydrophilic block to screen membrane

interaction/disruption. Overall, the triblock terpolymers offer an attractive composition profile that exhibited interesting properties as pDNA delivery vehicles.

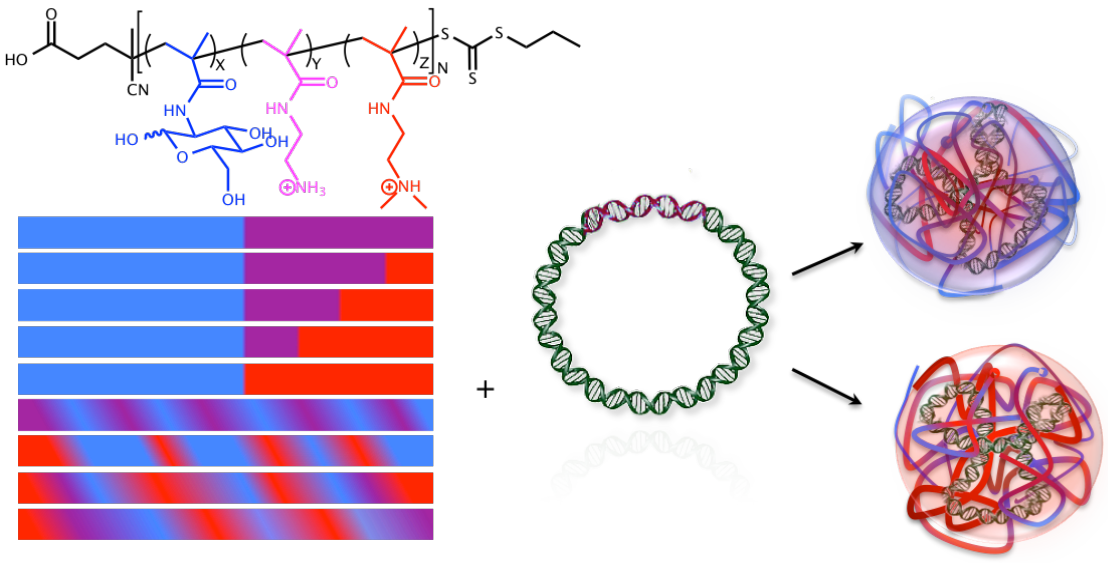

Figure 23. A depiction of the nine synthesized polymers forming polyplexes with pDNA.

2.2 Introduction

In the past decade there has been an increase in the search and development of alternative vehicles to condense and carry nucleic acids into cells. The delivery and expression of exogenous genetic material has shown potential in the fields of gene therapy, cancer treatment, organ transplants and vaccinations.[288-292] Delivery vehicles must be able to self-assemble with and protect nucleic acids from degradation, traverse vascular, cellular, and intracellular barriers, and finally efficiently deliver their payloads to the nucleus of cells where it can be transcribed and translated into protein.[288] Polymeric platforms have the potential to be developed as vehicles since the properties can be readily altered to enhance specificity and efficacy and they can be manufactured in bulk;[293] yet, much work is still needed to refine potential platforms for clinical application.

Typically, amines have been used to prepare cationic polymers for polyplex formation. Cationic polymers, such as polyethylenimine (PEI),[66,294] poly-L-lysine (PLL),[295] and polyamidoamine (PAMAM)[65,296] have been heavily studied for nucleic acid complexation in a fashion that promotes uptake, internalization, and transfection of cells. These polymers all have different compositions of charge centers ranging from primary, secondary, and tertiary amines. The difference in chemical properties of these polycations are of interest as they have different pK_a values and hydrophobicity profiles, which can affect cell membrane interaction, the polymer-nucleic acid binding strength, and dissociation of these species once within the cell.[122,297-300] PEI (linear PEI, pK_a = 8.44), a commercially available gene delivery vehicle, contains secondary amines along the backbone and has a general high transfection efficiency; however, it is toxic to some cell types.[122,172,301] The incorporation of carbohydrate moieties along a polycation backbone has been shown to reduce the cytotoxic response of polycation

vehicles.[27,172,301,302] In addition, glycopolymers have also been shown to interact with lectins, mimic biological functions, and can offer specificity in delivery.[172,303,304] Previously, a series of diblock copolymers containing a fixed length of carbohydrate block (2-deoxy-2-methacrylamido glucopyranose (MAG)) copolymerized with a cationic block consisting of primary amine (*N*-(2-amino)ethyl methacrylamide (AEMA)) were shown by our group to compact pDNA into polyplexes. These vehicles were found to be colloidally stable in physiological salt and serum conditions and exhibited high pDNA and siRNA internalization with low toxicity profiles. Interestingly, the efficacy for gene expression (pDNA) and gene knockdown (siRNA) was highly dependent on the cationic block length.[39] For pDNA, shorter AEMA block lengths lead to higher expression; it was speculated that the increase in cationic block length led to tighter binding and poor pDNA release once inside the cell. However, the opposite trend was found for siRNA, signifying that the short linear nucleic acid motif required a longer cationic block for stable encapsulation and effective gene knockdown.

Incorporating other charge center types (such as tertiary amines) and arrangement of these charges along the polycation backbone (i.e. statistical versus block) alters the pK_a value of the polycation. Indeed, this property can alter the strength of nucleic acid binding, pDNA release, polyplex charge, and possibly cellular interaction and toxicity. For example, 2-(*N,N*-dimethylamino)ethyl methacrylate has been incorporated into polymer vehicles and shown to successfully condense pDNA into polyplexes and facilitate transfection.[162,305-307] Incorporation of a tertiary amine into a polymeric vehicle is also thought to contribute to a buffering effect once within the acidic endosomal membranes in cells, whereas incorporating primary amine-containing aminoethyl methacrylate groups is thought to have a lower buffering effect.[161,308] Tertiary amines, such as *N,N*-(2-dimethyl-amino)ethyl methacrylamide (DMAEMA), may also impart a slight steric effect in comparison to primary amines (AEMA) when comparing the

binding of these cationic centers to the polyanionic DNA backbone.[300] Also, it has been reported that polymers containing a combination of AEMA and DMAEMA have an enhanced association with the cellular membrane due to hydrophobic interactions.[161] The two methyl groups on DMAEMA may allow insertion of the cationic amine into the phospholipid membrane, which can cause a negative Gaussian curvature.[309] Furthermore, statistical polymers composed of AEMA and 3-gluconamidopropyl methacrylamide have been shown to be less toxic and have higher gene expression than their block copolymer counterparts.[27] Dispersing the cationic charge throughout the entire length of the polymer, rather than confining it all into a block, may decrease binding affinity and promote pDNA release once within the cell. This could afford one the ability to add more amines per polymer chain and thus decrease the amount of polymer being added at the same N/P ratio, thus possibly making statistical polymers more efficient delivery vehicles.

To further understand the role of polymer composition in polyplex formation, delivery efficiency, and cellular cytotoxicity, a series of carbohydrate-containing polycations with varying ratios of primary and/or tertiary amines were synthesized via radical addition fragmentation chain transfer (RAFT) polymerization. Diblock, triblock, and statistical co- and terpolymers were created that contain a carbohydrate moiety (MAG), a primary amine (AEMA), and/or a tertiary amine (DMAEMA). Both the carbohydrate and cationic block lengths were kept constant while the content ratio of primary to tertiary amines was varied within the polymer models (Figure 23 and Figure 26). The goal of this study was to understand and compare the role of i) charge center composition (primary versus tertiary amines) and ii) polymer structure (statistical versus block) on polyplex formation, pDNA delivery, and in particular, cell membrane interaction and toxicity. Herein, we show that these factors play a large role in determining the efficiency of these delivery vehicles. Polycations containing primary

amines (AEMA) promote tight pDNA binding and form colloidally stable polyplexes. While these structures have a lower buffering effect in the cellular pH range they still promote high delivery and cell viability. Polyplexes formulated with polymers containing tertiary amine (DMAEMA) charges were found to have higher cellular internalization profiles but were significantly more toxic to cells (due to membrane destabilization). In addition, block versus statistical motifs were examined and it was found that as the amount of DMAEMA in the charge block increased, colloidal stability of the polyplexes and cell viability both significantly decreased.

2.3 Materials and Methods

2.3.1 Materials and Reagents

All solvents were purchased from Thermo Fisher Scientific. Cell Culture media and supplements were purchased from Life Technologies (Grand Island, NY). Human cervix adenocarcinoma (HeLa) cells were purchased from ATCC (Rockville, MD). For a comparison to previous literature and as a standard, JetPEI (linear PEI, PolyPlus Transfections, Illkirch, France) and Glycofect (Techulon, Blacksber, VA) polymers were also analyzed with the synthesized polymers. Glycofect is a degradable polymer (M_w = 4.6 kDa; degree of polymerization, n = 11, made at N/P = 20); JetPEI likely does not degrade during the time course of the experiment ($M_w \approx$ 22 kDa, N/P = 5). Polymers were analyzed with gel permeation chromatography (GPC) (Agilent, Santa Clara CA) equipped with refractive index and multiple angle light scattering detectors (Wyatt, Santa Barbara, CA) and nuclear magnetic resonance (NMR) (Bruker, Billerica, MA). A Bruker Avance III NMR equipped with BBFO Smart Probe operating at 500 MHz for ^{1}H and 125 MHz for ^{13}C was used for structural characterization. Polyplexes were analyzed with a gel electrophoresis kit (Invitrogen, Carlsbad, CA) and imaged using a Spectroline Bi-O-Vision UV transilluminator (Westbury, NY) and photographed with a 33mm lens 8 MP digital camera (Cupertino, CA). Zeta potential and dynamic light scattering (DLS) was measured on a Malvern Zetasizer Nano ZS (Worcestershire, UK). Lysed cells were analyzed on a BioTek Plate Reader (Winooski, VT) for absorbance and luminescence. Transfected cells were run on a BD FACSVerse (BD Biosciences**,** San Jose, CA) with dual lasers (λ = 488 nm and 640 nm), seven detectors, and analysed using FlowJo software (Ashland, OR). 2-deoxy-2-methacrylamido glucopyranose (MAG)[310] and 4-cyano-4-(propylsulfanylthiocarbonyl)sulfanylpentanoic acid (CPP)[311] were synthesized

as previously published. N-(2-amino)ethyl methacrylamide (AEMA) and *N,N*-(2-dimethylamino)ethyl methacrylamide (DMAEMA) were purchased from Polyscience (Warrington, PA) and 4,4'-azobis(4-cyanovaleric acid) (V-501) was purchased from Sigma-Aldrich (St. Louis, MO) and recrystallized twice from methanol.

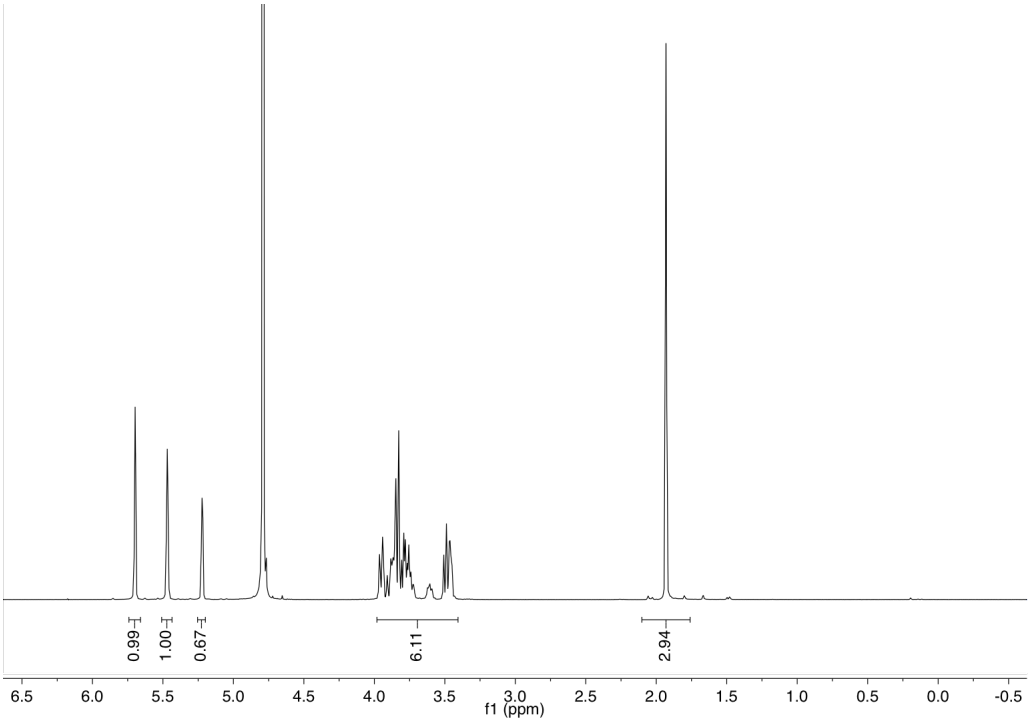

Figure 24. ^{1}H NMR spectra of the synthesized MAG monomer.

2.3.2 Methods

2.3.2.1 Polymer Synthesis

Polymers were synthesized by combining the monomer(s), chain transfer agent (CTA), and initiator at 1000:10:1 molar ratio respectively in 4:1 0.1 M acetate buffer (pH 5.2)/ethanol at 70 °C. The carbohydrate block was chain extended with AEMA and/or DMAEMA in 1 M acetate buffer (pH 5.2) at 70 °C.

2.3.2.2 Block Polymers

In a 50 mL round-bottom flask equipped with a magnetic stir bar, MAG (1.0 g, 4.04 mmol), CPP (11.22 mg, 40.4 μmols), and V-501 (1.13 mg, 4.04 μmols) were added in 40 mL 4:1 0.1 M sodium acetate buffer (pH 5.2)/ethanol. The vial was sealed with a rubber septum and purged with $N_{2(g)}$ for 2 hours before being heated in a hot oil bath at 70 °C for 1 hour. The reaction was quenched by exposure to air and purified via extensive dialysis with a molecular weight cut off (M.W.C.O.) membrane of 3500 g/mol against water for 4 days and then lyophilized. Poly-*block*(MAG) was characterized with GPC and NMR (Figure 25 and Figure 30).

Poly-*b*(MAG_{46}) (80 mg in each vial) was used as the macroCTA and chain extended with AEMA and/or DMAEMA in 1 M acetate buffer (pH 5.2) at 70 °C for varying amounts of time. The five block polymers were purified against water (pH 4) in a dialysis membrane for four days and then lyophilized. Polymers were characterized with GPC and NMR. (See Figure 30 and the Appendix)

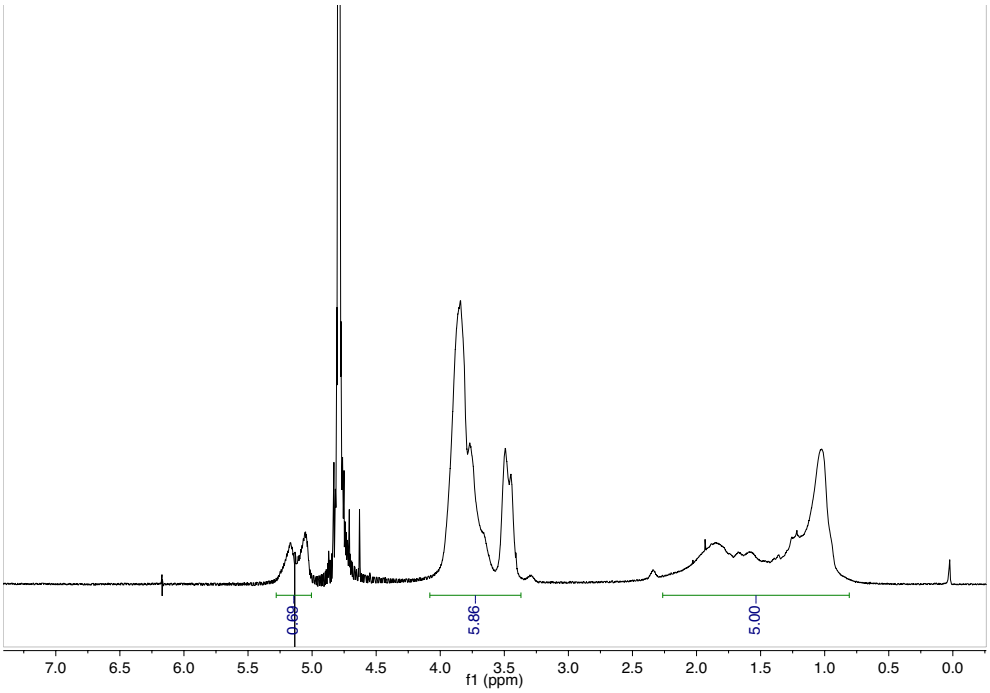

Figure 25. ^{1}H NMR spectra of poly($\mathbf{G}_{46}$)

2.3.2.3 Statistical Copolymers

In four separate 10 mL glass ampules equal molar amounts of a) MAG:AEMA; b) MAG:DMAEMA; c) MAG:AEMA:DMAEMA; and d) AEMA:DMAEMA:2×MAG (twice the molar equivalence of MAG to AEMA or DMAEMA) was added. The total monomer concentration was 0.25 M, dissolved in 4:1 0.1 M acetate buffer (pH 5.2)/ethanol. CPP and V-501 were added according to the previously specified ratios. Magnetic stir bars were added and the ampules were subjected to four freeze-pump-thaw cycles before being sealed and placed in a 70 °C oil bath for 2.5 hours. The reaction was stopped by quenching the ampule in liquid nitrogen and breaking open the seal. The polymers were purified against water (pH 4) via extensive dialysis (M.W.C.O 3500 g/mol membrane) for four days and then lyophilized before being characterized with GPC and

NMR (see figures in the Appendix). An example reaction of c) MAG:AEMA:DMAEMA is as follows: MAG (140 mg, 0.566 mmol), AEMA (93 mg, 0.566 mmol), and DMAEMA (88 mg, 0.566 mmols) was dissolved in 6.795 mL of 4:1 acetate buffer (pH 5.2)/ethanol solution. The chain transfer agent CPP (4.7 μg, 17 μmol) and initiator V-501 (0.48 μg, 1.7 μmol) were added last before the vial went through four freeze-pump-thaw cycles and was sealed and heated in an oil bath at 70 °C.

2.3.2.4 Reactivity Ratios

The kinetics of polymerization of each monomer and the reactivity ratios between the monomers were determined by NMR at 70 °C with pulses at regular intervals at specified times. The kinetics of each monomer was determined by plotting the conversion of each monomer to polymer over time. Monomer consumption was pseudo-first order (linear) when plotted.[297] For the reactivity ratios, monomers were combined in a pair wise manner and polymerized with V-501 in D_2O sodium acetate buffer (pH 5.2). The feed monomer mole fraction ranged from 0.10 to 0.90. The NMR tube was sealed with a rubber septum and purged with nitrogen gas for 30 minutes. An initial NMR was taken at room temperature, then the probe was heated to 70 °C and locked and shimmed on a dummy sample before insertion of the sample tube. The vinyl peak integration was monitored and the decrease in this signal was used to calculate monomer conversion into polymer (Figure 27). Total monomer conversion was kept below 10%. A Mayo-Lewis plot for f_1 and F_1 was utilized to determine the reactivity ratios (r_1 and r_2) - (the relative probabilities of monomer self-propagation to cross-propagation).[312-314] Gel permeation chromatography (GPC) was used to determine the molecular weight of the polymers while ^{1}H NMR was used to determine the molecular content of the polymers.

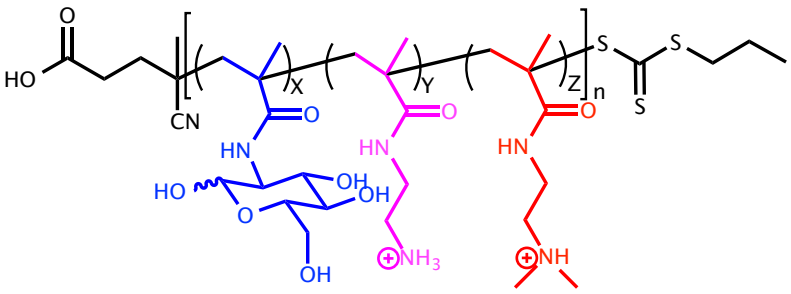

Figure 26. Synthesized copolymer structure, monomers are MAG_X (blue), $AEMA_Y$ (purple), and $DMAEMA_Z$ (red); poly($\mathbf{G}_X$-$\mathbf{P}_Y$-$\mathbf{T}_Z$) and where n is the total number of repeat units in the polymer.

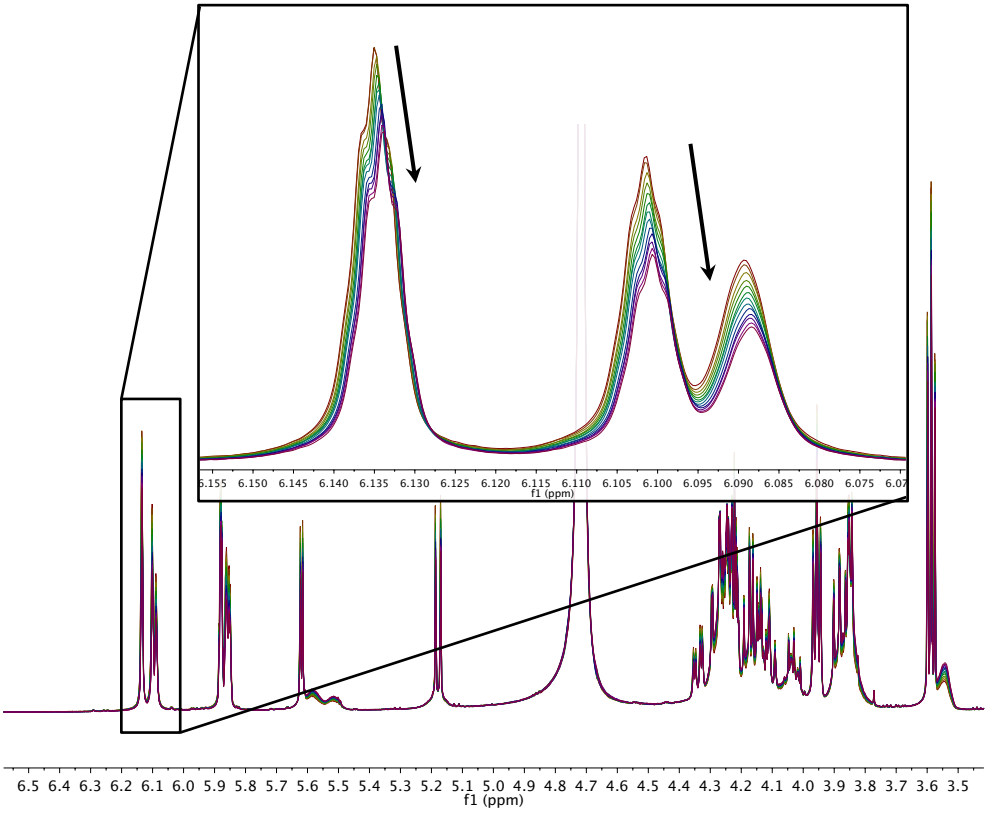

Figure 27. Overlays of ^{1}H NMR at 70 °C to monitor the consumption of two different monomers to find r_1 and r_2 in the reactivity ratio study. The monomers in this case were MAG and AEMA

2.3.2.5 Titrations

To measure the pK_a of the monomers, 0.10 M solutions of the AEMA and DMAEMA monomers were made in DI-water. The solution was first acidified to pH 1.0 with 1.00 M hydrochloric acid, and then 0.20 M NaOH was added in known increments at 25 °C and the pH was monitored with a AB15 digital pH electrode (Accumet Basic, Fisher Scientific, Pittsburg, PA). The potentiometer was standardized with buffers at pH 4, pH 7, and pH 10. Solutions of the same concentration (0.10 M, on a per monomer basis) of the homopolymers containing AEMA and DMAEMA were also made and similarly analyzed for pK_a and buffering capability in the same manner as above (Figure 28).

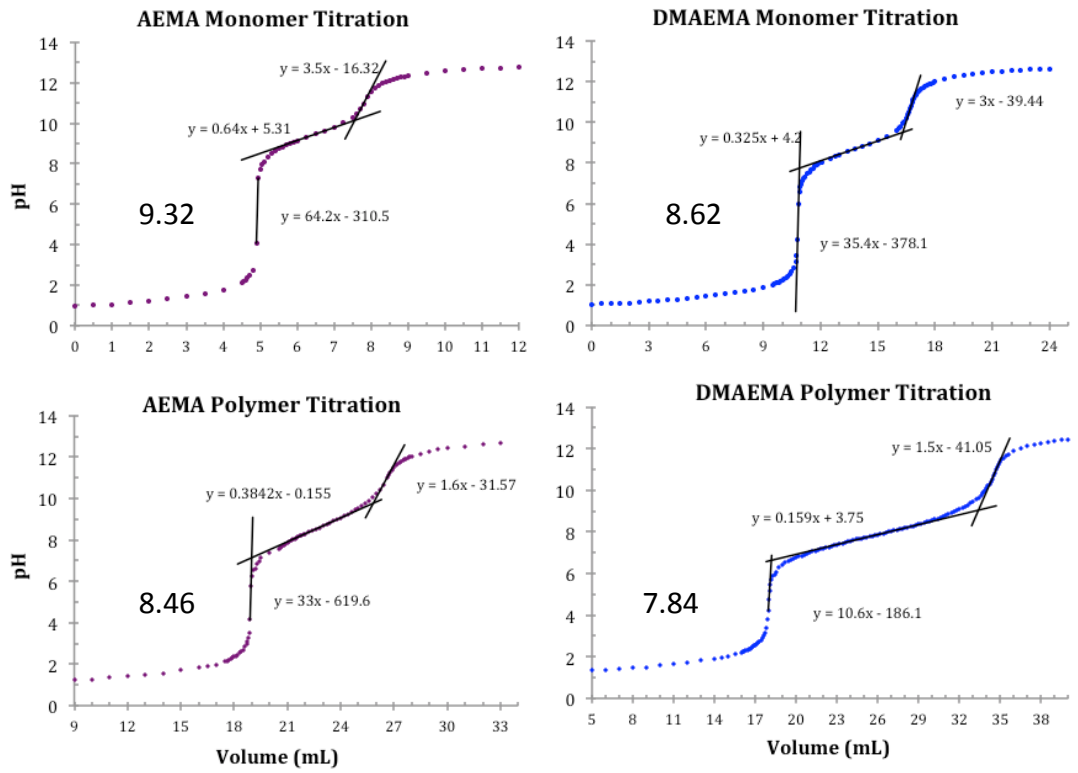

Figure 28**.** Potentiometric titration curves of AEMA and DMAEMA monomers and homopolymers. The solutions were acidified to pH 1 with 1M HCl and titrated with 0.20 mol L^{-1} NaOH. The pK_a of the AEMA and DMAEMA were 9.32 and 8.62 respectively while the pK_a of the primary and tertiary amine homopolymers were 8.46 and 7.84 respectively.

2.3.3 Polyplex Formation and Characterization

The polymers were solubilized in ultrapure H_2O to a determined N/P ratio/concentration before being used further in biological assays. All polyplexes were formed by adding equal volumes of the polymer solution to 0.02 µg/µL pDNA solution and the samples were then incubated for 45 minutes at room temperature. To determine the N/P ratio at which each polymer condenses the negatively charged phosphate groups on the backbone of DNA, a gel electrophoretic shift assay (Figure 29) was performed at N/P ratios from 0 to 10 in a 0.6% agarose gel containing ethidium bromide (6 µL/100 mL TAE buffer).

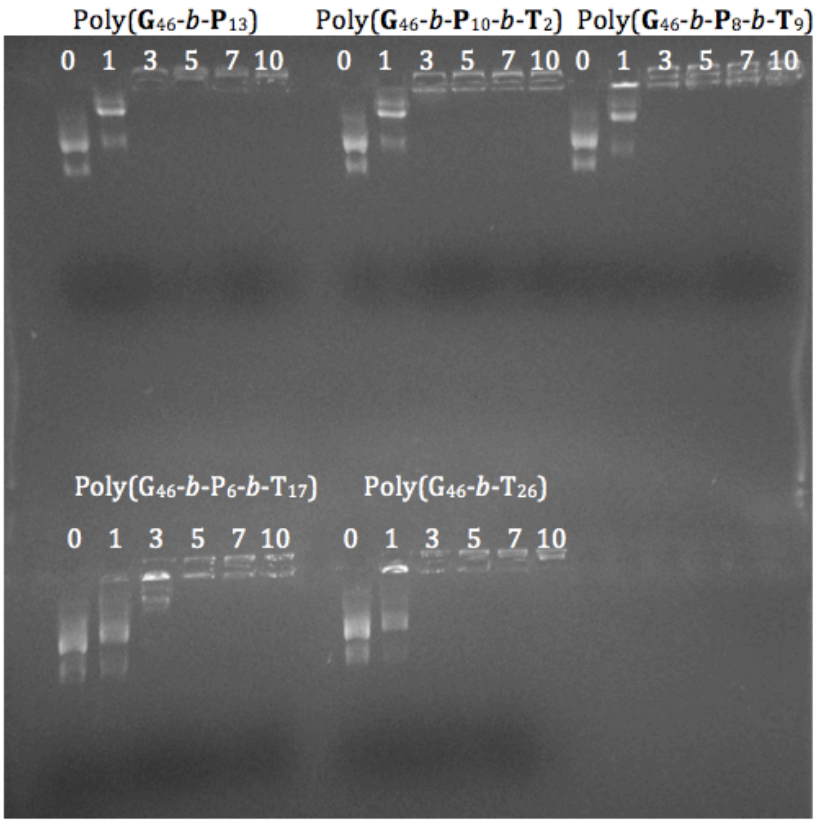

Figure 29. Gel Electrophoretic shift assay of the five block copolymers at N/P ratios 0, 1, 3, 5, 7 and 10.

2.3.3.1 Dynamic Light Scattering

The size of the polyplexes was measured by dynamic light scattering (DLS) at 633 nm on a Malvern Instruments Zetasizer Nano ZS (Worcestershire, UK) in water, Opti-MEM, and DMEM with 10% FBS. Stability was determined by measuring the size of the polyplexes at 0h, 2h, 4h, and 6 hours in water and media containing salts and proteins.

2.3.3.2 Cell Culture

Cell culture studies were done using HeLa cells. Cells were seeded at 100,000 cells/well in DMEM with 10% FBS in a 12 well plate (Corning, MA). Cells were cultured for 24 hours at 37 °C and 5% CO_2 to allow the cells to adhere to the plate before being washed with PBS and transfected with polyplexes. The total volume of the polyplex solution added was 600 µL (200 µL of polyplex solution and 400 µL of Opti-MEM). After four hours, 1 mL of DMEM with 10% FBS was added. 24 hours post transfection, the cells were washed with PBS and fresh DMEM (1 mL) was added. 48 hours post transfection the cells were analyzed in various assays to understand the toxicity and delivery efficiency of the polymers (described below).

2.3.3.2.1 Toxicity

The MTT (3-(4,5-dimethyl-2-thiazolyl)-2,5-diphenyltetrazolium bromide) assay has long been used as a reliable colorimetric assay for cell viability.[301,315] MTT assays were completed per the manufacture's instructions. In brief, 48 hours post transfection, the cells were washed with PBS and then 1 mL DMEM containing 0.5 mg MTT reagent was added to each well. The cells were incubated for 1 hour before being washed with PBS again and 600 µL DMSO was added to dissolve the purple formazan. The plate was

gently rocked for 10 minutes and 200 µL of the DMSO solution was removed and pipetted into a clear 96 well plate and analyzed by a BioTek (Winooski, VT) plate reader at 570 nm.

2.3.3.2.2 Gene Expression

Polyplexes were made with *gWiz-Luc* Luciferase Reporter plasmid DNA (*Photinus pyralis*) (Aldevron, Fargo, ND), coding for firefly luciferase gene. 48 hours post transfection, the cells were washed with PBS and lysed with 100 µL 1X Luciferase Cell Culture Lysis Reagent. After 30 minutes of incubation, 5 µL of lysed cells was pipetted into an opaque 96 well plate. After adding 95 µL of Luciferin Reagent to each well, the luminescence was measured with the BioTek plate reader.

2.3.3.2.3 Cell Viability, Membrane Permeabilization, and pDNA Internalization

A general protocol was used to analyze the polyplex formulations for toxicity, ability to permeabilize the cell membrane and promote pDNA internalization. pCMV-LacZ pDNA was labeled with Cy5 per the manufacture's instructions (Mirus Bio LLC, Madison, WI). Cells were plated at 100,000 cells/well in 1 mL DMEM in a 12 well plate. The cells were washed with PBS prior to transfection. Polyplexes (200 µL) were added to the cells in Opti-MEM (400 µL). Four hours post transfection, the cells were washed with PBS and trypsinized (500 µL) for 10 minutes before DMEM (500 µL) was added. The cells were transferred to a falcon tube and centrifuged at 1000 × g for 10 minutes at 4 °C. Most of the media was removed and 1 mL 1X Binding Buffer (eBioscience, San Diego, CA) was added to each falcon tube and vortexed before being centrifuged again for 10 minutes at 4 °C. The media was removed and 100 µL 1X Binding Buffer containing 2 µL Annexin V (eBioscience) was added. The falcon tubes were vortexed and allowed to sit

at room temperature for 10 minutes before another 1 mL aliquot of 1X Binding Buffer was added. The falcon tubes were then centrifuged again. The media was removed and 100 µL of 1X Binding Buffer containing 5 µL 7-AAD Viability Staining Solution (BD Biosciences, San Jose, CA) and 50 µL CountBright Absolute Counting Beads (Life Technologies, Grand Island, NY) were added. Each sample was vortexed again before being analyzed on the Flow Cytometer. 20,000 events were collected per falcon tube and the experiment was performed in triplicate. The data was analyzed in FlowJo software and gates were determined from the double negative (cells only) and negative staining samples (Cells + Annexin V, Cells + 7AAD, Cells + Cy5 pDNA) as seen in the Appendix (Figure 81).

2.3.3.2.4 Microscopy

Cells were plated on Delta T dishes (Bioptechs Inc., Butler, PA) 24 hours pre-transfection at 50,000 cells in 1 mL of DMEM. Cells were washed with PBS before being transfected with 100 µL of polyplex solution (0.01 µg/µL pDNA) at an N/P ratio of 10 in 1 mL of Opti-MEM. The Delta T dish was covered with a Delta T heated glass lid and fitted to the EVOS Digital Microscope adapter stage (AMG Life Technologies, Grand Island, NY) and warmed to 37 °C. Carbon dioxide gas was supplied to the Delta T dish at 1 mL/min. The cells were viewed at 40 × magnification under transmitted light and fluorescence at 628 nm. Images of the cells were captured every 10 seconds for four hours and later compiled at 60 fps into a 24 second movie clip. Cells were also transfected with a green fluorescent protein (GFP) encoding plasmid (pZGreen) (Clontech), cells were imaged 48 hours post-transfection at 40 × objective under transmitted light and fluorescence at 470 nm and 350 nm.

2.4 Results and Discusion

2.4.1 Synthesis and Characterization of Polymers

2.4.1.1 Synthesis

The block and statistical copolymer models were synthesized via RAFT polymerization. RAFT is compatible with aqueous solvents and gives excellent control over the degree of polymerization without using harmful metal catalysts. [288,293,310,316-318] The first polymer synthesized was the polyMAG CTA (MAG is denoted as **G** in the polymers) poly($\mathbf{G}_{46}$). The purified polymer was characterized with ^{1}H NMR (Figure 24 and Figure 25) and shows the disappearance of the vinyl resonances at σ 5.5 (1H) and 5.7 (1H) ppm and the appearance of the methylene groups, CH_2 (2H), in the polymer backbone from 1.5 – 2.3 ppm. GPC analysis revealed the M_n to be 11.7 kDa (n=46) and a low dispersity index ($Đ$ = 1.02) signifying high control in the polymerization. The poly(G_{46}) macroCTA was then chain extended with primary amine monomers (AEMA denoted as **P** in the polymers) and/or the tertiary amine monomers (DMAEMA denoted as **T** in the polymers). The statistical copolymers were prepared by adding the monomers with CTA and initiator together and then heated under a nitrogen atmosphere. To ensure that the statistical copolymers had a similar composition to that of the monomer feed ratio, the polymerizations were run to high conversions; thus, leading to longer polymers with slightly higher dispersities. Data for the nine block and statistical copolymer analogs are shown in Table 3 and ^{1}H NMR spectra can be found in the Appendix.

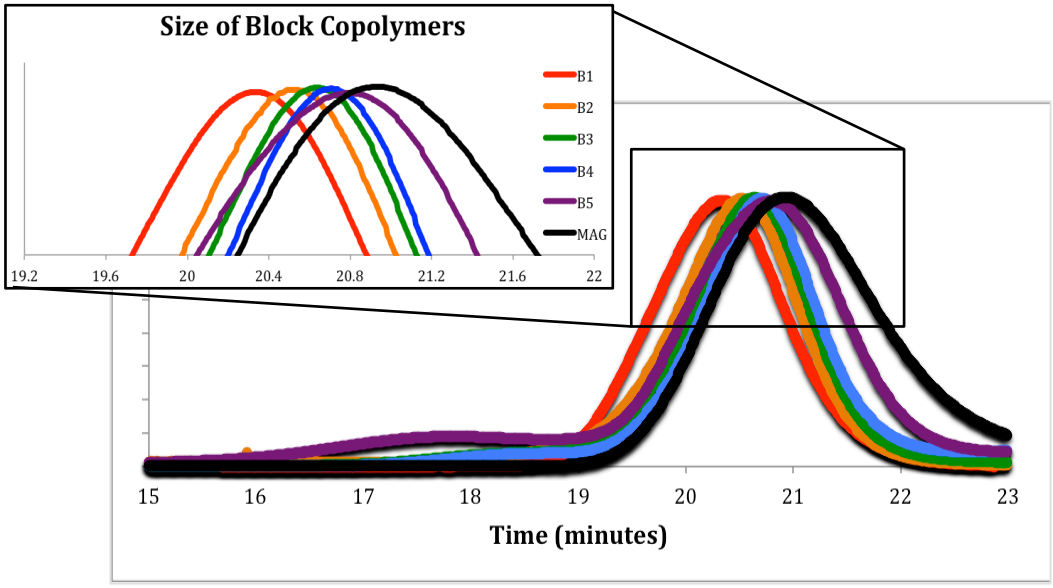

Figure 30. Aqueous Size exclusion chromatogram of the block polymers overlayed. M_w and $Đ$ can be found in Table 3.

Table 3. Molecular Characterization of the Synthesized Block and Statistical Copolymers". [a] Molecular weight (M_n) and dispersity (Đ) determined by gel permeation chromatography. [b] Number of repeating units (M_n/M_0) in each polymer determined by ^1H NMR spectroscopy in D_2O at 500 MHz with a relaxation delay of 10 seconds.

Polymers	M_n (kDa)[a]	Đ[a]	MAG[b]	AEMA[b]	DMAEMA[b]
Poly(G_{46}-*b*-P_{13})	13.1	1.02	46	13	
Poly(G_{46}-*b*-P_{10}-*b*-T_2)	13.2	1.02	46	10	2
Poly(G_{46}-*b*-P_8-*b*-T_9)	13.8	1.02	46	8	9
Poly(G_{46}-*b*-P_6-*b*-T_{17})	14.8	1.03	46	6	17
Poly(G_{46}-*b*-T_{26})	15.3	1.04	46		26
Poly(G_{45}-*s*-P_{35})	15.5	1.03	45	35	
Poly(G_{62}-*s*-T_{23})	19.1	1.16	62		23
Poly(G_{32}-*s*-P_{40}-*s*-T_{21})	16.3	1.14	32	40	21
Poly(G_{47}-*s*-P_{28}-*s*-T_{18})	18.0	1.14	47	28	18

2.4.1.2 Characterization

After the copolymers were synthesized and purified, ^{1}H NMR (Appendix) was utilized to characterize the polymer composition while GPC was used to analyze the molecular weight and dispersity. The four statistical copolymers are represented in Table 3. Although the composition of the statistical copolymers can be determined with NMR and GPC, the ordering of the repeating units can only be understood as a function of monomer relative reactivity ratios.[314] The reactivity of AEMA, DMAEMA, and MAG was examined in a pair-wise fashion using conventional free-radical polymerization. By varying the molar fraction feed (f_1) of monomer (r_1 and r_2) and monitoring the polymer composition (F_1) the reactivity ratios could be calculated using the non-linear Mayo-Lewis equation.[312,313]

$$F_1 = \frac{r_1 f_1^2 + f_1 f_2}{r_1 f_1^2 + 2 f_1 f_2 + r_2 f_2^2}$$

The reactivity ratios of the three monomers (Table 4) show that the statistical copolymers are slightly gradient in nature; being that $r_{MAG} > r_{AEMA}$ and r_{DMAEMA}. These data signify that the MAG monomer prefers to react with itself in the presence of the other two monomers and AEMA and DMAEMA prefer to cross-propagate in the presence of MAG; however, they do not have a preference for reacting with the other charged monomer or themselves. This leads to polymers that likely have a higher concentration of glucose moieties on one end of the polymer and alternating AEMA and DMAEMA charged moieties in the case of the statistical copolymers synthesized with all the monomers.

Table 4. The reactivity ratios of the three monomers used in the statistical copolymers, determined by altering the feed ratio (f_1) of each monomer and polymerizing using a free-radical approach at 70 °C in a 500 MHz variable temperature NMR. The r_1 and r_2 values were calculated from equation 1. $r_1 = (k_{11}/k_{12})$ and $r_2 = (k_{22}/k_{21})$.

↓ r_1 r_2 →	MAG	AEMA	DMAEMA
MAG	-	1.54	0.88
AEMA	0.30	-	0.63
DMAEMA	0.19	0.61	-

2.4.1.2.1 Titrations

Many previous studies have shown that the charge center type within polymeric vehicles has a large effect on the polymer-pDNA binding strength (polyplex stability), the interactions of the polymer with the cell membrane, and the buffering capacity in the biological pH range. Thus, incorporating primary and/or tertiary amines within these polymer structures alters the pK_a of the polymers significantly and thus, the above properties. To determine and compare the pK_a values of the AEMA and DMAEMA monomers and homopolymers, titrations were performed (Figure 28). As expected, the tertiary amine DMAEMA monomer and polymer was found to have a lower pK_a than that of the primary amine AEMA derivatives. It was also found that the homopolymers of these monomers had a lower pK_a than the monomers themselves (Table 5). This phenomenon has been studied in detail by Lee *et al.*[319] The values of DMAEMA in Table 3 closely match those reported by van de Wetering *et al.*, who reported pK_a values of 8.5 and 7.8 for the monomer and polymer, respectively.[166,288] Both the primary and tertiary amine groups are fully ionized in the monomers at a pH of 5.2, which was the rationale

for selecting this pH for statistical and block copolymer synthesis. The higher pK_a of the primary amine moieties leads us to hypothesize that polyplexes formed with AEMA charge centers could be more tightly bound than that of polyplexes formed with polymers containing DMAEMA. Additionally, the two methyl groups on the tertiary amine (particularly when not protonated) may also provide more of a hydrophobic character to the polymer, which could influence interactions with the cell surface and various biomolecules.

Table 5. The pK_a values of the AEMA and DMAEMA monomer and homopolymer. The pK_as were determined by adding 0.20 mol L^{-1} NaOH at 25 °C to a solution of AEMA and DMAEMA monomer and homopolymer.

	Monomer	Polymer
AEMA	9.32	8.46
DMAEMA	8.62	7.84

2.4.2 Polyplex Formation

The N/P ratio is a molar ratio between positively charged nitrogens (N) on the polymer and negative phosphate (P) groups on the backbone of the pDNA. It should be noted that N/P ratio (the concentration of amines) in solution is being compared between the different polymer systems (and the polymers are being compared at the same N/P value); therefore, depending on the composition of the polymer, the concentration of the polymer chains in solution will not be the same between the different systems analyzed (i.e. polymers containing a higher content of amines are typically less concentrated in solution). From the gel mobility shift assays (Figure 29 and Appendix) it can be observed

that the free pDNA (0 N/P) travels through the gel to the positive electrode but by 5 N/P, the pDNA is completely bound by the polymers, as it is stationary in the loading well. The Zeta potential (Figure 31) was also measured for the polyplexes formulated at 5 N/P. The Zeta potential for all polyplexes was positive, generally found to be between +10 mV and +35 mV for the polyplex solutions. Moving forward, two N/P ratios (5 and 10) were chosen to assess complex stability from aggregation in water, Opti-MEM, and DMEM (containing 10% FBS). Previously, we have shown that polyplexes formed with diblocks of MAG and varying lengths of AEMA were stable in cell culture media and did not flocculate over time.[39] It has also been shown by others that polyplexes formed with poly(*N,N*-(2-dimethylamino)ethyl methacrylate) have a size to N/P ratio relationship; at lower N/P ratios the polyplexes were larger (~1000 nm) but at high N/P ratios the polyplexes were uniformly smaller (<200 nm in water and ~600 nm in serum containing solution).[320] Our polyplexes were formed at N/P ratios of 5 and 10 to assess the biological relevance of the complexes with respect to complex stability, toxicity, cellular internalization, and transgene expression.

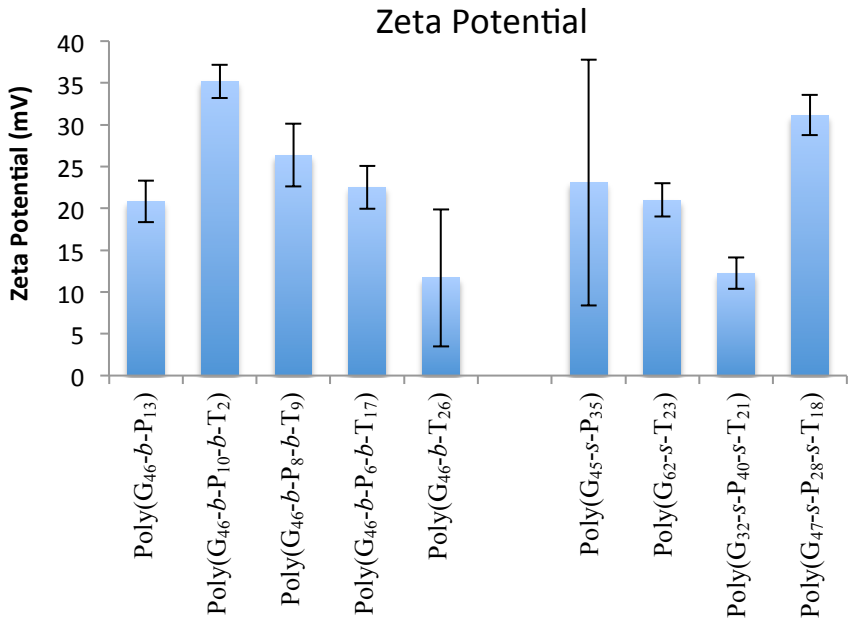

Figure 31. The zeta potential of the formulated polyplexes at 10 N/P diluted in water. Standard deviation was taken from three separate ζ measurements. All formulations had a positive zeta value.

2.4.3 Stability

The stability of these polyplexes was determined by monitoring the size/aggregation of particles in water, Opti-MEM, and DMEM containing 10% FBS over the period of 6 hours. All the polyplex types were stable in water as the size did not change (generally around 100 nm) over the course of 6 hours. When the polyplexes were added to cell culture media (Opti-MEM, Figure 32 and Table 10) some of the polyplex formulations aggregated with time, which was highly dependent on the polymer chemistry and tertiary polyplex structure. The flocculation seen in Opti-MEM is most likely occurring because the increased concentration of salts in solution decreases the Debye length.

It was presumed that all the block polymers would promote colloidal stability in the polyplex formulations by coating the core-shell polyplex structure with a hydrophilic polymer. This was clearly noticed in polyplex formulations with the AEMA charge centers Poly(G_{46}-*b*-P_{13}) compared to the analogous polyplexes formed with DMAEMA Poly(G_{46}-*b*-T_{26}). However, this was not the case with two of the triblock polymers, which aggregated to ~700 nm. It appears that polyplexes formed from the block polymers comprised of all three monomers had colloidal stability that diminished as more of the DMAEMA monomer was incorporated, leading to polyplexes that rapidly aggregated.

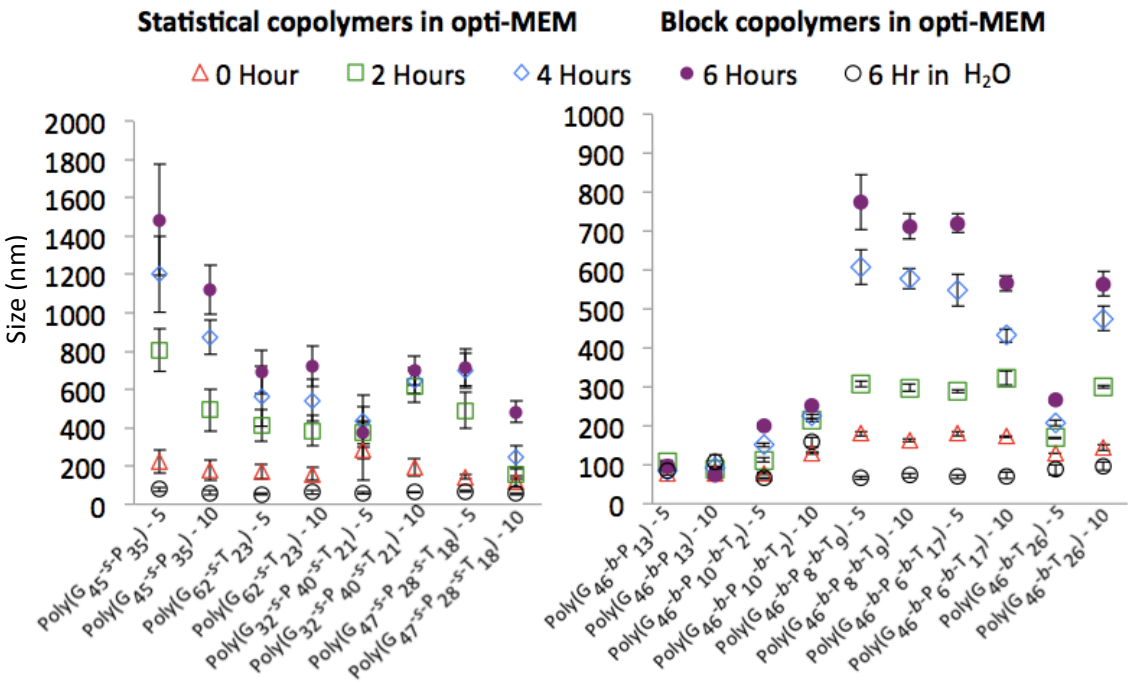

Figure 32. DLS measurements show the hydrodynamic diameter of the polyplexes formed at 5 and 10 N/P with the statistical and block copolymers developed herein. Polyplex size was analyzed in water and Opti-MEM and the size was measured by dynamic light scattering (DLS) at 633 nm on a Malvern Instruments Zetasizer Nano ZS at 173° back angle scatter; time zero is when the polyplexes (formulated in water) were added to Opti-MEM. Error bars are the standard deviation of all the data collected, a minimum of three replicates. A table of this data can be found in the Appendix.

This signifies that the polymers containing primary amine charges likely have a higher binding affinity to the pDNA in the diblock copolymer while the hydrophilic glycopolymer shields the polyplex from flocculation. When comparing the difference between the statistical and block copolymers, all the polyplexes formulated with the statistical copolymers aggregated over time in media; however, the statistical copolymers containing some fraction of DMAEMA formed smaller aggregates. Interestingly, statistical copolymers containing the MAG and AEMA, Poly(G_{45}-*s*-P_{35}), revealed the most rapid and largest aggregation, to particles over a micron in size. The lower aggregation seen in some of the other statistical copolymer formulations can be attributed to the reactivity ratios between the three monomers. As previously mentioned, the statistical copolymers likely have a gradient nature to their composition due to the reactivity ratios between the monomers (the MAG monomers are likely clustered at one end of the polymer). The short cationic block comprised of both primary and tertiary amines (triblocks) seems to not bind as tightly as the diblocks containing just one type of amine.

2.4.4 Cell Viability

Cell viability is one component to obtaining a higher delivery efficiency. To investigate the cytotoxicity of polyplexes at N/P ratios of 5 and 10, MTT assays were performed with HeLa cells. The cell viability was measured 48 hours post transfection (Figure 33a). A clear toxicity trend was observed; polyplex toxicity increased as the amount of tertiary amine in the polymer increased, particularly with the block polymers. Rawlinson *et al* reported that the cytotoxicity of pDMAEMA is cell type and molecular weight dependent.[321] With the statistical copolymers, a similar trend was noticed but was not as pronounced. Although the composition of Poly(G_{62}-*s*-T_{23}) and Poly(G_{46}-*b*-T_{26}) are

similar, the Poly(G_{62}-*s*-T_{23}) model is likely slightly less toxic possibly due to the cationic amine being spread throughout the polymer backbone with the glucose moiety. Ahmed and Narain have examined similar polymers created with AEMA and monomers containing glucose and showed a similar trend exists to what we have observed; statistical copolymers are less toxic than their block copolymer counterparts.[27,172] When considering the effect of free polymer on toxicity, it was interesting to note that both the statistical [Poly(G_{62}-*s*-T_{23})] and block [Poly(G_{46}-*b*-T_{26})] analogs containing only the tertiary amine charged groups caused a large portion of the cells to die (when not complexed with pDNA into polyplexes). Indeed, the toxicity of free polymer was higher than when the same concentration of polymer was contained in a polyplex. Thus, free polymer in solution interacts strongly with cells, may be internalized, and these interactions/pathways may be different than when the polymer is complexed with pDNA in a polyplex. This high toxicity was not observed in the MTT assays with the polymer only samples that contained the primary amine moieties.

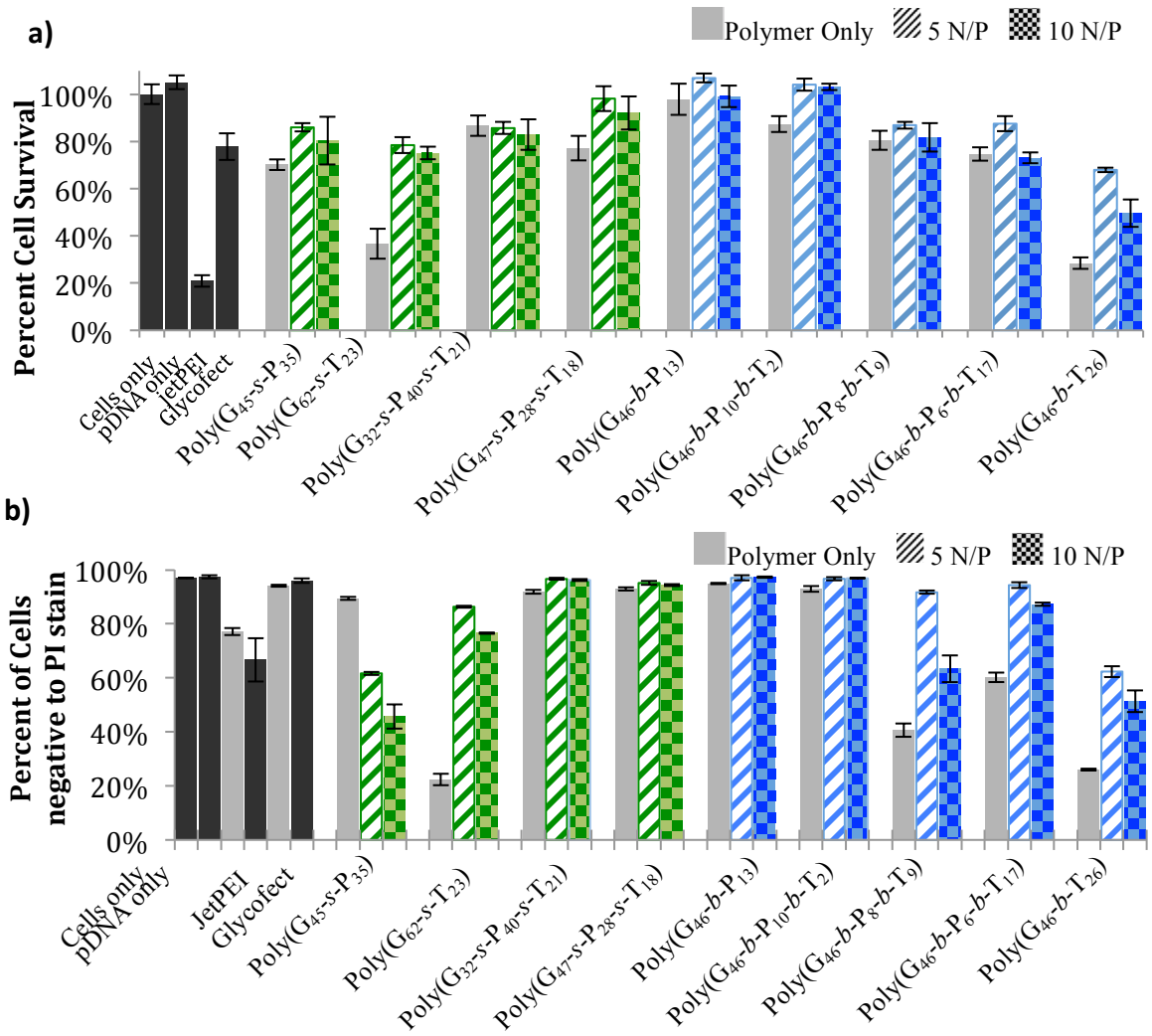

Figure 33 a) MTT assay (percent cell survival) of cells treated with polymer only or polyplexes formulated at N/P ratios of 5 or 10. Samples were analyzed 48 hours post transfection. b) The percent of cells whose membranes are intact and not permeable to propidium iodide stain as determined via flow cytometry. Cells were treated with polymer only or polyplexes at N/P ratios of 5 and 10. Samples were analyzed 4 hours post transfection. All data is standardized to cells only control and error bars are the standard deviation of three replicates.

The integrity of the cell membrane and thus cell viability was also evaluated by adding propidium iodide (PI) stain to the cells four hours post transfection (Figure 33b). Cells exposed to polymer only (no pDNA) and polyplexes were evaluated for membrane permeability by the number of cells positive to PI (PI is only internalized into cells with compromised membranes).[322] Again, it was noticed that as the amount of tertiary amine increased in the polymers, cell permeability to PI increased; this was particularly evident for the block copolymer formulations. When observing the effect of polymer only (no pDNA) with cells, poly(G_{62}-*s*-T_{23}), poly(G_{46}-*b*-P_8-*b*-T_9), poly(G_{46}-*b*-P_6-*b*-T_{17}), and poly(G_{46}-*b*-T_{26}) interacted with the cells to a high degree. Also, for polyplexes formulated with the block polymers at N/P 10, as the tertiary amine content increased, PI permeability increased indicating that the tertiary amine polymers have a very high membrane destabilization effect. Most of the statistical copolymers appeared more benign to cells (with the exception of polyplexes made from poly(G_{45}-*s*-P_{35}) and the polymer only formulation of poly(G_{62}-*s*-T_{23}); spacing the charge with the glucose units may "soften" the interaction of the charged polymers with the cell membrane so they are not as lytic. On the contrary, poly(G_{45}-*s*-P_{35}) polyplexes appeared to cause membrane destabilization but the block copolymer analog poly(G_{46}-*b*-P_{13}) did not. This could be due to two factors: i) the block system had a smaller number of charges copolymerized and/or ii) having a primary amine (high pK_a) close to the polyplex surface could increase the interactions with the cell membrane, causing destabilization. In the block formulation, the charge is buried in the polyplex core (complexed to pDNA) and the glucose shell on the polyplex surface may not have such a strong interaction/destabilizing effect with the cell membrane. These results indicate that cells that are PI positive may not necessarily be "dead" but rather have compromised membranes from interaction with the polymers; specifically the tertiary amine rich polymers. It should be noted that destabilization in the

cell membrane could be caused by direct polymer interactions with the cell membrane or from cytotoxic effects of the polymer (from the tertiary amines).

2.4.5 Cellular Membrane Integrity

To further examine and understand the toxicity and membrane destabilization, assays were performed with these formulations to monitor whether cells were going through apoptosis. An Annexin V assay was completed to determine whether cells were expressing phosphatidylserine, a marker for apoptosis, on their surface.[323,324] The Annexin protein has a low K_d for phosphatidylserine (5 x 10^{-10} M), a protein only found on the cytoplasmic side of the phospholipid bilayer – except during apoptosis.[325] The Annexin V assay was performed in conjugation with a dye exclusion assay to establish the cell membrane integrity during the experiment. While the Annexin protein is large (36 kDa), a small molecule dye, 7-AAD, was utilized to distinguish between cells with compromised membranes and dead/necrotic cells. This assay allows us to gain information on whether the polymers/polyplexes are causing small holes/destabilizing the phospholipid membrane (7-AAD positive) and/or if the polymers/polyplexes have triggered apoptosis (Annexin V positive) or necrosis (cells positive for both 7-AAD and Annexin V).[322]

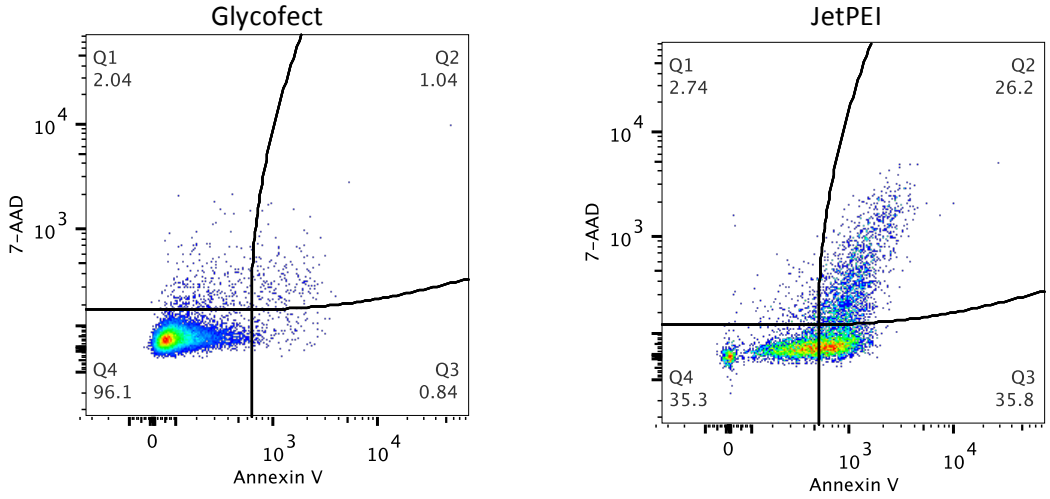

Figure 34. Controls Glycofect and JetPEI from flow cytometry data. The x-axis is the Annexin V (FITC) stain, the y-axis is the 7-AAD stain

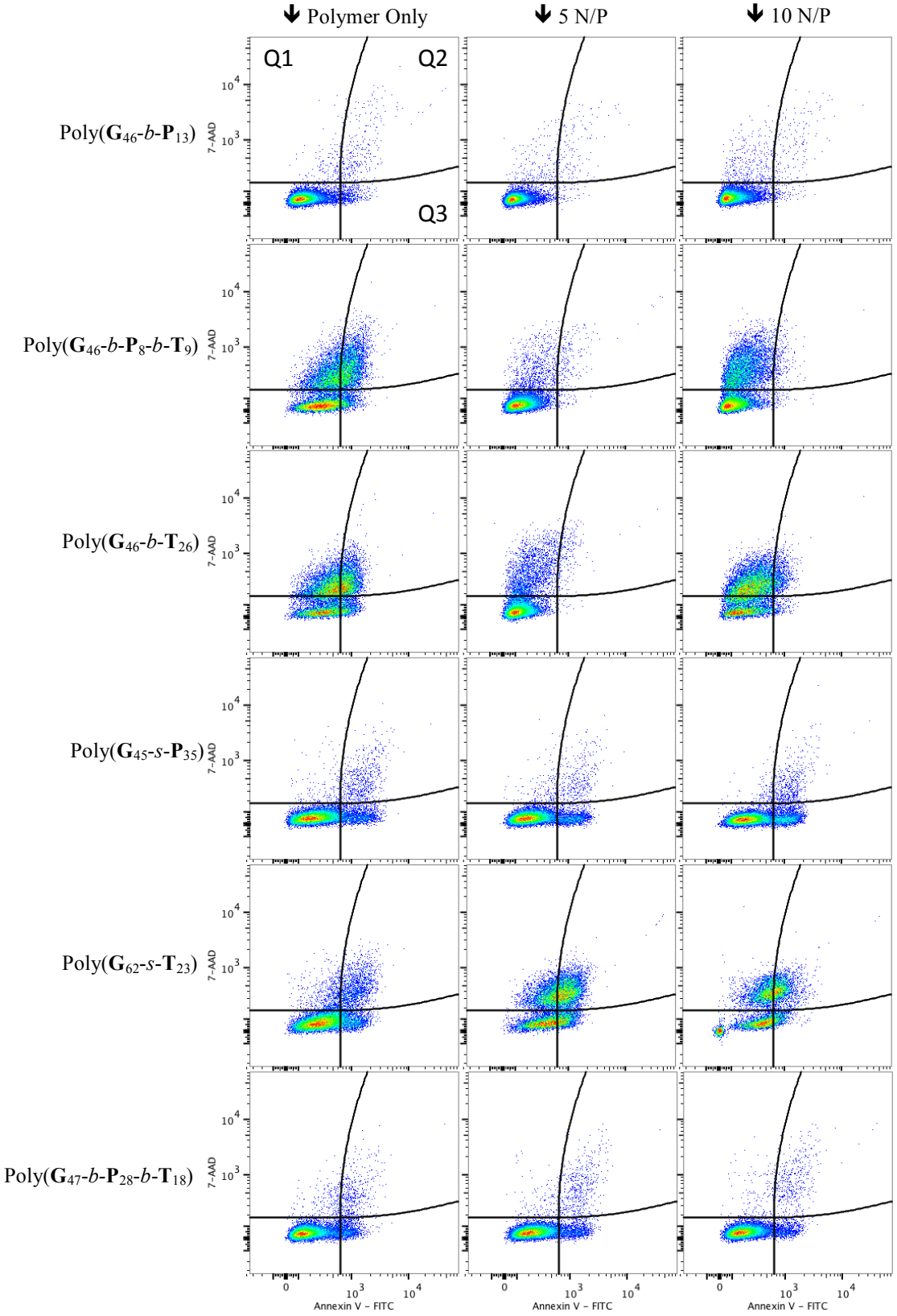
Polymer Only
5 N/P
10 N/P
Q1
Q2
Q3
Poly(G46-b-P13)
Poly(G46-b-P8-b-T9)
Poly(G46-b-T26)
Poly(G45-s-P35)
Poly(G62-s-T23)
Poly(G47-b-P28-b-T18)
7-AAD
Annexin V - FITC

Figure 35. Flow cytometry analysis of cells for membrane permeability (7-AAD positive), apoptosis (Annexin V positive), and necrosis (both 7-AAD and Annexin V positive). Data plotted as 7-AAD (y-axis) vs Annexin V (x-axis). Pseudo color represents the density of 20,000 events plotted. Quadrant 1 (Q1) depicts cells that are only 7-AAD positive (seen as red bars in Figure 36), Q2 denotes cells that are 7-AAD and Annexin V positive (double positive grey bars in Figure 36), and Q3 denotes apoptotic cells that are only Annexin V positive (blue bars in Figure 36).

The flow cytometry data (Figure 36, Figure 35, Figure 34, Figure 79, and Figure 80) showed very compelling evidence that some cells did have destabilized membranes/small holes (without causing a large population to be apoptotic), meaning that 7-AAD could pass through the membrane but were not positive for Annexin V. These populations came from cells treated with polymers containing tertiary amines: poly(G_{62}-*s*-T_{23}), poly(G_{46}-*b*-P_8-*b*-T_9), poly(G_{46}-*b*-P_6-*b*-T_{17}), and poly(G_{46}-*b*-T_{26}) (Figure 33, Figure 35, and red bars in Figure 36). The tertiary amine diblock [poly(G_{46}-*b*-T_{26})] at 10 N/P showed the highest membrane disruption, only 6.6% of the cells were dead, but 65% of the cells had destabilized membranes, showing cellular internalization of 7-AAD without cells being positive for Annexin V. The amount of Annexin V positive (apoptotic) cells indicates more information about the cytotoxicity of each polymer/polyplex formulation with HeLa cells. It was found that the two statistical formulations poly(G_{45}-*s*-P_{35}) and poly(G_{62}-*s*-T_{23}) caused a portion of the cell population (about 20%) to undergo apoptosis (Fig 6). With respect to the block polymers, the polyplex formulations were not toxic to cells (<7% dead); however, the polymer only samples of poly(G_{46}-*b*-P_8-*b*-T_9), poly(G_{46}-*b*-P_6-*b*-T_{17}), and poly(G_{46}-*b*-T_{26}) caused between 18-30% of the cells to die. A similar trend was noticed in the MTT and PI assays (Figure 33). It was indeed evident from these data that the control polyplex formulation with JetPEI caused over 60% of the cells analyzed to be dead and show signs of apoptotic markers on their surface after only 4 hours of polyplex exposure – and was the most toxic formulation examined here (similar to the MTT results in Figure 33). With the exception of poly(G_{45}-*s*-P_{35}), all other formulations (polymers and polyplexes) with the high primary amine content [poly(G_{32}-*s*-P_{40}-*s*-T_{21}), poly(G_{47}-*s*-P_{28}-*s*-T_{18}), poly(G_{46}-*b*-P_{13}), and poly(G_{46}-*b*-P_{10}-*b*-T_2)] were found to be quite benign to the cells (Figure 36).

These data further support our hypothesis that the tertiary amine polymers interact with the cell in a nonspecific manner and induce pore formation in the cellular

membrane, leading to high toxicity. Hong *et al.* has reported and imaged (with AFM) this behavior in cell membranes with polycations.[326] Interestingly, at 5 N/P, close to the complexation point, the cells had a higher survival rate (lower Annexin V signal than polymer only samples) whereas at 10 N/P apoptosis increases, due in part to the excess polymer in solution. This further reiterates that polyplexes and polymers enter the cell in a different fashion, interact with the membrane, and cause toxic side effects in alternative ways.

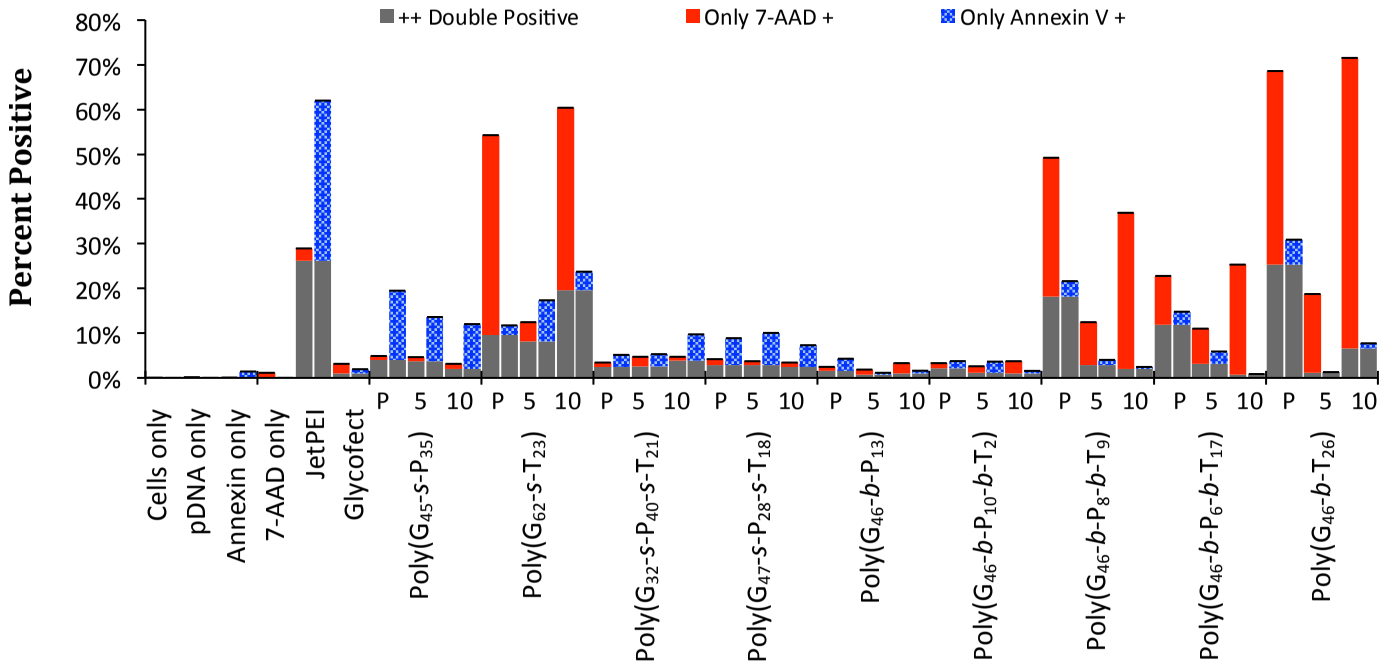

Figure 36. The percentage of cells that are fluorescent for 7-AAD positive (height at the top of the red bar) and Annexin V positive (height of blue bar). Each sample is represented by two bars. Cells that are double positive (cells in Q2 in Figure 35) are depicted as grey bars. Red bars correspond to percent of cells in Q1 and blue bars to Q3 in Figure 35. P, 5, and 10 correspond to the polymer only sample, the 5 N/P sample, and the 10 N/P sample for each polymer listed below. Error bars are the standard deviation of the data collected in triplicate.

2.4.6 Polyplex Internalization

Cellular internalization of the polyplex formulations was determined by monitoring Cy5-labeled pDNA. The percent of Cy5 positive live cells (Figure 37) indicates that the synthesized delivery vehicles were generally quite effective at delivering the Cy5-labeled pDNA into the cells. Some interesting trends were noticed with these data. While poly(G_{46}-*b*-P_{13}) at 5 N/P was the poorest polyplex formulation to promote cell entry (25% Cy5-pDNA positive cells), the internalization was much higher at a higher N/P ratio (10 N/P) as 75% of HeLa cells were positive for Cy5-pDNA. For the analogous tertiary amine system, poly(G_{46}-*b*-T_{26}), polyplex internalization was very high at N/P 5 (~90%) but lower at 10 N/P (43%); most of the cells positive for Cy5-pDNA were also found to be PI positive. All other polyplex formulations revealed high internalization percentages (80-90+ %) with the exception of JetPEI polyplexes (~25%); this polymer was also found to be highly toxic and cells positive for Cy5 were also PI positive.

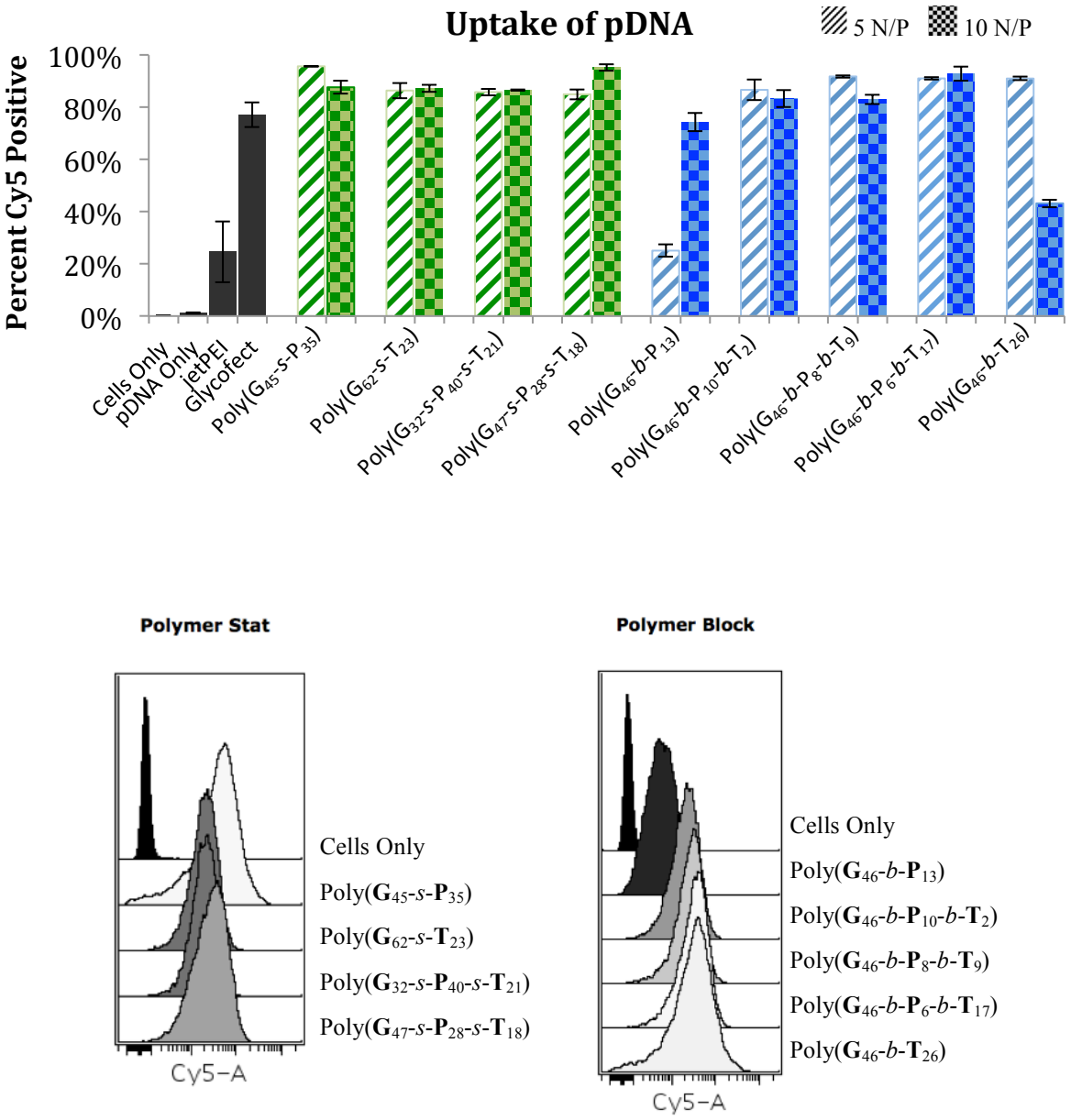

Figure 37. a) The amount of live cells that contain Cy-5 labeled pDNA and b) the intensity of the Cy-5 signal in cells transfected with polyplexes at 5 N/P. Cy5 represents the intensity of the Cy5 signal only in live cells – as determined by the negative population of propidium iodide.

2.4.7 Expression

It is generally thought that genetic cargo mostly enters the nucleus during mitosis when the nuclear membrane disassembles; however, it has been shown in previous research that polymers that induce membrane permeability also have higher expression efficiencies.[20] Previous work by our group demonstrated that PEI polyplexes induced plasma membrane permeabilization within half an hour of transfection and nuclear membrane permeabilization by four hours post transfection; this led to apoptosis and an increase in cellular toxicity/death but also appears to increase gene expression.[20] Knowing that the tertiary amine causes the plasma membrane to destabilize (and here it is also linked to toxicity), it was thought that the polymers containing the tertiary amines may also have higher delivery efficiency/gene expression. To test this hypothesis, HeLa cells were transfected with polyplexes formulated with pDNA containing the firefly luciferase gene. It was observed (Figure 38) that the poly(G_{45}-*s*-P_{35}), poly(G_{47}-*s*-P_{28}-*s*-T_{18}), poly(G_{46}-*b*-P_8-*b*-T_9), and poly(G_{46}-*b*-P_6-*b*-T_{17}) all revealed relatively high gene expression. Due to high membrane permeability, it was expected that poly(G_{46}-*b*-T_{26}) would have revealed higher expression; however, only half of the cells survived the transfection assay (MTT assay, Figure 33a). The two triblock polymers, poly(G_{46}-*b*-P_8-*b*-T_9) and poly(G_{46}-*b*-P_6-*b*-T_{17}) had high gene expression, likely because these polymers are nontoxic and may contain a slightly lower fraction of tertiary amines (to aid in permeabilizing cell membranes). It was surprising to find that poly(G_{45}-*s*-P_{35}) had a much higher expression profile than poly(G_{62}-*s*-T_{23}). While we currently do not understand this trend, we speculate that the statistical copolymer comprised of only tertiary amine charges, poly(G_{62}-*s*-T_{23}), may dissociate before the polyplex can traffic to the nucleus. For a similar reason this could be why the statistical copolymer made with only primary amines, poly(G_{45}-*s*-P_{35}), had higher gene expression than the block copolymer analog,

poly(G_{46}-*b*-P_{13}). Similar to previous work by Ahmed and Narain,[27] we have found that spreading the charge throughout the polymer in a statistical fashion can lead to increased gene expression (particularly with primary amine charges). We conclude that the incorporation of tertiary amines in cationic polymer vehicles does promote higher gene expression, due to their ability to permeabilize cell membranes. However, incorporating a large fraction of tertiary amines leads to an increase in cytotoxicity, apoptosis, and cell death. Thus, the composition of amine types on this vehicle class should be balanced by incorporating mostly primary amines that facilitate stable polyplex formation and are more benign to the cell.

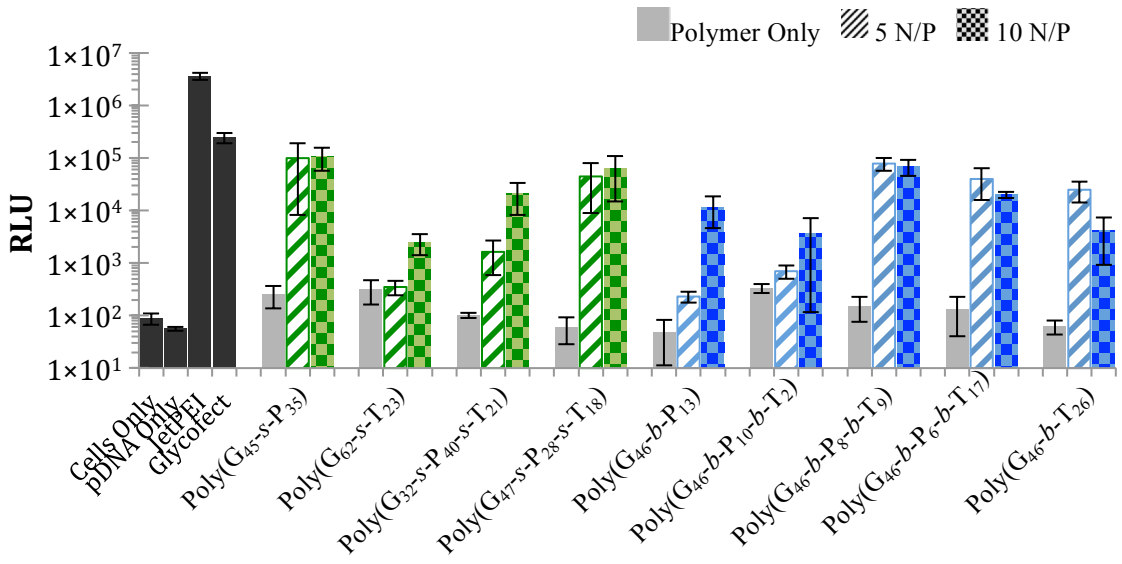

Figure 38. Luciferase gene expression measured 48 hours post-transfection in HeLa cells. Luminescence measured by a BioTek plate reader. RLU is the relative light units. Error bars are the standard deviation of three replicates.

2.4.8 Microscopy

Lastly, to monitor cells during the transfection process, selected polyplexes formulated with Cy5-pDNA were added to cultured HeLa cells and imaged for 4 hours (with the exception of JetPEI transfection, which was imaged for 1.5 hours due to severe toxicity and cell death by this time). The images were compiled into time-lapse videos to visualize cell behavior and morphology during this time period (Figure 39 shows the DIC image at t=0 and an overlay of the DIC and Cy-5 channel images at 4 hours, videos are available in the Supporting Information of the published paper[26]). Cells were also transfected with a GFP containing plasmid and imaged 48 hours post transfection at 350 nm and 470 nm (Figure 41). In Figure 40 and the videos online, the toxicity of some formulations was clearly evident. For cells exposed to JetPEI polyplexes, all cells appeared to be under severe stress as soon as 30 mins post transfection (the cells start blebbing and the cells shrink/shrivel up, Movie S1).[327] When the Cy5 channel was observed, the polyplexes appeared to interact with the cell membrane, the cytoplasm, and the nucleus (Figure 39). Of the polymer vehicles synthesized for this study, the most toxic formulation appeared to be poly(G_{46}-*b*-T_{26}), which agrees with the MTT (Figure 35), 7-AAD, and Annexin V assays (Figure 35 and Figure 36, and the Appendix). After four hours, almost all the cells appeared to have polyplexes within or on the cell surface and most the cells appear dead (severely shriveled/lysed, Figure 40, Movie S2). Similarly, poly(G_{62}-*s*-T_{23}) also caused the cells to bleb and shrivel (Figure 40, Movie S3). Cells exposed to poly(G_{46}-*b*-P_{13}) polyplexes did not appear to bleb (similar to previous toxicity studies); however, a slight decrease in cell volume was noted (Figure 40, Movie S4). The formulation with Poly(G_{45}-*s*-P_{35}) did not appear toxic to cells over the four hour time course of this experiment (Figure 40, Movie S5, no blebbing or decrease in cell volume noticed even though polyplexes were clearly internalized within cells). Cells that

were transfected with a plasmid that encodes for GFP protein were viewed under 470 nm wavelength light 48 hours post transfection (Figure 41). In the selected samples in can clearly be seen that the cells had GFP protein expressed with in them. Poly(G_{46}-*b*-P_{13}) appeared to have low amounts of GFP whereas poly(G_{46}-*b*-T_{26}) had higher GFP intensity, even in some of the blebs surrounding the cells.

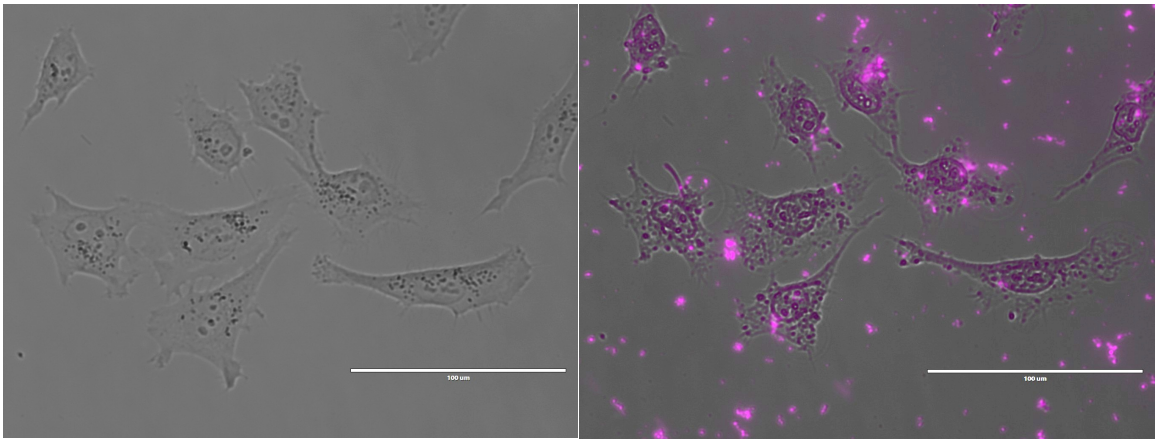

Figure 39. Microscopy images taken of the cells before Cy-5 labeled JetPEI polyplexes were added and four hours post transfection. Purple overlay is fluorescence microscopy taken at 679 nm. Scale bar represents 100 µm.

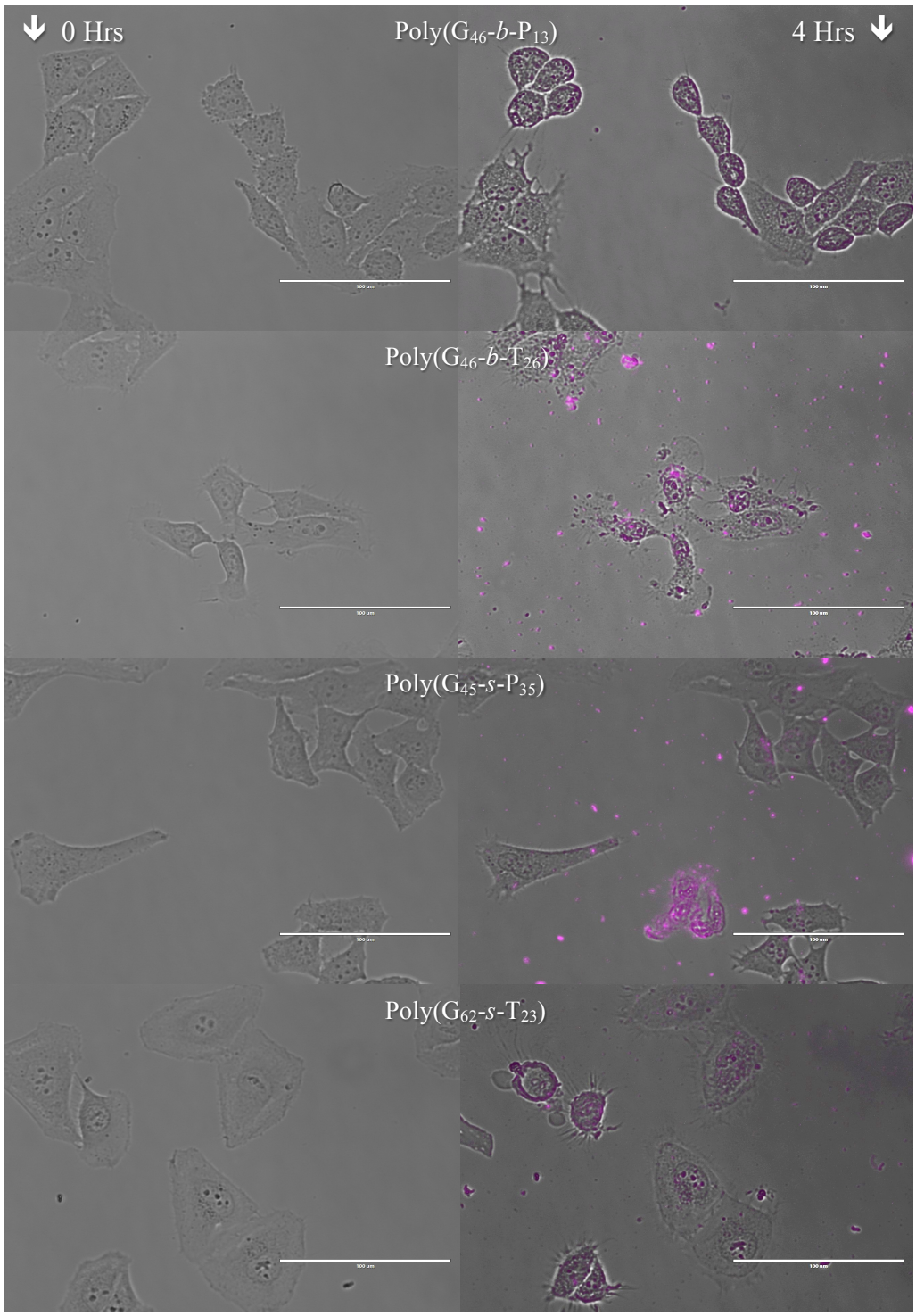

Figure 40. Microscopy images taken at the time polyplexes were added and four hours post transfection. Purple overlay on second column is fluorescence microscopy taken at 628 nm. Scale bar represents 100 μm.

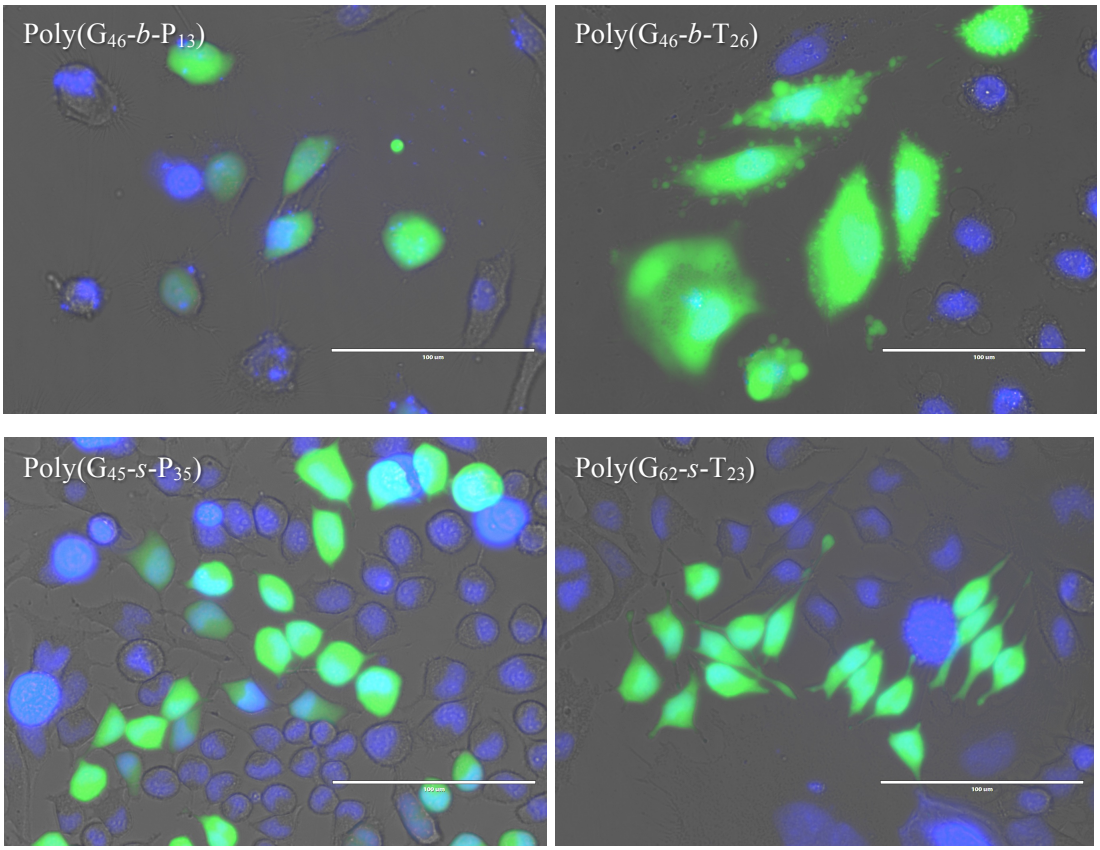

Figure 41. Microscopy images taken at 48 hours post transfection of HeLa cells that were transfected with a GFP containing plasmid. The fluorescence microscopy was taken at at 350 nm (DAPI) and 470 nm (GFP expression). Scale bar represents 100 μm.

2.5 Conclusion

In an effort to find the right balance among nucleic acid uptake, toxicity, membrane permeability, and gene expression, we have synthesized and characterized a family of nine polymers containing a variety of compositions using MAG, AEMA, and DMAEMA monomers. The polymers were similar in length, while the ratio of primary to tertiary amines was varied as well as block versus statistical formulations were compared. The polyplexes made with statistical copolymers flocculated in culture media (observed via DLS) over time but were stable in water. The triblock polymers generally flocculated over time, however, the triblock with the composition poly(G_{46}-*b*-P_{10}-*b*-T_2) was the most stable of the triblocks. The diblock formulations with poly(G_{46}-*b*-P_{13}) were completely stable in culture media over the experimental time course. It was apparent that the tertiary amine-containing systems were more toxic than the systems containing only primary amines and it was found that the presence of the tertiary amines could permeabilize cell membranes. This phenomenon was further investigated by staining transfected cells with an apoptotic marker, Annexin V, and a DNA intercalating molecule (7-AAD). Cells exposed to polymers containing tertiary amines were permeable to 7-AAD and formulations containing a higher ratio of tertiary amines allowed cellular internalization of some Annexin V, thus promoting cell membrane permability and toxicity at the higher tertiary amine ratios. As a result, these polymers exhibited higher gene expression levels, however, polymers with highest tertiary amine ratios resulted in very high toxicity. The terpolymer with a high primary amine and very low tertiary amine ratio [Poly(G_{46}-*b*-P_{10}-*b*-T_2)] overall yielded the optimal combination of forming colloidally-stable polyplexes that had high cellular uptake, and low toxicity while still retaining high levels of gene expression.

Overall, we conclude that there is a delicate balance between higher uptake and transgene expression (caused by membrane disruption) and an increase in toxicity (from membrane destabilization). It appears that triblock polymers containing longer blocks of both carbohydrate (MAG) and primary amine (AEMA) units with a small block of tertiary amine (DMAEMA) moieties offer a potential platform to further optimize vehicles for in vivo examination.

The Appendix includes: NMR spectra of polymers, SEC chromatograms of the polymers, reactivity ratio NMR overlay, pK_a comparison between the monomers and polymers, gel electrophoretic shift assays, flow cytometry diagrams, histograms from flow cytometry data, microscopy images, and a table of the DLS results. Video of the cells can be found online free of charge via the Internet at http://pubs.acs.org.

Chapter 3.

INVESTIGATING THE pH AND IONIC STRENGTH DEPENDENCE OF THE CORONA IN CATIONIC AMPHIPHILIC POLYMERS/MICELLES

Synopsis

Amphiphilic block polymers were designed to comprise of a weak polyelectrolyte and a hydrophobic block length, both with low glassy transition temperatures. Four different block polymers were synthesized and characterized in which the molecular weights varied. The amphiphilic polymers self assembled into core-shell micelles that were then probed in defferent buffers. The size of the corona and surface potential were measured as a function of pH and ionic strength of the buffers.

This chapter is adapted and is to be submitted for publication by the following authors:

Sprouse, D.; Jiang, Y.; Laaser, J. E.; Lodge, T. P.; Reineke, T. M.

3.1 Abstract

The enthalpically driven formation of macromolecular assemblies/micelles from amphiphilic polymers can provide a basic template for building more complex macrostructures. While micelles have a wide array of uses, herein we study the fundamentals of micelle formation, morphology, and properties (relevant to future development of biomedical applications, e.g. the complexation of cationic micelles with DNA). This complexation can be utilized for drug or gene delivery, targeted immune responses, air and water purification, or theranostics. Four diblock polymers composed of a hydrophilic/cationic block of *N,N*-dimethylaminoethyl methacrylate (DMAEMA) and a hydrophobic/nonionic block of *n*-butyl methacrylate (BMA) were synthesized and characterized *via* ^{1}H NMR, size-exclusion chromatography (SEC), matrix assisted laser desorption ionization - time of flight - mass spectrometry (MALDI-TOF-MS), and ultraviolet-visible spectrophotometry (UV-Vis). The amphiphilic polymers self-assembled into core-shell micelles that were characterized by dynamic light scattering (DLS), static light scattering (SLS), zeta potential, and cryo-TEM. The micelles were also studied in buffers at a wide range of ionic strengths and pH. It was noticed that the micelles had a range of sizes depending on the extension and contraction of the corona in different media. We report the correlation between corona size and the aqueous solution's pH and ionic strength, and the relationship between zeta potential and ionic strength of the buffers. The size and charge of the micelles as well as the ionic strength of the surrounding media will play a fundamental role in the interaction with and binding of a polyanion, like DNA, to a positively charged micelle.

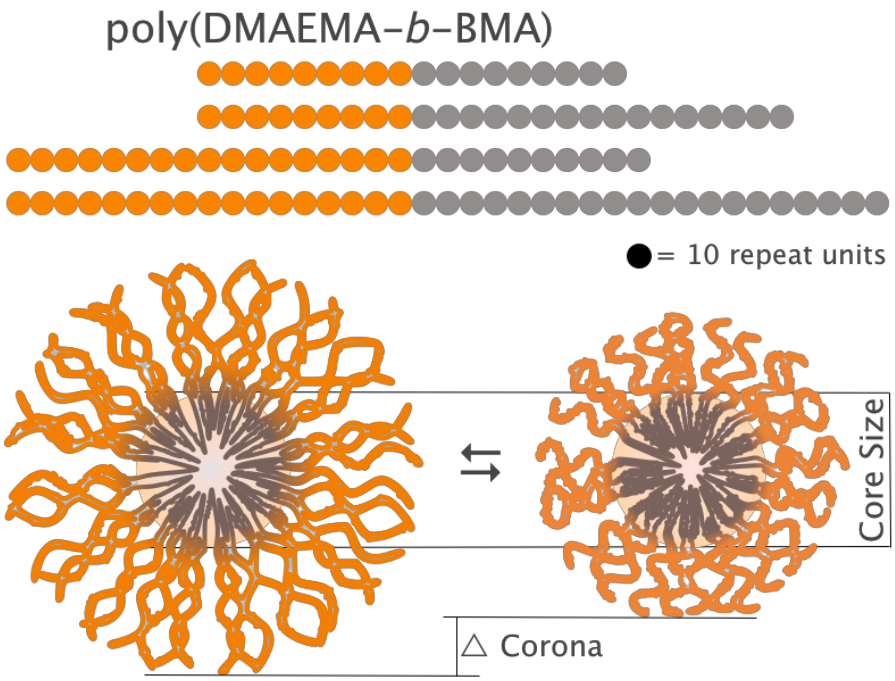

Figure 42. A depiction of the contraction and extension of the corona.

3.2 Introduction

The formation of micelles from amphiphilic polymers has been widely studied over the past two decades. Amphiphilic block polymers are of interest as they have many practical uses including drug delivery, cosmetics, dispersant technology, water purification, sensors, nano reactors, and emulsifiers.[188,189,328] Through polymer design and synthesis, amphiphilic polymers can be tailored to constitute specific assembly characteristics. For example, increasing the volume ratio of the hydrophobic block (to the hydrophilic block) can change the shape of the micelle from spherical to cylindrical and incorporating a polyelectrolyte in the water-soluble component allows the charge density to be adjusted.[329-331] Therefore, assembly behavior can be adjusted and tailored to various applications.[331,332] For example, control in the size, shape, and assembly behavior would specifically benefit the design of reproducible drug and nucleic acid delivery vehicles.[179,333] Our group and many others have investigated the assembly of polycations with nucleic acids to form polyplexes, which are known to improve stability and cellular delivery efficiency. While packaging polynucleotides into polyplexes have their uses and advantages, their assembly behavior is complicated by many factors including the lack of control in polycation over charging, pH- and serum-mediated aggregation or unpackaging, which present difficulties in reproducing defined complex formation and biological behavior. To this end, preassembly of polycations into micelles may have advantages over polyplexes in that the assemblies can be reproduced and well characterized prior to DNA complexation for further *in vitro* or *in vivo* studies.[1,26,182,217,305] Utilizing pre-assembled micelles for as vehicles also provide an alternative approach to carefully characterize and understand the binding, complexation, behavior, and dissociation between well-defined cationic micelles and polyanions in

physiological conditions. In addition, micelles also have the potential to incorporate multiple delivery modalities such as drugs, genes, proteins, and/or contrast agents.[187,189,334]

The length of polymer, ratio of hydrophilic to hydrophobic block lengths, and choice of monomers all have a large impact on micelle formation, shape, size, and dispersity. It has been reported that micelles containing a rubbery core have a higher transfection efficiency than glassy cores,[305] and polymers with lower glass transition temperatures are more biodegradable.[335,336] Two polymers with low glass transition temperatures (T_g) that are of interest for our work are poly(*N*,*N*-dimethylaminoethyl methacrylate) (DMAEMA) and poly(*n*-butyl methacrylate) (BMA). Poly(DMAEMA) is a weak polyelectrolyte[337] and when incorporated in a polymer micelle corona acts as a polymer brush (polymer chains anchored to an interface (the micelle core) by their ends).[338-340] The poly(DMAEMA) chains are extended outward due to the osmotic pressure of counter ions within the micelle corona.[341,342] Poly(BMA) is a water-insoluble polymer with a T_g below that of room temperature. When above the critical micelle concentration (CMC), micelle assembly is enthalpically driven by the hydrophobic BMA block through burial into the micelle core, where it expels solvent molecules.[343] Previously statistical copolymers of BMA and DMAEMA, and poly(BMA-*co*-DMAEMA)-*b*-PEG polymers have shown promise as pH and temperature sensitive drug and gene delivery vehicles, tunable hydrogels, and antimicrobial agents.[184,217,337,344-346] These results agreed with previous studies in which the hydrophobic nature of the polymers and polyplexes helped increase membrane permeability; however, they were toxic and unstable in biological media. More recently, a self-assembled micelleplex made from poly(ethylene glycol-*b*-BA-*b*-DMAEMA) complexed with siRNA was found to have improved gene silencing in vitro and had increased tumor uptake relative to PEG-*b*-DMAEMA polyplexes.[182]

Herein we detail the synthesis of poly(DMAEMA-*b*-BMA) (Figure 43 and Figure 47) and the formation of cationic micelles with a rubbery core. Our aim was to create a series of four distinct copolymer compositions for micelle formation and characterize their behavior in various pH and ionic strength environments to assess the shape, size, and charge of the micelle corona in different media. Micelle formation and stability was analyzed in buffers from pH 5 to 10 and with ionic strengths from 20 mM to 1 M, as well as with Opti-MEM, a common biological media in which cells are usually transfected.[347] Understanding the impact of block length and solution environment on micelle morphology and charge is important for the future development of well-defined and stable micelleplexes that can form complexes with polyanions such as nucleic acids for a number of applications.

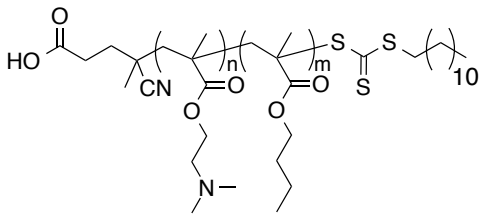

Figure 43. Synthesized diblock polymer structure composed of DMAEMA and BMA.

3.3 Experimental Section

3.3.1 Materials

All solvents were purchased from Thermo Fisher Scientific. Opti-MEM culture media was purchased from Life Technologies (Grand Island, NY). 2-(Dimethylamino)ethyl methacrylate (DMAEMA), n-butyl methacrylate (BMA), 2,2′-azobis(2-methylpropionitrile) (AIBN), 4,4′-azobis(4-cyanovaleric acid) (V-501), and 4-cyano-4-(dodecylsulfanylthiocarbonyl)sulfanyl pentanoic acid (CDT) were purchased from Sigma-Aldrich (St. Louis, MO) and were either recrystallized or distilled before use. Polymers were analyzed with size exclusion chromatography (SEC) (Agilent, Santa Clara CA) equipped with multi angle light scattering and refractive index detectors (Wyatt, Santa Barbara, CA), a Bruker Avance III nuclear magnetic resonance (NMR) (Bruker, Billerica, MA) equipped with Prodigy TCI CryoProbe operating at 500 MHz for ^{1}H and 125 MHz for ^{13}C, and a AB SCIEX TOF/TOF 5800 matrix-assisted laser desorption/ionization-time-of-flight mass spectrometry (MALDI-TOF-MS) (Framingham, MA) equipped with a 1 kHz solid-state laser at 355 nm. Zeta potential and single-angle dynamic light scattering (DLS) measurements were performed on a Malvern Zetasizer Nano ZS (λ=637 nm) (Worcestershire, UK). Multi-angle DLS and static light scattering (SLS) were performed on a Brookhaven Instruments BI-200SM light scattering system (λ=617 nm). Cryogenic transmission electron microscopy (CryoTEM) was completed using a FEI Tecnai G^2 Spirit BioTWIN (Hillsboro, Oregon) equipped with an Eagle 4 megapixel CCD camera; samples were vitrified in a FEI Vitrobot Mark III at -178 ºC. Image analysis was performed using ImageJ. UV-Vis was completed with a Spectronic Genesys 5 spectrophotometer (Houston, Texas) over a wavelength (λ) range of 200-600 nm using quartz cuvettes of 10 mm path length.

3.3.2 Methods

3.3.2.1 Polymer Synthesis

Two lengths of the DMAEMA block were added to two different lengths of the BMA block to synthesize four different polymer structures to understand role of block length in micelle formation and behavior (Figure 47). The first longer cationic macro-chain transfer agent (macroCTA) was synthesized by adding DMAEMA (15.0 g, 95.4 mM), V-501 (13.4 mg, 0.048 mM), and CDT (193 mg, 0.478 mM) to a 100 mL round-bottom flask with a magnetic stir bar that was dissolved in 63 mL of a mixture of DMF, water, and THF 5:3:2 by volume ratio. The solution was then acidified to pH 5 with 6 M HCl. The round bottom flask was sealed with a septum and purged with nitrogen gas for 1 hour before being heated to 70 °C in an oil bath and stirred for 3 hours. The reaction was stopped by exposure to the atmosphere and purified *via* dialysis (in a M.W.C.O 3500 g/mol membrane) against deionized-water for 4 days and then lyophilized. The dry polymer powder was characterized with SEC, NMR, and MALDI-TOF-MS (see the Appendix). The second shorter block length was made by adding DMAEMA (11.0 g, 70.0 mM), V-501 (18.4 mg, 0.0655 mM), and CDT (265 mg, 0.655 mM) to a 100 mL round-bottom and dissolved in 65 mL of a mixture of DMF, water, and THF, 5:3:2 by volume ratio and acidified to pH 5 with HCl. The round bottom flask was purged with N_2 gas and then stirred and heated for 3 hours in a 60 °C oil bath. The polymer was purified as mentioned above and characterized with SEC, NMR, and MALDI-TOF-MS (see Figure 44, Figure 45, Figure 46, and the Appendix). The two homopolymers were then chain extended with BMA in four separate reactions to yield four block polymers with either a short or long cationic/hydrophilic block and a short or long hydrophobic block. For the short DMAEMA-short BMA diblock, BMA (2.39 g, 16.5 mM), macroCTA (1.19 g, 0.0828 mM), and AIBN (1.36 mg, 0.00828 mM) were added to a 50 mL round bottom

and dissolved in 28 mL of a mixture of DMF, THF, and water, 20:5:3 by ratio. For the short DMAEMA – long BMA diblock, BMA (2.72 g, 19.1 mM), macroCTA (1.10 g, 0.0761 mM), and AIBN (1.25 mg, 0.00761 mM) were added to a 50 mL round bottom and dissolved in 33 mL of a mixture of DMF, THF, and water, 23:6:4 by volume ratio. For the long DMAEMA – short BMA diblock, BMA (1.74 g, 12.2 mM), macroCTA (1.86 g, 0.0512 mM), and AIBN (0.841 mg, 0.00512 mM) were added to a 50 mL round bottom and dissolved in 20 mL of a mixture of DMF, THF, and water 14:4:2 by volume ratio. For the long DMAEMA – long BMA diblock, BMA (1.32 g, 9.27 mM), macroCTA (1.13 g, 0.0309 mM), and AIBN (0.51 mg, 0.00309 mM) were added to a 25 mL round bottom and dissolved in 20 mL of a DMF, THF, and water, 14:4:2 by volume ratio. The round bottom flasks were equipped with a stir bar, sealed with a rubber septum, and purged with N_2 gas for 1 hour before being heated in a 60 °C oil bath for varying amounts of time. The polymer solutions were all purified *via* dialysis against water with a (8,000 g/mol M.W.C.O.) membrane for 4 days and lyophilized to dry polymer powder and then characterized *via* NMR and MALDI-TOF-MS (see Figure 44, Figure 45, Figure 46, and the Appendix).

3.3.2.2 Polymer Characterization

Size exclusion chromatography (SEC) was used to determine the molecular weight (number average (M_n) and weighted average (M_w)) and dispersity (Đ) for the macroCTAs using a 1.0 wt. % acetic acid/0.1 M Na_2SO_4 aqueous eluent. A flow rate of 0.4 mL/min, Eprogen (Downers Grove, IL) columns [CATSEC1000 (7 μm, 50 × 4.6), CATSEC100 (5 μm, 250 × 4.6), CATSEC300 (5 μm, 250 × 4.6), and CATSEC1000 (7 μm, 250 × 4.6)], a Wyatt HELEOS II light scattering detector (λ = 662 nm), and an Optilab rEX refractometer (λ = 658 nm) were used. Astra V (version 5.3.4.18, Wyatt

Technologies, Santa Barbara, CA) was utilized for the determination of M_n, Đ, and dn/dc of the polymers. ^{1}H NMR measurements were performed with a temperature-controlled Bruker 500 MHz spectrometer. Samples were prepared in MeOD, THF, and various combinations thereof. Spectra were recorded for each polymer at a temperature of 30 °C. Block copolymer compositions were determined by comparing resonances of the DMAEMA block with those associated with the BMA block. The known M_n from SEC was then used to compare the DMAEMA/BMA ratio to calculate the final polymer molecular weights. For MALDI-TOF-MS the polymer samples were dissolved in methanol and THF and spotted on the MALDI sample plate with an equal amount of dihydroxybenzoic acid (DHB) matrix mixed with α-cyano-4-hydroxycinnamic acid (CHCA) matrix. In some occasions a doping agent was added to enhance the resolution or assist the higher molecular weight polymers to fly. This was done by adding either a cationic resin (DOWEX 50w X2 hydrogen form) or triflouroacetic acid (TFA) after the spot had air-dried. Other doping agents were attempted but these only decreased the resolution. The MALDI-TOF-MS was calibrated with fresh myoglobin before each experiment and the laser power was adjusted for each spot and polymer/matrix type accordingly.

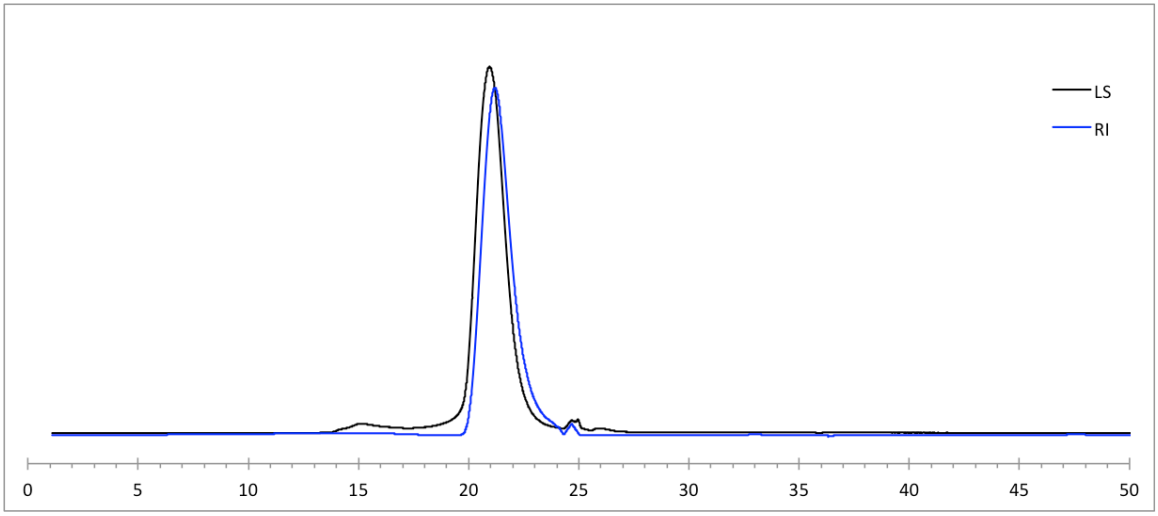

Figure 44. Size Exclusion Chromatography of Poly(DMAEMA14). As determined by SEC using an aqueous eluent of 0.1 M Na2SO4 in 1.0 wt. % acetic acid at a flow rate of 0.4 mL/min on Eprogen columns [CATSEC1000 (7 µm, 50 × 4.6), CATSEC100 (5 µm, 250 × 4.6), CATSEC300 (5 µm, 250 × 4.6), and CATSEC1000 (7 µm, 250 × 4.6)] with a Wyatt HELEOS II light scattering detector (λ = 662 nm), and an Optilab rEX refractometer (λ = 658 nm).

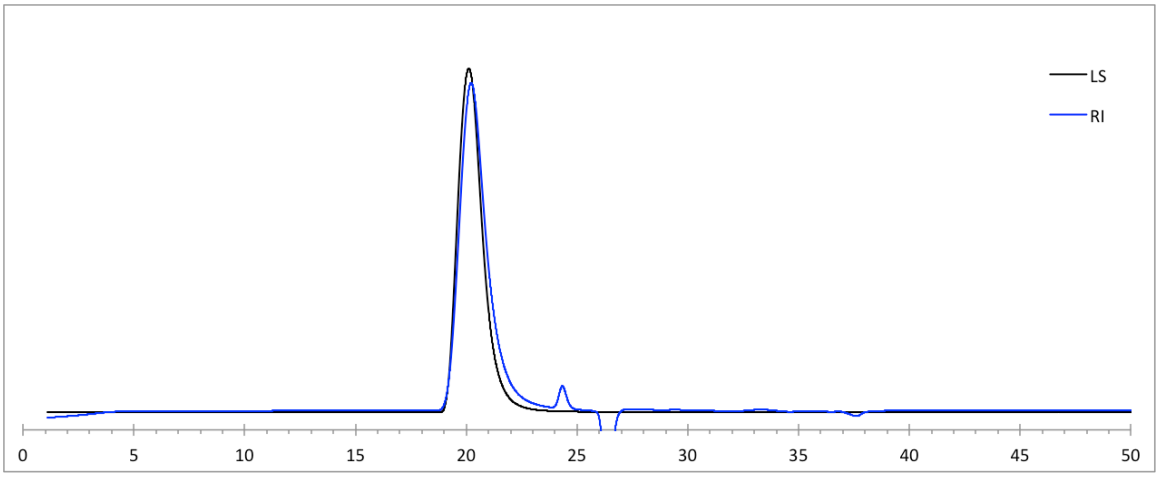

Figure 45 Size Exclusion Chromatography of Poly($DMAEMA_{27}$).

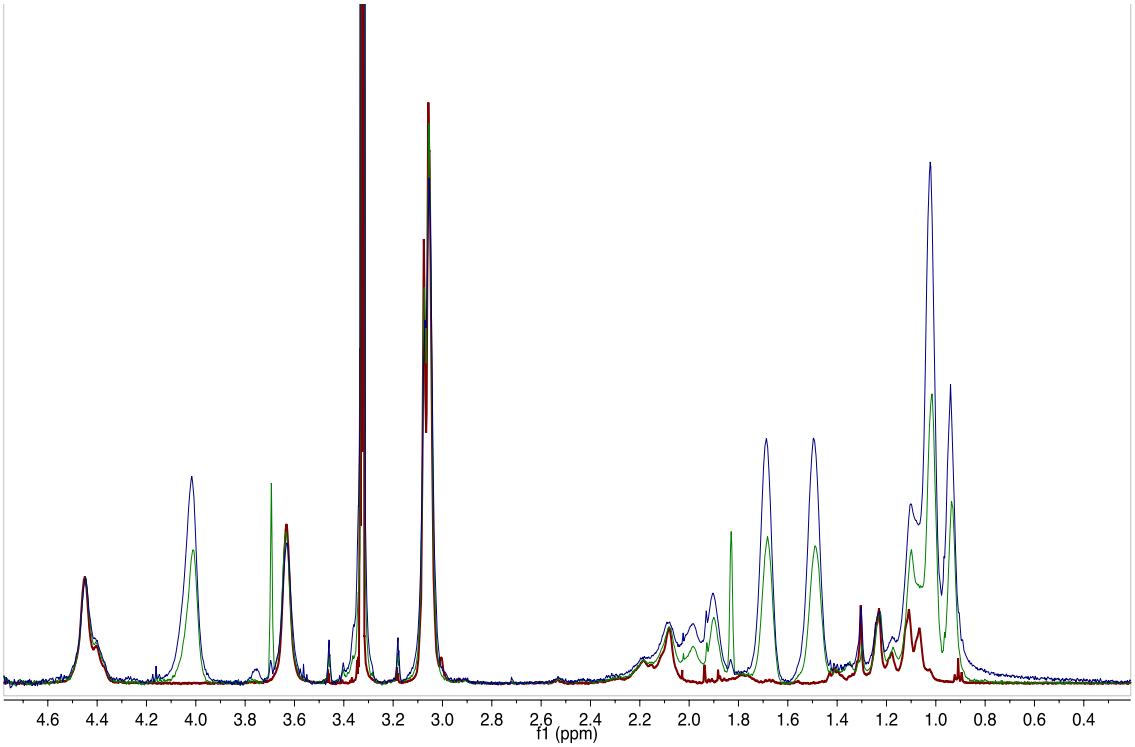

Figure 46 ^{1}H NMR 500 MHz of Poly(DMAEMA$_{14}$), Poly(DMAEMA$_{14}$-*b*-BMA$_{13}$), and Poly(DMAEMA$_{14}$-*b*-BMA$_{23}$) in 1:1 *d*-methanol:Tetrahydrofuran mixture

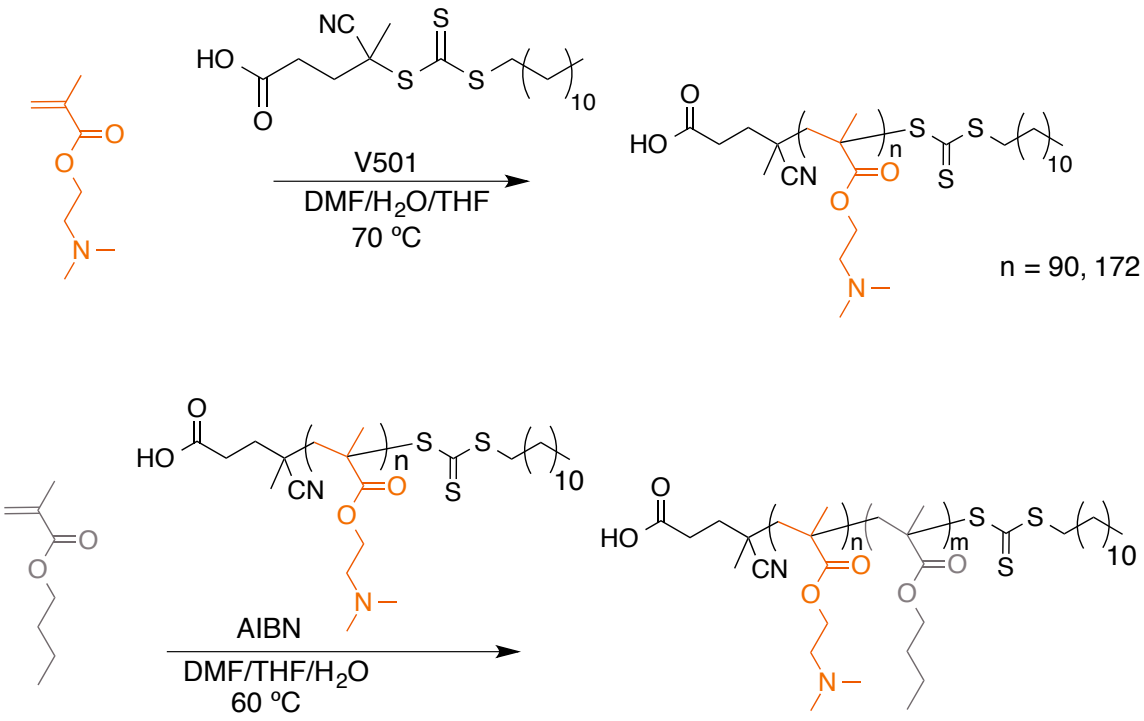

Figure 47. The synthetic scheme of poly(DMAEMA) and poly(DMAEMA-*b*-BMA)

3.3.2.3 Micelle formation

Dry polymer powder was dissolved in ultrapure water at a concentration of 1 mg/mL. The solution was vortexed for 2-3 minutes to aid dissolution, and then the solution was left to equilibrate for at least 24 hours. Other micelle preparatory methods were attempted, including thin film, sonication, heating, and cosolvent preparation methods; however, direct dissolution resulted in the most consistent preparation method to yield micelles with low polydispersities (Figure 48). The micelle stock solutions were then pipetted into dialysis bags (8,000 g/mol M.W.C.O.) and dialyzed against different buffers and ionic strengths (detailed below) for 4 days with media changed every 12 hours.

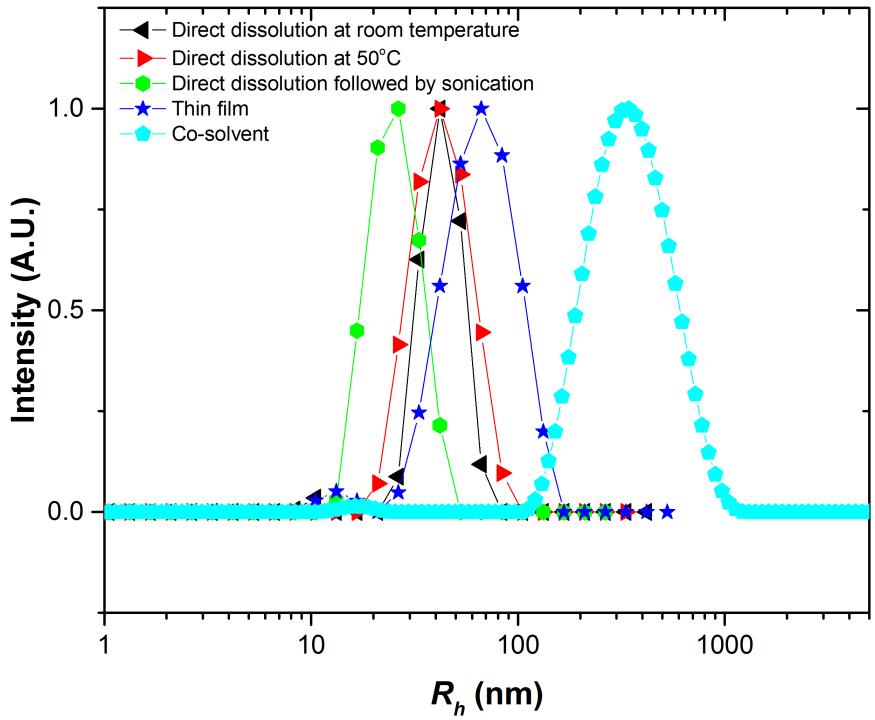

Figure 48. The size and dispersity of micelles formed with different techniques using Poly(DMAEMA$_{27}$-*b*-BMA$_{14}$).

3.3.2.4 Buffer Preparation

Buffers of different pH and ionic strengths were created to test the effects of pH and ionic strength. It should be noted that in this study all micelles were prepared in water first unless stated otherwise and then dialyzed into each buffer condition. The ionic strength of the buffers was held constant at 20 mM, monoprotic buffers were chosen to yield a range of pHs, and sodium chloride was added to adjust the total ionic strength. The buffers chosen for each pH was as follows: pH 5 - acetate; pH 6 - MES; pH 7 - MOPS; pH 7.5 - HEPES; pH 8 - TRIS; pH 9 - TRIS; pH 10 – CHES (see the Appendix for acronyms). Opti-MEM was also used as a model of biological media; the measured pH of Opti-MEM was 7.2, and the ionic strength was estimated to be 140 mM according to the specifications provided by the manufacturer. Also, the role of buffer ionic strength was examined and MOPS, CHES, and Tris buffers were used and the ionic strengths were adjusted to 20 mM, 50 mM, 100 mM, 200 mM, 500 mM, and 1 M solutions with added NaCl.

3.3.2.5 Micelle concentration determination

After the micelles were dialyzed in different buffers to a specific pH and ionic strength, their concentration was determined by UV-Vis. First, each of the polymer types were dissolved in water at known concentrations, and absorbance was measured from 200 nm to 600 nm. The spectra were baseline corrected using equation 3, where A, B, and C are constants and λ is the wavelength. The absorbance was measured at λ_{max} 311 nm (Figure 50a). The data for all the micelle concentrations were then plotted as a function of CTA concentration (trithiocarbonate endgroup) and fit to a line, the slope of which was used to calculate the final concentration of all the micelles after dialysis (Figure 50b).

$$Absorption = log\left(\frac{A-B}{\lambda^n}\right)^{-1} + C \qquad \textbf{(3)}$$

3.3.2.6 Micelle Size and Zeta Potential Measurements

3.3.2.6.1 Dynamic Light Scattering (DLS)

The average size of each micelle formulation was determined with dynamic light scattering, either with five angles (60°, 75°, 90°, 105°, 120°) or two angles (17°, 173°) at 23 or 25 °C for the multi-angle and dual-angle instruments, respectively. Prior to the final size determination with the dialyzed micelles, the size was correlated to concentration, temperature, and buffer type to establish the stability of the micelles over time.

3.3.2.6.2 Static Light Scatternig (SLS)

For all samples used in SLS, micelle solutions were prepared by dialyzing 1 mg/mL micelle solutions in milliQ water against pH 7, 100 mM MOPS buffer for 4 days. The concentration of dialyzed micelles was determined with UV-Vis as mentioned above, and dilutions were then performed to obtain desired concentrations. The dn/dc value of each micelle solution was measured using the refractometer described for Size Exclusion Chromatography (SEC) analysis. For each micelle solution, a minimum of four different concentrations were used to measure scattering intensity with 10 data points (between 45° and 135°) for each concentration. Berry plots were used to calculate the molar mass M_w, radius of gyration R_g and second viral coefficient A_2 for each micelle composition.

3.3.2.6.3 Cryogenic Transmission Electron Microscopy (CryoTEM)

The morphologies of the Poly(DMAEMA-BMA) micelles in water were visualized by cryo-TEM. For each specimen, 3-4 μL of micelle solution was loaded onto a carbon-coated and lacey film-supported copper TEM grid in the climate chamber of a FEI Vitrobot Mark III vitrification robot. The climate chamber was kept at 26 °C with saturated water vapor. The loaded grid was blotted and then plunged into liquid ethane that was cooled by liquid N_2. Vitrified samples were kept under liquid N_2 before being imaged. Images were taken under focus for adequate phase contrast.

3.3.2.6.4 Zeta Potential

The dialyzed micelles were put in a cuvette equipped with gold plated electrodes, and the zeta potential was measured with a Malvern Zetasizer Nano ZS (Malvern Instrument Ltd., Worcestershire, United Kingdom). The zeta potential was calculated from the measured electrophoretic mobility using the Smoluchowski equation. All measurements were taken at 25 °C, and the viscosity was adjusted according to the amount of NaCl added to the buffered solution.

3.4 Results and Discussion

3.4.1 Synthesis and Characterization

The two monomers, DMAEMA and BMA, were chosen for this study due to both their reported homopolymer T_g's of 20 °C, providing 'rubbery' polymer blocks that would easily self assemble in aqueous conditions.[348] While previous reports have indicated that acrylate monomers may be lower in toxicity than methacrylates,[349,350] we chose to synthesize the latter as methacrylates are much less susceptible to hydrolysis in aqueous media (and polymer stability was important to ensure reproducibility for this study).[332] The CTA was chosen for its ability to adequately control polymerization of both monomers; the DMAEMA block was synthesized first followed by chain extension with BMA so that the trithiocarbonate and aliphatic dodecyl CTA end group would be buried in the core of the micelle. Two lengths of the hydrophilic/cationic DMAEMA block were synthesized and characterized with NMR, SEC, and MALDI. The SEC revealed that the macroCTAs had molecular weights [M_w of 15 KDa 29 KDa and M_n of 14 KDa and 27 KDa with low dispersity (Đ < 1.10)], corresponding to block lengths of 90 and 172 repeat units. These macroCTAs were chain extended with BMA to yield four novel polymers, consisting of four hydrophilic-hydrophobic block lengths short-short, short-long, long-short, and long-long. It should be noted that after chain extension the four diblock polymers were not able to be characterized via SEC-SLS due to their low critical micelle concentration (CMC) and affinity to form micelles in all solvents/mobile phases tested. This was particularly noticeable in the ^{1}H NMR spectra of the diblock polymers was taken in deuterated methanol at 50 °C. Under these conditions, the BMA moiety was undetectable (Figure 49); however, upon addition of deuterated tetrahydrofuran (2:1 MeOD:THF vol) the BMA block could clearly be seen (Figure 49). The broadening of the BMA resonances was a result of the micelle's core behaving as

one large particle sequestered from the solvent, as has previously been reported by Convertine et al.[345] The core of the micelle behaves as a large particle, and it is presumed that the chains are kinetically trapped within each core, thus the overall core size and aggregation number should be fixed.[188] The NMR integration of DMAEMA to BMA blocks allowed calculation of the final polymer weighs/composition as seen in Table 6. MALDI-TOF-MS was used to determine the dispersity of the four diblocks, all of which were less than 1.09.

Table 6. A summary of the four block polymers made and characterized with GPC, NMR, and MALDI-TOF-MS.

Mol % DMAEMA	Vol % DMAEMA	DMAEMA M_n[a] (kDa)	BMA M_n[b] (kDa)	M_n[b] (kDa)	Đ[c] (M_w/M_n)	N_n[b]
100		14			1.07	90
49	46	14	13	27	1.07	184
36	33	14	23	37	1.09	250
100		27			1.08	172
64	62	27	14	41	1.09	270
46	43	27	29	56	1.08	374

[a] Determined by SEC-SLS; [b] Determined via ^{1}H NMR; [c] Determined using MALDI-TOF/TOF-MS; N_n is the number of repeat units (M_n/M_0) for each polymer and Đ is the dispersity (M_w/M_n).

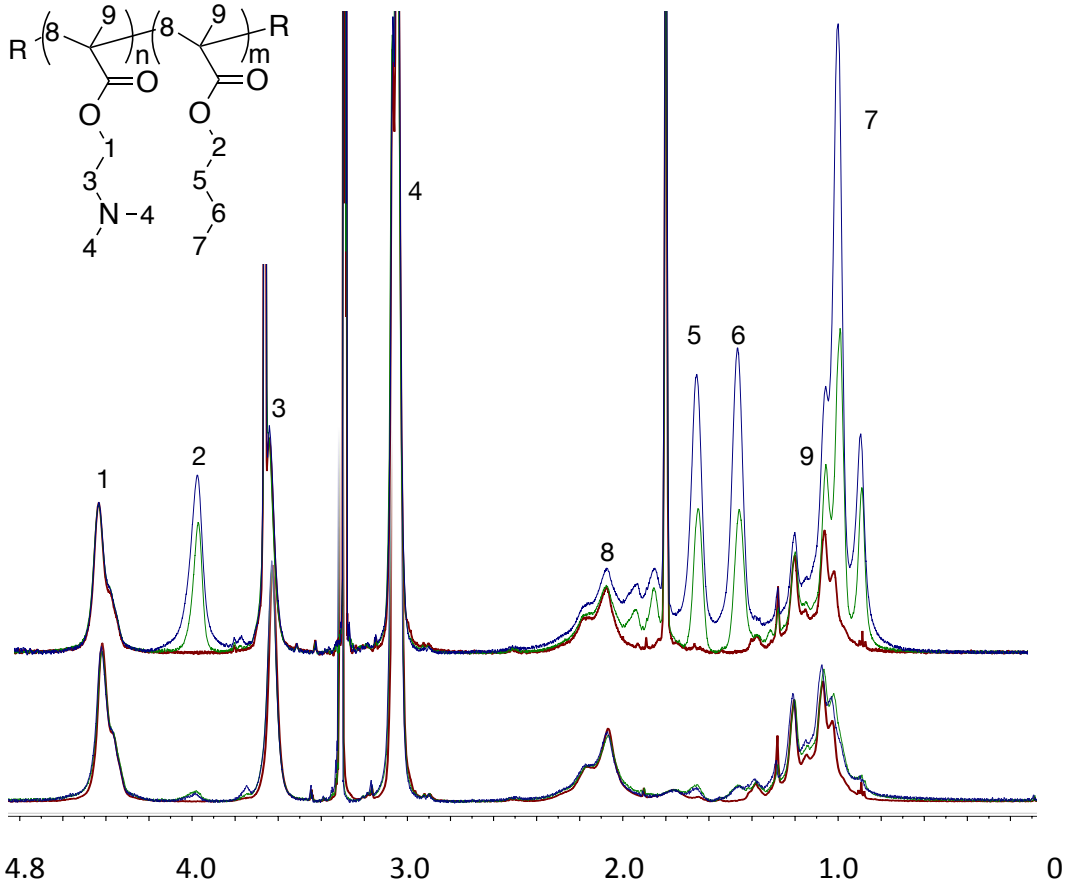

Figure 49. ^{1}H NMR of Poly(DMAEMA$_{27}$), Poly(DMAEMA$_{27}$-*b*-BMA$_{14}$), and Poly(DMAEMA$_{27}$-*b*-BMA$_{29}$) in δ-methanol (bottom) and 2:1 methanol:THF (top). Internally referenced to CD_3OD.

Following synthesis, the four diblock copolymers were purified *via* dialysis, to which hydrochloric acid was added (to a pH~4) to protonate the tertiary amines. During dialysis, micelles are formed. However, upon lyophilization the enthalpic driving force to form micelles drops, but there could still be some microphase structures or a core memory size in the dried polymer powder. The purified amphiphilic polymer proved difficult to characterize via SEC-SLS, as in both aqueous and organic conditions the SEC-SLS chromatogram/light scattering signal was that of the micelles (See Figure 82 and Figure 83). To further characterize the polymers, we turned to MALDI-TOF-MS, which uses a soft ionization method to charge the polymer species. A combination of cationic matrices had to be used with the dried droplet method to ionize the polymers. The MALDI results closely resemble those from NMR but consistently underestimate the M_n by as much as 10%. This can be attributed to the fact that it is challeging to get the higher molecular weight fraction of the polymer samples to fly on MALDI,[351-355] thus a lower than actual M_n and M_w are reported.

3.4.2 Micelle formation and Characterization

The assembly method used to promote micelle formation with amphiphilic polymers can greatly affect their final size and morphology. Therefore, it is important to investigate the average sizes and dispersities of micelle solutions resulting from the different formation techniques. Consistently, we aimed to make 1 mg/mL solutions by dissolving each polymer structure in water and vortexing it for several mins to yield the micelles/particles. Alternative methods of micelle formation were also examined, *i.e.*, *via* self assembly at 50 °C and continuous heating for one hour, which resulted in micelles with higher dispersities even though the average sizes were similar to that of the direct dissolution technique without heating. Sonication of polymer solutions for 30 minutes yielded very small particles, presumable disintegrated micelles or broken up polymers. Other techniques were attempted such as thin film techniques and co-solvent dialysis methods, which led to micelles with both larger sizes and higher dispersities (see Figure 48). Due to the ease of formation (and general lower micelle dispersity) with the direct dissolution technique, this method used for all micelle formation. The size of the micelles formed by direct dissolution in pure water are displayed in Figure 51. It was observed that as the total polymer molecular weight increases, the micelle's radius of hydration increases, while the dispersities of the micelles remained low. As it has been reported by Borisov et al.[341] the size of polyelectrolyte assemblies in non-ionic microenvironments is proportional to the degree of polymerization, as the stretched out chains are governed more by long-range intermolecular coulomb repulsion than short-ranged intramolecular repulsion/sterics. These micelles were also imaged with cryo-TEM to visualize the size and shape of the micelles in water (Figure 53).

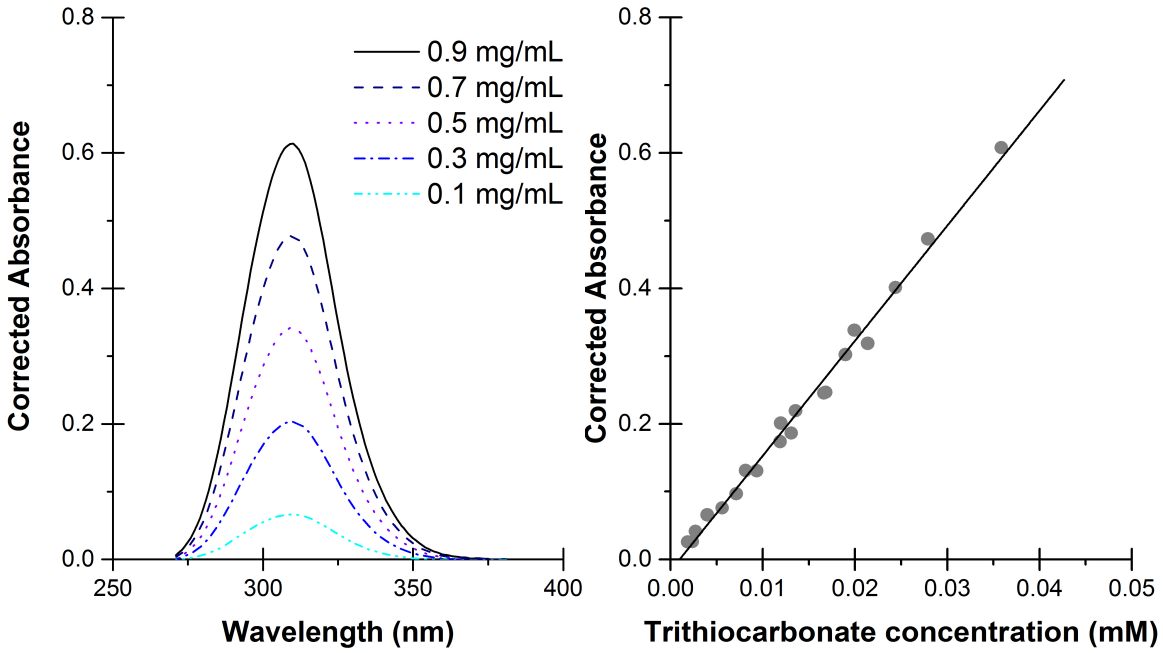

Figure 50a. a) The corrected absorbance of Poly(DMAEMA$_{14}$-*b*-BMA$_{13}$) at various concentrations in pure water at different wavelengths. b.) The corrected maximum absorbance of Poly(DMAEMA$_{14}$-*b*-BMA$_{13}$), Poly(DMAEMA$_{14}$-*b*-BMA$_{23}$), Poly(DMAEMA$_{27}$-*b*-BMA$_{14}$), and Poly(DMAEMA$_{27}$-*b*-BMA$_{29}$) micelles in water at various concentrations and plotted vs. CTA concentration (mM) in solution. A linear fit was applied. The coefficient of determinant $R^2 = 0.991$ and the extinction coefficient was $(1.70 \pm 0.04) \times 10^4$ cm^{-1} M^{-1}.

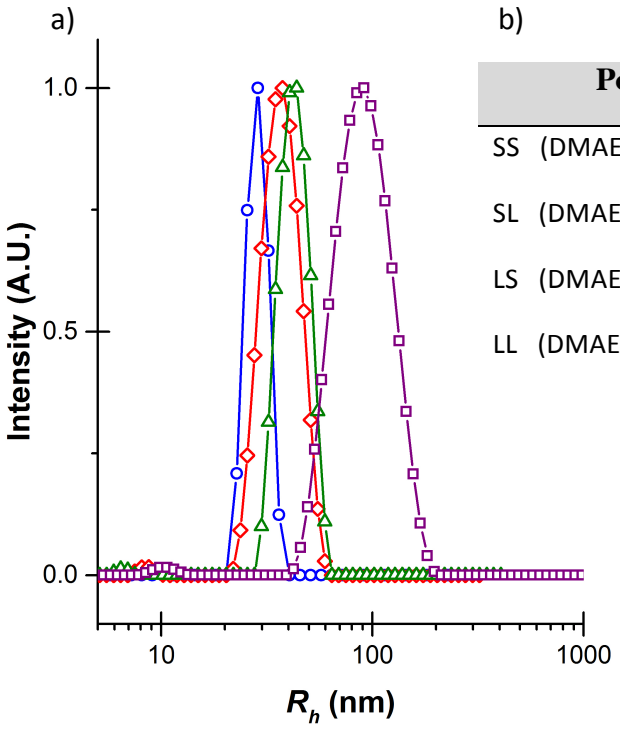

b)

Polymer	R_h (nm)	μ_2/Γ^2
SS (DMAEMA$_{14}$-*b*-BMA$_{13}$)	29	0.04
SL (DMAEMA$_{14}$-*b*-BMA$_{23}$)	37	0.04
LS (DMAEMA$_{27}$-*b*-BMA$_{14}$)	48	0.07
LL (DMAEMA$_{27}$-*b*-BMA$_{29}$)	79	0.10

Figure 51. a) The hydrodynamic radius of micelles formed by direct dissolution in water at 1 mg/mL. Data are represented as follows: Blue circles is poly(DMAEMA$_{14}$-*b*-BMA$_{13}$), red diamonds is poly(DMAEMA$_{14}$-*b*-BMA$_{23}$), green triangles is poly(DMAEMA$_{27}$-*b*-BMA$_{14}$), and purple squares is poly(DMAEMA$_{27}$-*b*-BMA$_{29}$). b) The reported R_h (nm) from DLS and the dispersity (μ_2/Γ^2) of the micelles.

3.4.3 Cryo-TEM

The micelle structure, among other things, plays an important role for nucleic acid binding.[345] CryoTEM was used to visualize the shape and size of each micelle sample. , This technique allowed visualization of the micelle core (as can easily be seen in the cyro-TEM images shown below), however, the micelle corona does not have enough contrast to be visualized. It was found that the micelles all adopted a spherical morphology with the exception ofthe poly(DMAEMA$_{27}$-*b*-BMA$_{29}$) sample where about 10% of the micelles appear to be worm-like in morphology. This small population of worm-like micelles explains why the dispersity (μ_2/Γ^2) of poly(DMAEMA$_{27}$-*b*-BMA$_{29}$) (as measured with DLS) is more broad than the other samples (Figure 50). When this sample was sonicated, the dispersity decreased (Figure 52) from the original dispersity of 0.10 to 0.05 (1 min sonication), and 0.04 (10 mins. sonication), indicating disruption of the wormlike micelles and formation of more spherical monodisperse micelle samples (See Figure 53). With the use of imaging software, we calculated the core size (radius) of the micelles to be 12 ± 2 nm for the micelles formed with poly(DMAEMA$_{14}$-*b*-BMA$_{13}$) and poly(DMAEMA$_{27}$-*b*-BMA$_{14}$) respectively (small hydrophobic block), and 20 nm for poly(DMAEMA$_{14}$-*b*-BMA$_{23}$) (longer hydrophobic block). For poly(DMAEMA$_{27}$-*b*-BMA$_{29}$) micelles (also long hydrophobic block), the spherical core size (radius) was calculated to 25 nm; however, the average core size (radius) including the worm-like micelles was 30 ± 8 nm . Here it should be noted that in some of our images, the worms extend up to 500 nm in length (but the fraction was small). For ease of calculations and comparison, the data reported is of the sonicated sample of this polymer. While the size of the core (R_{core}) appeared proportional to the hydrophobic BMA block lengths, the cores in the cryo-TEM image could also include part of the corona, which is discussed more in the next section. We attempted to visualize the corona in the cryo-TEM image by

increasing its contrast with the staining reagent, sodium phosphotungstate hydrate, (1 wt% in final solution). This caused the micelles to aggregate into large clumps and made it difficult to accurately resolve the corona with certainty (see Figure 100), but from a few individual micelles we calculated the core sizes to be smaller than those reported by cryo-TEM.

Figure 52. The hydrodynamic radius of micelles formed by directed dissolution in deionized water at 1 mg/mL. The size and dispersity decrease of poly(DMAEMA$_{27}$-*b*-

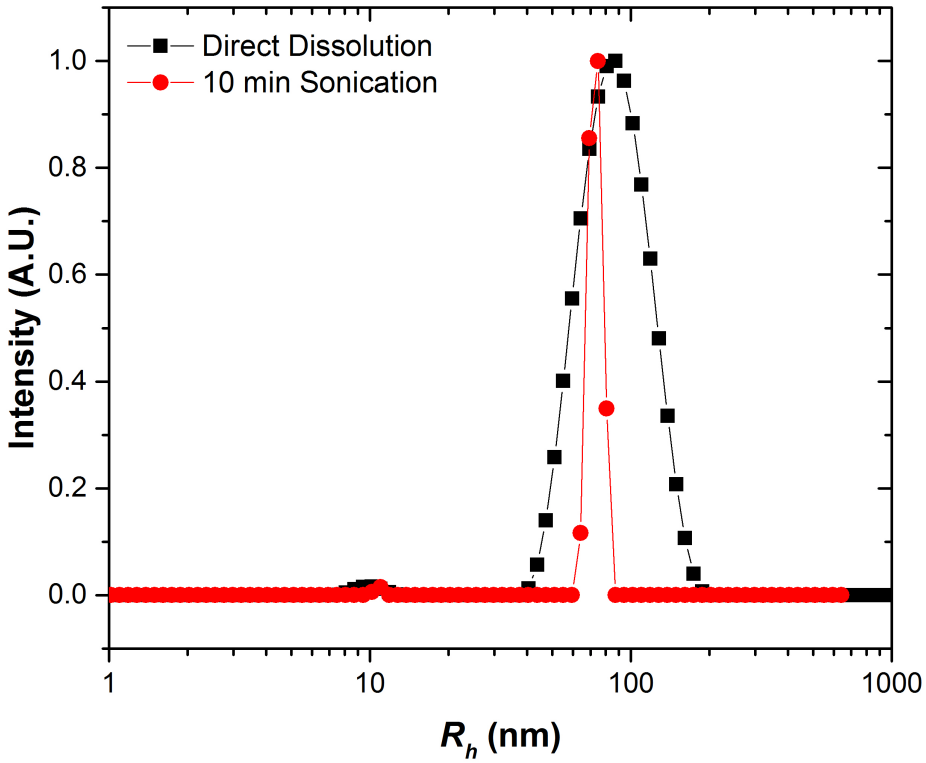

BMA$_{14}$) with 10 minutes of sonication. Suggesting that that the wormlike micelles are broken apart and more uniform spherical micelles are formed.

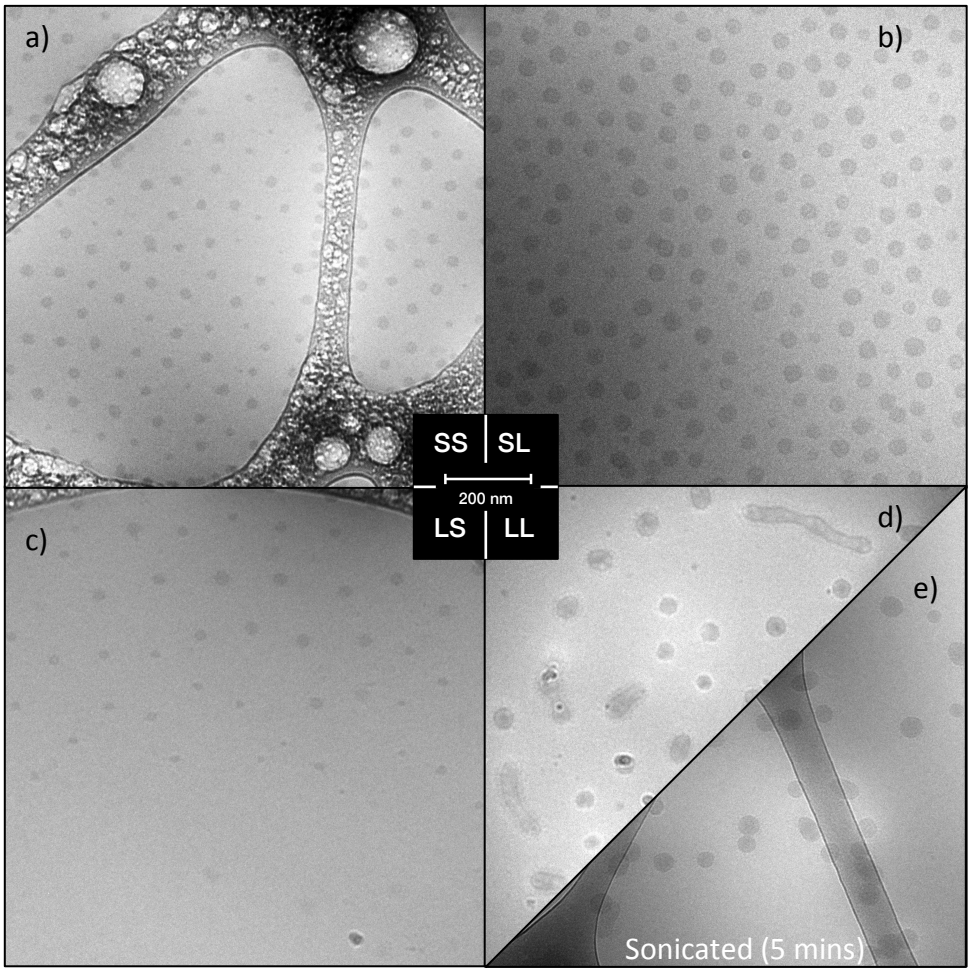

Figure 53. Cryo-TEM images of micelles made in deionized water. a) (SS) refers to poly(DMAEMA$_{14}$-*b*-BMA$_{13}$), b) (SL) is poly(DMAEMA$_{14}$-*b*-BMA$_{23}$), c) (LS) is poly(DMAEMA$_{27}$-*b*-BMA$_{14}$), and d) (LL) is poly(DMAEMA$_{27}$-*b*-BMA$_{29}$) top half is unsonicated LL while the bottom half (e) was sonicated for 5 mins. Scale bar represents 200 nm.

3.4.4 Static Light Scattering

The micelles were probed with static light scattering to ascertain the molecular weight (M_w), radius of gyration R_g, and aggregation number (N_g) of the micelles at pH 7 and 100 mM ionic strength. The importance of determining M_w of the micelles is to be able to calculate the number of chains in each micelle and therefore the number of nitrogen atoms (molar amine content), which is necessary to calculate number binding ratios of DNA and micelles. From SLS, the radius of gyration can also be calculated, but here it should be noted that SLS has the tendency to overestimate the R_g if a very small fraction of aggregates with high molar mass is present in the dispersion.[356] Some of the R_g/R_h values ascertained by SLS are less than 0.775, the value for a hard sphere. This trend has been reported previously with core-corona micelles by Helmstedt et al. and can be attributed to the different refractive index increments (dn/dc) of the two blocks within the polymers that form the micelle.[357] Kunz et al has also investigated this phenomenon with porous/soft spheres (microgels) and kappa-casein micelles and found that several parameters can affect the R_g or R_h measurement, including the density of each block polymer, the depth of solvent penetration into the micelle corona and core, and the packing/arrangement of chains within the micelle (sometimes resembling a loosely crosslinked material).[358] As seen in Table 7, the R_g/R_h is close to that of a hard sphere model, with some of the systems having a smaller value than 0.775, iterating soft/porous spheres. A closer inspection of the micelle characterization data suggests that when the corona volume is much larger than the core volume and thus the R_h is much larger than the densely packed core's radius, this leads to a decreased R_g/R_h value. The micelles can be described as having smaller densely packed cores with larger highly extended coronas in water.

Table 7. Static light scattering data collected.

Polymer	R_h (nm)	R_g (nm)	R_g/R_h	M_w (10^6 g/mol)	N_g
SS	25	15	0.61	4.8	170
SL	34	27	0.79	9.9	270
LS	33	23	0.70	3.3	80
LL	57	43	0.75	19	344

From the combination of cryo-TEM data and SLS aggregation values (N_g), we were able to calculate the density of chains at the core-corona interface and the core density (Table 8) in water. While it appears that the aggregation number is driven by the length of the hydrophobic block,[359,360] (longer BMA blocks have higher N_g), it seems that the packing density is somewhat independent. As was previously mentioned, the core and part of the corona is being viewed in the cryo-TEM images. From the calculated core densities from cryo-TEM (Table 8), the BMA core is much lower than its reported density of 1.07 g/cm^3, thus, indicating that part of the corona is being visualized in the image.[361] In Table 8 we have calculated the corrected radius of the core using equation 2 [assuming the literature density (ρ) of poly(BMA)].

$$R_{core} = \sqrt[3]{\frac{3\, N_g\, M_w}{4\, \pi\, \rho\, N_{Av}}} \qquad \textbf{(2)}$$

These R_{core} values are slightly less than those seen in cryo-TEM and yield a packing density at the core/corona interface to be 8 nm^2/chain ± 2 nm^2 for all four micelle systems (Table 8).

Table 8. Summary and analysis of the micelle's core from cryo-TEM and SLS data.

Polymer	BMA M_n (kg/mol)	R_{core} [a] (nm)	R_{core} [b] (nm)	N_g	Ca. Core Density[a] (g/cm^3)	Packing Density [b] (nm^2/chain)
SS	13	12	9	170	0.507	6.5
SL	23	20	13	270	0.307	8.1
LS	14	13	8	80	0.204	8.7
LL	29	25	16	340	0.253	8.7

[a] was determined by cryo-TEM and [b] determined from SLS assuming the core density to be 1.07 g/cm^3.

3.4.5 Dynamic Light Scattering

DLS was used to determine the size of the micelles, in particular the characteristics of the corona. Micelles were all created *via* direct dissolution, and several experimental controls were performed. Previously it has been shown that micelles with very low T_g (-58 °C) and short hydrophobic chains (3.2 KDa) are able to rearrange and exchange chains[188] and that the length of hydrophobic chain greatly affects the rate of chain exchange kinetics.[362] We hypothesize that because our polymers have long hydrophobic block lengths (13-29 KDa) and glass transition temperatures close to room temperature, polymer chain exchange would likely not be observable. To test this hypothesis, we performed two experiments: we made micelles at 1 mg/mL and diluted them to several concentrations to examine if the micelles would change size according to their concentration in solution, and we mixed two different micelle solutions together to examine if size changed over time. In both these experiments, we did not observe micelle size deformation - which may indicate no [observable] polymer chain exchange and that the micelle core could be in a fixed state in aqueous conditions once formed.

Previously, Gil *et al*. noted that polymers with similar structures to those studied here may one day be used as temperature responsive micelles for gene delivery.[344] It is

important to understand the temperature dependence of micelle stability as they may be subjected to a number of different temperatures, e.g. storage 4 ºC or to promote delivery in biological systems at 37 ºC. We studied the micelles over a wide range of temperatures (see the Appendix) to analyze the dependence of temperature on structure and stability. Here, it should be noted that poly(DMAEMA) does have a reported lower critical solution temperature (LCST) of 38 °C at pH 9, 45 °C at pH 7, and 69 °C at pH 4,[164] and to this end, we conducted LCST measurement and no observable cloud point was observed at the conditions tested with the micelles in water at 1 g/L. This result could be due to the fact that the poly(DMAEMA) is not molecularly dissolved in solution but it is confined to the corona of a micelle with high osmotic pressure in the poly(DMAEMA) layer/corona. The effects of pH and ionic strength on the phase transition temperatures of poly(DMAEMA)[337] and poly(DMAEMA-co-BA)[363] has previously been studied in detail. To summarize, the temperature response is attributed to the collapse of DMAEMA moieties. Increasing the pH of the bulk decreased the transition temperature of the temperature-sensitive phase transition and increasing the BMA content lead to a reduction in the transition pH and temperature of the phase transition.[337,363] While the micelle size was measured over a range of temperatures (20 - 60 °C + 4 ºC), no change in size was detected at constant pH and ionic strength (see the Appendix).

The molecular weights and molar mass ratio between the hydrophilic and hydrophobic block lengths have a direct impact on the size, shape, and stability of the micelles.[333] Previously it has been shown that micelle stability is strongly correlated with core polymer length.[364] To assess the stability of the micelles over time and in various buffers, we consequently formed and measured the size of the micelles. Over the period of a month the micelles did not change size, indicating that these cationic polymer micelles are at a stable size when formed by direct dissolution in water at 1 g/L (see the Appendix). To evaluate the effect of the salt and pH on micelle formation, the diblock

polymers were directly dissolved in different buffers (pH 7 100 mM, pH 8 100 mM and water at 1 g/L). The micelles made in each buffer were consistently the same size over time suggesting that formation and equilibrium (but not size) are unaffected by the media (see the Appendix). Even at high pH, close to the isoelectric point, and in a range where hydrolysis can happen, the sizes remained constant. Polymer integrity from hydrolysis was also examined by forming micelles in D_2O with sodium deuteroxide (40 wt. %). Hydrolysis was not observed by ^1H NMR over three days.

3.4.6 Buffered micelles

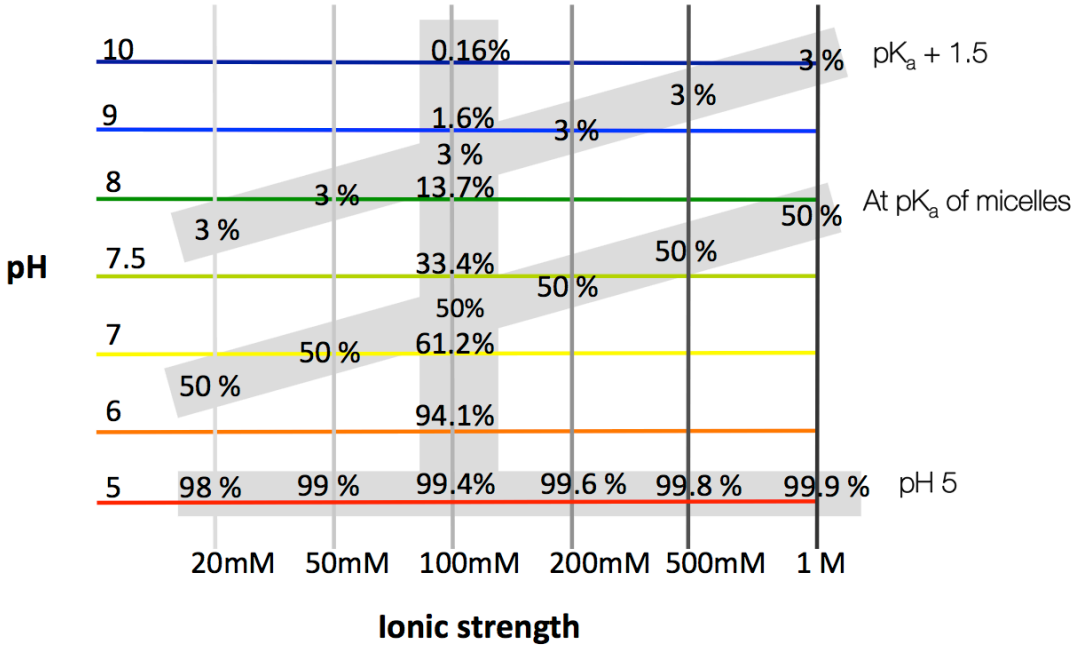

Figure 54. A plot representing the pH and ionic strength values at which we dialyzed the micelles and their corresponding protonation state (%).

3.4.6.1 The effects of pH Varience

Once determined that micelles made *via* direct dissolution are stable with respect to time, concentration, temperature, and buffered solutions, we set about to test the effects of varying the pH and ionic strength on the formed micelles. DMAEMA is a weakly ionizable polyelectrolyte, meaning that the fraction of charged monomers is governed by an ionization equilibrium and is strongly affected by the local proton and ionic strength concentrations (Figure 54).[341] The four polymers were dissolved in water and then dialyzed over four days to several pH values and ionic strengths (Figure 54 and Figure 57 and the Appendix). The size (R_h) and zeta potential (ζ) of the micelles were measured after the dialyzed samples were filtered through a 0.2 μm filter (in Figure 51 there were no particles > 200 nm). As seen in Figure 56, the size of the micelles decreases as the pH increases; however, the correlation observed was not linear with respect to pH. The micelle core, being nonionic, should not change with pH, whereas the corona, being a weak polyelectrolyte, is greatly affected by the change in pH (and protonation state) (see Figure 55 for schematic representation). When the pH is less than the pK_a, the DMAEMA moiety is protonated, the monomer units are slightly repelled by intramolecular coulombic forces, the polymer/corona is swollen by the positive osmotic pressure within, and the cationic polymer chains are extended outward. The micelles can be viewed as swollen (positive osmotic pressure within the corona) cationic polymer brushes with a rubbery kinetically 'locked' core. Duly, when the pH increases, the tertiary amines become deprotonated and the electrostatic repulsion and osmotic pressure decreases, thus allowing the DMAEMA polymer chains to relax and decrease in length. Protonated poly(DMAEMA) is highly water soluble; however, the methyl groups on DMAEMA induce hydrophobicity and provide a compact conformation (hypercoiled morphology) at high pH, therefore the unprotonated DMAEMA is slightly hydrophobic

in nature.[344,365] This, along with the decrease in osmotic pressure, leads to the contraction of the corona at high pH values. The poly(DMAEMA) is fully neutralized/deprotonated at pH 9.9 and above. Knowing the aggregation number (N_g), DMAEMA M_w, and R_h, we calculated the average monomer concentrations in the corona when at pH 5, 100 mM ionic strength to be 410 mM, 240 mM, 145 mM, and 130 mM for SS, SL, LS, and LL, respectively. Also, the concentration of DMAEMA monomers when the corona is contracted at pH 10, 100 mM is 1040 mM, 500 mM, 480 mM, and 350 mM for micelles SS, SL, LS, and LL, respectively. The collapse of the corona is expected to happen when the ionic strength in the osmotic brush approaches that of the bulk solution, which in our system appears to happen at 0.3 units above the pK_a. This pK_a is higher than expected for some of our osmotic brushes, which could arise from the variation of the monomer concentration throughout the corona. The increase in corona size with respect to protonation state appears proportional from 0 to 33% protonation (pK_a + 0.3) in 100 mM salted buffer (see Figure 96 and the Appendix) showing that there is an initial correlation between the two; however, thereafter the size plateaus off as protonation increases. It is interesting to note that the two micelle systems of identical DMAEMA block length [poly($DMAEMA_{27}$-*b*-BMA_{14}) and poly($DMAEMA_{27}$-*b*-BMA_{29})] do not have the same change in corona size between pH 5 and 10; however they do scale proportionally on a log scale. Further comparing poly($DMAEMA_{27}$-*b*-BMA_{14}) and poly($DMAEMA_{27}$-*b*-BMA_{29}), the change in size of the micelle with the smaller hydrophobic block is 11 nm (green triangles), while the micelle with the larger hydrophobic block has a corona change of 16 nm (purple squares). Earlier we pointed out that poly($DMAEMA_{27}$-*b*-BMA_{14}) and poly($DMAEMA_{27}$-*b*-BMA_{29}) have very different aggregation numbers, and while poly($DMAEMA_{27}$-*b*-BMA_{14}) is less densely packed (more area/chain in the corona), it does have a greater DMAEMA corona concentration; poly($DMAEMA_{27}$-*b*-BMA_{14}) also has a larger curvature, thus when the corona begins to contract the chains

become more densely packed in a faster manner than the lower density models.[366] It is our hypothesis that the micelle with the larger core block [poly(DMAEMA$_{27}$-*b*-BMA$_{29}$)] appears to be able to contract its corona more due to its lower monomer concentration, lower curvature, and larger corona volume. Having a larger volume means that the change in volume from pH 5 to pH 10 is actually less in poly(DMAEMA$_{27}$-*b*-BMA$_{29}$) than the analogous model with a smaller core [poly(DMAEMA$_{27}$-*b*-BMA$_{14}$)], and because the curvature is higher with poly(DMAEMA$_{27}$-*b*-BMA$_{14}$), the corona is more densely packed at pH 10. Another interesting observation is the size of the corona of poly(DMAEMA$_{27}$-*b*-BMA$_{29}$) at pH 5; the R_h of the corona is roughly 40 nm (Figure 56 and Table 7). Taking into account the M_n of the hydrophilic block (27 kDa, 172 repeat units), the maximum end-to-end distance (L_{max}) of poly(DMAEMA$_{27}$) would be about 45 nm, meaning that the DMAEMA block length is approaching its maximum stretched out length, emphasizing the highly extended state of the corona.

Table 9. Summary of the corona's parameters from SLS and DLS.

Polymer	DMAEMA (kg/mol)	R_h [a] (nm)	R_h [b] (nm)	Surf. Density [a] (nm^2/chain)	Vol. change in corona	Corona ρ [a] (g/cm^3)*	Corona ρ [b] (g/cm^3)*
SS	14	25	19	46	61 %	0.064	0.162
SL	14	35	28	57	53 %	0.037	0.078
LS	27	34	23	177	70 %	0.023	0.075
LL	27	57	41	119	63 %	0.020	0.055

[a] data obtained at pH 5; [b] data obtained at pH 10; ρ = density; *density of the DMAEMA polymer component, excluding the water volume, which is the majority of filled space.

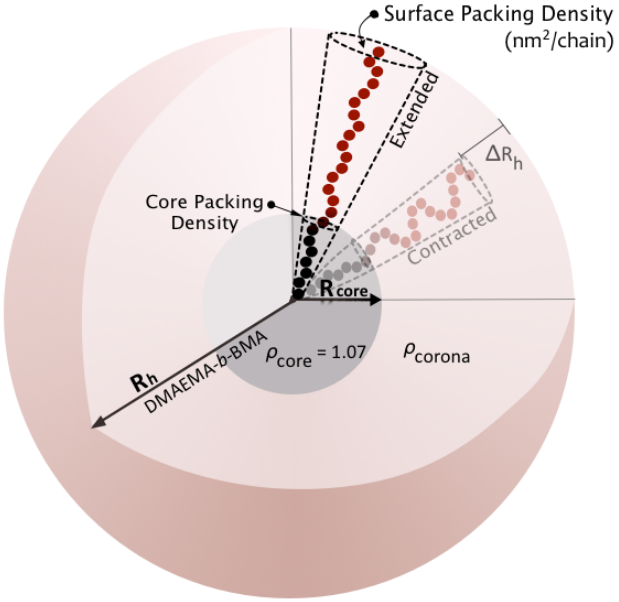

Figure 55. A schematic illustration of the micelle structure with an extended corona (low pH) and a contracted corona (high pH), depicting the change in R_h, corona density, and the packing density of chains.

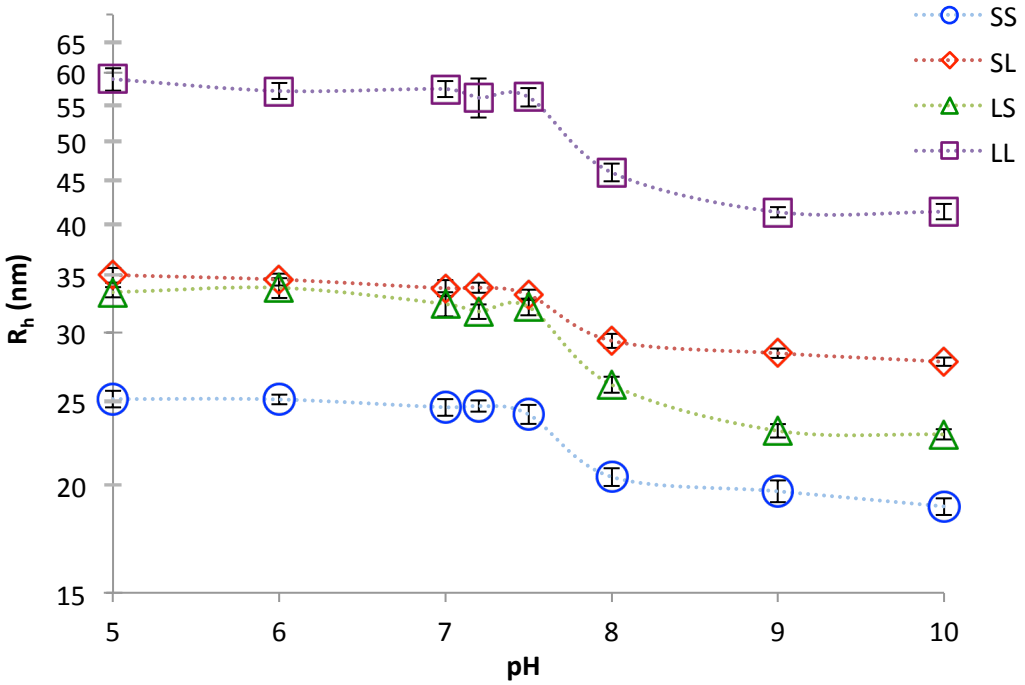

Figure 56. The DLS analysis revealing the size (R_h) of the four micelle types in different buffers (pH) prepared at an ionic strength of 100 mM at 173 °. Blue circles (SS) is poly(DMAEMA$_{14}$-*b*-BMA$_{13}$), red diamonds (SL) is poly(DMAEMA$_{14}$-*b*-BMA$_{23}$), green triangles (LS) is poly(DMAEMA$_{27}$-*b*-BMA$_{14}$), and purple squares (LL) is poly(DMAEMA$_{27}$-*b*-BMA$_{29}$). Error bars are the standard deviation of all the data collected, a minimum of three replicates.

3.4.6.2 The effects of Ionic Strength Varience

Understanding these interactions/dynamics is important for the future development of stable micelles in a variety of environmental conditions, e.g. physiological. To assess the size of the corona with respect to the ionic strength, the poly(DMAEMA$_{27}$-*b*-BMA$_{14}$) micelles were dialyzed to pH 5, the individual pK_a for each micelle formulation, and pK_a +1.5 within different ionic strengths ranging from 20-1000 mM (Figure 57a). Here it should be noted that i) the concentration of the buffer is 20 mM and the total ionic strength was adjusted by the addition of NaCl, and ii) the pK_a of poly(DMAEMA) is always lower than that of the DMAEMA monomer; however, these values become increasingly closer at higher salt concentrations.[319,365,367] As shown in Figure 57a, the relationship between micelle size and ionic strength is almost linear (on a log scale). Although the protonation state of the poly(DMAEMA) chains is greater than 98% at pH 5, and equal to 50% at the pK_a, and 3% at 1.5 units above the pK_a, intramolecular columbic charge repulsion and osmotic pressure is varied between samples. For simplicity, we shall discuss osmotic pressure and charge repulsion as two separate phenomena, but these are both dependent upon the protonation/deprotonation state of poly(DMAEMA). It should also be noted that osmotic pressure governs the corona extension more than charge repulsion.[368] At pH 5, the DMAEMA is almost fully protonated and the micelles are strongly charged and therefore accommodate a large number of counterions, highly increasing the osmotic pressure within the brush layer. The added salt screens the charge 'visibility' of polyprotonated tertiary amines, and therefore as salt increases the osmotic pressure decreases and so does the Debye screening length. The decrease in size can be attributed to two effects: first, the increase in salt leads to a decrease in osmotic pressure within the corona and second, the added salt decreases the Debye screening length (κ^{-1}) of the electrolyte. These two properties lead to a cationic

corona that contracts at higher ionic strengths. Micelles at the pK_a (50% charged) have less osmotic pressure than those at pH 5 and therefore are less influenced by the osmotic pressure/ionic strength of the bulk. Thus the change in size is less pronounced, especially at higher salt concentrations. The micelles dialyzed at the pK_a + 1.5 are almost completely neutralized, in 20 mM buffer they are not very swollen to begin and are hardly influenced by intramolecular charge repulsion; osmotic pressure in the corona is low, the DMAEMA polymers are only slightly water soluble, and therefore already somewhat collapsed. At low degrees of ionization, the micelle conformation is controlled by a balance between the short range chain-chain repulsion and the conformational entropy of stretched out chains.[341] The addition of salt steadily collapses the corona as the osmotic pressure decreases in the corona, yet even these micelles still have enough charge to still be stable in solution as no precipitation was noted. It can also be seen (Figure 57a) between the three samples that as the salt concentration approaches 1 M, the change in size decreases/plateaus, indicating the limit of corona collapse is being approached, or the polymers could be adopting a random coil morphology.

In Figure 57b the four polymer micelles are each at their pK_a and the ionic strength was systematically increased, which follows a similar trend as that seen at pH 5 and pK_a + 1.5. The size of poly($DMAEMA_{14}$-*b*-BMA_{23}) and poly($DMAEMA_{27}$-*b*-BMA_{14}) are of almost identical sizes when the coronas are extended (low ionic strength), but as the salt concentration increases the longer DMAEMA block length collapses [6%] more than the short, and thus at higher salt concentration the poly($DMAEMA_{27}$-*b*-BMA_{14}) is slightly smaller in size than poly($DMAEMA_{14}$-*b*-BMA_{23}). As it was seen above in size versus pH, the change in size between LS and LL [poly($DMAEMA_{27}$-*b*-BMA_{14}), poly($DMAEMA_{27}$-*b*-BMA_{29})] was moderately different (ΔLS_{size} = 7 nm vs. ΔLL_{size} = 13 nm) considering these micelles have the same length of DMAEMA block;

again this is due to the larger cored micelle having less corona density, lower curvature, and over four times the volume.

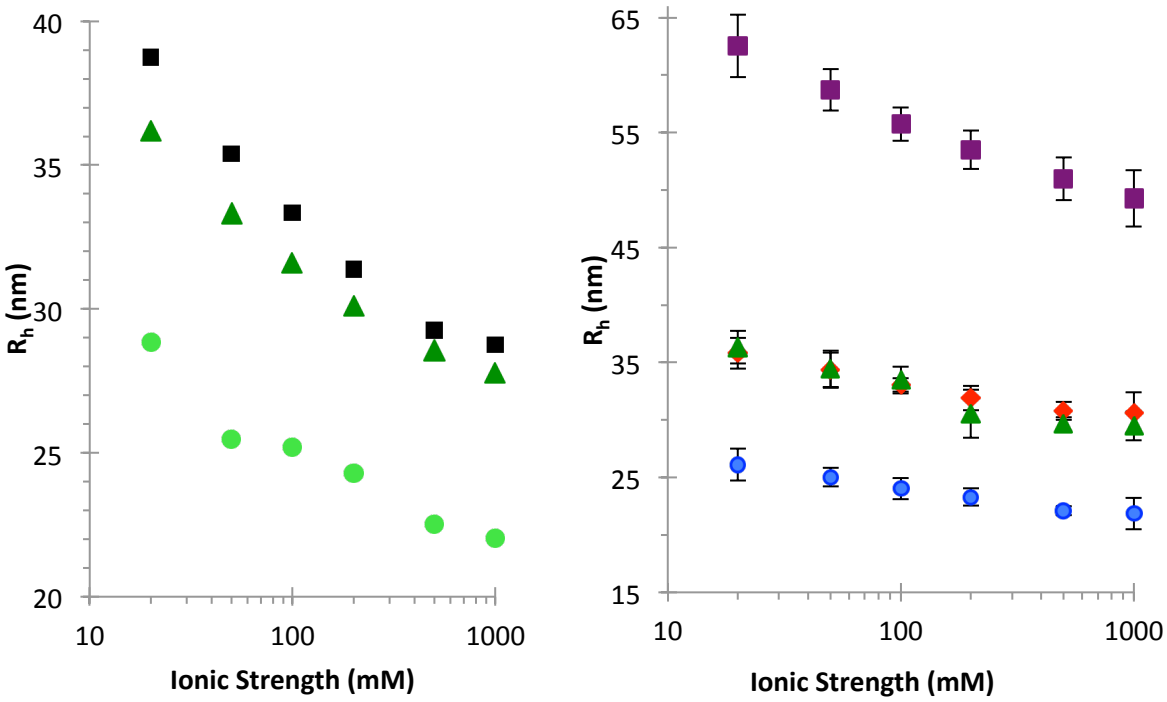

Figure 57a. The size (R_h) of poly(DMAEMA$_{27}$-*b*-BMA$_{14}$) micelles as measured by DLS at various ionic strengths and protonation states. Black squares represent samples at pH 5, green triangles are micelles where pH = pK_a, and circles are micelles at pK_a + 1.5 (3% protonated). (Multi-angle DLS error is less than 1%, but accuracy is about 5%)

Figure 57b. The size (R_h) of the four micelles at their pK_a (50% protonated) at different ionic strengths ranging from 20 mM to 1 M as measured by DLS. Blue circles (SS) is poly(DMAEMA$_{14}$-*b*-BMA$_{13}$), red diamonds (SL) is poly(DMAEMA$_{14}$-*b*-BMA$_{23}$), green triangles (LS) is poly(DMAEMA$_{27}$-*b*-BMA$_{14}$), and purple squares (LL) is poly(DMAEMA$_{27}$-*b*-BMA$_{29}$). Error bars are the standard deviation of three replicates.

3.4.7 Zeta Potential

3.4.7.1 The effects of pH Varience

The zeta potential, the potential difference at the slipping plane (inside the double layer), of the micelle formulations can indicate much about the stability of particles in dispersion.[369] It was our goal to investigate the zeta potential of our micelles in these pH and ionic strength monoprotic buffers and monovalent salts to understand how zeta potential may affect future binding and complexation experiments. Zeta potential is an important electrokinetic property, in addition to indicating colloid stability from aggregation, it can play a role in understanding the adsorption of particles on the colloid dispersion/solution interface through differences in the electrophoretic mobility.[369] Our results were calculated from the measured electrophoretic mobility using Henry's equation and the Smoluchowski approximation.[370] The environment of the sample (pH, ionic strength, additives, concentration, etc.) greatly affects the zeta potential, it has been shown with similar micelles (RAFT polymerized poly(acrylamidophenylboronic acid-*b*-acrylamidoethylamine) and ATRP synthesized poly(2-diisopropylaminoethyl methacrylate-*b*-aminoethyl methacrylate) modified with succinic anhydride) that at low pH, the zeta potential is usually positive and at high pH the zeta potential is negative.[371,372] The point at which the zeta potential is zero (isoelectric point) is significant as this is normally the point at which the colloidal system is least stable to aggregation.[370,371,373] According to our results (Figure 58), the zeta potential is positive at all pH values except at pH 10. There also appears to be a logarithmic relationship between zeta potential and protonation state (see the Appendix). The isoelectric point falls between pH 8 and 10 at 100 mM ionic strength (1% protonated) - this is very close to the point where the poly(DMAEMA) is fully deprotonated (pH 9.9). This small discrepancy between fully deprotonated poly(DMAEMA) and zero zeta potential is likely

a result of the CTA head group. Remembering that at the end of each polymer chain is a carboxylic acid, which is deprotonated at high pH and does result in a hard fixed negative charge on the surface of the micelles, this artifact produces micelles that can be negatively charged before all of the DMAEMA moieties have been neutralized. From pH 6-5 the zeta potential changes little, and one can expect this trend to continue as pH drops from 5 to 2; similarly, a similar trend should hold above pH 10, as has been previously shown.[369,371-377] In our system the $\Delta\zeta$ (change in ζ vs. pH) is greatest when the pH is slightly greater than that of the pK_a of the micelles, this coincides with the point at which it is easiest to remove charge (H^+) from the micelle's corona and therefore reduce its surface charge – this was also the point at which the size of the corona decreased the most with respect to change in pH (Figure 56).

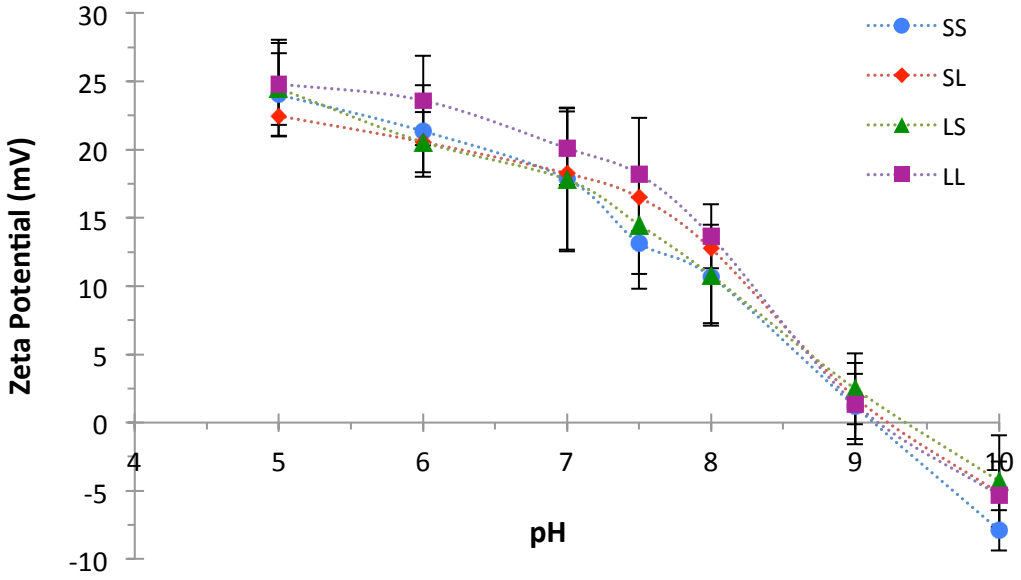

Figure 58. The measured zeta potential of the four polymer micelles at 100 mM ionic strength from pH 5 to pH 10. Error bars represent the standard deviation of a triplicate measurement. Blue circles (SS) is poly(DMAEMA$_{14}$-*b*-BMA$_{13}$), red diamonds (SL) is poly(DMAEMA$_{14}$-*b*-BMA$_{23}$), green triangles (LS) is poly(DMAEMA$_{27}$-*b*-BMA$_{14}$), and purple squares (LL) is poly(DMAEMA$_{27}$-*b*-BMA$_{29}$).

3.4.7.2 The effects of Ionic Strength Varience

Wang and Keller have demonstrated that multivalent ions decrease the zeta potential of a particle to a higher degree than monovalent ions and monoprotic buffers.[375] The double layer theory predicts that increasing electrolyte concentration and valency will decrease the thickness of an electric double layer which should result in a decrease in the magnitude of zeta potential.[378,379] We found this consistent with our results, as seen in Figure 59, the zeta potential decreases as the salt concentration increases. This is because the size of the double layer (κ^{-1}) is dependent on the concentration of ions present in solution; the more ions present – the more compressed the double layer becomes.[374] Here it should be emphasized that the accuracy (signal to noise ratio) of the measurement decreases when the salt concentration is above 0.1 M (according to the instrument manufacturer). Therefore values higher than 200 mM have been excluded from our results. It is important to study zeta potential for future binding applications, such as the complexation between micelles and polyanions (like DNA). Because complexation is usually an entropically driven process, higher salt concentration not only decreases zeta potential and charge screening but also hinders micelleplex formation. As seen in our data, at low ionic strengths the zeta potential is highly positive, making this a good starting point for future binding assays of these micelles to various polyanions.

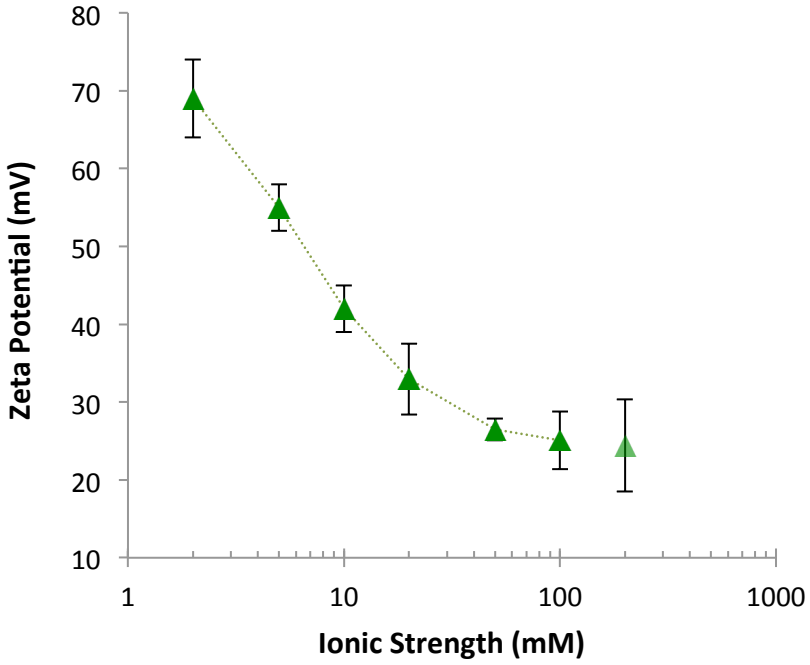

Figure 59. The measured zeta potential of the poly(DMAEMA$_{27}$-*b*-BMA$_{14}$) micelle at pH 7 at various ionic strengths. Values higher than 200 mM have been excluded due to the instrument manufacturer's guidelines. Error bars are the standard deviation of the data measured in triplicate.

Understanding the zeta potential, size, and protonation state of the micelles in different pH and ionic strength environments is crucial for the investigation of the fundamentals of binding between cationic micelles and polyanions such as proteins, nucleic acids, or polymers. Along with the change between the environment of the initial complexation point and the environment of the final end point, i.e. biological media, intravenous conditions, or intracellular cytoplasm – all these factors may greatly alter the binding and release profiles of these potential payloads.

3.5 Conclusion

Herein we have detailed the synthesis and characterization of two macroCTAs and four diblock polymers comprised of a cationic hydrophilic DMAEMA block and a hydrophobic BMA block. These polymers spontaneously formed micelles in many solution conditions and proved to be exceptionally stable over time even at high pH, temperatures, and concentration. Micelles were made *via* direct dissolution and dialyzed to several pHs and ionic strengths before being analyzed by UV-Vis, cryo-TEM, SLS, DLS, and zeta potential. Cryo-TEM revealed that we had formed spherical micelles, except with poly($DMAEMA_{27}$-*b*-BMA_{29}) which formed some worm-like micelles, but could be readily broken up with sonication. SLS revealed that R_g/R_h was close to that of a hard sphere (0.75), and the density of the micelles at the core-corona interface and on the surface of the micelle increased as the length of polymer increased. The change in corona size depended on three factors: the packing density of the polymer chains, the charge repulsion between protonated DMAEMA moieties, and the osmotic pressure within the micelle vs. its environment. The micelles were then investigated in buffers, and the effects of pH and ionic strength were evaluated while maintaining a constant protonation state. The corona, being a weak polyelectrolyte brush, was pH and ionic strength sensitive, and the size of the corona contracted and extended accordingly. Finally we measured the zeta potential of our micelles and found the isoelectric point to be between pH 8 and 10. The size of the micelles at physiological conditions varied (23-55 nm), which mainly correlated to the length of the polymer, while the average zeta potential at physiological conditions was around 20 mV, making these micelles prime candidates for future binding assays and possible delivery vehicles with a variety of functional polyanions.

The Appendices include: ^{1}H NMR spectra, SEC chromatograms, MALDI-TOF-MS, DLS size distribution and preparatory methods and sonication, UV-Vis, Micelle stability over time, temperature, and in buffers, DLS size vs. protonation state, DSL size vs. Debye length, Cryo-TEM images, dn/dc plots, static light scattering berry plots.

Chapter 4.

FINAL CONCLUSION AND FUTURE DIRECTIONS

4.1 Continuation of the Polyplex Project with Block and Statistical Copolymers for DNA Delivery

The future direction of this project has many avenues, some of which could lead to in vivo testing and more definitive mechanisms of entry into the nucleus. To this note, some of the polymers synthesized herein have already been tested and compared with galactose polymers in vitro and in vivo (mice).

To summarize this research: a series of cationic diblock glycopolymers derived from *N*-acetyl-D-galactosamine (GNA) were synthesized and evaluated to create delivery systems specifically targeted to asialoglycoprotein receptors on hepatocytes. These ASGP receptors are only present on hepatocytes. The liver is a common target for the treatment of many diseases such as hemophilia and several lysosomal storage diseases.[264,380-382]

The diblock polymers were composed of a GNA-derived block of fixed length and cationic 2-aminoethylmethacrylamide (AEMA) blocks of varying lengths. GNA-derived polymers showed cell type-specific gene expression in vitro, with higher protein expression in HepG2 (human hepatocellular carcinoma) as compared to HeLa (human cervix adenocarcinoma) cells. In vivo studies show higher accumulation of pDNA and GNA-derived polymers in the mouse liver compared with the glucose-derived [poly(MAG)] non-targeted control polymers.

While the galactose-based polymers had higher gene expression in HepG2 cells the glucose polymers had higher expression in HeLa cells. This shows that presence of GNA ligands on the MAGNA block promotes cell type-dependent delivery, with higher transgene expression with HepG2 (contains the ASGP receptor) as compared to HeLa (lacks ASGP receptor) cells. In the animal studies the glucose polymers tented to accumulate in the kidney more so than the galactose polymers; however, the galactose

polymers were more prone to localization in the liver cells. The targeted delivery of drugs and nucleic acids to specific tissues has been a long sought after goal and a major hurdle for the field of nano medicine. Tissue-specific delivery offers advantages of increased therapeutic efficacy, lower toxicity, and reduced immune response.[383]

These initial findings emphasize that more polymers and polyplexes need to be tested in vivo to better our understanding of how non-viral vehicles interact with and affect biological hosts and organs. The future direction of these projects is to test these polymers in more living systems and to further probe their ability to penetrate cellular membranes, including nuclear.[20]

4.2 Continuation of the Micelleplex Project with Amphiphilic Polymers for studying the binding of DNA to Micelles and the Delivery thereof

The goal of this project stems from the second thrust of the MRSEC IRG3 (Hierarchical Multifunctional Macromolecular Materials), and that is to control the structure and properties of block-polymer-based "amphiplexes" and assemblies of the polyanions (like DNA) with cationic polymer micelles. But before I mention future work I should comment on what has already been done with this project.

With the carefully synthesized polymers and monodisperse micelles already made and studied, we needed precise lengths of DNA in order to accurately study the binding of nucleic acids with the cationic micelles. Lengths of 20, 200, and 2000 base pairs were chosen; these represent 12.2 kDa, 123 kDa, and 1.24 mDa and 6.6 nm, 66 nm, and 660 nm respectively. The different lengths of DNA were cloned from a double stranded plasmid DNA. Lengths of 200 and 2000 base pairs were cloned from a plasmid by designing and custom ordering three unique primers. The pDNA

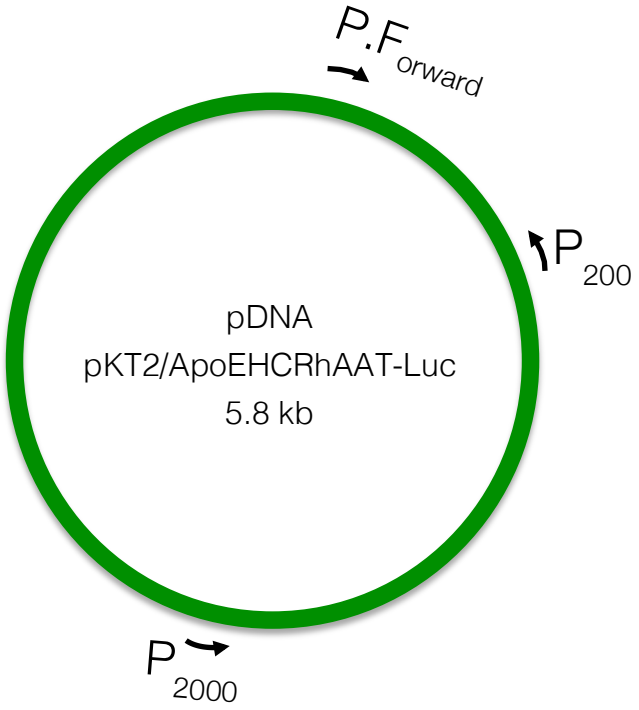

was cloned in a PCR machine for 30 cycles, and purified and imaged to ascertain its validity. To make the short 20 base pair oligomer two complimentary strands of 20mer primers were bought and annealed. The sequences of the 20 bp lengths of DNA are:

CCCATACAAGCGATAGATTT
AAATCTATCGCTTGTATGGG

The sequence of the 200 bp length of DNA is:

TATCCGCTGGAAGATGGAACCGCTGGAGAGCAACTGCATAAGGCTATGAAGA
GATACGCCCTGGTTCCTGGAACAATTGCTTTTACAGATGCACATATCGAGGTG
GACATCACTTACGCTGAGTACTTCGAAATGTCCGTTCGGTTGGCAGAAGCTAT
GAAACGATATGGGCTGAATACAAATCACAGAATCGTCGTATG

The sequence of the 2000 bp length of DNA is:

CTGAATCCGGTGAGAATGGCAAAAGTTTATGCATTTCTTTCCAGACTTGTTCA
ACAGGCCAGCCATTACGCTCGTCATCAAAATCACTCGCATCAACCAAACCGT
TATTCATTCGTGATTGCGCCTGAGCGAGACGAAATACGCGATCGCTGTTAAA
AGGACAATTACAAACAGGAATCGAATGCAACCGGCGCAGGAACACTGCCAG
CGCATCAACAATATTTTCACCTGAATCAGGATATTCTTCTAATACCTGGAATG
CTGTTTTTCCGGGGATCGCAGTGGTGAGTAACCATGCATCATCAGGAGTACG
GATAAAATGCTTGATGGTCGGAAGAGGCATAAATTCCGTCAGCCAGTTTAGT
CTGACCATCTCATCTGTAACATCATTGGCAACGCTACCTTTGCCATGTTTCAG
AAACAACTCTGGCGCATCGGGCTTCCCATACAAGCGATAGATTGTCGCACCT
GATTGCCCGACATTATCGCGAGCCCATTTATACCCATATAAATCAGCATCCAT
GTTGGAATTTAATCGCGGCCTCGACGTTTCCCGTTGAATATGGCTCATAACAC
CCCTTGTATTACTGTTTATGTAAGCAGACAGTTTTATTGTTCATGATGCAGCT
GGATCCAGATCCCTATACAGTTGAAGTCGGAAGTTTACATACACTTAAGTTG
GAGTCATTAAAACTCGTTTTTCAACTACTCCACAAATTTCTTGTTAACAAACA
ATAGTTTTGGCAAGTCAGTTAGGACATCTACTTTGTGCATGACACAAGTCATT
TTTCCAACAATTGTTTACAGACAGATTATTTCACTTATAATTCACTGTATCAC
AATTCCAGTGGGTCAGAAGTTTACATACACTAAGTTGACTGTGCCTTTAAACA
GCTTGGAAAATTCCAGAAAATGATGGTCTCCCTATAGTGAGTCGTATTAGATC
CCGGGTAGTAGGCTCAGAGGCACACAGGAGTTTCTGGGCTCACCCTGCCCCC
TTCCAACCCCTCAGTTCCCATCCTCCAGCAGCTGTTTGTGTGCTGCCTCTGAA
GTCCACACTGAACAAACTTCAGCCTACTCATGTCCCTAAAATGGGCAAACAT
TGCAAGCAGCAAACAGCAAACACACAGCCCTCCCTGCCTGCTGACCTTGGAG
CTGGGGCAGAGGTCAGAGACCTCTCTGGGCCCATGCCACCTCCAACATCCAC
TCGACCCCTTGGAATTTCGGTGGAGAGGAGCAGAGGTTGTCCTGGCGTGGTT
TAGGTAGTGTGAGAGGGGTACCCGGGGATCTTGCTACCAGTGGAACAGCCAC
TAAGGATTCTGCAGTGAGAGCAGAGGGCCAGCTAAGTGGTACTCTCCCAGAG
ACTGTCTGACTCACGCCACCCCCTCCACCTTGGACACAGGACGCTGTGGTTTC
TGAGCCAGGTACAATGACTCCTTTCGGTAAGTGCAGTGGAAGCTGTACACTG
CCCAGGCAAAGCGTCCGGGCAGCGTAGGCGGGCGACTCAGATCCCAGCCAG
TGGACTTAGCCCCTGTTTGCTCCTCCGATAACTGGGGTGACCTTGGTTAATAT

TCACCAGCAGCCTCCCCCGTTGCCCCTCTGGATCCACTGCTTAAATACGGACG
AGGACAGGGCCCTGTCTCCTCAGCTTCAGGCACCACCACTGACCTGGGACAG
TGAATGATCGGAGCCCCGATCATCGCTGCGTTGCCTTCGCCCCGTGCCCCGCT
CCGCGCCGCCTCGCGCCGCCCGCCCCGGCTCTGACTGACCGCGTTACTCCCAC
AGGTGAGCGGGCGGGACGGCCCTTCTCCTCCGGGCTGTAATTAGCGCTTGGT
TTAATGACGGCTCGTTTCTTTTCTGTGGCTGCGTGAAAGCCTTAAAGGGCTCC
GGGAGCTAGAGCCTCTGCTAACCATGTTCATGCCTTCTTCTTTTTCCTACAGCT
CCTGGGCAACGTGCTGGTTGTTGTGCTGTCTCATCATTTTGGCAAAGAATTCG
GGCCC

With the three lengths of DNA cloned and purified, they were complexed with the micelles in different conditions. First the Poly(DMAEMA$_{27}$-*b*-BMA$_{14}$) micelle and 2000bp linear DNA were chosen to be complexed at a ratio of 1 micelle to 1 strand of DNA (Figure 60) in di-water and in buffers at 100 mM and 1 M ionic strength (both at the pK_a of the micelles). This equates to a charge ratio (N^+/P^-) of 3.56, 1.81, and 1.78 for the water, 100 mM, and 1 M samples respectively. The results show that the size of the aggregates formed depends on the salt concentration of the solution. Interestingly, the size of the aggregates formed is almost instantaneous according to DLS time studies (Figure 61). The process of complexation between the micelles and DNA is entropically driven and thus in the 1 M salted buffer there was no observable complexation between the polycation and polyanion, even after 10 days.

As well as the buffers and ionic strength being tested to form the micelleplexes, the order of addition was experimented with. Poly(DMAEMA$_{27}$-*b*-BMA$_{14}$) was complex with the 20bp DNA in pH 5, 20 mM buffer, by varying the order of addition. That is by adding DNA to micelles and adding micelles to DNA. Here it can be seen that the order of addition can affect the size, distribution, and stability of the formed micelleplexes. More work in this area needs to be done in order to fully understand the binding and interactions of polycations with polyanions, perhaps by experimenting with isothermal titration calorimetry (ITC) and 3D NMR techniques such as DOSY-TOCSY.

The overarching goal of this project is to control the structure and properties of block-polymer-based "amphiplexes" and assemblies of the polyanions (like DNA) with cationic polymer micelles. More specifically it is important to develop an understanding of DNA-polycation interactions through the continued study of micelleplexes. With this goal in mind the future direction of this project can be summarized in two phases. The first is the evaluation of micelleplex formation and identifying the key determining factors that govern this process. The second is to be able to quantify the micelleplex structure, composition, stability, and dynamic behaviors thereof.

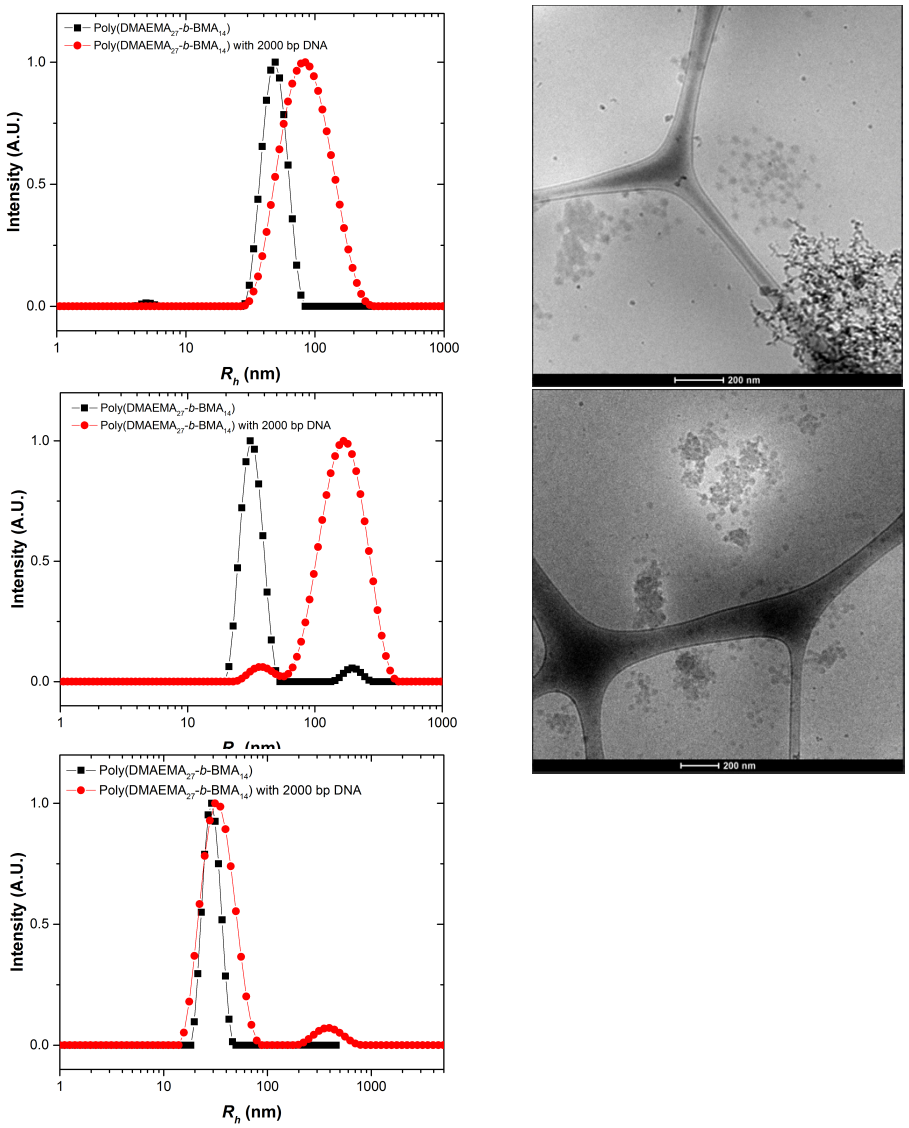

Figure 60. R_h and Cryo-TEM image of micelleplex formed by Poly(DMAEMA$_{27}$-*b*-BMA$_{14}$) and 2000bp linear DNA. From top to bottom, the formation solvent is water, pH 7.2 100 mM and pH 7.88 1 M.

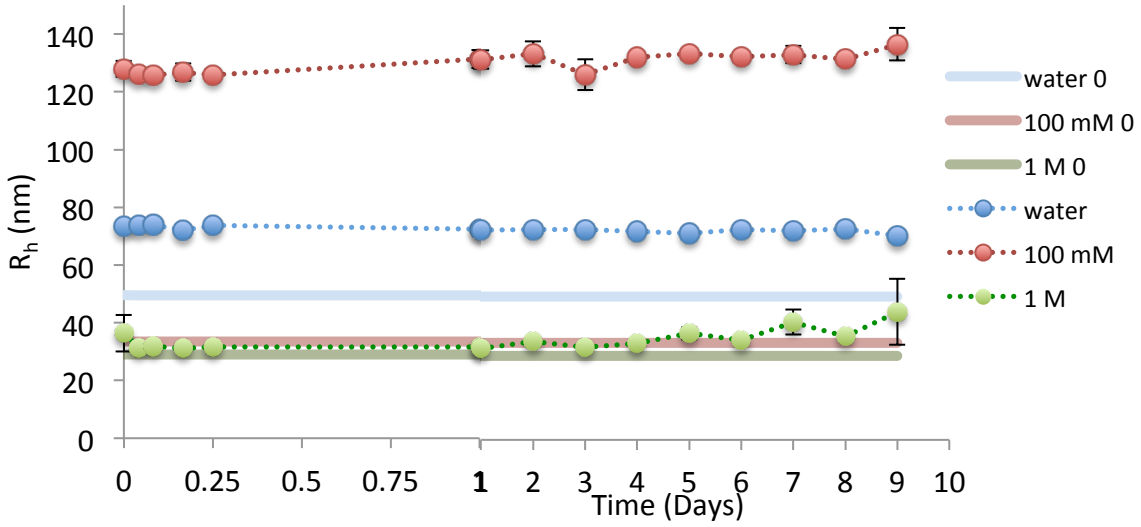

Figure 61. DLS of the micelleplexes formed in water (blue), 100 mM buffer (red), and 1 M buffer (green) with Poly(DMAEMA$_{27}$-*b*-BMA$_{14}$) and 2000bp DNA. The solid lines represent the original sizes of the micelles in the associated media/buffer. DLS of the complexes were taken at the time of mixing, 1, 2, 4, 6, and 8 hours, then on consecutive days.

Figure 62 Poly(DMAEMA$_{27}$-*b*-BMA$_{14}$) complexed with 20 bp DNA in pH 5, 20 mM buffer. Showing the difference in transmittance and size of the aggregates upon the order of addition

References:

(1) Wu, Y.; Wang, M.; Sprouse, D.; Smith, A. E.; Reineke, T. M. *Biomacromolecules* **2014**, *15*, 1716–1726.

(2) Choi, Y. H.; Liu, F.; Kim, J. S.; Choi, Y. K.; Park, J. S.; Kim, S. W. *J. Controlled Release* **1998**, *54*, 39–48.

(3) Oupický, D.; Howard, K. A.; Konák, C.; Dash, P. R.; Ulbrich, K.; Seymour, L. W. *Bioconjugate Chem.* **2000**, *11*, 492–501.

(4) MacLaughlin, F. C.; Mumper, R. J.; Wang, J. J.; Tagliaferri, J. M.; Gill, I.; Hinchcliffe, M.; Rolland, A. P. *J. Controlled Release* **1998**, *56*, 259–272.

(5) Srinivasachari, S.; Liu, Y.; Zhang, G.; Prevette, L.; Reineke, T. M. *J. Am. Chem. Soc.* **2006**, *128*, 8176–8184.

(6) Erbacher, P.; Bettinger, T.; Belguise-Valladier, P.; Zou, S. M.; Coll, J. L.; Behr, J. P.; Remy, J. S. *J. Gene Med.* **1999**, *1*, 210–222.

(7) Parimi, S.; Barnes, T. J.; Callen, D. F.; Prestidge, C. A. *Biomacromolecules* **2010**, *11*, 382–389.

(8) Reineke, T. M.; Davis, M. E. *Bioconjugate Chem.* **2003**, *14*, 255–261.

(9) Gonzalez, H.; Hwang, S. J.; Davis, M. E. *Bioconjugate Chem.* **1999**, *10*, 1068–1074.

(10) Davis, M.; Pun, S.; Bellocq, N.; Reineke, T.; Popielarski, S.; Mishra, S.; Heidel, J. *Curr. Med. Chem.* **2004**, *11*, 179–197.

(11) Prevette, L. E.; Kodger, T. E.; Reineke, T. M.; Lynch, M. L. *Langmuir* **2007**, *23*, 9773–9784.

(12) Prevette, L. E.; Lynch, M. L.; Kizjakina, K.; Reineke, T. M. *Langmuir* **2008**, *24*, 8090–8101.

(13) Grandinetti, G.; Smith, A. E.; Reineke, T. M. *Mol. Pharmaceutics* **2012**, *9*, 523–538.

(14) Kabanov, A. V.; Batrakova, E. V.; Sriadibhatla, S.; Yang, Z.; Kelly, D. L.; Alakov, V. Y. *J. Controlled Release* **2005**, *101*, 259–271.

(15) Gratton, S. E. A.; Ropp, P. A.; Pohlhaus, P. D.; Luft, J. C.; Madden, V. J.; Napier, M. E.; DeSimone, J. M. *Proc. Natl. Acad. Sci. USA* **2008**, *105*, 11613–11618.

(16) Mishra, S.; Webster, P.; Davis, M. E. *Eur. J. Cell Biol.* **2004**, *83*, 97–111.

(17) Davis, M. E.; Chen, Z. G.; Shin, D. M. *Nat. Rev. Drug Discov.* **2008**, *7*, 771–782.

(18) Corey, D. R.; Abrams, J. M. *Genome Biol.* **2001**, *2*, Reviews1015.

(19) Aboul-Fadl, T. *Curr. Med. Chem.* **2005**, *12*, 2193–2214.

(20) Grandinetti, G.; Reineke, T. M. *Mol. Pharmaceutics* **2012**, *9*, 2256–2267.

(21) Li, C.; Liu, H.; Sun, Y.; Wang, H.; Guo, F.; Rao, S.; Deng, J.; Zhang, Y.; Miao, Y.; Guo, C.; Meng, J.; Chen, X.; Li, L.; Li, D.; Xu, H.; Wang, H.; Wang, H.; Li, B.; Jiang, C. *J. Mol. Cell Biol.* **2009**, *1*, 37–45.

(22) Aberle, A. M.; Bennett, M. J.; Malone, R. W. *Biochim. Biophys. Acta* **1996**, *1299*, 281–283.

(23) Asgatay, S.; Franceschi-Messant, S.; Perez, E.; Vicendo, P.; Rico-Lattes, I.; Phez, E.; Rols, M. P. *Int. J. Pharm.* **2004**, *285*, 121–133.
(24) Lee, C.-C.; Liu, Y.; Reineke, T. M. *Bioconjugate Chem.* **2008**, *19*, 428–440.
(25) Vicennati, P.; Giuliano, A.; Ortaggi, G.; Masotti, A. *Curr. Med. Chem.* **2008**, *15*, 2826–2839.
(26) Sprouse, D.; Reineke, T. M. *Biomacromolecules* **2014**, *15*, 2616–2628.
(27) Ahmed, M.; Narain, R. *Biomaterials* **2011**, *32*, 5279–5290.
(28) Godbey, W. T.; Wu, K. K.; Mikos, A. G. *J. Biomed. Mater. Res.* **1999**, *45*, 268–275.
(29) Huang, M.; Fong, C.-W.; Khor, E.; Lim, L.-Y. *J. Controlled Release* **2005**, *106*, 391–406.
(30) Srinivasachari, S.; Liu, Y.; Prevette, L. E.; Reineke, T. M. *Biomaterials* **2007**, *28*, 2885–2898.
(31) Bartlett, D. W.; Davis, M. E. *Bioconjugate Chem.* **2007**, *18*, 456–468.
(32) Bartlett, D. W.; Su, H.; Hildebrandt, I. J.; Weber, W. A.; Davis, M. E. *Proc. Natl. Acad. Sci. USA* **2007**, *104*, 15549–15554.
(33) Fahrmeir, J.; Gunther, M.; Tietze, N.; Wagner, E.; Ogris, M. *J. Controlled Release* **2007**, *122*, 236–245.
(34) Yue, Y.; Jin, F.; Deng, R.; Cai, J.; Chen, Y.; Lin, M. C. M.; Kung, H.-F.; Wu, C. J. *J. Controlled Release* **2011**, *155*, 67–76.
(35) Shcharbin, D.; Pedziwiatr, E.; Bryszewska, M. *J. Controlled Release* **2009**, *135*, 186–197.
(36) Liu, Y.; Reineke, T. M. *J. Am. Chem. Soc.* **2005**, *127*, 3004–3015.
(37) Popielarski, S. R.; Mishra, S.; Davis, M. E. *Bioconjugate Chem.* **2003**, *14*, 672–678.
(38) Liu, Y.; Reineke, T. M. *Bioconjugate Chem.* **2006**, *17*, 101–108.
(39) Smith, A. E.; Sizovs, A.; Grandinetti, G.; Xue, L.; Reineke, T. M. *Biomacromolecules* **2011**, *12*, 3015–3022.
(40) Tang, M. X.; Szoka, F. C. *Gene. Ther.* **1997**, *4*, 823–832.
(41) Knorr, V.; Allmendinger, L.; Walker, G. F.; Paintner, F. F.; Wagner, E. *Bioconjugate Chem.* **2007**, *18*, 1218–1225.
(42) Neu, M.; Germershaus, O.; Behe, M.; Kissel, T. *J. Controlled Release* **2007**, *124*, 69–80.
(43) Gerelli, Y.; Barbieri, S.; Di Bari, M. T.; Deriu, A.; Cantu, L.; Brocca, P.; Sonvico, F.; Colombo, P.; May, R.; Motta, S. *Langmuir* **2008**, *24*, 11378–11384.
(44) Kato, H.; Suzuki, M.; Fujita, K.; Horie, M.; Endoh, S.; Yoshida, Y.; Iwahashi, H.; Takahashi, K.; Nakamura, A.; Kinugasa, S. *Toxicol. In Vitro* **2009**, *23*, 927–934.
(45) Lai, E.; van Zanten, J. H. *Biophys. J.* **2001**, *80*, 864–873.
(46) Hwang, S. J.; Bellocq, N. C.; Davis, M. E. *Bioconjugate Chem.* **2001**, *12*, 280–290.
(47) Ross, P. D.; Shapiro, J. T. *Biopolymers* **1974**, *13*, 415–416.
(48) Shcharbin, D.; Pedziwiatr, E.; Blasiak, J.; Bryszewska, M. *J. Controlled Release* **2010**, *141*, 110–127.

(49) Shim, M. S.; Kwon, Y. J. *Bioconjugate Chem.* **2009**, *20*, 488–499.
(50) Liu, M.; Chen, J.; Xue, Y.-N.; Liu, W.-M.; Zhuo, R.-X.; Huang, S.-W. *Bioconjugate Chem.* **2009**, *20*, 2317–2323.
(51) Zimmermann, T. S.; Lee, A. C. H.; Akinc, A.; Bramlage, B.; Bumcrot, D.; Fedoruk, M. N.; Harborth, J.; Heyes, J. A.; Jeffs, L. B.; John, M.; Judge, A. D.; Lam, K.; McClintock, K.; Nechev, L. V.; Palmer, L. R.; Racie, T.; Röhl, I.; Seiffert, S.; Shanmugam, S.; Sood, V.; Soutschek, J.; Toudjarska, I.; Wheat, A. J.; Yaworski, E.; Zedalis, W.; Koteliansky, V.; Manoharan, M.; Vornlocher, H.-P.; MacLachlan, I. *Nature* **2006**, *441*, 111–114.
(52) Heidel, J. D.; Liu, J. Y. C.; Yen, Y.; Zhou, B.; Heale, B. S. E.; Rossi, J. J.; Bartlett, D. W.; Davis, M. E. *Clin. Cancer Res.* **2007**, *13*, 2207–2215.
(53) Dheda, K.; Huggett, J. F.; Bustin, S. A.; Johnson, M. A.; Rook, G.; Zumla, A. *BioTechniques* **2004**, *37*, 112–119.
(54) Juhasz, A.; Vassilakos, A.; Chew, H. K.; Gandara, D.; Yen, Y. *Oncol. Rep.* **2006**, *15*, 1299–1304.
(55) Bejjani, R.; BenEzra, D.; Cohen, H.; Rieger, J.; Andrieu, C.; Jeanny, J. C.; Gollomb, G.; Behar-Cohen, F. *Mol. Vis.* **2005**, *11*, 124–132.
(56) Kunath, K.; Harpe, von, A.; Fischer, D.; Peterson, H.; Bickel, U.; Voigt, K.; Kissel, T. *J. Controlled Release* **2003**, *89*, 113–125.
(57) Decker, T.; Lohmann-Matthes, M.-L. *J. Immunol. Methods* **1988**, *115*, 61–69.
(58) Kunath, K.; Harpe, von, A.; Fischer, D.; Kissel, T. *J. Controlled Release* **2003**, *88*, 159–172.
(59) Srinivasachari, S.; Fichter, K. M.; Reineke, T. M. *J. Am. Chem. Soc.* **2008**, *130*, 4618–4627.
(60) Tominaga, H.; Ishiyama, M.; Ohseto, F.; Sasamoto, K.; Hamamoto, T.; Suzuki, K.; Watanabe, M. *Anal. Commun.* **1999**, *36*, 47–50.
(61) Ishiyama, M.; Miyazono, Y.; Sasamoto, K.; Ohkura, Y.; Ueno, K. *Talanta* **1997**, *44*, 1299–1305.
(62) Solly, K.; Wang, X.; Xu, X.; Strulovici, B.; Zheng, W. *Assay Drug Dev. Technol.* **2004**, *2*, 363–372.
(63) Boussif, O.; Lezoualc'h, F.; Zanta, M. A.; Mergny, M. D.; Scherman, D.; Demeneix, B.; Behr, J. P. *Proc. Natl. Acad. Sci. USA* **1995**, *92*, 7297–7301.
(64) Fischer, D.; Bieber, T.; Li, Y.; Elsässer, H. P.; Kissel, T. *Pharm. Res.* **1999**, *16*, 1273–1279.
(65) Fischer, D.; Li, Y.; Ahlemeyer, B.; Krieglstein, J.; Kissel, T. *Biomaterials* **2003**, *24*, 1121–1131.
(66) Neu, M.; Fischer, D.; Kissel, T. *J. Gene Med.* **2005**, *7*, 992–1009.
(67) Ma, Y.; Chen, B.; He, N.; Chen, G.; Li, L.; Wu, C. J. *Macromol. Biosci.* **2014**, *14*, 1807–1815.
(68) Ma, Y.; Wu, C. J. *J. Mater. Chem. B* **2014**, *2*, 3282.
(69) Dai, Z.; Wu, C. J. *Macromolecules* **2012**, *45*, 4346–4353.
(70) Dai, Z.; Gjetting, T.; Mattebjerg, M. A.; Wu, C. J.; Andresen, T. L. *Biomaterials* **2011**, *32*, 8626–8634.
(71) Yue, Y.; Jin, F.; Deng, R.; Cai, J.; Dai, Z.; Lin, M. C. M.; Kung, H.-F.; Mattebjerg, M. A.; Andresen, T. L.; Wu, C. J. *J. Controlled Release* **2011**, *152*,

143–151.
(72) Deng, R.; Yue, Y.; Jin, F.; Chen, Y.; Kung, H.-F.; Lin, M. C. M.; Wu, C. J. *J. Controlled Release* **2009**, *140*, 40–46.
(73) Vinogradov, S. V.; Bronich, T. K.; Kabanov, A. V. *Bioconjugate Chem.* **1998**, *9*, 805–812.
(74) Nguyen, H. K.; Lemieux, P.; Vinogradov, S. V.; Gebhart, C. L.; Guérin, N.; Paradis, G.; Bronich, T. K.; Alakhov, V. Y.; Kabanov, A. V. *Gene. Ther.* **2000**, *7*, 126–138.
(75) Petersen, H.; Fechner, P. M.; Martin, A. L.; Kunath, K.; Stolnik, S.; Roberts, C. J.; Fischer, D.; Davies, M. C.; Kissel, T. *Bioconjugate Chem.* **2002**, *13*, 845–854.
(76) Mao, S.; Neu, M.; Germershaus, O.; Merkel, O.; Sitterberg, J.; Bakowsky, U.; Kissel, T. *Bioconjugate Chem.* **2006**, *17*, 1209–1218.
(77) Gary, D. J.; Puri, N.; Won, Y.-Y. *J. Controlled Release* **2007**, *121*, 64–73.
(78) Namgung, R.; Kim, J.; Singha, K.; Kim, C. H.; Kim, W. J. *Mol. Pharmaceutics* **2009**, *6*, 1826–1835.
(79) Forrest, M. L.; Meister, G. E.; Koerber, J. T.; Pack, D. W. *Pharm. Res.* **2004**, *21*, 365–371.
(80) Pun, S. H.; Bellocq, N. C.; Liu, A.; Jensen, G.; Machemer, T.; Quijano, E.; Schluep, T.; Wen, S.; Engler, H.; Heidel, J.; Davis, M. E. *Bioconjugate Chem.* **2004**, *15*, 831–840.
(81) Wu, G. Y.; Wu, C. H. *J. Biol. Chem.* **1987**, *262*, 4429–4432.
(82) Wu, G. Y.; Wu, C. H. *J. Biol. Chem.* **1988**, *263*, 14621–14624.
(83) Wolfert, M. A.; Schacht, E. H.; Toncheva, V.; Ulbrich, K.; Nazarova, O.; Seymour, L. W. *Hum. Gene Ther.* **1996**, *7*, 2123–2133.
(84) Wolfert, M. A.; Seymour, L. W. *Gene. Ther.* **1996**, *3*, 269–273.
(85) Katayose, S.; Kataoka, K. *Bioconjugate Chem.* **1997**, *8*, 702–707.
(86) Kano, A.; Moriyama, K.; Yamano, T.; Nakamura, I.; Shimada, N.; Maruyama, A. *J. Controlled Release* **2011**, *149*, 2–7.
(87) Zhang, Z.-Y.; Smith, B. D. *Bioconjugate Chem.* **2000**, *11*, 805–814.
(88) Zama, M.; Ichimura, S. *Biochem. Biophys. Res. Commun.* **1971**, *44*, 936–942.
(89) Kabanov, A. V.; Kabanov, V. A. *Bioconjugate Chem.* **1995**, *6*, 7–20.
(90) Futaki, S.; Ohashi, W.; Suzuki, T.; Niwa, M.; Tanaka, S.; Ueda, K.; Harashima, H.; Sugiura, Y. *Bioconjugate Chem.* **2001**, *12*, 1005–1011.
(91) Green, M.; Loewenstein, P. M. *Cell* **1988**, *55*, 1179–1188.
(92) Frankel, A. D.; Pabo, C. O. *Cell* **1988**, *55*, 1189–1193.
(93) Fawell, S.; Seery, J.; Daikh, Y.; Moore, C.; Chen, L. L.; Pepinsky, B.; Barsoum, J. *Proc. Natl. Acad. Sci. USA* **1994**, *91*, 664–668.
(94) Schwarze, S. R.; Ho, A.; Vocero-Akbani, A.; Dowdy, S. F. *Science* **1999**, *285*, 1569–1572.
(95) Futaki, S.; Suzuki, T.; Ohashi, W.; Yagami, T.; Tanaka, S.; Ueda, K.; Sugiura, Y. *J. Biol. Chem.* **2001**, *276*, 5836–5840.
(96) Wang, H.-Y.; Chen, J.-X.; Sun, Y.-X.; Deng, J.-Z.; Li, C.; Zhang, X.-Z.; Zhuo, R.-X. *J. Controlled Release* **2011**, *155*, 26–33.
(97) Wender, P. A.; Mitchell, D. J.; Pattabiraman, K.; Pelkey, E. T.; Steinman, L.;

Rothbard, J. B. *Proc. Natl. Acad. Sci. USA* **2000**, *97*, 13003–13008.
(98) Tünnemann, G. Toxicity, Uptake and Applications of Intracellular Delivery by Cell Penetrating Peptides, Munich, Germany, 2009, pp. 1–107.
(99) Tünnemann, G.; Ter-Avetisyan, G.; Martin, R. M.; Stöckl, M.; Herrmann, A.; Cardoso, M. C. *J. Pept. Sci.* **2008**, *14*, 469–476.
(100) Ter-Avetisyan, G.; Tünnemann, G.; Nowak, D.; Nitschke, M.; Herrmann, A.; Drab, M.; Cardoso, M. C. *J. Biol. Chem.* **2009**, *284*, 3370–3378.
(101) Kim, Y.; Binauld, S.; Stenzel, M. H. *Biomacromolecules* **2012**, *13*, 3418–3426.
(102) Rothbard, J. B.; Jessop, T. C.; Wender, P. A. *Adv. Drug Deliv. Rev.* **2005**, *57*, 495–504.
(103) Veiseh, O.; Kievit, F. M.; Mok, H.; Ayesh, J.; Clark, C.; Fang, C.; Leung, M.; Arami, H.; Park, J. O.; Zhang, M. *Biomaterials* **2011**, *32*, 5717–5725.
(104) Zhao, Z.-X.; Gao, S.-Y.; Wang, J.-C.; Chen, C.-J.; Zhao, E.-Y.; Hou, W.-J.; Feng, Q.; Gao, L.-Y.; Liu, X.-Y.; Zhang, L.-R.; Zhang, Q. *Biomaterials* **2012**, *33*, 6793–6807.
(105) Haensler, J.; Szoka, F. C. *Bioconjugate Chem.* **1993**, *4*, 372–379.
(106) Kukowska-Latallo, J. F.; Bielinska, A. U.; Johnson, J.; Spindler, R.; Tomalia, D. A.; Baker, J. R. *Proc. Natl. Acad. Sci. USA* **1996**, *93*, 4897–4902.
(107) Tang, M. X.; Redemann, C. T.; Szoka, F. C. *Bioconjugate Chem.* **1996**, *7*, 703–714.
(108) Sonawane, N. D.; Szoka, F. C.; Verkman, A. S. *J. Biol. Chem.* **2003**, *278*, 44826–44831.
(109) Thomas, T. P.; Majoros, I.; Kotlyar, A.; Mullen, D.; Banaszak Holl, M. M.; Baker, J. R., Jr. *Biomacromolecules* **2009**, *10*, 3207–3214.
(110) Imamura, M.; Kodama, Y.; Higuchi, N.; Kanda, K.; Nakagawa, H.; Muro, T.; Nakamura, T.; Kitahara, T.; Sasaki, H. *Biol. Pharm. Bull.* **2014**, *37*, 552–559.
(111) Merkel, O. M.; Mintzer, M. A.; Sitterberg, J.; Bakowsky, U.; Simanek, E. E.; Kissel, T. *Bioconjugate Chem.* **2009**, *20*, 1799–1806.
(112) Dodane, V.; Vilivalam, V. D. *PSTT* **1998**, *1*, 246–253.
(113) Aranaz, I.; Mengibar, M.; Harris, R.; Panos, I.; Miralles, B.; Acosta, N.; Galed, G.; Heras, A. *Curr. Chem. Biol.* **2009**, *3*, 203–230.
(114) Mao, H.-Q.; Roy, K.; Troung-Le, V. L.; Janes, K. A.; Lin, K. Y.; Wang, Y.; August, J. T.; Leong, K. W. *J. Controlled Release* **2001**, *70*, 399–421.
(115) Borchard, G. *Adv. Drug Deliv. Rev.* **2001**, *52*, 145–150.
(116) Aiba, S.-I. *Int. J. Biol. Macromol.* **1991**, *13*, 40–44.
(117) Mima, S.; Miya, M.; Iwamoto, R.; Yoshikawa, S. *J. Appl. Polym. Sci.* **1983**, *28*, 1909–1917.
(118) Mumper, R. J.; Wang, J.; Claspell, J. M.; Rolland, A. P. *J. Controlled Release* **1995**, *22*, 178.
(119) Ishii, T.; Okahata, Y.; Sato, T. *Biochim. Biophys. Acta* **2001**, *1514*, 51–64.
(120) Kiang, T.; Wen, J.; Lim, H. W.; Leong, K. W. *Biomaterials* **2004**, *25*, 5293–5301.
(121) Liu, X.; Howard, K. A.; Dong, M.; Andersen, M. Ø.; Rahbek, U. L.; Johnsen, M. G.; Hansen, O. C.; Besenbacher, F.; Kjems, J. *Biomaterials* **2007**, *28*, 1280–1288.

(122) Richard, I.; Thibault, M.; De Crescenzo, G.; Buschmann, M. D.; Lavertu, M. *Biomacromolecules* **2013**, *14*, 1732–1740.
(123) Kim, T. H.; Kim, S. I.; Akaike, T.; Cho, C. S. *J. Controlled Release* **2005**, *105*, 354–366.
(124) Wong, K.; Sun, G.; Zhang; Dai, H.; Liu, Y.; He; Leong, K. W. *Bioconjugate Chem.* **2006**, *17*, 152–158.
(125) Shi, B.; Zhang, H.; Bi, J.; Dai, S. *Colloids Surf., B.* **2014**, *119*, 55–65.
(126) Liu, Y.; Wenning, L.; Lynch, M.; Reineke, T. M. *J. Am. Chem. Soc.* **2004**, *126*, 7422–7423.
(127) Reineke, T. M. *J. Polym. Sci., Part A Polym. Chem.* **2006**, *44*, 6895–6908.
(128) Liu, Y.; Reineke, T. M. *Bioconjugate Chem.* **2007**, *18*, 19–30.
(129) Fichter, K. M.; Ingle, N. P.; McLendon, P. M.; Reineke, T. M. *ACS Nano* **2013**, *7*, 347–364.
(130) Taori, V. P.; Lu, H.; Reineke, T. M. *Biomacromolecules* **2011**, *12*, 2055–2063.
(131) Grandinetti, G.; Ingle, N. P.; Reineke, T. M. *Mol. Pharmaceutics* **2011**, *8*, 1709–1719.
(132) Ingle, N. P.; Malone, B.; Reineke, T. M. *Trends Biotechnol.* **2011**, *29*, 443–453.
(133) Liu, Y.; Reineke, T. M. *Biomacromolecules* **2010**, *11*, 316–325.
(134) Taori, V. P.; Liu, Y.; Reineke, T. M. *Acta Biomater.* **2009**, *5*, 925–933.
(135) Paiva, C. L.; Panek, A. D. *Biotechnol. Annu. Rev.* **1996**, *2*, 293–314.
(136) Lins, R. D.; Pereira, C. S.; Hünenberger, P. H. *Proteins* **2004**, *55*, 177–186.
(137) Davis, M. E. *Curr. Opin. Biotechnol.* **2002**, *13*, 128–131.
(138) Wagner, E. *Pharm. Res.* **2004**, *21*, 8–14.
(139) Reineke, T. M.; Davis, M. E. *Bioconjugate Chem.* **2003**, *14*, 247–254.
(140) Ingle, N. P.; Xue, L.; Reineke, T. M. *Mol. Pharmaceutics* **2013**, *10*, 4120–4135.
(141) Kitagishi, H.; Hatada, S.; Itakura, T.; Maki, Y.; Maeda, Y.; Kano, K. *Org. Biomol. Chem.* **2013**, *11*, 3203–3211.
(142) Hwang, S. J.; Bellocq, N. C.; Davis, M. E. *Bioconjugate Chem.* **2001**, *12*, 280–290.
(143) Plank, C.; Mechtler, K.; Szoka, F. C.; Wagner, E. *Hum. Gene Ther.* **1996**, *7*, 1437–1446.
(144) Cromwell, W. C.; Bystrom, K.; Eftink, M. R. *J. Phys. Chem.* **1985**, *89*, 326–332.
(145) Amiel, C.; Sébille, B. *Adv. Colloid Interface Sci.* **1999**, *79*, 105–122.
(146) Buckwalter, D. J.; Sizovs, A.; Ingle, N. P.; Reineke, T. M. *ACS Macro Lett.* **2012**, *1*, 609–613.
(147) Pun, S. H.; Davis, M. E. *Bioconjugate Chem.* **2002**, *13*, 630–639.
(148) Zuckerman, J. E.; Gritli, I.; Tolcher, A.; Heidel, J. D.; Lim, D.; Morgan, R.; Chmielowski, B.; Ribas, A.; Davis, M. E.; Yen, Y. *Proc. Natl. Acad. Sci. USA* **2014**, *111*, 11449–11454.
(149) Heidel, J. D.; Yu, Z.; Liu, J. Y. C.; Rele, S. M.; Liang, Y.; Zeidan, R. K.; Kornbrust, D. J.; Davis, M. E. *Proc. Natl. Acad. Sci. USA* **2007**, *104*, 5715–5721.
(150) Srinivasachari, S.; Reineke, T. M. *Biomaterials* **2009**, *30*, 928–938.

(151) Xue, L.; Ingle, N. P.; Reineke, T. M. *Biomacromolecules* **2013**, *14*, 3903–3915.
(152) Lynn, D. M.; Anderson, D. G.; Putnam, D.; Langer, R. *J. Am. Chem. Soc.* **2001**, *123*, 8155–8156.
(153) Anderson, D. G.; Lynn, D. M.; Langer, R. *Angew. Chem. Int. Ed. Engl.* **2003**, *42*, 3153–3158.
(154) Akinc, A.; Anderson, D. G.; Lynn, D. M.; Langer, R. *Bioconjugate Chem.* **2003**, *14*, 979–988.
(155) Green, J. J.; Shi, J.; Chiu, E.; Leshchiner, E. S.; Langer, R.; Anderson, D. G. *Bioconjugate Chem.* **2006**, *17*, 1162–1169.
(156) Anderson, D. G.; Peng, W.; Akinc, A.; Hossain, N.; Kohn, A.; Padera, R.; Langer, R.; Sawicki, J. A. *Proc. Natl. Acad. Sci. USA* **2004**, *101*, 16028–16033.
(157) Huang, Y. H.; Zugates, G. T.; Peng, W.; Holtz, D.; Dunton, C.; Green, J. J.; Hossain, N.; Chernick, M. R.; Padera, R. F.; Langer, R.; Anderson, D. G.; Sawicki, J. A. *Cancer Res.* **2009**, *69*, 6184–6191.
(158) Lee, J.-S.; Green, J. J.; Love, K. T.; Sunshine, J.; Langer, R.; Anderson, D. G. *Nano Lett.* **2009**, *9*, 2402–2406.
(159) Green, J. J.; Zugates, G. T.; Langer, R.; Anderson, D. G. *Methods Mol. Biol.* **2009**, *480*, 53–63.
(160) Cherng, J. Y.; van de Wetering, P.; Talsma, H.; Crommelin, D. J. A.; Hennink, W. E. *Pharm. Res.* **1996**, *13*, 1038–1042.
(161) Zhu, C.; Jung, S.; Si, G.; Cheng, R.; Meng, F.; Zhu, X.; Park, T. G.; Zhong, Z. *J. Polym. Sci., Part A Polym. Chem.* **2010**, *48*, 2869–2877.
(162) Asha, M.; Cao, H.; Collin, E.; Wang, W.; Pandit, A. *Int. J. Pharm.* **2012**, *434*, 99–105.
(163) Jones, R. A.; Poniris, M. H.; Wilson, M. R. *J. Controlled Release* **2004**, *96*, 379–391.
(164) Loh, X. J. *J. Appl. Polym. Sci.* **2013**, *127*, 992–1000.
(165) Agarwal, S.; Zhang, Y.; Maji, S.; Greiner, A. *Materials Today* **2012**, *15*, 388–393.
(166) van de Wetering, P.; Moret, E. E.; Schuurmans-Nieuwenbroek, N. M.; van Steenbergen, M. J.; Hennink, W. E. *Bioconjugate Chem.* **1999**, *10*, 589–597.
(167) van de Wetering, P.; Cherng, J. Y.; Talsma, H.; Hennink, W. E. *J. Controlled Release* **1997**, *49*, 59–69.
(168) Hinton, T. M.; Guerrero-Sanchez, C.; Graham, J. E.; Le, T.; Muir, B. W.; Shi, S.; Tizard, M. L. V.; Gunatillake, P. A.; McLean, K. M.; Thang, S. H. *Biomaterials* **2012**, *33*, 7631–7642.
(169) Rungsardthong, U.; Deshpande, M.; Bailey, L.; Vamvakaki, M.; Armes, S. P.; Garnett, M. C.; Stolnik, S. *J. Controlled Release* **2001**, *73*, 359–380.
(170) Yue, X.; Zhang, W.; Xing, J.; Zhang, B.; Deng, L.; Guo, S.; Yang, J.; Zhang, Q.; Dong, A. *Soft Matter* **2012**, *8*, 2252–2260.
(171) van de Wetering, P.; Cherng, J. Y.; Talsma, H.; Crommelin, D. J.; Hennink, W. E. *J. Controlled Release* **1998**, *53*, 145–153.
(172) Ahmed, M.; Narain, R. *Prog. Polym. Sci.* **2013**, *38*, 767–790.
(173) Ahmed, M.; Jawanda, M.; Ishihara, K.; Narain, R. *Biomaterials* **2012**, *33*, 7858–7870.

(174) Li, H.; Cortez, M. A.; Phillips, H. R.; Wu, Y.; Reineke, T. M. *ACS Macro Lett.* **2013**, *2*, 230–235.
(175) Xiu, K. M.; Yang, J. J.; Zhao, N. N.; Li, J. S.; Xu, F. J. *Acta Biomater.* **2013**, *9*, 4726–4733.
(176) Xu, F. J.; Zhang, Z. X.; Ping, Y.; Li, J.; Kang, E. T.; Neoh, K. G. *Biomacromolecules* **2009**, *10*, 285–293.
(177) Nakayama, Y. *Acc. Chem. Res.* **2012**, *45*, 994–1004.
(178) Wang, Y.; Zhou, K.; Huang, G.; Hensley, C.; Huang, X.; Ma, X.; Zhao, T.; Sumer, B. D.; DeBerardinis, R. J.; Gao, J. *Nat. Mater.* **2013**, *13*, 204–212.
(179) Aw, M. S.; Kurian, M.; Losic, D. *Chemistry* **2013**, *19*, 12586–12601.
(180) Yu, H.; Xu, Z.; Chen, X.; Xu, L.; Yin, Q.; Zhang, Z.; Li, Y. *Macromol. Biosci.* **2013**, *14*, 100–109.
(181) Sharma, R.; Lee, J.-S.; Bettencourt, R. C.; Xiao, C.; Konieczny, S. F.; Won, Y.-Y. *Biomacromolecules* **2008**, *9*, 3294–3307.
(182) Gary, D. J.; Lee, H.; Sharma, R.; Lee, J.-S.; Kim, Y.; Cui, Z. Y.; Jia, D.; Bowman, V. D.; Chipman, P. R.; Wan, L.; Zou, Y.; Mao, G.; Park, K.; Herbert, B.-S.; Konieczny, S. F.; Won, Y.-Y. *ACS Nano* **2011**, *5*, 3493–3505.
(183) Yu, H.; Zou, Y.; Wang, Y.; Huang, X.; Huang, G.; Sumer, B. D.; Boothman, D. A.; Gao, J. *ACS Nano* **2011**, *5*, 9246–9255.
(184) Manganiello, M. J.; Cheng, C.; Convertine, A. J.; Bryers, J. D.; Stayton, P. S. *Biomaterials* **2012**, *33*, 2301–2309.
(185) Gary, D. J.; Min, J.; Kim, Y.; Park, K.; Won, Y.-Y. *Macromol. Biosci.* **2013**, *13*, 1059–1071.
(186) Cheng, C.; Convertine, A. J.; Stayton, P. S.; Bryers, J. D. *Biomaterials* **2012**, *33*, 6868–6876.
(187) Koyamatsu, Y.; Hirano, T.; Kakizawa, Y.; Okano, F.; Takarada, T.; Maeda, M. *J. Controlled Release* **2014**, *173*, 89–95.
(188) Kelley, E. G.; Murphy, R. P.; Seppala, J. E.; Smart, T. P.; Hann, S. D.; Sullivan, M. O.; Epps, T. H. *Nat. Commun.* **2014**, *5*, 3599–3599.
(189) Yokoyama, M. *J. Drug Targeting* **2014**, *22*, 576–583.
(190) Hwang, S. J.; Davis, M. E. *Curr. Opin. Mol. Ther.* **2001**, *3*, 183–191.
(191) Davis, M. E. *Mol. Pharmaceutics* **2009**, *6*, 659–668.
(192) Zauner, W.; Ogris, M.; Wagner, E. *Adv. Drug Deliv. Rev.* **1998**, *30*, 97–113.
(193) Banaszczyk, M. G.; Lollo, C. P.; Kwoh, D. Y.; Phillips, A. T.; Amini, A.; Wu, D. P.; Mullen, P. M.; Coffin, C. C.; Brostoff, S. W.; Carlo, D. J. *J. Macromol. Sci., Pure Appl. Chem.* **1999**, *A36*, 1061–1084.
(194) Kwok, K. Y.; McKenzie, D. L.; Evers, D. L.; Rice, K. G. *J. Pharm. Sci.* **1999**, *88*, 996–1003.
(195) Toncheva, V.; Wolfert, M. A.; Dash, P. R.; Oupický, D.; Ulbrich, K.; Seymour, L. W.; Schacht, E. H. *Biochim. Biophys. Acta* **1998**, *1380*, 354–368.
(196) Ogris, M.; Brunner, S.; Schüller, S.; Kircheis, R.; Wagner, E. *Gene. Ther.* **1999**, *6*, 595–605.
(197) Maruyama, A.; Katoh, M.; Ishihara, T.; Akaike, T. *Bioconjugate Chem.* **1997**, *8*, 3–6.
(198) Cherng, J. Y.; Talsma, H.; Crommelin, D. J.; Hennink, W. E. *Pharm. Res.*

1999, *16*, 1417–1423.
(199) Anchordoquy, T. J.; Koe, G. S. *J. Pharm. Sci.* **2000**, *89*, 289.
(200) Kasper, J. C.; Troiber, C.; Kuechler, S.; Wagner, E.; Friess, W. *Eur. J. Pharm. Biopharm.* **2013**, *85*, 294–305.
(201) Cherng, J. Y. J.; van de Wetering, P. P.; Talsma, H. H.; Crommelin, D. J. D.; Hennink, W. E. W. *Pharm. Res.* **1997**, *14*, 1838–1841.
(202) Talsma, H.; Cherng, J.; Lehrmann, H.; Kursa, M.; Ogris, M.; Hennink, W.; Cotten, M.; Wagner, E. *Int. J. Pharm.* **1997**, *157*, 233–238.
(203) Chollet, P.; Favrot, M. C.; Hurbin, A.; Coll, J. L. *J. Gene Med.* **2002**, *4*, 84–91.
(204) Lv, H.; Zhang, S.; Wang, B.; Cui, S.; Yan, J. *J. Controlled Release* **2006**, *114*, 100–109.
(205) Goula, D.; Remy, J. S.; Erbacher, P.; Wasowicz, M.; Levi, G.; Abdallah, B.; Demeneix, B. A. *Gene. Ther.* **1998**, *5*, 712–717.
(206) Shinoda, T.; Maeda, A.; Kagatani, S.; Konno, Y.; Goto, M.; Sonobe, T.; Akaike, T. *Drug Deliv.* **1999**, *6*, 127–133.
(207) Richardson, S.; Kolbe, H.; Duncan, R. *Int. J. Pharm.* **1999**, *178*, 231–243.
(208) Lynn, D. M.; Langer, R. *J. Am. Chem. Soc.* **2000**, *122*, 10761–10768.
(209) Boussif, O.; Delair, T.; Brua, C.; Veron, L.; Pavirani, A.; Kolbe, H. *Bioconjugate Chem.* **1999**, *10*, 877–883.
(210) Kwoh, D. Y.; Coffin, C. C.; Lollo, C. P.; Jovenal, J.; Banaszczyk, M. G.; Mullen, P.; Phillips, A.; Amini, A.; Fabrycki, J.; Bartholomew, R. M.; Brostoff, S. W.; Carlo, D. J. *Biochim. Biophys. Acta* **1999**, *1444*, 171–190.
(211) Dash, P. R.; Read, M. L.; Barrett, L. B.; Wolfert, M.; Seymour, L. W. *Gene. Ther.* **1999**, *6*, 643–650.
(212) Dash, P. R.; Read, M. L.; Fisher, K. D.; Howard, K. A.; Wolfert, M.; Oupický, D.; Subr, V.; Strohalm, J.; Ulbrich, K.; Seymour, L. W. *J. Biol. Chem.* **2000**, *275*, 3793–3802.
(213) Garrett, S. W.; Davies, O. R.; Milroy, D. A.; Wood, P. J.; Pouton, C. W.; Threadgill, M. D. *Bioorg. Med. Chem.* **2000**, *8*, 1779–1797.
(214) Gref, R.; Lück, M.; Quellec, P.; Marchand, M.; Dellacherie, E.; Harnisch, S.; Blunk, T.; Müller, R. H. *Colloids Surf., B.* **2000**, *18*, 301–313.
(215) Finsinger, D.; Remy, J. S.; Erbacher, P.; Koch, C.; Plank, C. *Gene. Ther.* **2000**, *7*, 1183–1192.
(216) Laga, R.; Carlisle, R.; Tangney, M.; Ulbrich, K.; Seymour, L. W. *J. Controlled Release* **2012**, *161*, 537–553.
(217) Nelson, C. E.; Kintzing, J. R.; Hanna, A.; Shannon, J. M.; Gupta, M. K.; Duvall, C. L. *ACS Nano* **2013**, *7*, 8870–8880.
(218) Fattal, E.; Bochot, A. *Int. J. Pharm.* **2008**, *364*, 237–248.
(219) Howard, K. A. *Adv. Drug Deliv. Rev.* **2009**, *61*, 710–720.
(220) Malek, A.; Merkel, O.; Fink, L.; Czubayko, F.; Kissel, T.; Aigner, A. *Toxicol. Appl. Pharmacol.* **2009**, *236*, 97–108.
(221) Dobrovolskaia, M. A.; Germolec, D. R.; Weaver, J. L. *Nat. Nanotechnol.* **2009**, *4*, 411–414.
(222) Dobrovolskaia, M. A.; Mcneil, S. E. *Nat. Nanotechnol.* **2007**, *2*, 469–478.
(223) Jiskoot, W.; van Schie, R. M. F.; Carstens, M. G.; Schellekens, H. *Pharm. Res.*

2009, *26*, 1303–1314.
(224) Murad, Y. M.; Clay, T. M. *BioDrugs* **2009**, *23*, 361–375.
(225) Robbins, M.; Judge, A.; MacLachlan, I. *Oligonucleotides* **2009**, *19*, 89–101.
(226) Cubillos-Ruiz, J. R.; Engle, X.; Scarlett, U. K.; Martinez, D.; Barber, A.; Elgueta, R.; Wang, L.; Nesbeth, Y.; Durant, Y.; Gewirtz, A. T.; Sentman, C. L.; Kedl, R.; Conejo-Garcia, J. R. *J. Clin. Invest.* **2009**, *119*, 2231.
(227) Tomlinson, S. *Curr. Opin. Immunol.* **1993**, *5*, 83–89.
(228) Chonn, A.; Cullis, P. R.; Devine, D. V. *J. Immunol.* **1991**, *146*, 4234–4241.
(229) Henry, S. P.; Giclas, P. C.; Leeds, J.; Pangburn, M.; Auletta, C.; Levin, A. A.; Kornbrust, D. J. *J. Pharmacol. Exp. Ther.* **1997**, *281*, 810–816.
(230) Ishida, T.; Ichihara, M.; Wang, X.; Yamamoto, K.; Kimura, J.; Majima, E.; Kiwada, H. *J. Controlled Release* **2006**, *112*, 15–25.
(231) Ishihara, T.; Takeda, M.; Sakamoto, H.; Kimoto, A.; Kobayashi, C.; Takasaki, N.; Yuki, K.; Tanaka, K.-I.; Takenaga, M.; Igarashi, R.; Maeda, T.; Yamakawa, N.; Okamoto, Y.; Otsuka, M.; Ishida, T.; Kiwada, H.; Mizushima, Y.; Mizushima, T. *Pharm. Res.* **2009**, *26*, 2270–2279.
(232) Judge, A.; McClintock, K.; Phelps, J. R.; Maclachlan, I. *Mol. Ther.* **2006**, *13*, 328–337.
(233) Semple, S. C.; Harasym, T. O.; Clow, K. A.; Ansell, S. M.; Klimuk, S. K.; Hope, M. J. *J. Pharmacol. Exp. Ther.* **2005**, *312*, 1020–1026.
(234) Sroda, K.; Rydlewski, J.; Langner, M.; Kozubek, A.; Grzybek, M.; Sikorski, A. F. *Cell. Mol. Biol. Lett.* **2005**, *10*, 37–47.
(235) Szebeni, J.; Baranyi, L.; Savay, S.; Milosevits, J.; Bunger, R.; Laverman, P.; Metselaar, J. M.; Storm, G.; Chanan-Khan, A.; Liebes, L.; Muggia, F. M.; Cohen, R.; Barenholz, Y.; Alving, C. R. *J. Liposome Res.* **2002**, *12*, 165–172.
(236) Tagami, T.; Nakamura, K.; Shimizu, T.; Ishida, T.; Kiwada, H. *J. Controlled Release* **2009**, *137*, 234–240.
(237) Wang, X. Y.; Ishida, T.; Ichihara, M.; Kiwada, H. *J. Controlled Release* **2005**, *104*, 91–102.
(238) Minakuchi, Y.; Takeshita, F.; Kosaka, N.; Sasaki, H.; Yamamoto, Y.; Kouno, M.; Honma, K.; Nagahara, S.; Hanai, K.; Sano, A.; Kato, T.; Terada, M.; Ochiya, T. *Nucleic Acids Res.* **2004**, *32*, e109–e109.
(239) Sano, A.; Maeda, M.; Nagahara, S.; Ochiya, T.; Honma, K.; Itoh, H.; Miyata, T.; Fujioka, K. *Adv. Drug Deliv. Rev.* **2003**, *55*, 1651–1677.
(240) Pun, S. H.; Tack, F.; Bellocq, N. C.; Cheng, J.; Grubbs, B. H.; Jensen, G. S.; Davis, M. E.; Brewster, M.; Janicot, M.; Janssens, B.; Floren, W.; Bakker, A. *Cancer Biol. Ther.* **2004**, *3*, 641–650.
(241) Bellocq, N. C.; Davis, M. E.; Engler, H.; Jensen, G. S.; Liu, A.; Machemer, T.; Maneval, D. C.; Quijano, E.; Pun, S. H.; Schluep, T.; Wen, S. *Mol. Ther.* **2003**, *7*, S290.
(242) Hu-Lieskovan, S.; Heidel, J. D.; Bartlett, D. W.; Davis, M. E.; Triche, T. J. *Cancer Res.* **2005**, *65*, 8984–8992.
(243) Kirpotin, D. B.; Drummond, D. C.; Shao, Y.; Shalaby, M. R.; Hong, K.; Nielsen, U. B.; Marks, J. D.; Benz, C. C.; Park, J. W. *Cancer Res.* **2006**, *66*, 6732–6740.

(244) Choi, C. H. J.; Alabi, C. A.; Webster, P.; Davis, M. E. *Proc. Natl. Acad. Sci. USA* **2010**, *107*, 1235–1240.
(245) Bartlett, D. W.; Davis, M. E. *Biotechnol. Bioeng.* **2008**, *99*, 975–985.
(246) Davis, M. E.; Zuckerman, J. E.; Choi, C. H. J.; Seligson, D.; Tolcher, A.; Alabi, C. A.; Yen, Y.; Heidel, J. D.; Ribas, A. *Nature* **2010**, *464*, 1067–1070.
(247) Levine, A. S.; Levy, H. B. *Cancer Treat. Rep.* **1978**, *62*, 1907–1913.
(248) Schreiber, S.; Kämpgen, E.; Wagner, E.; Pirkhammer, D.; Trcka, J.; Korschan, H.; Lindemann, A.; Dorffner, R.; Kittler, H.; Kasteliz, F.; Küpcü, Z.; Sinski, A.; Zatloukal, K.; Buschle, M.; Schmidt, W.; Birnstiel, M.; Kempe, R. E.; Voigt, T.; Weber, H. A.; Pehamberger, H.; Mertelsmann, R.; Bröcker, E. B.; Wolff, K.; Stingl, G. *Hum. Gene Ther.* **1999**, *10*, 983–993.
(249) Konstan, M. W.; Davis, P. B.; Wagener, J. S.; Hilliard, K. A.; Stern, R. C.; Milgram, L. J. H.; Kowalczyk, T. H.; Hyatt, S. L.; Fink, T. L.; Gedeon, C. R.; Oette, S. M.; Payne, J. M.; Muhammad, O.; Ziady, A. G.; Moen, R. C.; Cooper, M. J. *Hum. Gene Ther.* **2004**, *15*, 1255–1269.
(250) Sidi, A. A.; Ohana, P.; Benjamin, S.; Shalev, M.; Ransom, J. H.; Lamm, D.; Hochberg, A.; Leibovitch, I. *J. Urol.* **2008**, *180*, 2379–2383.
(251) Ohana, P.; Gofrit, O.; Ayesh, S.; Al-Sharef, W.; Mizrahi, A.; Birman, T.; Schneider, T.; Matouk, I.; de Groot, N.; Tavdy, E.; Sidi, A. A.; Hochberg, A. *Gene Ther. Mol. Biol.* **2004**, *8*, 181–192.
(252) Gofrit, O. N.; Benjamin, S.; Halachmi, S.; Leibovitch, I.; Dotan, Z.; Lamm, D. L.; Ehrlich, N.; Yutkin, V.; Ben-Am, M.; Hochberg, A. *J. Urol.* **2014**, *191*, 1697–1702.
(253) Coelho, T.; Adams, D.; Silva, A.; Lozeron, P.; Hawkins, P. N.; Mant, T.; Perez, J.; Chiesa, J.; Warrington, S.; Tranter, E.; Munisamy, M.; Falzone, R.; Harrop, J.; Cehelsky, J.; Bettencourt, B. R.; Geissler, M.; Butler, J. S.; Sehgal, A.; Meyers, R. E.; Chen, Q.; Borland, T.; Hutabarat, R. M.; Clausen, V. A.; Alvarez, R.; Fitzgerald, K.; Gamba-Vitalo, C.; Nochur, S. V.; Vaishnaw, A. K.; Sah, D. W. Y.; Gollob, J. A.; Suhr, O. B. *N. Engl. J. Med.* **2013**, *369*, 819–829.
(254) Jayaraman, M.; Ansell, S. M.; Mui, B. L.; Tam, Y. K.; Chen, J.; Du, X.; Butler, D.; Eltepu, L.; Matsuda, S.; Narayanannair, J. K.; Rajeev, K. G.; Hafez, I. M.; Akinc, A.; Maier, M. A.; Tracy, M. A.; Cullis, P. R.; Madden, T. D.; Manoharan, M.; Hope, M. J. *Angew. Chem.* **2012**, *124*, 8657–8661.
(255) Burnett, J. C.; Rossi, J. J.; Tiemann, K. *Biotechnology Journal* **2011**, *6*, 1130–1146.
(256) Xu, C.-F.; Wang, J. *Asian J. Pharm. Sci. (Hong Kong, China)* **2014**.
(257) Golan, T. Novel Kras-directed therapy in combination with chemotherapy for locally advanced pancreatic adenocarcinoma. *2014 ASCO Annual Meeting*, 2014.
(258) Landau, G.; Bercovich, Z.; Park, M. H.; Kahana, C. *J. Biol. Chem.* **2010**, *285*, 12474–12481.
(259) Scuoppo, C.; Miething, C.; Lindqvist, L.; Reyes, J.; Ruse, C.; Appelmann, I.; Yoon, S.; Krasnitz, A.; Teruya-Feldstein, J.; Pappin, D.; Pelletier, J.; Lowe, S. W. *Nature* **2012**, *487*, 244–248.
(260) Taylor, C. A.; Zheng, Q.; Liu, Z.; Thompson, J. E. *Mol. Cancer* **2013**, *12*, 35–

35.
(261) Browne, L. J. *NJTC* **2011**, *1*, 23.
(262) Dondero, R.; Taylor, C.; Liu, Z.; Terence, T.; Thompson, J. **Pharmacodynamic, Biodistribution and Toxicology Results for SNS01-T, a Nanoparticle That Targets eIF5A for the Treatment of Multiple Myeloma**. *American Society of Hematology Annual Meeting and Exposition*, 2011.
(263) Kanasty, R.; Dorkin, J. R.; Vegas, A.; Anderson, D. *Nat. Mater.* **2013**, *12*, 967–977.
(264) Rozema, D. B.; Lewis, D. L.; Wakefield, D. H.; Wong, S. C.; Klein, J. J.; Roesch, P. L.; Bertin, S. L.; Reppen, T. W.; Chu, Q.; Blokhin, A. V.; Hagstrom, J. E.; Wolff, J. A. *Proc. Natl. Acad. Sci. USA* **2007**, *104*, 12982–12987.
(265) Wooddell, C. I.; Rozema, D. B.; Hossbach, M.; John, M.; Hamilton, H. L.; Chu, Q.; Hegge, J. O.; Klein, J. J.; Wakefield, D. H.; Oropeza, C. E.; Deckert, J.; Roehl, I.; Jahn-Hofmann, K.; Hadwiger, P.; Vornlocher, H.-P.; McLachlan, A.; Lewis, D. L. *Mol. Ther.* **2013**, *21*, 973–985.
(266) Schneider, B.; Grote, M.; John, M.; Haas, A.; Bramlage, B.; Ickenstein, L. M.; Jahn-Hofmann, K.; Bauss, F.; Cheng, W.; Croasdale, R.; Daub, K.; Dill, S.; Hoffmann, E.; Lau, W.; Burtscher, H.; Ludtke, J. L.; Metz, S.; Mundigl, O.; Neal, Z. C.; Scheuer, W.; Stracke, J.; Herweijer, H.; Brinkmann, U. *Mol. Ther. Nucleic Acids* **2012**, *1*, e46–e46.
(267) Wong, S. C.; Klein, J. J.; Hamilton, H. L.; Chu, Q.; Frey, C. L.; Trubetskoy, V. S.; Hegge, J.; Wakefield, D.; Rozema, D. B.; Lewis, D. L. *Nucleic Acid Ther.* **2012**, *22*, 380–390.
(268) Aouadi, M.; Tesz, G. J.; Nicoloro, S. M.; Wang, M.; Chouinard, M.; Soto, E.; Ostroff, G. R.; Czech, M. P. *Nature* **2009**, *458*, 1180–1184.
(269) Kim, Y.-C.; Park, J.-H.; Prausnitz, M. R. *Adv. Drug Deliv. Rev.* **2012**, *64*, 1547–1568.
(270) Hickerson, R. P.; Wey, W. C.; Rimm, D. L.; Speaker, T.; Suh, S.; Flores, M. A.; Gonzalez-Gonzalez, E.; Leake, D.; Contag, C. H.; Kaspar, R. L. *Mol. Ther. Nucleic Acids* **2013**, *2*, e129–e129.
(271) Daddona, P. E.; Matriano, J. A.; Mandema, J.; Maa, Y.-F. *Pharm. Res.* **2011**, *28*, 159–165.
(272) Davtyan, H.; Ghochikyan, A.; Movsesyan, N.; Ellefsen, B.; Petrushina, I.; Cribbs, D. H.; Hannaman, D.; Evans, C. F.; Agadjanyan, M. G. *Neurodegener. Dis.* **2012**, *10*, 261–264.
(273) Graham, B. S.; Enama, M. E.; Nason, M. C.; Gordon, I. J.; Peel, S. A.; Ledgerwood, J. E.; Plummer, S. A.; Mascola, J. R.; Bailer, R. T.; Roederer, M.; Koup, R. A.; Nabel, G. J.; Team, T. V. 0. S. *PLoS ONE* **2013**, *8*, e59340.
(274) Boudreau, E. F.; Josleyn, M.; Ullman, D.; Fisher, D.; Dalrymple, L.; Sellers-Myers, K.; Loudon, P.; Rusnak, J.; Rivard, R.; Schmaljohn, C.; Hooper, J. W. *Vaccine* **2012**, *30*, 1951–1958.
(275) Walther, W.; Stein, U.; Fichtner, I.; Schlag, P. M. *Mol. Biotechnol.* **2004**, *28*, 121–128.
(276) Kebriaei, P.; Huls, H.; Singh, H.; Olivares, S.; Figliola, M.; Kumar, P. R.; Jena,

B.; Forget, M. A.; Ang, S.; Jackson, R. N.; Liu, T.; Bosque, D.; McNiece, I. K.; Rondon, G.; Hackett, P.; Hosing, C. M.; Shpall, E. J.; Champlin, R. E.; Cooper, L. J. N. *Blood* **2013**, *122*, 166–166.

(277) Aronovich, E. L.; McIvor, R. S.; Hackett, P. B. *Human Molecular Genetics* **2011**, *20*, 14–20.

(278) Saha, S.; Woodard, L. E.; Charron, E. M.; Welch, R. C.; Rooney, C. M.; Wilson, M. H. *Nucleic Acids Res.* **2015**, *43*, 1770–1782.

(279) Kang, Y.; Zhang, X.-Y.; Jiang, W.; Wu, C.-Q.; Chen, C.-M.; Gu, J.-R.; Zheng, Y.-F.; Xu, C.-J. *Cell Biol. Int.* **2009**, *33*, 509–515.

(280) Mandal, P. K.; Ferreira, L. M. R.; Collins, R.; Meissner, T. B.; Boutwell, C. L.; Friesen, M.; Vrbanac, V.; Garrison, B. S.; Stortchevoi, A.; Bryder, D.; Musunuru, K.; Brand, H.; Tager, A. M.; Allen, T. M.; Talkowski, M. E.; Rossi, D. J.; Cowan, C. A. *Cell Stem Cell* **2014**, *15*, 643–652.

(281) Kim, D.; Bae, S.; Park, J.; Kim, E.; Kim, S.; Yu, H. R.; Hwang, J.; Kim, J.-I.; Kim, J.-S. *Nat Methods* **2015**, *12*, 237–243.

(282) Wu, Y.; Zhou, H.; Fan, X.; Zhang, Y.; Zhang, M.; Wang, Y.; Xie, Z.; Bai, M.; Yin, Q.; Liang, D.; Tang, W.; Liao, J.; Zhou, C.; Liu, W.; Zhu, P.; Guo, H.; Pan, H.; Wu, C.; Shi, H.; Wu, L.; Tang, F.; Li, J. *Cell Research* **2015**, *25*, 67–79.

(283) High, K.; Gregory, P. D.; Gersbach, C. *Nat. Med.* **2014**, *20*, 476–477.

(284) Gantz, V. M.; Bier, E. *Science* **2015**, aaa5945.

(285) Baltimore, B. D.; Berg, P.; Botchan, M.; Carroll, D.; Charo, R. A.; Church, G.; Corn, J. E.; Daley, G. Q.; Doudna, J. A.; Fenner, M.; Greely, H. T.; Jinek, M.; Martin, G. S.; Penhoet, E.; Puck, J.; Sternberg, S. H.; Weissman, J. S.; Yamamoto, K. R. *Science* **2015**, aab1028.

(286) Kaufmann, K. B.; Büning, H.; Galy, A.; Schambach, A.; Grez, M. *EMBO Molecular Medicine* **2013**, *5*, 1642–1661.

(287) Ginn, S. L.; Alexander, I. E.; Edelstein, M. L.; Abedi, M. R.; Wixon, J. *J. Gene Med.* **2013**, *15*, 65–77.

(288) Lollo, C. P.; Banaszczyk, M.; Chiou, H. *Curr. Opin. Mol. Ther.* **2000**, *2*, 136–142.

(289) DeMuth, P. C.; Min, Y.; Huang, B.; Kramer, J. A.; Miller, A. D.; Barouch, D. H.; Hammond, P. T.; Irvine, D. J. *Nat. Mater.* **2013**, *12*, 367–376.

(290) Bagley, J.; Iacomini, J. *Gene. Ther.* **2003**, *10*, 605–611.

(291) Sizovs, A.; McLendon, P. M.; Srinivasachari, S.; Reineke, T. M. *Top. Curr. Chem.* **2010**, *296*, 131–190.

(292) Halama, A.; Kulinski, M.; Librowski, T.; Lochynski, S. *Pharmacol. Rep.* **2009**, *61*, 993–999.

(293) van Gaal, E. V. B.; Oosting, R. S.; Hennink, W. E.; Crommelin, D. J. A.; Mastrobattista, E. *Int. J. Pharm.* **2010**, *390*, 76–83.

(294) Boussif, O.; Lezoualc'h, F.; Zanta, M. A.; Mergny, M. D.; Scherman, D.; Demeneix, B.; Behr, J. P. *Proc. Natl. Acad. Sci. USA* **1995**, *92*, 7297–7301.

(295) Bettinger, T.; Carlisle, R. C.; Read, M. L.; Ogris, M.; Seymour, L. W. *Nucleic Acids Res.* **2001**, *29*, 3882–3891.

(296) Braun, C. S.; Vetro, J. A.; Tomalia, D. A.; Koe, G. S.; Koe, J. G.; Middaugh, C.

R. *J. Pharm. Sci.* **2004**, *94*, 423–436.
(297) Alidedeoglu, A. H.; York, A. W.; McCormick, C. L.; Morgan, S. E. *J. Polym. Sci., Part A Polym. Chem.* **2009**, *47*, 5405–5415.
(298) Morse, A. J.; Dupin, D.; Thompson, K. L.; Armes, S. P.; Ouzineb, K.; Mills, P.; Swart, R. *Langmuir* **2012**, *28*, 11733–11744.
(299) Evans, C. C.; Christie, R. J.; Nishiyama, N.; Zasadzinski, J.; Kataoka, K. *Endocrinology* **2010**, *151*, 466–473.
(300) Paslay, L. C.; Abel, B. A.; Brown, T. D.; Koul, V.; Choudhary, V.; McCormick, C. L.; Morgan, S. E. *Biomacromolecules* **2012**, *13*, 2472–2482.
(301) Tranter, M.; Liu, Y.; He, S.; Gulick, J.; Ren, X.; Robbins, J.; Jones, W. K.; Reineke, T. M. *Mol. Ther.* **2012**, *20*, 601–608.
(302) McLendon, P. M.; Fichter, K. M.; Reineke, T. M. *Mol. Pharmaceutics* **2010**, *7*, 738–750.
(303) Voit, B.; Appelhans, D. *Macromol. Chem. Phys.* **2010**, *211*, 727–735.
(304) Ting, S. R. S.; Chen, G.; Stenzel, M. H. *Polym. Chem.* **2010**, *1*, 1392–1412.
(305) Alhoranta, A. M.; Lehtinen, J. K.; Urtti, A. O.; Butcher, S. J.; Aseyev, V. O.; Tenhu, H. J. *Biomacromolecules* **2011**, *12*, 3213–3222.
(306) Won, Y.-Y.; Sharma, R.; Konieczny, S. F. *J. Controlled Release* **2009**, *139*, 88–93.
(307) Samsonova, O.; Pfeiffer, C.; Hellmund, M.; Merkel, O. M.; Kissel, T. *Polymers* **2011**, *3*, 693–718.
(308) Lim, D. W.; Yeom, Y. I.; Park, T. G. *Bioconjugate Chem.* **2000**, *11*, 688–695.
(309) Schmidt, N.; Mishra, A.; Lai, G. H.; Wong, G. C. L. *FEBS Lett.* **2010**, *584*, 1806–1813.
(310) Yin, L.; Dalsin, M. C.; Sizovs, A.; Reineke, T. M.; Hillmyer, M. A. *Macromolecules* **2012**, *45*, 4322–4332.
(311) Xu, X.; Smith, A. E.; Kirkland, S. E.; McCormick, C. L. *Macromolecules* **2008**, *41*, 8429–8435.
(312) Mayo, F. R.; Lewis, F. M. *J. Am. Chem. Soc.* **1944**, *66*, 1594–1601.
(313) Odian, G. *Principles of polymerization*; 4 ed.; John Wiley & Sons, Inc.: Hoboken, NJ, 2004; pp. 464–543.
(314) Alfrey, T.; Goldfinger, G. *J. Chem. Phys.* **1944**, *12*, 205–209.
(315) Mosmann, T. *J. Immunol. Methods* **1983**, *65*, 55–63.
(316) Mayadunne, R. T. A.; Rizzardo, E.; Chiefari, J.; Chong, Y. K.; Moad, G.; Thang, S. H. *Macromolecules* **1999**, *32*, 6977–6980.
(317) Vasilieva, Y. A.; Thomas, D. B.; Scales, C. W.; McCormick, C. L. *Macromolecules* **2004**, *37*, 2728–2737.
(318) McCormick, C. L.; Lowe, A. B. *Acc. Chem. Res.* **2004**, *37*, 312–325.
(319) Lee, H.; Son, S. H.; Sharma, R.; Won, Y.-Y. *J. Phys. Chem.* **2011**, *115*, 844–860.
(320) Cherng, J. Y.; van de Wetering, P.; Talsma, H.; Crommelin, D. J.; Hennink, W. E. *Pharm. Res.* **1996**, *13*, 1038–1042.
(321) Rawlinson, L.-A. B.; O'Brien, P. J.; Brayden, D. J. *J. Controlled Release* **2010**, *146*, 84–92.
(322) Van Engeland, M.; Nieland, L. J.; Ramaekers, F. C.; Schutte, B.;

Reutelingsperger, C. P. *Cytometry* **1998**, *31*, 1–9.
(323) Dong, H. P.; Holth, A.; Kleinberg, L.; Ruud, M. G.; Elstrand, M. B.; Tropé, C. G.; Davidson, B.; Risberg, B. *Am. J. Clin. Pathol.* **2009**, *132*, 756–762.
(324) Vermes, I.; Haanen, C.; Steffens-Nakken, H.; Reutelingsperger, C. *J. Immunol. Methods* **1995**, *184*, 39–51.
(325) Andree, H. A.; Reutelingsperger, C. P.; Hauptmann, R.; Hemker, H. C.; Hermens, W. T.; Willems, G. M. *J. Biol. Chem.* **1990**, *265*, 4923–4928.
(326) Hong, S.; Leroueil, P. R.; Janus, E. K.; Peters, J. L.; Kober, M.-M.; Islam, M. T.; Orr, B. G.; Baker, J. R.; Banaszak Holl, M. M. *Bioconjugate Chem.* **2006**, *17*, 728–734.
(327) Khmaladze, A.; Matz, R. L.; Epstein, T.; Jasensky, J.; Banaszak Holl, M. M.; Chen, Z. *J. Struct. Biol.* **2012**, *178*, 270–278.
(328) Su, T. J.; Styrkas, D. A.; Thomas, R. K.; Baines, F. L.; Billingham, N. C.; Armes, S. P. *Macromolecules* **1996**, *29*, 6892–6900.
(329) Pergushov, D. V.; Müller, A. H. E.; Schacher, F. H. *Chem. Soc. Rev.* **2012**, *41*, 6888–6901.
(330) Müller, M. In *Polyelectrolyte Complexes in the Dispersed and Solid State II*; Müller, M., Ed.; Advances in Polymer Science; Springer Berlin Heidelberg: Berlin, Heidelberg, 2013; Vol. 256, pp. 103–195.
(331) Zheng, Y.; Won, Y.-Y.; Bates, F. S.; Davis, H. T.; Scriven, L. E.; Talmon, Y. *J. Phys. Chem.* **1999**, *103*, 10331–10334.
(332) Yusa, S. I.; Fukuda, K.; Yamamoto, T.; Ishihara, K.; Morishima, Y. *Biomacromolecules* **2005**, *6*, 663–670.
(333) Owen, S. C.; Chan, D. P.; Shoichet, M. S. *Nano Today* **2012**, *7*, 53–65.
(334) Loh, X. J.; Ong, S. J.; Tung, Y. T.; Choo, H. T. *Mater. Sci. Eng. C* **2013**, *33*, 4545–4550.
(335) Lee, T. H.; Wang, J.; Wang, C.-H. *J. Controlled Release* **2002**, *83*, 437–452.
(336) Nikolic, M. S.; Djonlagic, J. *Polym. Degrad. Stab.* **2001**, *74*, 263–270.
(337) Emileh, A.; Vasheghani-Farahani, E.; Imani, M. *Eur. Polym. J.* **2007**, *43*, 1986–1995.
(338) Yang, Y. Q.; Lin, W. J.; Zhao, B.; Wen, X. F.; Guo, X. D.; Zhang, L. J. *Langmuir* **2012**, *28*, 8251–8259.
(339) Lee, H.; Kim, D. H.; Witte, K. N.; Ohn, K.; Choi, J.; Akgun, B.; Satija, S.; Won, Y.-Y. *J. Phys. Chem.* **2012**, *116*, 7367–7378.
(340) Zengin, A.; Karakose, G.; Caykara, T. *Eur. Polym. J.* **2013**, *49*, 3350–3358.
(341) Borisov, O. V.; Zhulina, E. B.; Leermakers, F. A. M.; Ballauff, M.; Mueller, A. H. E. *Self Organized Nanostructures of Amphiphilic Block Copolymers I* **2011**, *241*, 1–55.
(342) Borisov, O. V.; Zhulina, E. B. *Eur. Phys. J. B* **1998**, *4*, 205–217.
(343) Fanun, M. *Colloids in Drug Delivery*; Fanun, M., Ed.; CRC Press: Boca Raton, 2010; Vol. 150, pp. 1–652.
(344) Gil, E. S.; Hudson, S. M. *Prog. Polym. Sci.* **2004**, *29*, 1173–1222.
(345) Convertine, A. J.; Diab, C.; Prieve, M.; Paschal, A.; Hoffman, A. S.; Johnson, P. H.; Stayton, P. S. *Biomacromolecules* **2010**, *11*, 2904–2911.
(346) Álvarez-Paino, M.; Muñoz-Bonilla, A.; López-Fabal, F.; Gómez-Garcés, J. L.;

Heuts, J. P. A.; Fernández-García, M. *Biomacromolecules* **2015**, *16*, 295–303.
(347) Li, W.; Nakayama, M.; Akimoto, J.; Okano, T. *Polymer* **2011**, *52*, 3783–3790.
(348) Claeys, B.; De Coen, R.; De Geest, B. G.; la Rosa, de, V. R.; Hoogenboom, R.; Carleer, R.; Adriaensens, P.; Remon, J. P.; Vervaet, C. *Eur. J. Pharm. Biopharm.* **2013**, *85*, 1206–1214.
(349) Yoshii, E. *J. Biomed. Mater. Res.* **1997**, *37*, 517–524.
(350) Dillingham, E. O.; Lawrence, W. H.; Autian, J.; Schmalz, G. *J. Biomed. Mater. Res.* **1983**, *17*, 945–957.
(351) Housheya, O. J.; Wilkins, C. *Int. J. Chem. (Toronto, ON, Can.)* **2012**, *4*, 14–23.
(352) Okamoto, K. Maldi Mass Spectrometry of Snythetic Polymers http://www.tytlabs.com/english/review/rev413epdf/e413_029okamoto.pdf (accessed Apr 1, 2014).
(353) Montaudo, G.; Montaudo, M. S.; Puglisi, C.; Samperi, F. *Rapid Commun. Mass Spectrom.* **1995**, *9*, 1158–1163.
(354) Lou, X.; van Dongen JL. *J. Mass Spectrom.* **2000**, *35*, 1308–1312.
(355) Yalcin, T.; Dai, Y.; Li, L. *J. Am. Soc. Mass Spectrom.* **1998**, *9*, 1303–1310.
(356) Helmstedt, M.; Schäfer, H. *Polymer* **1994**, *35*, 3377–3383.
(357) Hirzinger, B.; Helmstedt, M.; Stejskal, J. *Polymer* **2000**, *41*, 2883–2891.
(358) Kunz, D.; Thurn, A.; Burchard, W. *Colloid Polym. Sci.* **1983**, *261*, 635–644.
(359) Vyhnalkova, R.; Müller, A. H. E.; Eisenberg, A. *Langmuir* **2014**, *30*, 13152–13163.
(360) Chelushkin, P. S.; Lysenko, E. A.; Bronich, T. K.; Eisenberg, A.; Kabanov, V. A.; Kabanov, A. V. *J. Phys. Chem.* **2008**, *112*, 7732–7738.
(361) Shanmuganathan, K.; Capadona, J. R.; Rowan, S. J.; Weder, C. *ACS Appl. Mater. Interfaces* **2010**, *2*, 165–174.
(362) Zinn, T.; Willner, L.; Lund, R.; Pipich, V.; Richter, D. *Soft Matter* **2012**, *8*, 623–626.
(363) Liu, F.; Urban, M. W. *Macromolecules* **2008**, *41*, 6531–6539.
(364) Van Domeselaar, G. H.; Kwon, G. S.; Andrew, L. C.; Wishart, D. S. *Colloids Surf., B.* **2003**, *30*, 323–334.
(365) Hur, J.; Witte, K. N.; Sun, W.; Won, Y.-Y. *Langmuir* **2010**, *26*, 2021–2034.
(366) Choucair, A.; Lavigueur, C.; Eisenberg, A. *Langmuir* **2004**, *20*, 3894–3900.
(367) Laaser, J. E.; Jiang, Y.; Sprouse, D.; Reineke, T. M.; Lodge, T. P. *Macromolecules* **2015**, *48*, 2677–2685.
(368) Chun, M.-S.; Bowen, W. R. *J. Colloid Interface Sci.* **2004**, *272*, 330–339.
(369) Zadaka, D.; Radian, A.; Mishael, Y. G. *J. Colloid Interface Sci.* **2010**, *352*, 7–7.
(370) Hunter, R. J. *Colloids Surf., A.* **1998**, *141*, 37–66.
(371) Zou, J.; Zhang, S.; Shrestha, R.; Seetho, K.; Donley, C. L.; Wooley, K. L. *Polym. Chem.* **2012**, *3*, 3146–3156.
(372) Wu, W.; Zhang, Q.; Wang, J.; Chen, M.; Li, S.; Lin, Z.; Li, J. *Polym. Chem.* **2014**, *5*, 5668–5679.
(373) Selmani, A.; Lützenkirchen, J.; Kallay, N.; Preocanin, T. *J Phys Condens Matter* **2014**, *26*, 244104–244104.
(374) Hiemstra, T. *Langmuir* **2012**, *28*, 15614–15623.
(375) Wang, P.; Keller, A. A. *Langmuir* **2009**, *25*, 6856–6862.

(376) Lyklema, J.; Golub, T. *Croat. Chem. Acta* **2007**, *80*, 303–311.
(377) Lyklema, J. *Fundamentals of interface and colloid science. Volume I: Fundamentals.*; 1st ed.; Academic Press: London, 2000; Vol. 1, pp. 1–844.
(378) Lyklema, H. In *Liquid-Fluid Interface*; Fundamentals of Interface and Colloid Science; Elsevier, 2000; Vol. 3, pp. i–ii.
(379) Pfeiffer, C.; Rehbock, C.; Hühn, D.; Carrillo-Carrion, C.; de Aberasturi, D. J.; Merk, V.; Barcikowski, S.; Parak, W. J. *J. R. Soc. Interface* **2014**, *11*, 20130931–20130931.
(380) Akinc, A.; Querbes, W.; De, S.; Qin, J.; Frank-Kamenetsky, M.; Jayaprakash, K. N.; Jayaraman, M.; Rajeev, K. G.; Cantley, W. L.; Dorkin, J. R.; Butler, J. S.; Qin, L.; Racie, T.; Sprague, A.; Fava, E.; Zeigerer, A.; Hope, M. J.; Zerial, M.; Sah, D. W.; Fitzgerald, K.; Tracy, M. A.; Manoharan, M.; Koteliansky, V.; Fougerolles, A. de; Maier, M. A. *Mol. Ther.* **2010**, *18*, 1357–1364.
(381) van Rossenberg, S. M. W.; Sliedregt-Bol, K. M.; Koning, G.; van den Elst, H.; van Berkel, T. J. C.; van Boom, J. H.; van der Marel, G. A.; Biessen, E. A. L. *ChemBioChem* **2003**, *4*, 633–639.
(382) Wang, H.-X.; Xiong, M.-H.; Wang, Y.-C.; Zhu, J.; Wang, J. *J. Controlled Release* **2013**, *166*, 106–114.
(383) Follenzi, A.; Battaglia, M.; Lombardo, A.; Annoni, A.; Roncarolo, M. G.; Naldini, L. *Blood* **2004**, *103*, 3700–3709.

Appendix

List of Abbreviations and Acronyms

7-AAD	7-Amino-actinomycin D
Acetate	Acetic Acid
AEMA	*N*-(2-amino)ethyl methacrylamide
AIBN	Azobisisobutyronitrile (2,2′-Azobis(2-methylpropionitrile))
BMA	Butly methacrylate
BPA	Bisphenol A
CD	Cyclodextrin
CHCA	α-cyano-4-hydroxycinnamic acid
CHES	*N*-Cyclohexyl-2-aminoethanesulfonic acid
CMC	Critical micelle concentration
CPP	4-Cyano-4-(propylsulfanylthiocarbonyl)sulfanylpentanoic acid
CRISPR	Clustered regularly interspaced short palindromic repeats
CTA	Chain transfer agent
Cy-5	Cyanine 5
Đ	Dispersity
Da	Daltons
DCM	Dichloromethane
DHB	Dihydroxybenzoic acid
DI	De-ionized
DLS	Dynamic light scattering
DMAEMA	*N,N*-(2-dimethylamino)ethyl methacrylamide
DMEM	Dulbecco modified Eagle's minimal essential medium

DMSO	Dimethylsulfoxide
DPC	Dynamic PolyConjugates
DSC	Differential scanning calorimetry
F_1 and f_1	Molar polymer composition and feed fraction
FACS	Fluorescence-activated cell sorting
FBS	Fetal bovine serum
GalNAc	N-Acetyl Galactosamine
GC-MS	Gas chromatography–mass spectrometry
GFP	Green fluorescent protein
GPC	Gel permeation chromatography
HEPES	4-(2-hydroxyethyl)-1-piperazineethanesulfonic acid
JetPEI	Linear polyethylenimine
MAG	2-Deoxy-2-methacrylamido glucopyranose
MALDI-TOF-MS	Matrix-assisted laser desorption/ionization-time of flight-mass spectrometry
MeOH	Methanol
MES	2-(*N*-morpholino)ethanesulfonic acid
M_n	Number-average molecular weight
MOPS	3-(*N*-morpholino)propansulfonic acid
MTT	3-(4,5-dimethyl-2-thiazolyl)-2,5-diphenyltetrazolium bromide
M_w	Weight-average molecular weight
MWCO	Molecular weight cut off
N/P	Nitrogen to posphate ratio
NMR	Nuclear magnetic resonance spectroscopy
PAMAM	Polyamidoamine
PBS	Phosphate Buffer Saline

PEG	Polyethyleneglycol
PEI	Polyethylenimine
PGAA	Polyglycoamidoamine
PI	Propidium iodide
PLL	Poly-L-lysine
PS	Polystyrene
RAFT	Reversible Addition-Fragmentation chain Transfer
R_g	Radius of gyration
R_h	Radius of hydration
RLU	Relative light units
ROMP	Ring opening metathesis polymerization
SAX	Small-angle X-ray scattering
SEC	Size-exclusion chromatography
SMP	Shape memory polymer
Tf	Transferrin protein
TFA	Triflouroacetic acid
T_g	Glass transition temperature
TGA	Thermogravimetric analysis
THAP	2,4,6-trihydroxyacetophenone
THF	Tetrahydrofuran
TLR	Toll-like receptor
T_m	Melting temperature
TRIS	tris(hydroxymethyl)aminomethane
T_{trans}	Shape memory transition temperature
V-501	4,4'-Azobis(4-cyanovaleric acid)
WAXS	Wide-angle X-ray scattering

w_x	Weight-fraction of copolymer
ε	Strain
ζ	Zeta potential
λ	Lambda (wavelength)
σ	Stress

List of Figures

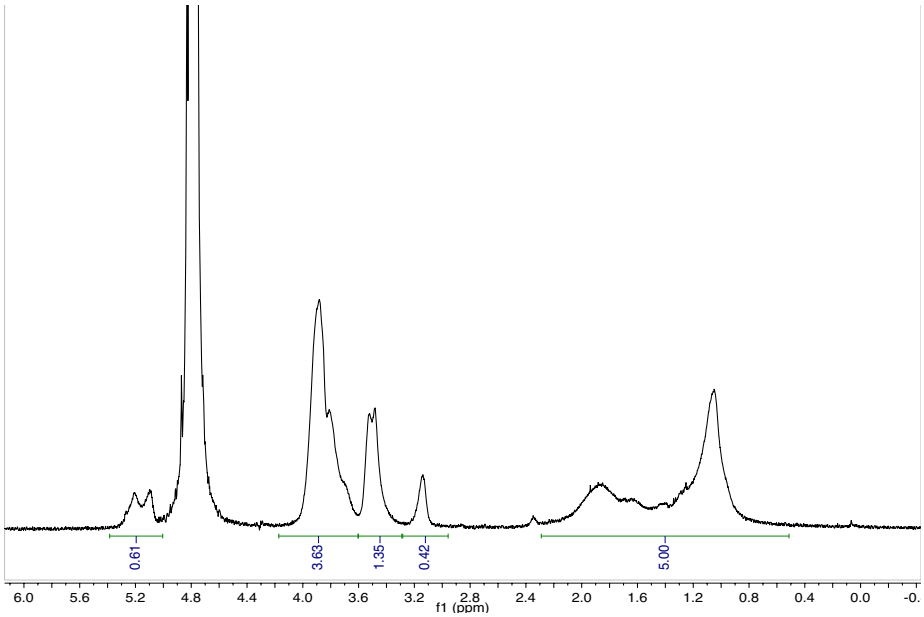

Figure 63. ^{1}H NMR spectra of poly($\mathbf{G}_{46}$-*b*-$\mathbf{P}_{13}$) in D_2O at 500 MHz with a relaxation delay of 10 seconds. Spectra are internally refrenced to the HOD peak.

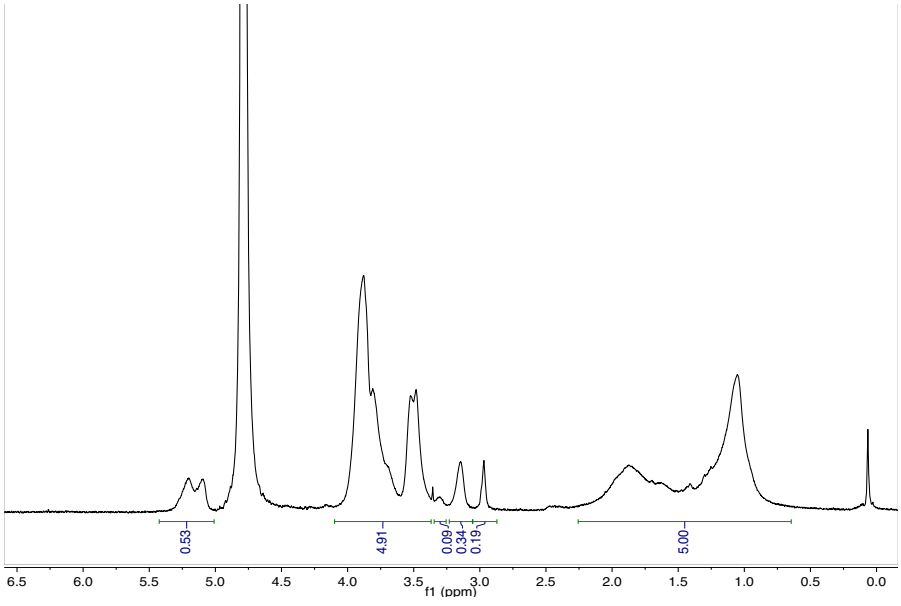

Figure 64. ^{1}H NMR spectra of poly($\mathbf{G}_{46}$-*b*-$\mathbf{P}_{10}$-*b*-$\mathbf{T}_{2}$) in D_2O at 500 MHz with a relaxation delay of 10 seconds. Spectra are internally refrenced to the HOD peak.

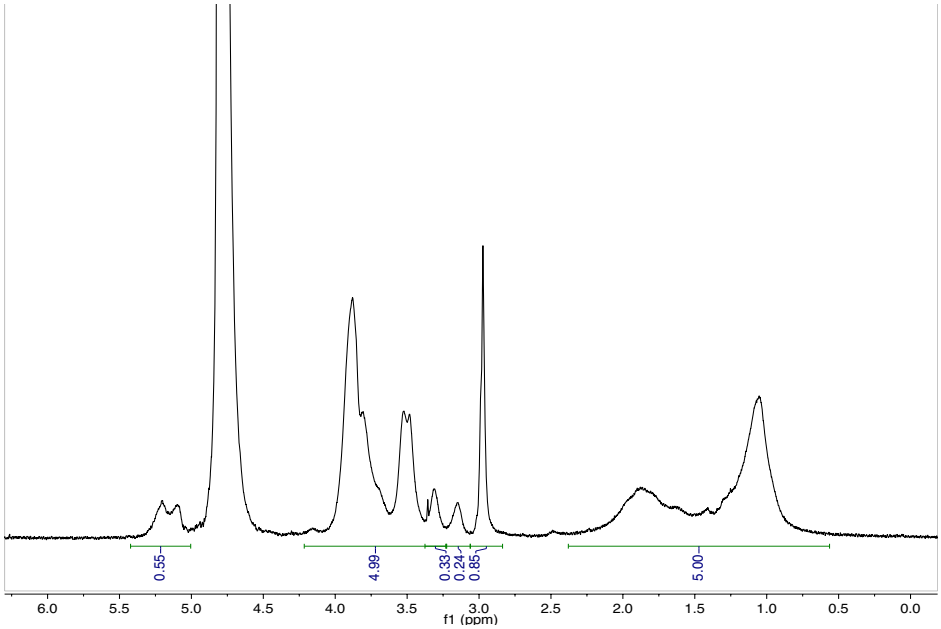

Figure 65. ^{1}H NMR spectra of poly(**G**$_{46}$-*b*-**P**$_{8}$-*b*-**T**$_{9}$) in D_2O at 500 MHz with a relaxation delay of 10 seconds. Spectra are internally refrenced to the HOD peak.

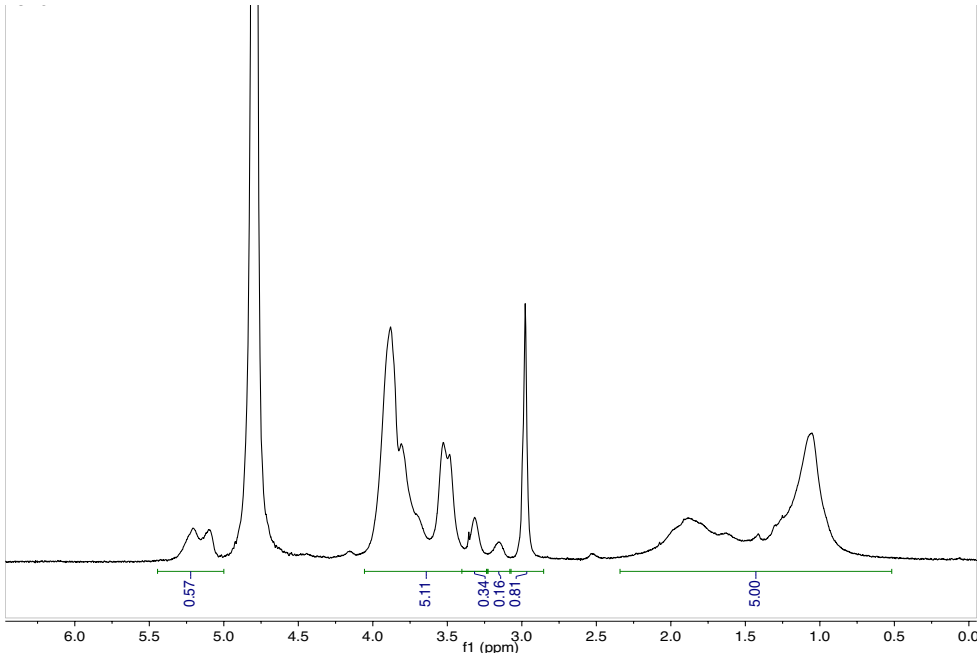

Figure 66. ^{1}H NMR spectra of poly(**G**$_{46}$-*b*-**P**$_{6}$-*b*-**T**$_{17}$) in D_2O at 500 MHz with a relaxation delay of 10 seconds. Spectra are internally refrenced to the HOD peak.

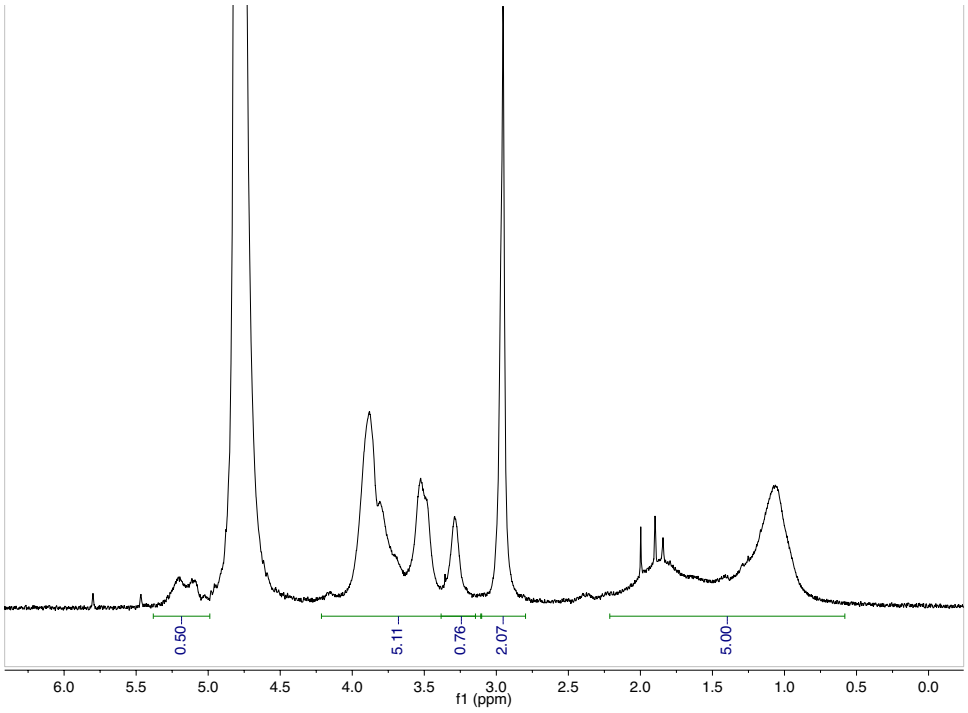

Figure 67. ^{1}H NMR spectra of poly(**G**$_{46}$-*b*-**T**$_{26}$) in D_2O at 500 MHz with a relaxation delay of 10 seconds. Spectra are internally refrenced to the HOD peak.

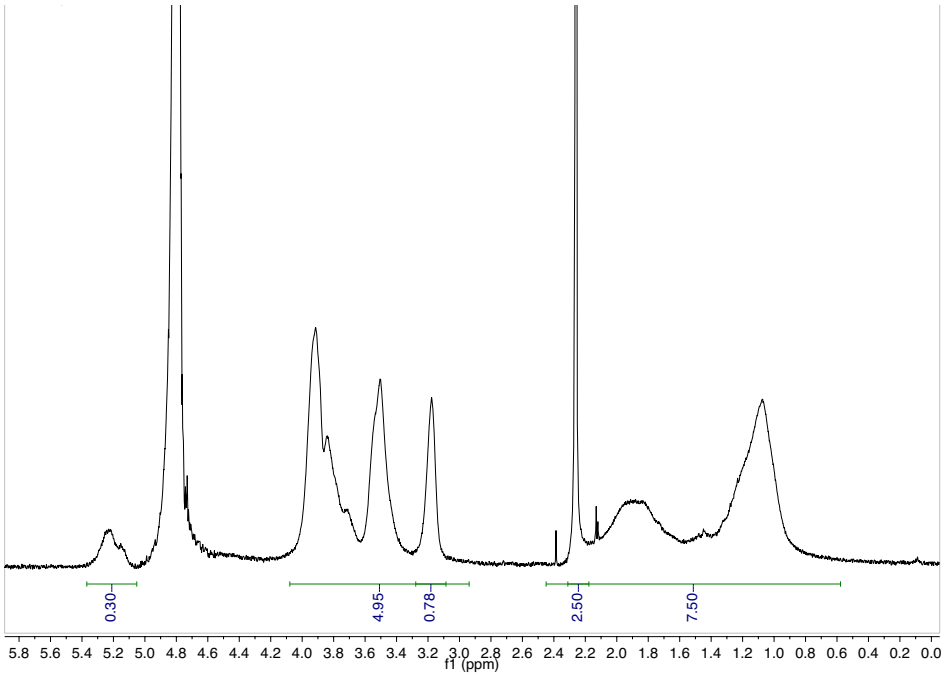

Figure 68. ^{1}H NMR spectra of poly(**G**$_{45}$-*s*-**P**$_{35}$) in D_2O at 500 MHz with a relaxation delay of 10 seconds. Spectra are internally refrenced to the HOD peak.

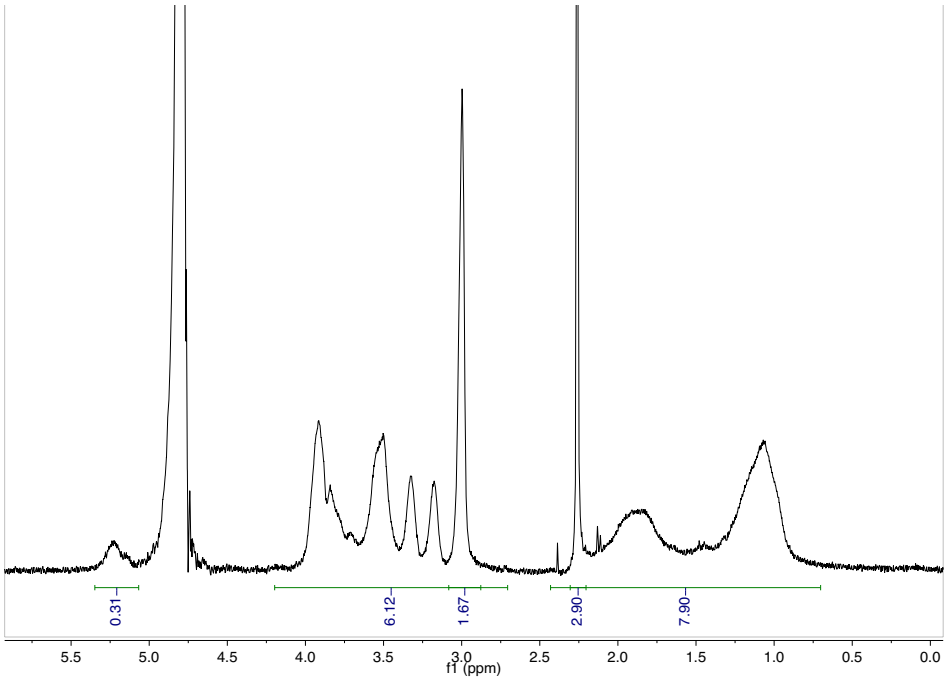

Figure 69. ^{1}H NMR spectra of poly(**G**$_{62}$-*s*-**T**$_{23}$) in D_2O at 500 MHz with a relaxation delay of 10 seconds. Spectra are internally refrenced to the HOD peak.

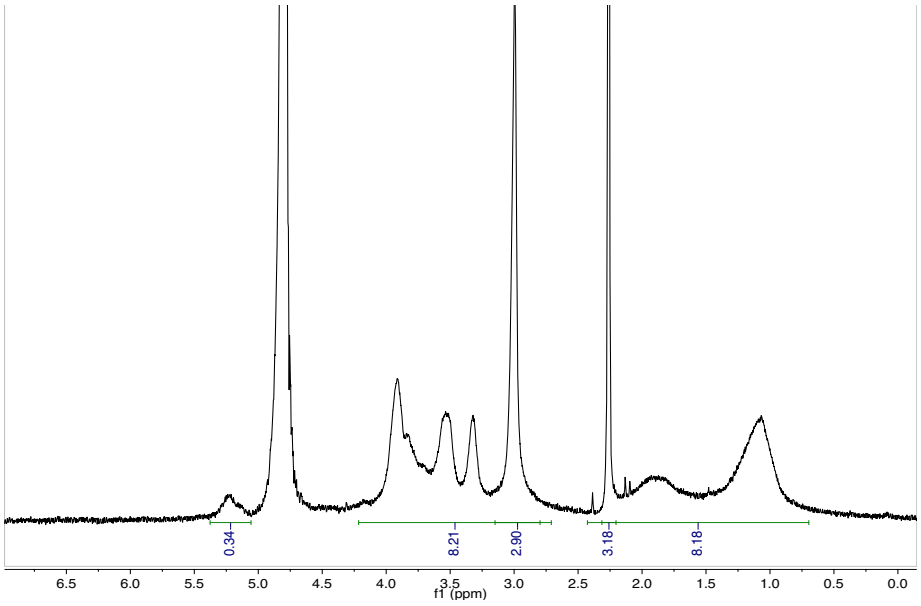

Figure 70 ^{1}H NMR spectra of poly(**G**$_{32}$-*s*-**P**$_{40}$-*s*-**T**$_{21}$) in D_2O at 500 MHz with a relaxation delay of 10 seconds. Spectra are internally refrenced to the HOD peak.

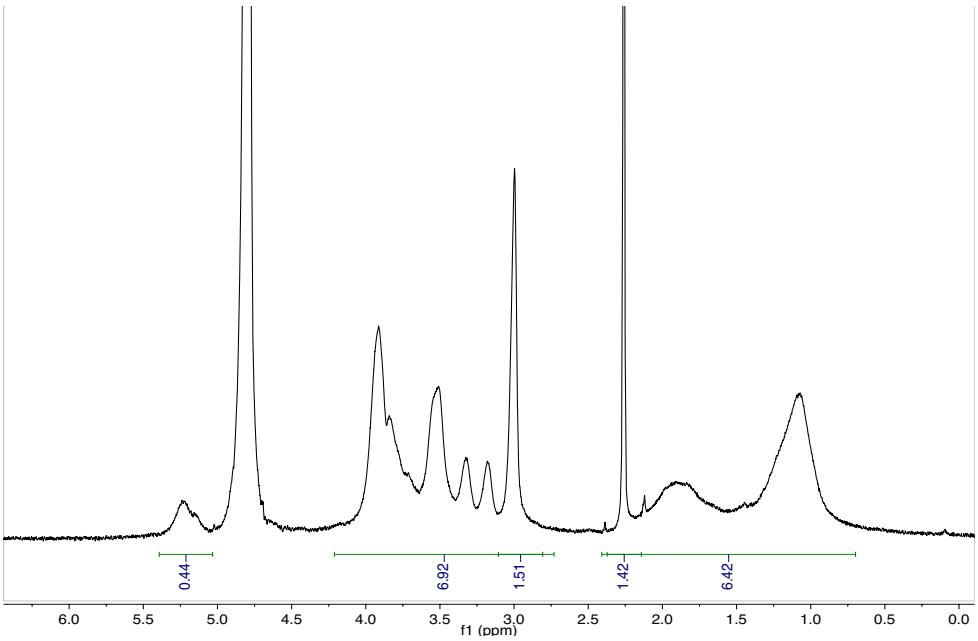

Figure 71. ^{1}H NMR spectra of poly(**G**$_{47}$-*s*-**P**$_{28}$-*s*-**T**$_{18}$) in D_2O at 500 MHz with a relaxation delay of 10 seconds. Spectra are internally refrenced to the HOD peak.

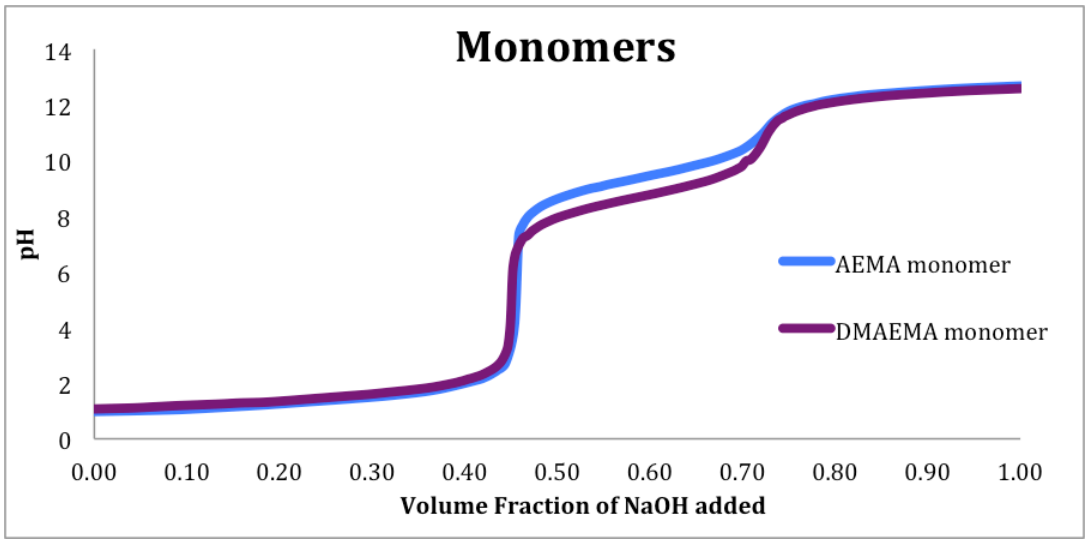

Figure 72. Comparison of the titration curves between AEMA and DMAEMA monomers.

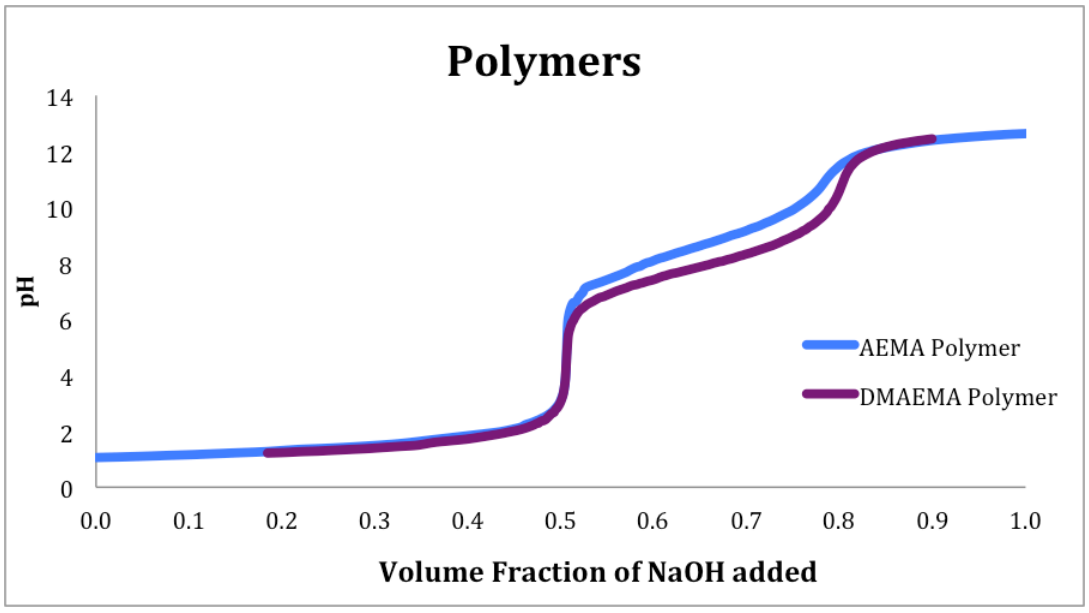

Figure 73. Comparison of the titration curves between AEMA and DMAEMA polymers.

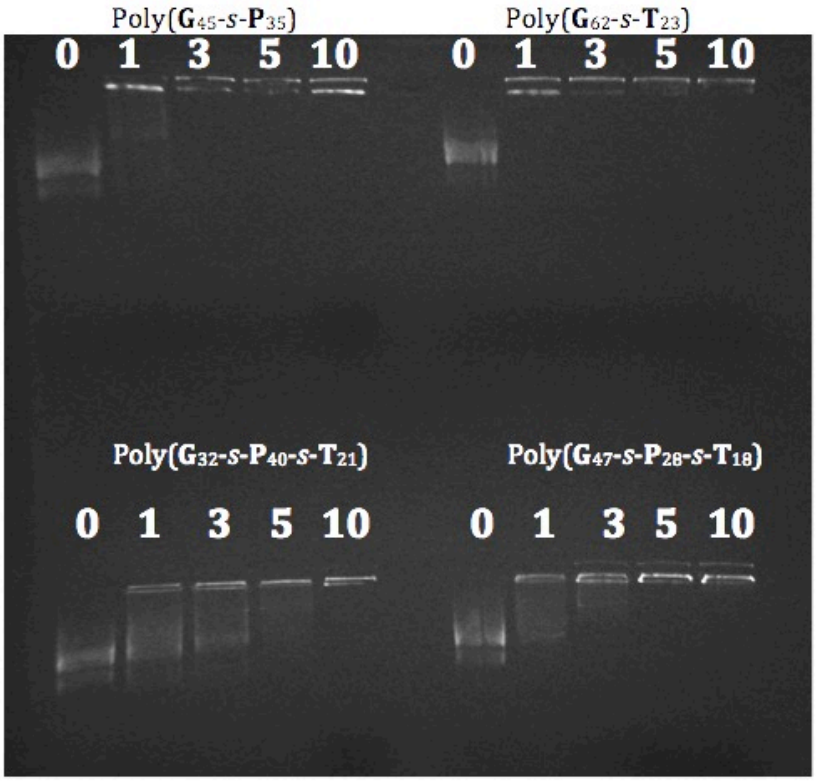

Figure 74. Gel Electrophoretic shift assay of the four statistical copolymers at N/P ratios 0, 1, 3, 5 and 10.

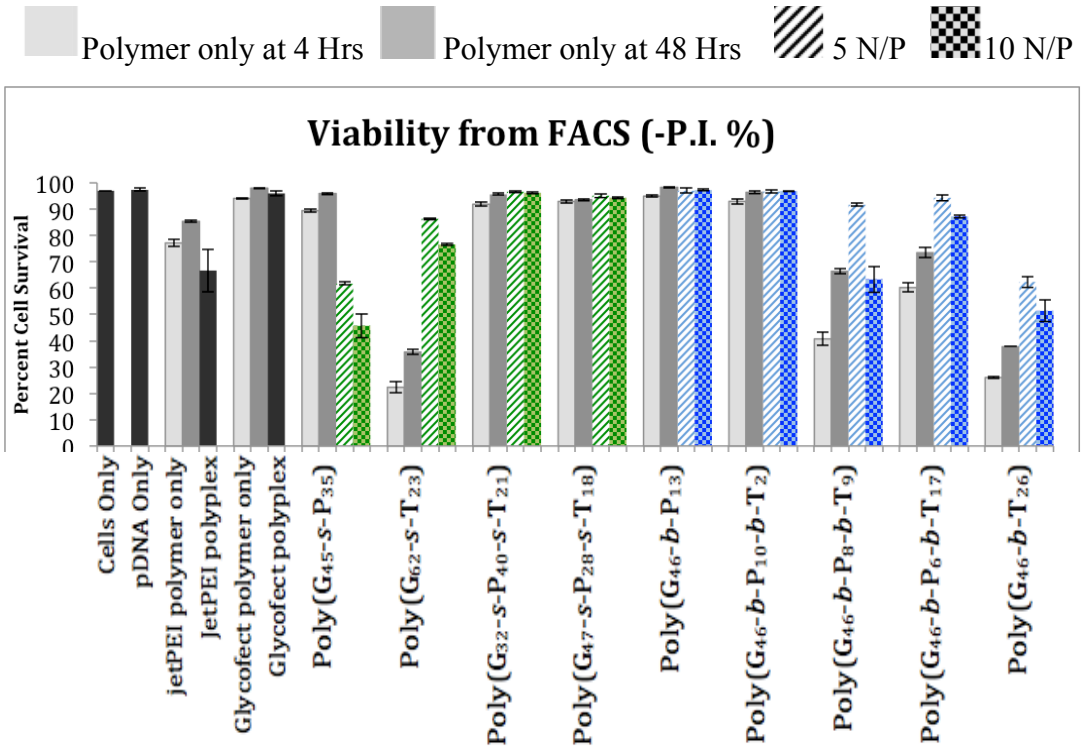

Figure 75. From Flow Cytometry – the percent cell survival according to negative propidium iodide staining of cells. Cells were treated with polymer only, and polyplexes at 5 N/P and 10 N/P. Polymer only samples were analyzed at 4 and 48 hours post transfection.

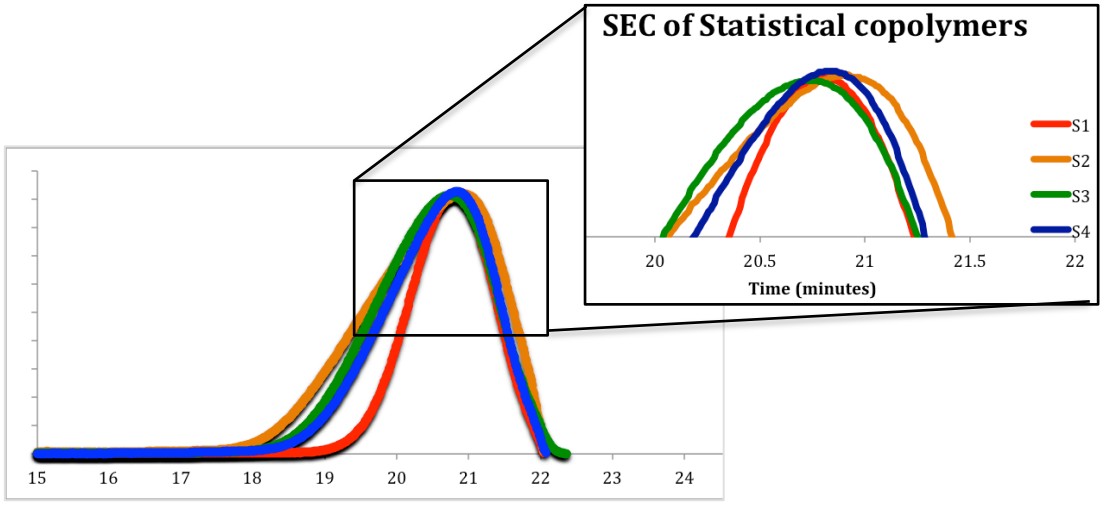

Figure 76. Aqueous Size exclusion chromatogram of the block polymers overlayed. M_w and $Đ$ can be found in Table 3.

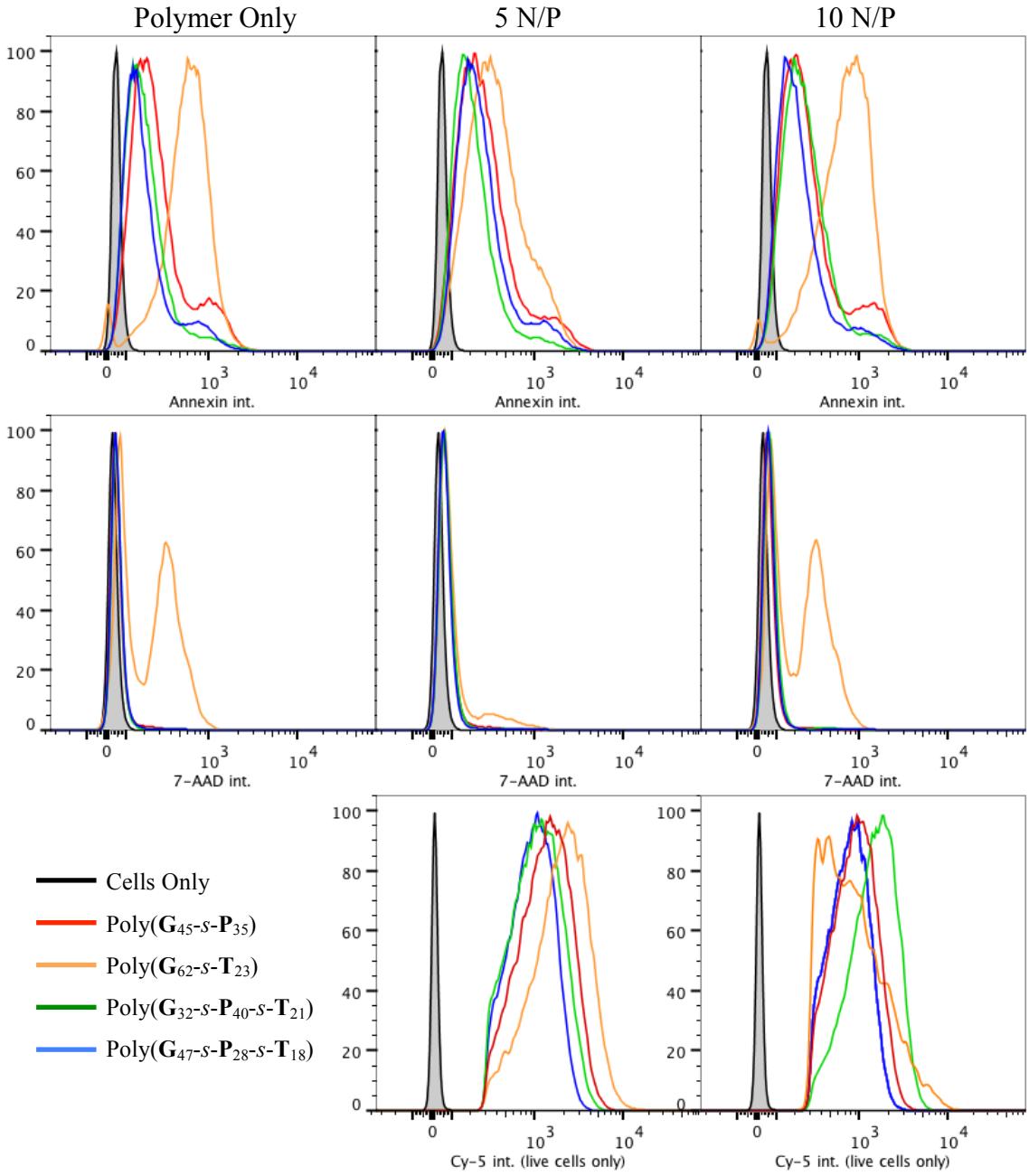

Figure 77. Normalized concatenated histogram overlays of the four statistical copolymers. The x-axis is Annexin V, 7-AAD, and Cy5 intensity for the rows and the columns are Polymer Only, 5 N/P, and 10 N/P, respectively. Cy5 represents the intensity of the Cy5 signal only in live cells – as determined by Annexin V negative population.

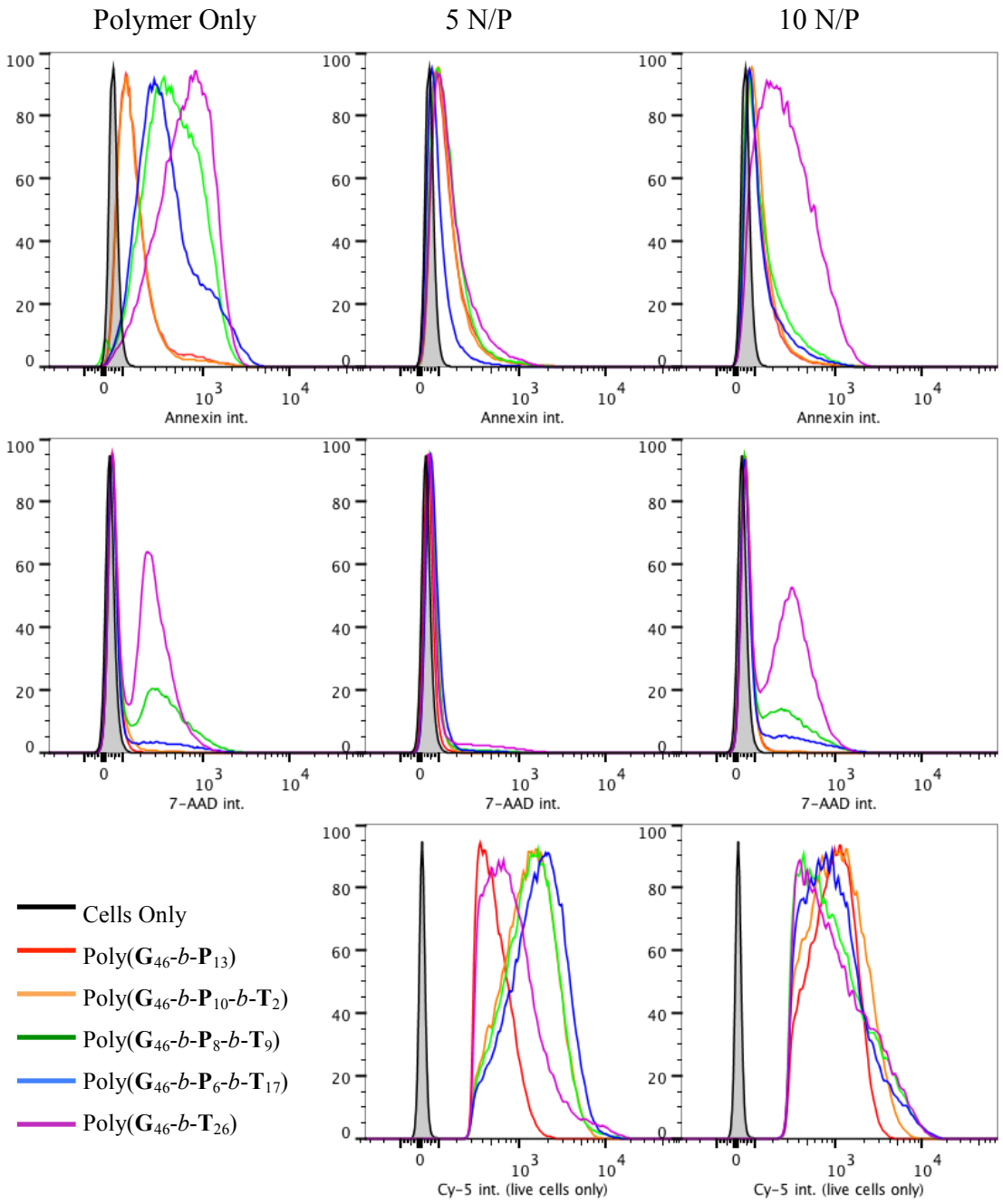

Figure 78. Normalized concatenated histogram overlays of the five block copolymers. The x-axis is Annexin V, 7-AAD, and Cy5 intensity for the rows and the columns are Polymer Only, 5 N/P, and 10 N/P, respectively. Cy5 represents the intensity of the Cy5 signal only in live cells – as determined by Annexin V negative population.

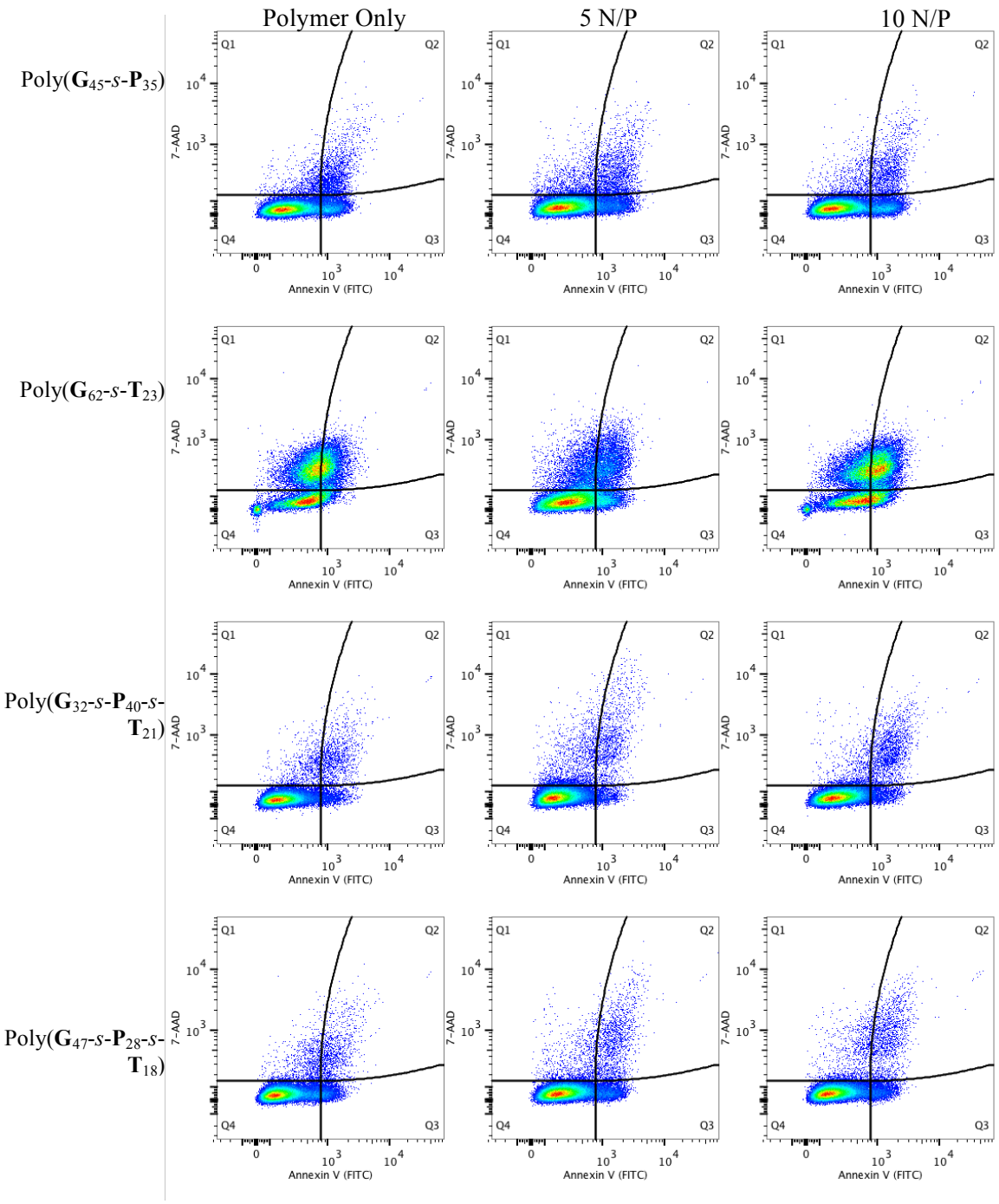

Figure 79. Flow cytomertry data for the four statistical copolymers. Triplicate sample was concatenated into one file. The x-axis is the Annexin V (FITC) stain, the y-axis is the 7-AAD stain, and the columns represent the Polymer only, 5 N/P, and the 10 N/P samples.

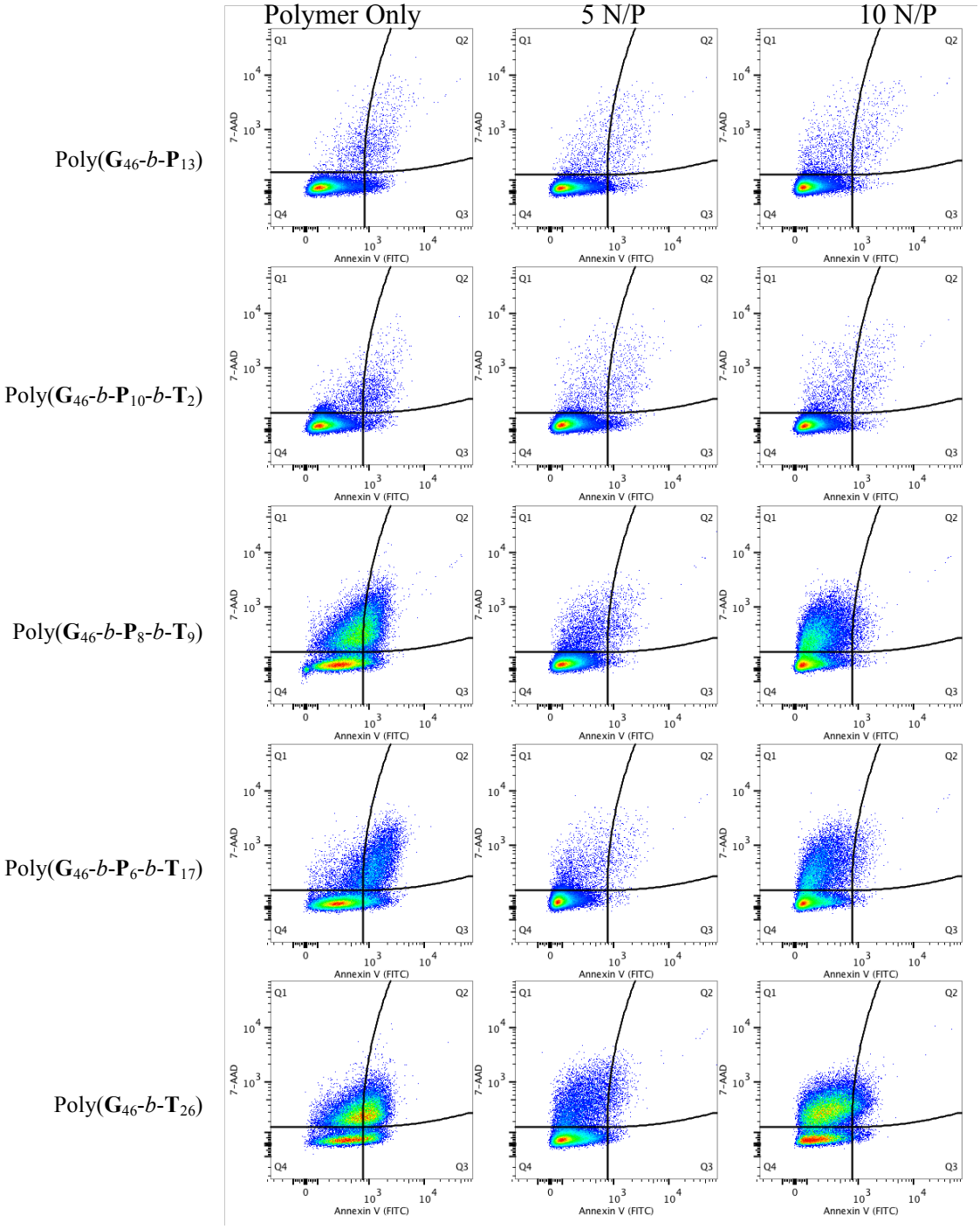

Figure 80. Flow cytomertry data for the five block copolymers. Triplicate sample was concatenated into one file. The x-axis is the Annexin V (FITC) stain, the y-axis is the 7-AAD stain, and the columns represent the Polymer only, 5 N/P, and the 10 N/P samples.

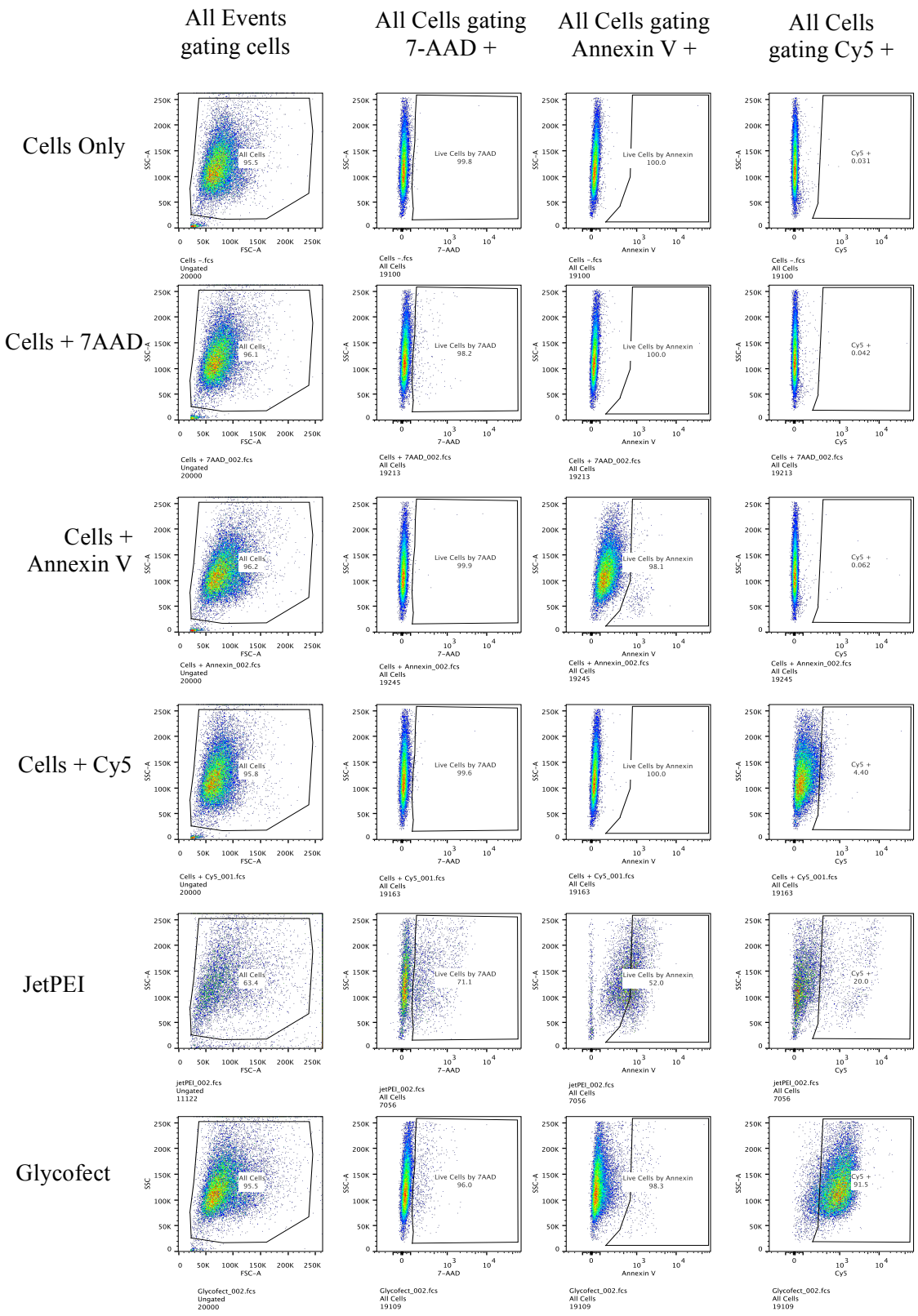

Figure 81. Gating hierarchy and controls for flow cytometry data.

Table 10 The size of the polyplexes measured by DLS, polyplexes were formed in water and then added to opti-MEM and size was measured at 0, 2, 4, and 6 hours.

Polymer	N/P	0 Hour	2 Hours	4 Hours	6 Hrs	6 Hr in H_2O
Poly(G_{45}-*s*-P_{35})	5	221	806	1200	1485	78
	10	176	491	871	1121	59
Poly(G_{62}-*s*-T_{23})	5	170	410	563	689	53
	10	158	385	544	722	64
Poly(G_{32}-*s*-P_{40}-*s*-T_{21})	5	281	374	432	371	58
	10	192	613	645	697	65
Poly(G_{47}-*s*-P_{28}-*s*-T_{18})	5	143	491	700	715	68
	10	118	159	249	483	55
Poly(G_{46}-*b*-P_{13})	5	79	108	85	96	84
	10	78	89	92	73	109
Poly(G_{46}-*b*-P_{10}-*b*-T_2)	5	78	113	151	202	66
	10	130	214	224	252	159
Poly(G_{46}-*b*-P_8-*b*-T_9)	5	180	308	607	776	66
	10	163	298	577	712	72
Poly(G_{46}-*b*-P_6-*b*-T_{17})	5	181	289	549	720	69
	10	173	322	432	567	72
Poly(G_{46}-*b*-T_{26})	5	130	169	208	266	87
	10	145	301	476	564	97

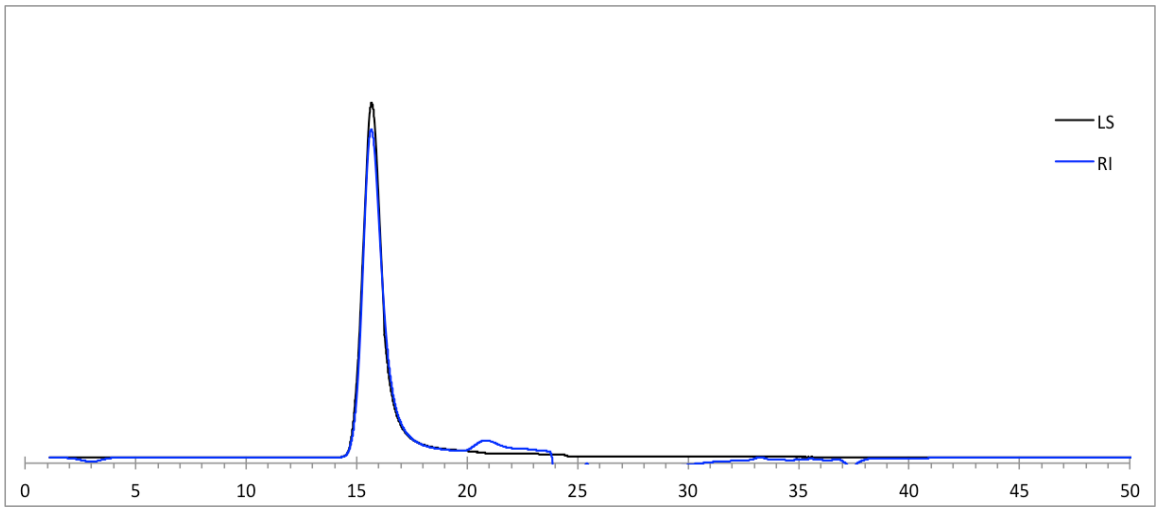

Figure 82. Size Exclusion Chromatography of Poly(DMAEMA$_{14}$-*b*-BMA$_{13}$).

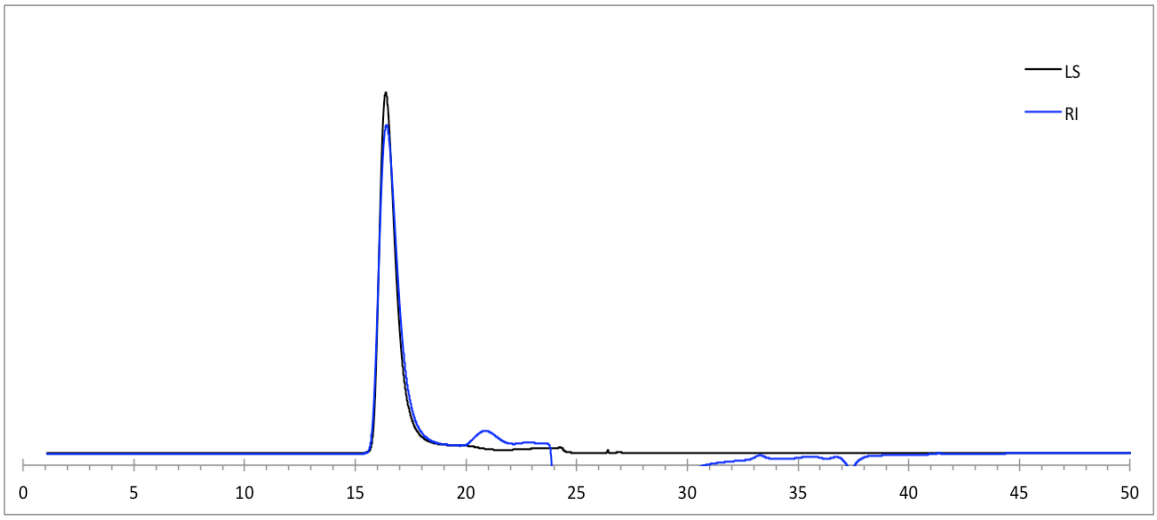

Figure 83. Size Exclusion Chromatography of Poly(DMAEMA$_{14}$-*b*-BMA$_{23}$)

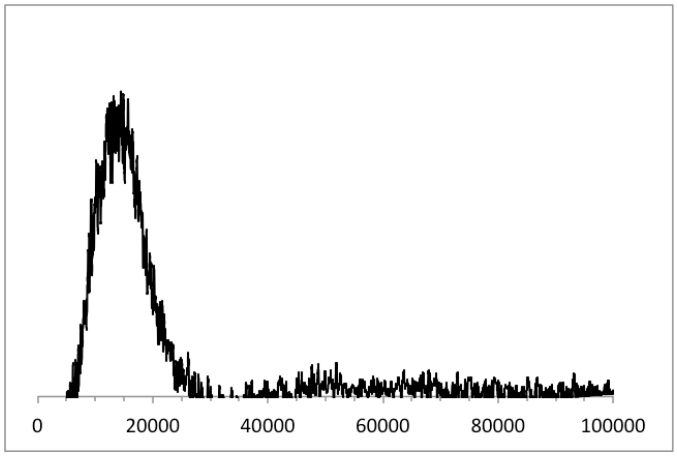

Figure 84. MALDI-TOF/TOF-MS of Poly(DMAEMA$_{14}$)

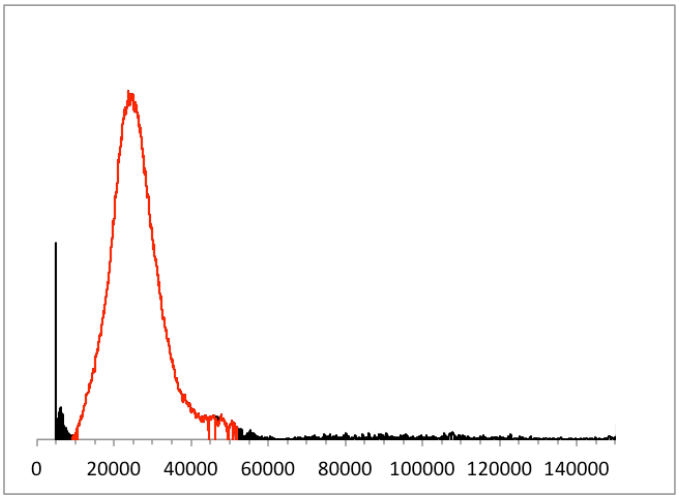

Figure 85. MALDI-TOF/TOF-MS of Poly(DMAEMA$_{14}$-*b*-BMA$_{13}$). The red line shows the area of integration.

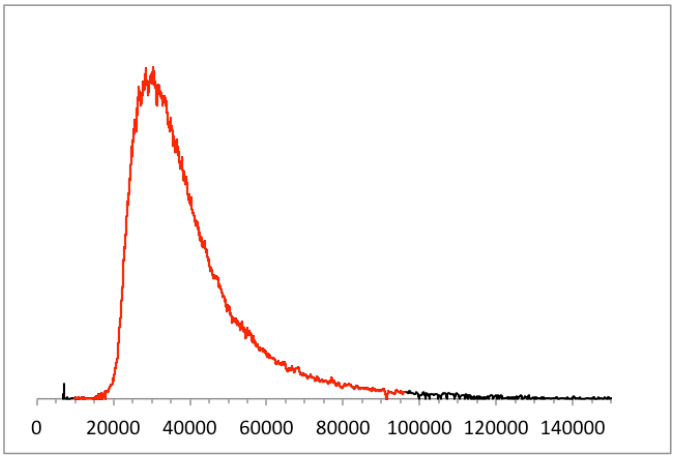

Figure 86. MALDI-TOF/TOF-MS of Poly(DMAEMA$_{14}$-*b*-BMA$_{23}$)

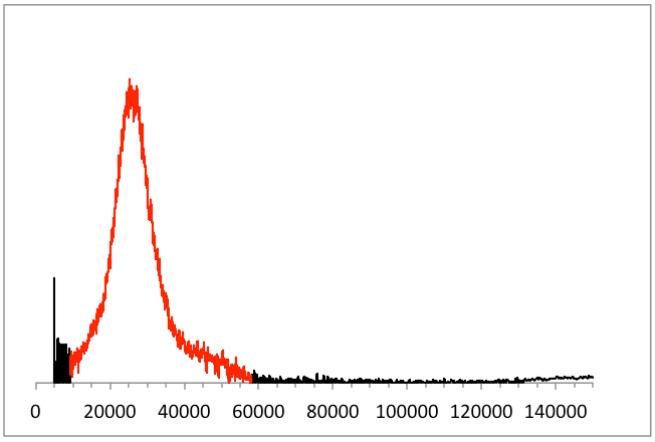

Figure 87. MALDI-TOF/TOF-MS of Poly(DMAEMA$_{27}$)

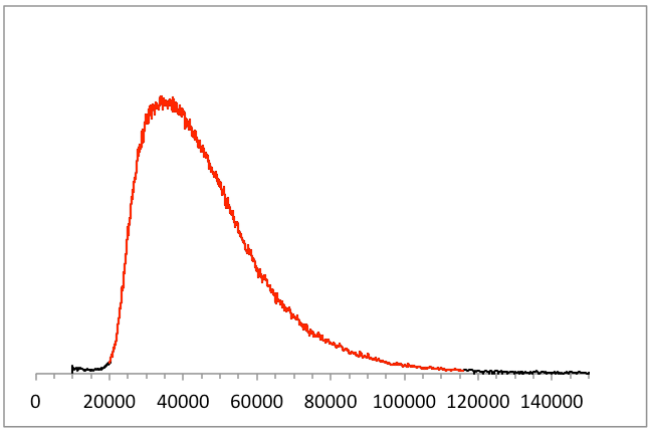

Figure 88. MALDI-TOF/TOF-MS of Poly(DMAEMA$_{27}$-*b*-BMA$_{14}$)

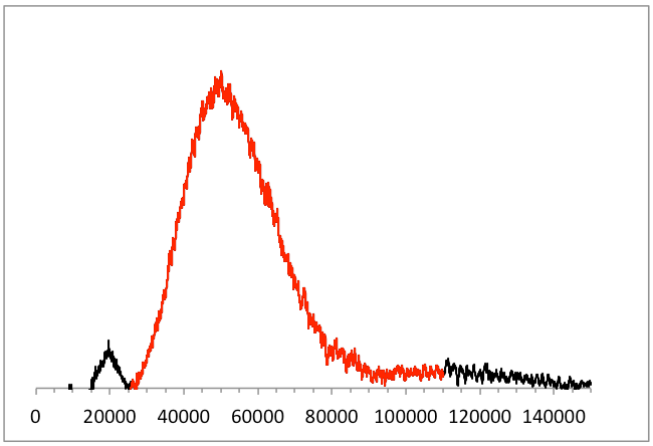

Figure 89. MALDI-TOF/TOF-MS of Poly(DMAEMA$_{27}$-*b*-BMA$_{29}$)

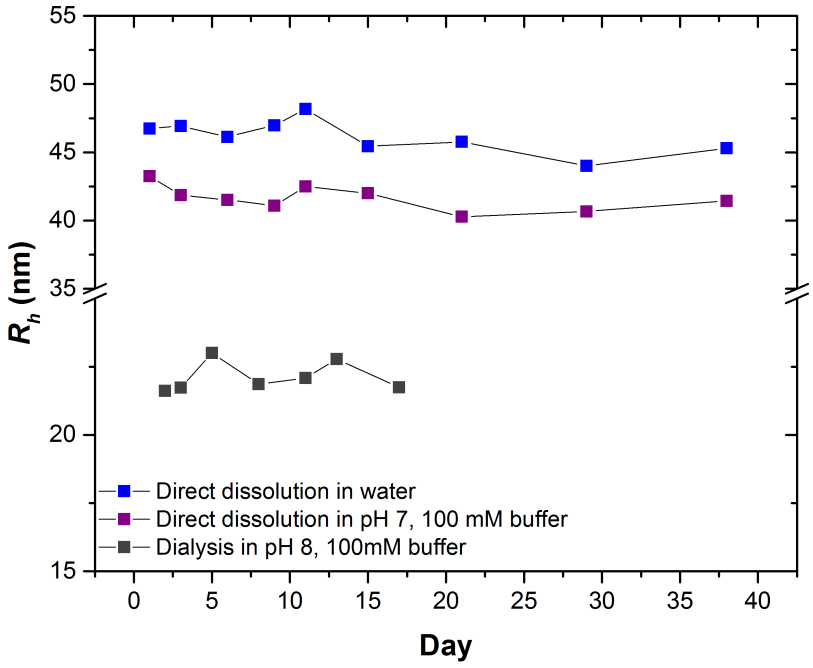

Figure 90. R_h stability of Poly(DMAEMA$_{27}$-*b*-BMA$_{14}$)

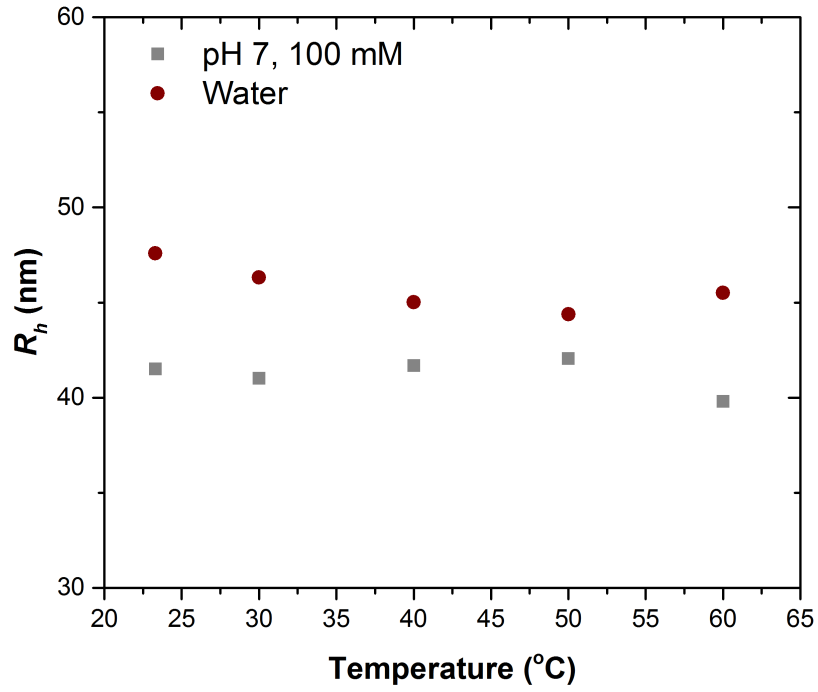

Figure 91. R_h of Poly(DMAEMA$_{27}$-*b*-BMA$_{14}$) at increasing temperatures. The temperature was increased by 10°C every 48 hours. Micelle solution in buffer was obtained by dialysis.

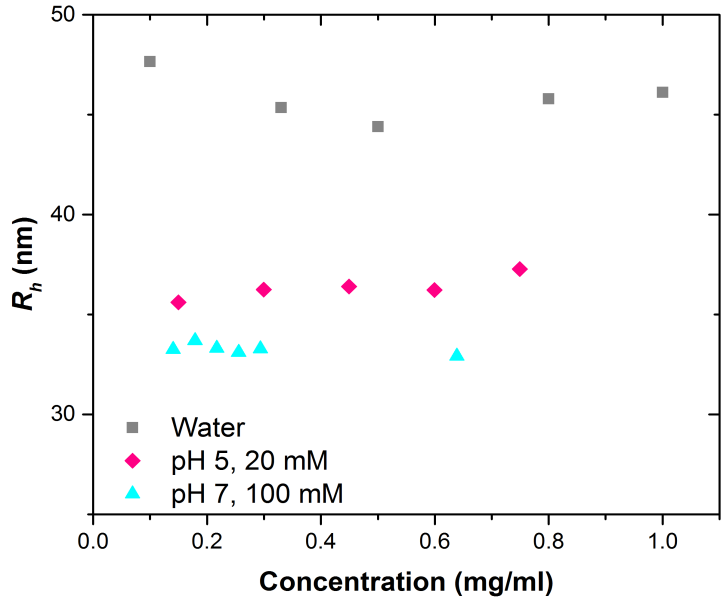

Figure 92. R_h of Poly(DMAEMA$_{27}$-*b*-BMA$_{14}$) at various concentration. Micelle solutions in buffer were obtained by dialysis.

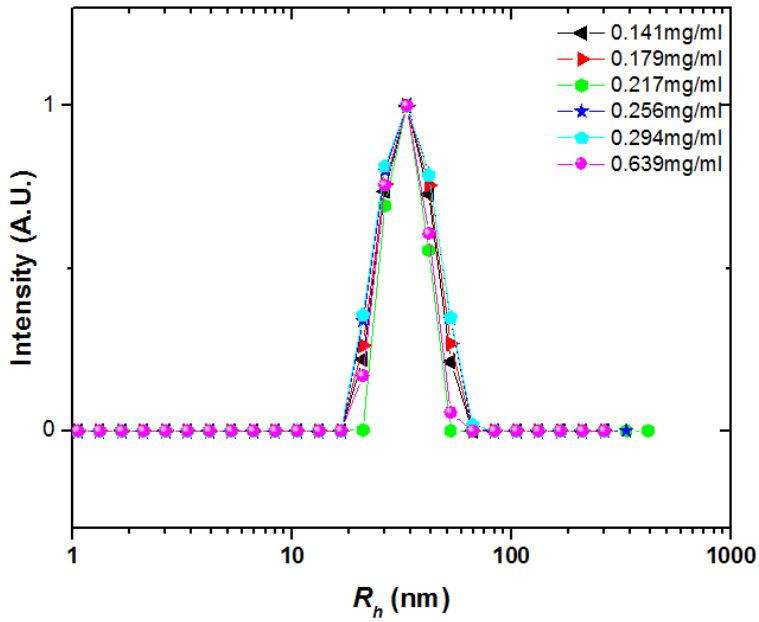

Figure 93. The size (R_h) of poly(DMAEMA$_{27}$-*b*-BMA$_{14}$) micelles made via direct dissolution and then dialyzed to pH 7 - 100 mM ionic strength and diluted to several concentrations to analyze size vs. concentration dependence. The size of the micelles once formed does not change with regard to their concentration in solution.

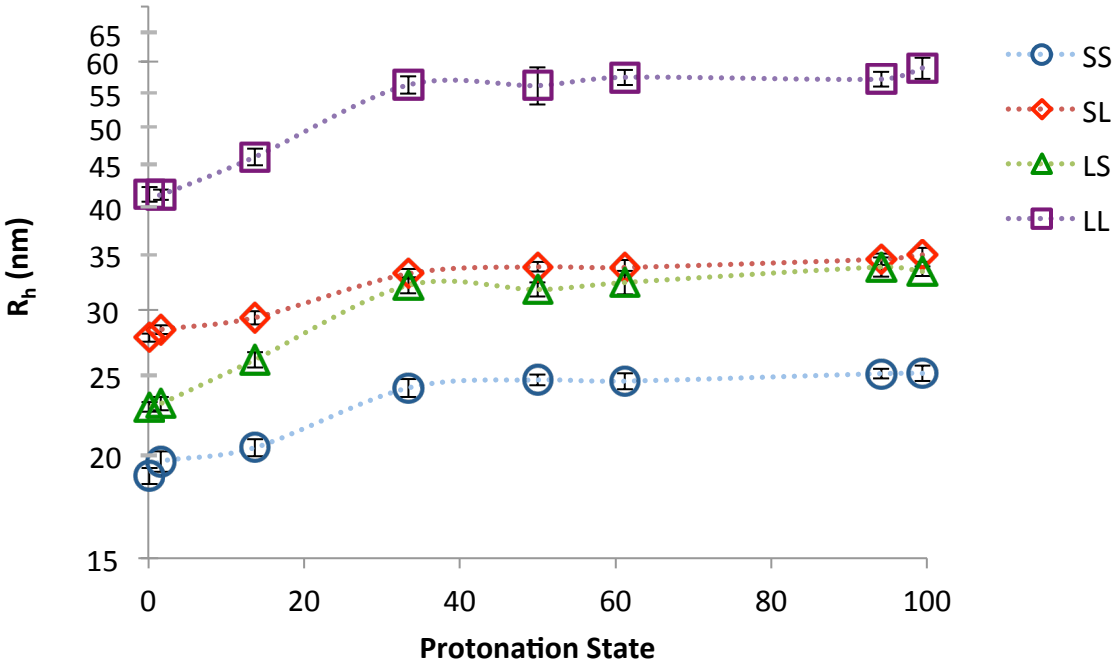

Figure 94. The size (R_h) of the four micelles at different protonation states (pH) at 100 mM ionic strength as measured by DLS. Blue circles (SS) is poly(DMAEMA$_{14}$-*b*-BMA$_{13}$), red diamonds (SL) is poly(DMAEMA$_{14}$-*b*-BMA$_{23}$), green triangles (LS) is poly(DMAEMA$_{27}$-*b*-BMA$_{14}$), and purple squares (LL) is poly(DMAEMA$_{27}$-*b*-BMA$_{29}$). Error bars are the standard deviation of all the data collected, a minimum of three replicates

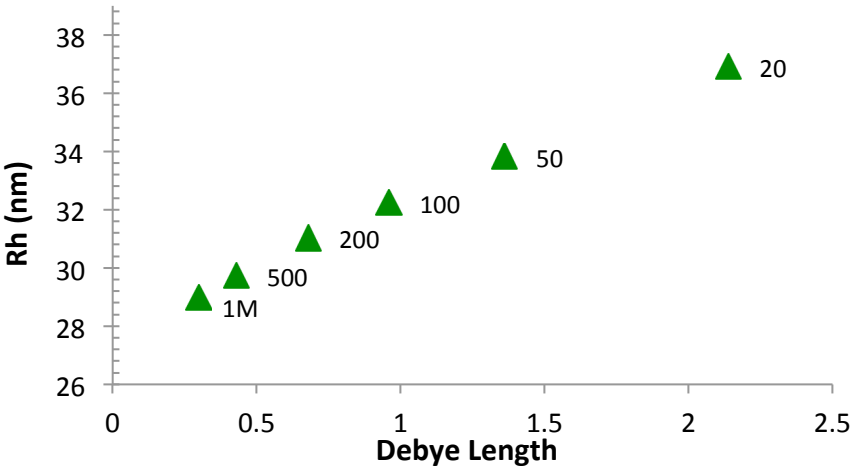

Figure 95. The size (R_h) of poly(DMAEMA$_{27}$-*b*-BMA$_{14}$) micelles at 50% protonation state (pK_a) at different ionic strengths (mM).

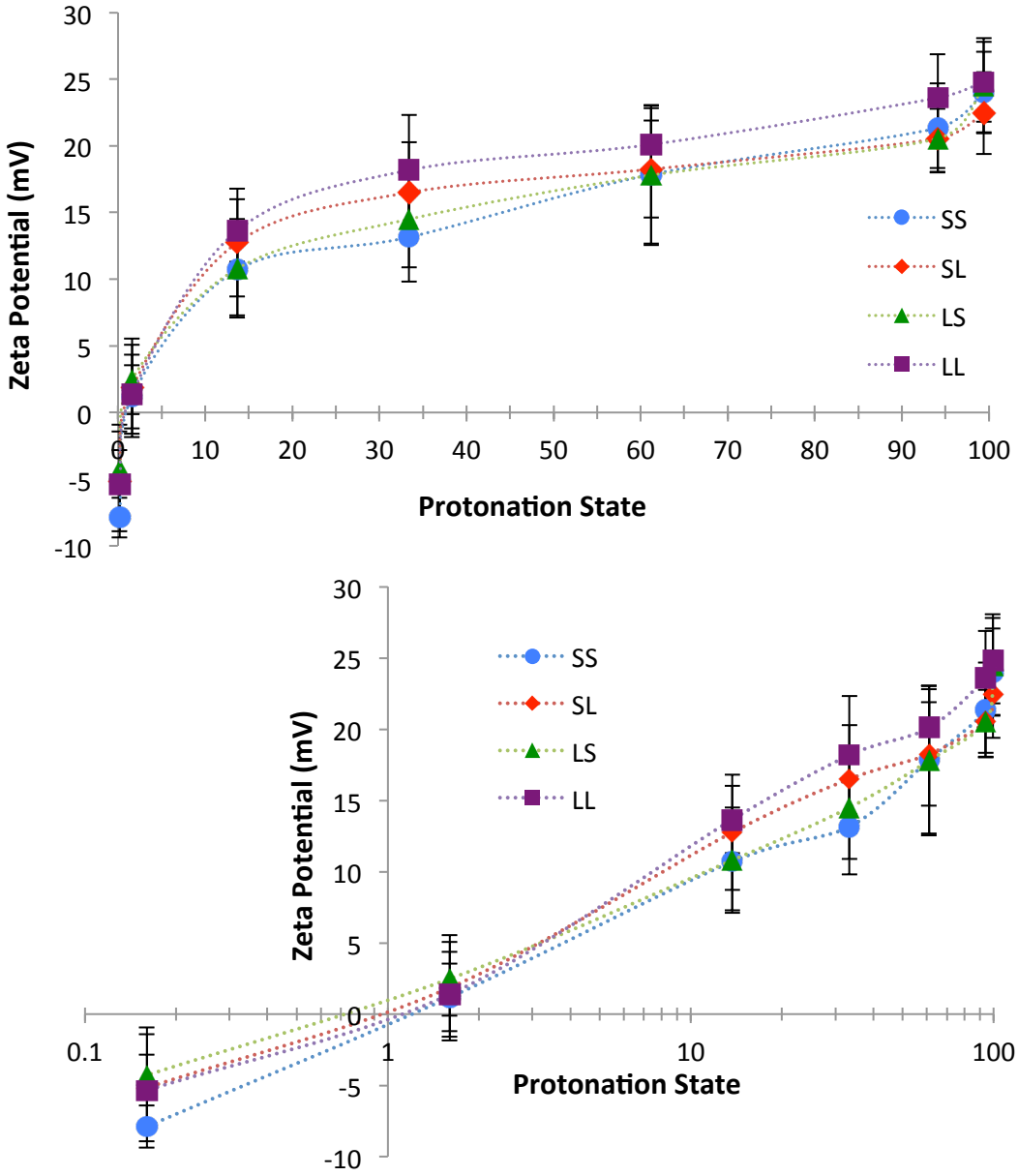

Figure 96a. The zeta potential (mV) of the four micelles at different protonation states (pH) at 100 mM ionic strength. Blue circles (SS) is poly(DMAEMA$_{14}$-*b*-BMA$_{13}$), red diamonds (SL) is poly(DMAEMA$_{14}$-*b*-BMA$_{23}$), green triangles (LS) is poly(DMAEMA$_{27}$-*b*-BMA$_{14}$), and purple squares (LL) is poly(DMAEMA$_{27}$-*b*-BMA$_{29}$). Figure 96b. The same data plotted on a log scale. Error bars are the standard deviation of all the data collected, a minimum of three replicates

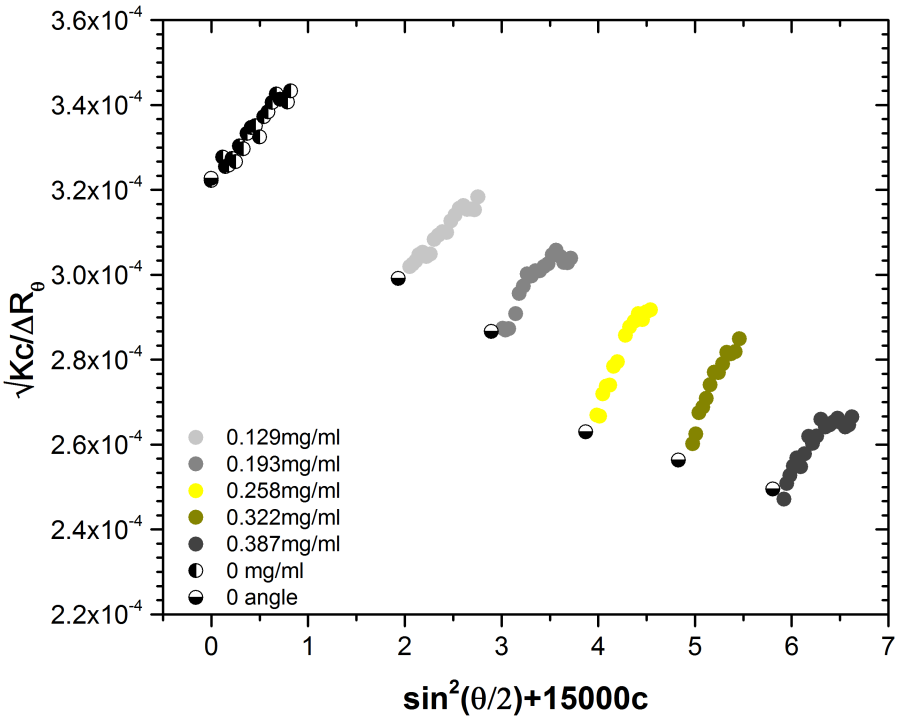

Figure 97. An example of one of the berry plots of the ploymers, used to calculate the molecular weight of the micelles. This berry plot is of the Poly(DMAEMA$_{14}$-*b*-BMA$_{23}$) micelle at pH 7, 100mM

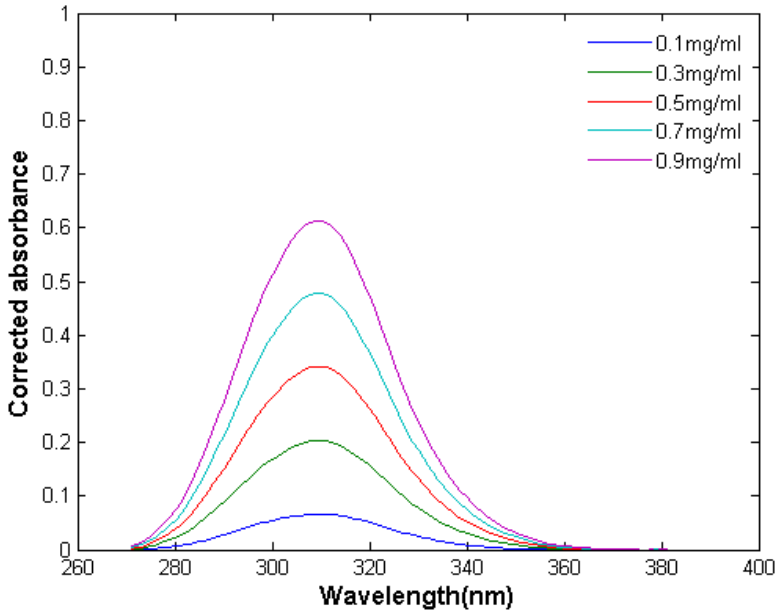

Figure 98. Corrected absorbance of Poly(DMAEMA$_{14}$-*b*-BMA$_{13}$).

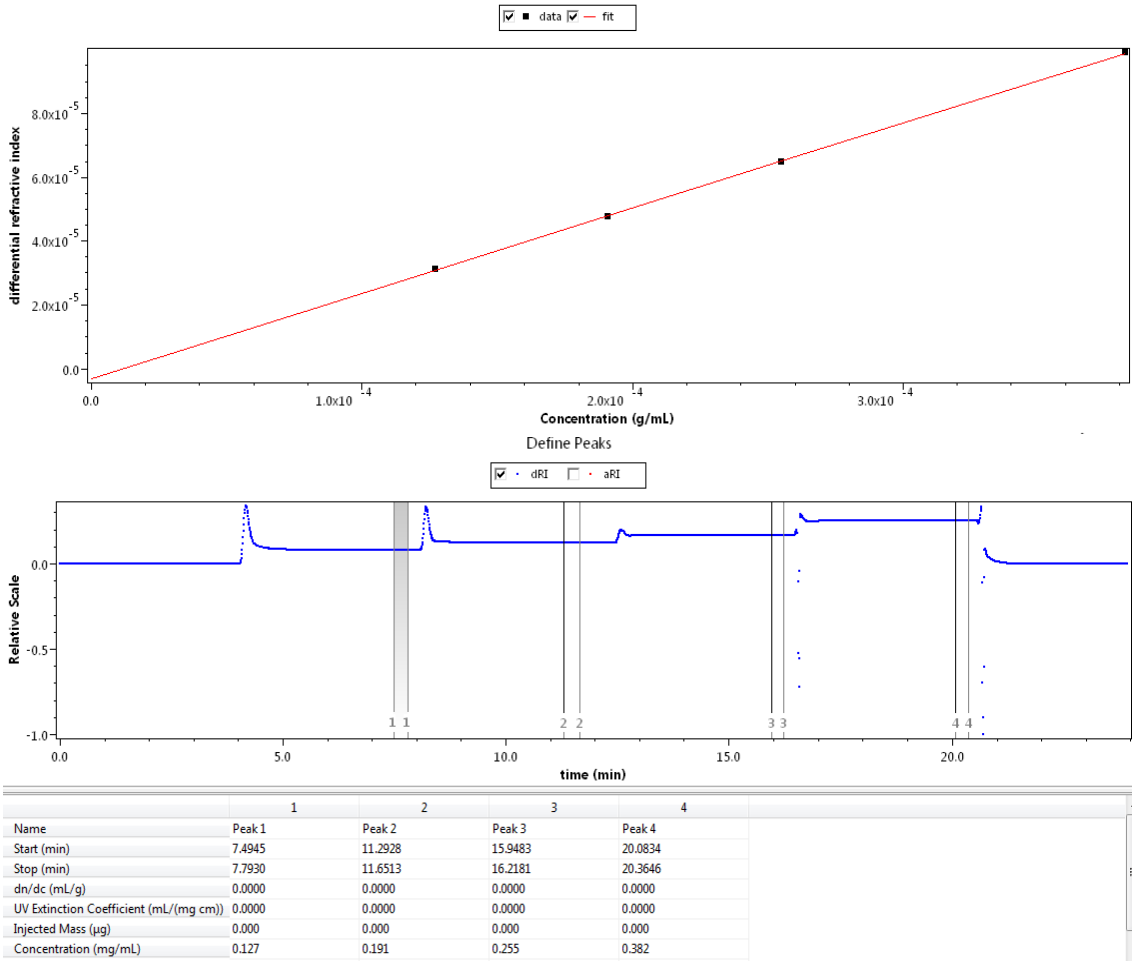

	1	2	3	4
Name	Peak 1	Peak 2	Peak 3	Peak 4
Start (min)	7.4945	11.2928	15.9483	20.0834
Stop (min)	7.7930	11.6513	16.2181	20.3646
dn/dc (mL/g)	0.0000	0.0000	0.0000	0.0000
UV Extinction Coefficient (mL/(mg cm))	0.0000	0.0000	0.0000	0.0000
Injected Mass (µg)	0.000	0.000	0.000	0.000
Concentration (mg/mL)	0.127	0.191	0.255	0.382

Figure 99. D*n*/D*c* calculation of micelles made in water with Poly(DMAEMA$_{27}$-*b*-BMA$_{14}$) and dialyzed to pH 5 100 mM ionic strength conditions. Concentration was predetermined with UV-Vis before being passed through a refractometer

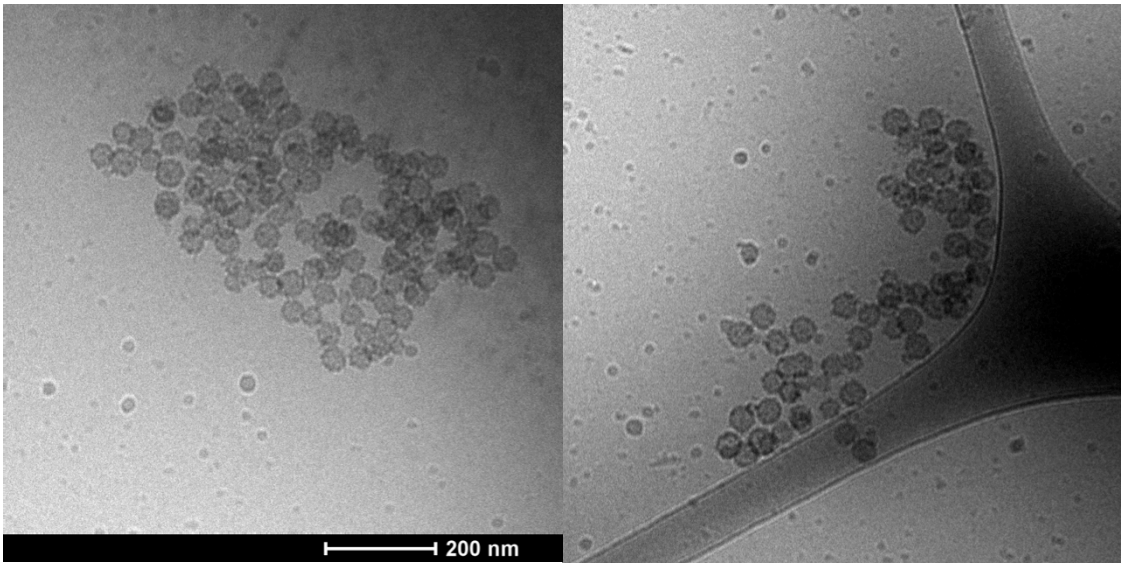

Figure 100. Stained Cryo-TEM images of poly(DMAEMA$_{14}$-*b*-BMA$_{23}$).

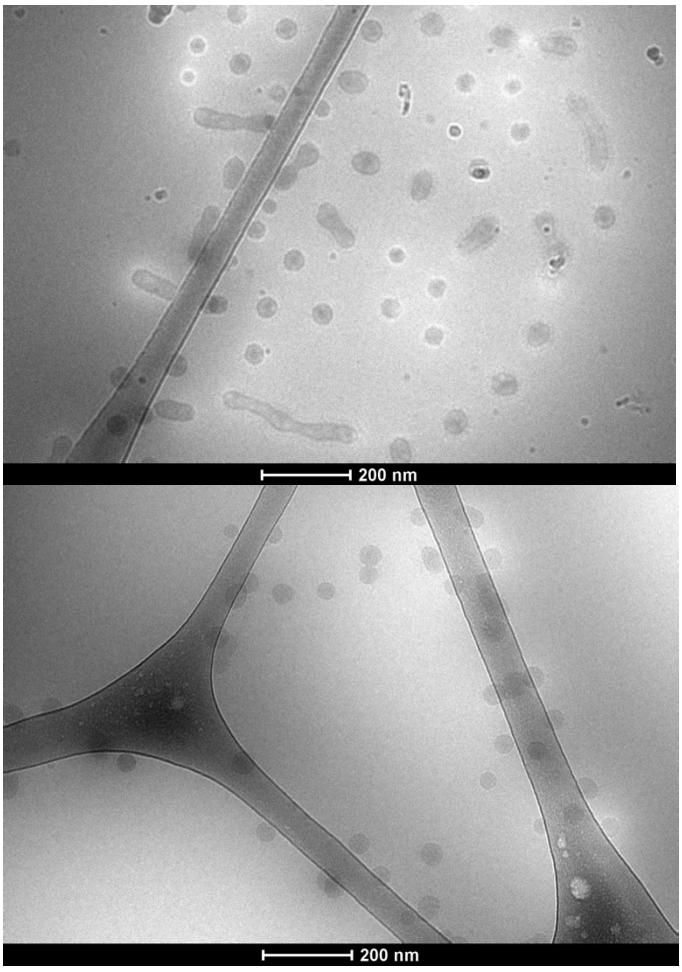

Figure 101. Cryo-TEM image of a before and after 5 mins of sonication with poly(DMAEMA$_{27}$-*b*-BMA$_{29}$).